

Prevention of radiotherapy-induced side effects in retinoblastoma animal models

Dissertation

der Mathematisch-Naturwissenschaftlichen Fakultät
der Eberhard Karls Universität Tübingen
zur Erlangung des Grades eines
Doktors der Naturwissenschaften
(Dr. rer. nat.)

vorgelegt von
Alexander Viktor Tschulakow
aus Gomel/Belarus

Tübingen
2018

Gedruckt mit Genehmigung der Mathematisch-Naturwissenschaftlichen Fakultät der
Eberhard Karls Universität Tübingen.

Tag der mündlichen Qualifikation:

17.07.2018

Dekan:

Prof. Dr. Wolfgang Rosenstiel

1. Berichterstatter:

Prof. Dr. Ulrich Schraermeyer

2. Berichterstatter:

Prof. Dr. Hans-Georg Rammensee

Das Strahlen von *Kinderaugen*
bringt mehr Licht in unsere Seele,
als der hellste Sonnenschein.

B. Geller-Wollentin

Взгляните в детские глаза!
Когда тоска и груз забот...
Там сказки свет и чудеса,
Там вся вселенная живёт.

Алена Глазова

List of Contents

| | |
|---|-----------|
| List of Contents | 4 |
| 1. List of abbreviations, Acronyms | 6 |
| 2. Summary | 7 |
| 2.1 Summary | 7 |
| 2.2 Zusammenfassung | 8 |
| 3. Introduction..... | 10 |
| 3.1 Retinoblastoma (Rb) | 10 |
| 3.1.1 History of Rb..... | 10 |
| 3.1.2 Aetiology and Epidemiology of Rb | 11 |
| 3.1.3 Biology of Rb | 12 |
| 3.1.4 RB1 gene | 14 |
| 3.1.5 Rbp interactions and its role in cancer | 15 |
| 3.1.6 Rb research..... | 18 |
| 3.1.7 Diagnosis of Rb..... | 18 |
| 3.1.8 Radiotherapy and other treatment options for Rb treatment | 19 |
| 3.2 Radioprotectors | 20 |
| 3.2.1 Epidermal growth factor receptor (EGFR) | 22 |
| 3.2.2 Ortho-phospho-L-tyrosine (pTyr) | 25 |
| 4. Objectives | 28 |
| 5. Results..... | 29 |
| 5.1 Is there a relevant mouse model, which can be used for radiotherapeutic approaches? | 29 |
| 5.1.1 Establishment of a novel retinoblastoma (Rb) nude mouse model by intravitreal injection of human Rb Y79 cells – Comparison of <i>in vivo</i> analysis versus histological follow up | 31 |
| 5.1.1.1 Additional unpublished material..... | 32 |
| 5.2 Can the application of pTyr protect tissues that are affected by irradiation during radiotherapy and prevent radiotherapy-induced secondary tumours?..... | 33 |
| 5.3 Does the application of pTyr interfere with the radiotherapy of retinoblastoma?..... | 37 |
| 5.3.1 <i>In vitro</i> studies..... | 37 |
| 5.3.1.1. Western blot | 38 |

List of Contents

| | |
|---|-----------|
| 5.3.1.2 Pre-plating and delayed plating limited dilution assay- studies with Y79 cells | 38 |
| 5.3.2 Irradiation studies in our Rb Y79-xenograft nude mouse model..... | 38 |
| 5.4 The radioprotector ortho-phospho-L-tyrosine (pTyr) attenuates the side effects of fractionated irradiation in retinoblastoma mouse models but also decreases the local tumour control | 40 |
| 6. Discussion | 41 |
| 6.1 Is there a relevant mouse model, which can be used for radiotherapeutic approaches? | 41 |
| 6.2 Can the application of pTyr protect tissues that are affected by irradiation during radiotherapy and prevent the induction of secondary tumours? | 42 |
| 6.3. Does the application of pTyr interfere with the radiotherapy of retinoblastoma? | 43 |
| 6.4 Additional finding | 44 |
| 7. Final conclusions | 44 |
| 8. Perspectives | 45 |
| 9. Appendix | 47 |
| 9.1 List of references..... | 47 |
| 9.2 Declaration according to § 5 Abs. 2 No. 8 of the PromO of the Faculty of Science - Share in publications done in team work..... | 56 |
| 9.3 List of publications..... | 57 |
| 9.4 Articles from other projects published during PhD study..... | 62 |
| 9.4.1 The anatomy of the foveola reinvestigated | 63 |
| 9.4.2 Effects of intravitreally injected Fc fragment on rat eyes..... | 64 |
| 9.4.3 The effects of VEGF-A-inhibitors aflibercept and ranibizumab on the ciliary body and iris of monkeys..... | 65 |
| 9.4.4 Effects of a Single Intravitreal Injection of Aflibercept and Ranibizumab on Glomeruli of Monkeys | 66 |
| 9.5 Curriculum Vitae | 67 |
| 9.5 Erklärungen..... | 69 |
| 9.6 Acknowledgements..... | 70 |

1. List of abbreviations, Acronyms

| | |
|--------|------------------------------------|
| ChT – | chemotherapy |
| DNA - | deoxyribonucleic acid |
| EGF - | epidermal growth factor |
| EGFR - | epidermal growth factor receptor |
| EM – | electron microscopy |
| IR- | irradiation |
| MDMX - | mouse double minute X |
| OCT - | optical coherence tomography |
| PBS – | phosphate buffered saline |
| PCR - | polymerase chain reaction |
| pTyr - | ortho-phospho-L-tyrosine |
| Rb – | retinoblastoma |
| Rbp – | retinoblastoma protein |
| RPE – | retinal pigment epithelium |
| RNA - | ribonucleic acid |
| RT - | radiotherapy |
| SLO - | scanning laser ophthalmoscopy |
| VEGF - | vascular endothelial growth factor |
| WT - | wild type |

2. Summary

2.1 Summary

Retinoblastoma is the most common intraocular malignancy of infancy which is thought to originate from progenitor cells of the developing retina. The modern therapeutic approaches for retinoblastoma treatment including radiotherapy have very high success rates if the tumour is diagnosed at an early time point. But these therapies, especially radiotherapy, have side effects such as damage to healthy tissues and increasing the risk of induction of secondary tumours. As the radiotherapy has to be performed in a very young age and the risk of the therapy's side effects persist over lifetime, the quality of the patients' lives is strongly impaired. The risk of developing secondary tumours after radiotherapy is particularly high for patients with a family history of retinoblastoma, which leads to a deterioration in the quality of these patients' lives. In this context, the aim of our project was to analyse a new option for the prevention of side effects of radiotherapy of the retinoblastoma through the use of the radioprotector ortho-phospho-L-tyrosine (pTyr). Three main questions had to be answered:

1. Is there a relevant retinoblastoma-mouse-model which can be used for radiotherapy?
2. Can the application of pTyr protect tissues that are damaged by irradiation during radiotherapy and prevent the induction of secondary tumours?
3. Does the application of pTyr interfere with the radiotherapy?

To answer question 1., the retinoblastoma mouse models described in the literature were analysed. Since none of them fully met our requirements, we decided to establish a new retinoblastoma-xenograft-mouse model by performing intravitreal injections of human Y79 cells in immunodeficient nude mice. The growth of the xenograft tumours in the eyes was monitored *in vivo* by scanning laser ophthalmoscopy (SLO) and optical coherence tomography (OCT). These results were compared to the results of the corresponding histological analysis. The *in vivo* and histological results showed a good correlation. The xenograft-tumours in the mouse-model showed very similar growth, histological and ultrastructural characteristics to Rb patients' tumours and therefore our model can be used for the study of retinoblastoma.

To answer the second question, Rb^{+/-} mice as a model for patients who have defects in the homologue human RB1 gene were used. These patients have a higher risk of developing a retinoblastoma and other tumours like sarcomas, additionally they are prone to radiotherapy-induced tumours. The animals were irradiated in a retinoblastoma radiotherapy-like procedure with and without a pTyr pre-treatment (100 mg/kg bodyweight, 16 hours before irradiation). A bleaching of the hair coat in the irradiated area started five weeks after irradiation in the animals which were not treated with pTyr. However, in the pTyr pre-treated animals the bleaching started later, about eight weeks after irradiation, and was significantly weaker. Importantly our *in vivo* (OCT) as well as our histological results have shown that pTyr protects the retina, which is a radiosensitive tissue, against the radiation-induced damage: the irradiation induced degenerative changes in the retina, such as thickness reduction, and loss of photoreceptors were significantly higher in the non-pTyr pretreated animals as compared to the pTyr-treated ones three, six and nine months after irradiation. No induced tumours or distant metastasis were found for any of the analysed mice. Since it is known that in retinoblastoma patients induced tumours are mostly diagnosed some 30 years after radiotherapy, the maximum lifespan of 16 months of our mice might be too short for the side effects to appear.

Finally, in order to check if the application of pTyr would interfere with radiotherapy, the ability of pTyr to protect Y79 cells *in vitro* and *in vivo* was tested. For the *in vitro*

2. Summary

testing Y 79 cell cultures were irradiated with and without pTyr pretreatment and their survival was analysed using different "limited dilution assays". No significant radioprotection of pTyr on Y79 cells was detected.

For the *in vivo* analysis of the radioprotection of Y79 cells by pTyr, our new established nude mouse model was used for a radiotherapeutic experiment with and without pTyr pre-treatment. The radiotherapy was successful as 80% of the mice which were not pre-treated with pTyr, stayed tumour-free for at least nine months after radiotherapy. However, in all pTyr pretreated animals a retinoblastoma reappeared. It has become apparent, that pTyr is a potent radioprotector for Y79-xenografts in contrast to Y79 cell cultures. This makes pTyr contraindicated for the radiotherapy of retinoblastoma. However, the radioprotective abilities of pTyr might make it interesting for the radiotherapy of other cancers, especially those with p53 mutations.

2.2 Zusammenfassung

Das Retinoblastom ist der häufigste intraokulare Tumor im Kindesalter. Moderne Therapien für Retinoblastom-Patienten wie z.B. die Strahlentherapie führen bei frühzeitiger Erkennung des Tumors mit sehr hoher Wahrscheinlichkeit zur Heilung. Allerdings hat die Strahlentherapie Nebenwirkungen wie z.B. Normalgewebsschädigungen und ein erhöhtes Risiko für das Entstehen von Sekundärtumoren. Da die Therapie im sehr frühen Lebensalter stattfindet und das Risiko der Folgeschäden der Therapie ein Leben lang bestehen bleibt, wird die Lebensqualität der Patienten dadurch nachhaltig beeinträchtigt. Das Risiko ist besonders hoch für Patienten mit familiärer Retinoblastomvorbelastung. Vor diesem Hintergrund war es das Ziel unseres Projektes einen Ansatz zur Prävention dieser therapiebedingten Nebenwirkungen für die Strahlentherapie des Retinoblastoms durch den Einsatz des Normalgewebs-spezifischen Radioprotektors Ortho-phospho-L-tyrosin (pTyr) zu untersuchen. Dabei sollten drei wichtige Fragen geklärt werden:

1. Gibt es ein passendes radiotherapeutisch einsetzbares Retinoblastom-Mausmodell?
2. Kann pTyr Radiotherapie-bedingte Nebenwirkungen und die Entstehung von Sekundärtumoren verhindern?
3. Wird durch pTyr Gabe eine Beeinträchtigung des Erfolges der Strahlentherapie verursacht?

Um die erste Frage zu beantworten, wurde zunächst die Literatur nach Retinoblastom-Modellen durchsucht. Da keines der beschriebenen Modelle unseren Vorstellungen voll entsprach, wurde beschlossen ein neues eigenes Modell zu etablieren. Dazu wurden humane Y79 Tumorzellen intravitreal in immundefiziente Nacktmäuse injiziert. Das Wachstum der Xenograft-Tumore in den Augen wurde *in vivo* mit Hilfe von scanning laser ophthalmoscopy (SLO) und optical coherence tomography (OCT) untersucht und die Resultate mit denen der entsprechenden histologischen Untersuchungen verglichen. Die Resultate der *in vivo* Untersuchungen konnten gut mit den Resultaten der histologischen Untersuchungen korreliert werden. Das Wachstum der Xenograft-Tumore in unserem neu etablierten Retinoblastom-Nacktmausmodell, sowie deren zelluläre und ultrastrukturellen Charakteristika waren dem menschlicher Retinoblastome sehr ähnlich. Somit ist unser Modell gut für Untersuchungen zum Wachstum und Entwicklung des Retinoblastoms geeignet. Somit sind die von uns verwendeten *in vivo* Verfahren für die Detektion und morphologische Beschreibung von Retinoblastomen im frühen Entwicklungsstadium einsetzbar.

Um die zweite Frage zu klären wurden Rb+/- Mäuse eingesetzt. Diese dienten als Modell für Patienten mit Defekten im homologen RB1 Gen, die ein höheres Risiko haben ein Retinoblastom und Sekundärtumore nach einer Strahlentherapie zu

2. Summary

entwickeln. Die Mäuse wurden mit und ohne pTyr-Vorbehandlung in einer eine Retinoblastom-Radiotherapie simulierenden Art bestrahlt. Die erste feststellbare Reaktion der Mäuse auf die Bestrahlung war eine Veränderung des Fells im bestrahlten Bereich von schwarz zu grau/weiß. Bei allen nicht mit pTyr behandelten Tieren erfolgte diese Reaktion ca. 5 Wochen nach der Behandlung. Diese ist bei den mit pTyr behandelten Tieren später (ca. 8 Wochen nach Behandlung) und signifikant weniger stark ausgeprägt erfolgt. Fell und Hautveränderungen sind bekannte Begleiterscheinungen nach Bestrahlungs- und Radiotherapeutischen Versuchen bei Mäusen. Eine weitere wichtige Frage unserer Untersuchung war, ob die Retina, die ein bestrahlungsempfindliches Gewebe darstellt, durch die pTyr Behandlung vor Strahlenschäden geschützt werden kann. Sowohl unsere *in vivo* als auch unsere histologischen Untersuchungen lassen eine schützende Wirkung von pTyr auf bestrahltes Gewebe erkennen, da die degenerativen Retinaveränderungen in den mit pTyr vorbehandelten Tieren 3, 6 und 9 Monate nach Bestrahlung deutlich schwächer ausgeprägt waren als in den nicht mit pTyr vorbehandelten. Im Beobachtungszeitraum dieses Versuches konnten keine induzierten Tumore beobachtet werden. Wir gehen davon aus, dass diese sich erst zu späteren Zeitpunkten manifestieren würden. Bei Retinoblastom-Patienten, die mit Radiotherapie behandelt wurden, werden Therapie-induzierte Tumore meist erst ungefähr 30 Jahre nach der Behandlung diagnostiziert.

Um zu testen, ob pTyr die Radiotherapie beeinträchtigt, wurden *in vitro* und *in vivo* Studien zur Radioprotektion von pTyr auf Y79 Zellen durchgeführt. Für die *in vitro* Untersuchung wurden Y79-Tumorzellkulturen mit und ohne pTyr Vorbehandlung bestrahlt und das Überleben der Zellen mittels „limited dilution assays“ analysiert. Es konnte keine signifikante Radioprotektion von pTyr in Y79 Zellen in unseren *in vitro* Studien nachweisen werden.

Um die Radioprotektion von pTyr auf Y 79 Zellen *in vivo* zu untersuchen, wurde unser neu etabliertes Xenograft-Retinoblastom-Nacktmausmodell eingesetzt. Die Mäuse wurden mit und ohne pTyr Vorbehandlung radiotherapeutisch behandelt, wobei das gleiche Bestrahlungs-Schema wie für die Bestrahlungen der Rb+/- Mäuse angewendet wurde. Der Erfolg der Radiotherapie mit und ohne pTyr-Vorbehandlung wurde untersucht.

Die Bestrahlungen haben die Y79 Krebszellen effektiv eliminiert. 80% der Mäuse, die nicht mit pTyr vorbehandelt wurden, sind über einen Zeitraum von mindestens neun Monaten Tumor-frei geblieben. pTyr hat sich allerdings als ein potenter Radioprotektor für Y79 Xenograft-Tumore erwiesen, im Gegensatz zu Y79 Zellkulturen. In allen mit pTyr behandelten Mäusen haben sich nach der Radiotherapie wieder Retinoblastome entwickelt, was den Einsatz von pTyr für die Radiotherapie des Retinoblastoms ausschließt.

pTyr könnte allerdings für den Einsatz in der Radiotherapie anderer Tumore, vor allem derer mit p53 Defekten in Frage kommen.

3. Introduction

3.1 Retinoblastoma (Rb)

3.1.1 History of Rb

It seems that retinoblastoma (Rb) is a very old problem of human beings. There are hints that the ancient Mayans already suffered from Rb. Thus in the national museum of Mexico there is a stone sculpture of a head with Rb-like symptoms such as a hanging lip and a swollen eye, which is estimated to be 4000 years of age (fig. 1 A) (Gaitan-Yanguas, 1978).

The first person to report about patients with Rb-like symptoms in Europe was Pieter Pauws (Petrus Pawius of Amsterdam) a noted anatomist and later professor at the University of Leiden in 1597 (Kivela & Polkunen, 2003). James Wardrop, a famous Scottish surgeon, described an Rb-like disease- *fungus haematodes*, as an entity in 1809 and suggested enucleation as the preferred treatment (fig. 1 B) (Albert, 1987). Numerous famous ophthalmologists like Friedrich Wilhelm Ernst Albrecht von Graefe, pathologists like Rudolf Virchow, who claimed that Rb is of glial origin and used the term *glioma of the retina*, and many others made their contributions to the understanding and treatment of Rb (Pandey, 2014).

The name *retinoblastoma* for this kind of tumour was first suggested by the American ophthalmic pathologist, Friedrich Herman Verhoeff in the 1920's, a term that was adopted by the American Ophthalmological Society in 1926 (Grossniklaus, 2014). He was also the first person to report about the first Rb patient who received radiotherapy (RT), whose eye was cured, who kept his vision and stayed tumour-free for over 50 years (Verhoeff, 1921, 1952).

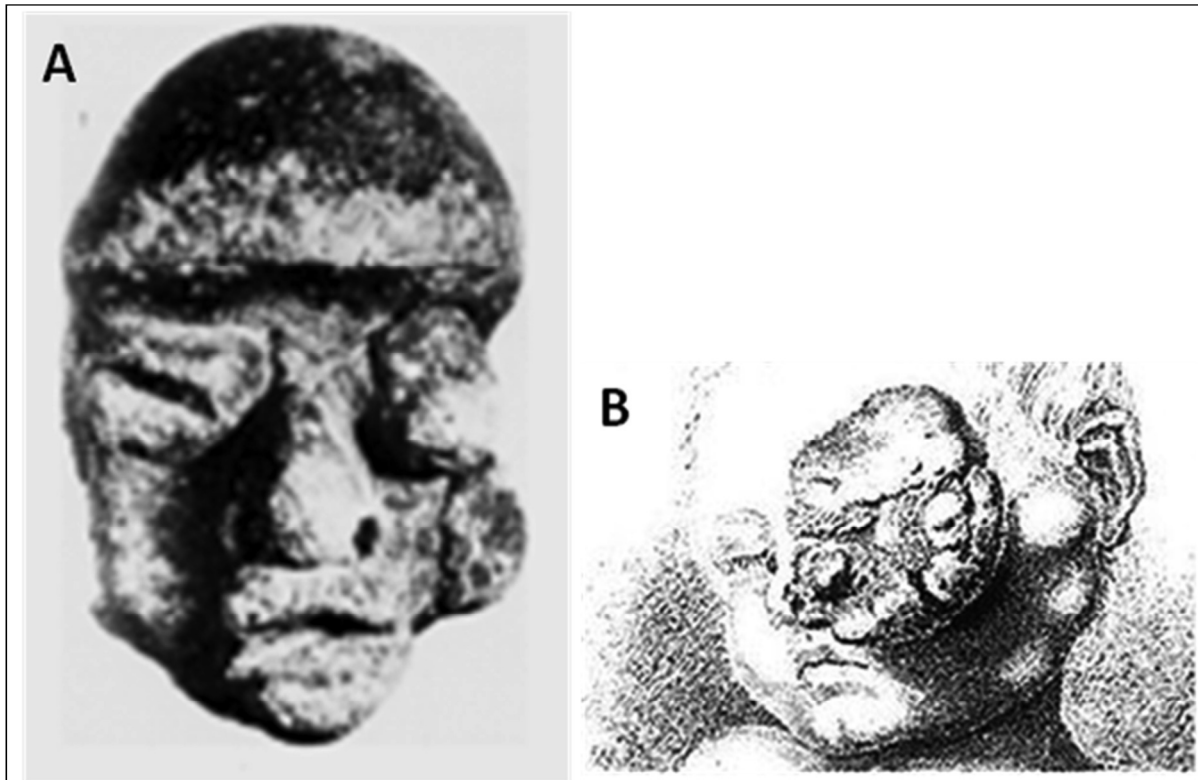


Fig. 1: **Historical representations of retinoblastoma. (A):** stone sculpture of a head with Rb-like symptoms such as a hanging lip and a swollen eye National museum of Mexico (ca. 2000 BC) **(B):** illustration from “Observations on fungus haematodes or soft cancer in several of the most important organs of the human body: containing also a comparative view of the structure of fungus haematodes and cancer: with cases and dissections” by Wardrop James (1809).

3.1.2 Aetiology and Epidemiology of Rb

A family history of Rb is a major risk factor for the development of the tumour. The genetic background for these kinds of Rb-tumours will be discussed in more detail in the Chapters 3.1.3 Biology of Rb and 3.1.4 RB1 gene.

Risk factors for the development of sporadic (without family history) Rb are poorly understood. There are hints that the exposure of the parents to pesticides (Kristensen et al., 1996), higher age of the parents (Moll et al., 1996) and *in vitro* fertilization (IVF) (Moll et al., 2003) are risk factors. Additionally, climate, race, socioeconomic development (Jemal et al., 2000), UV exposure (Hooper, 1999), and diet are discussed as risk factors (M. A. Orjuela et al., 2005). The human papilloma virus (HPV) protein E7 leads to Rbp degradation. HPV could be found in 36% of Rb tumours according to an epidemiological study with Mexican patients (Boyer et al., 1996; M. Orjuela et al., 2000), which makes a HPV infection of the mother a risk factor (Bhuvaneshwari et al., 2012) because the virus can be transferred to the child. Additionally it was shown that Rb1 expression is negatively regulated in cells containing replicating genomic RNA from hepatitis C virus, a human virus strongly

3. Introduction

associated with hepatocellular carcinoma (Munakata et al., 2005). These studies suggest intriguing possible factors that may contribute towards the incidence of retinoblastoma, but further work to better elucidate the etiology of Rb is needed.

There is no clear gender-specific difference in the incidence of Rb. Global incidence data for retinoblastoma show an approximate 50-fold variation, which is highly atypical for a paediatric tumour. According to population-based registry data of the International Agency for Research in Cancer (IARC), incidence rates are generally similar in North America, Europe, and Australia; slightly higher rates are observed in Central and South America; a wide range of rates are reported in Asia with the highest in the Chennai region in India; and generally higher rates are observed in Africa (Parkin et al., 1988).

Great efforts are being made to investigate the variations in the incidence of Rb and risk factors for the development of the disease. The study of geographic and ethnic variations, factors that may differ between populations with different incidence rates for Rb may help to recognize the risk factors for Rb and those populations with a higher risk of developing Rb. This information could be used to inform the populations about the risk and develop monitoring programs.

3.1.3 Biology of Rb

Retinoblastoma is the most common intraocular malignancy of infancy which is thought to originate from progenitor cells of the developing retina (Aerts et al., 2016; Aerts et al., 2006). A controversial discussion about the exact cell type of the origin of Rb is still going on (Ajioka et al., 2007).

The tumour can grow within the retina (endophytic), extending into the vitreous body (fig. 2 A), or beneath the retina, subretinal (exophytic), which results in a detachment of the retina lying above it (fig. 2 B). There are also combined forms as well as diffuse infiltrating forms of retinoblastoma. In addition, the tumours can occur in just one part of the eye (unifocal) or in several places at once (multifocal) (fig. 2 C) (Balmer et al., 2006).

3. Introduction

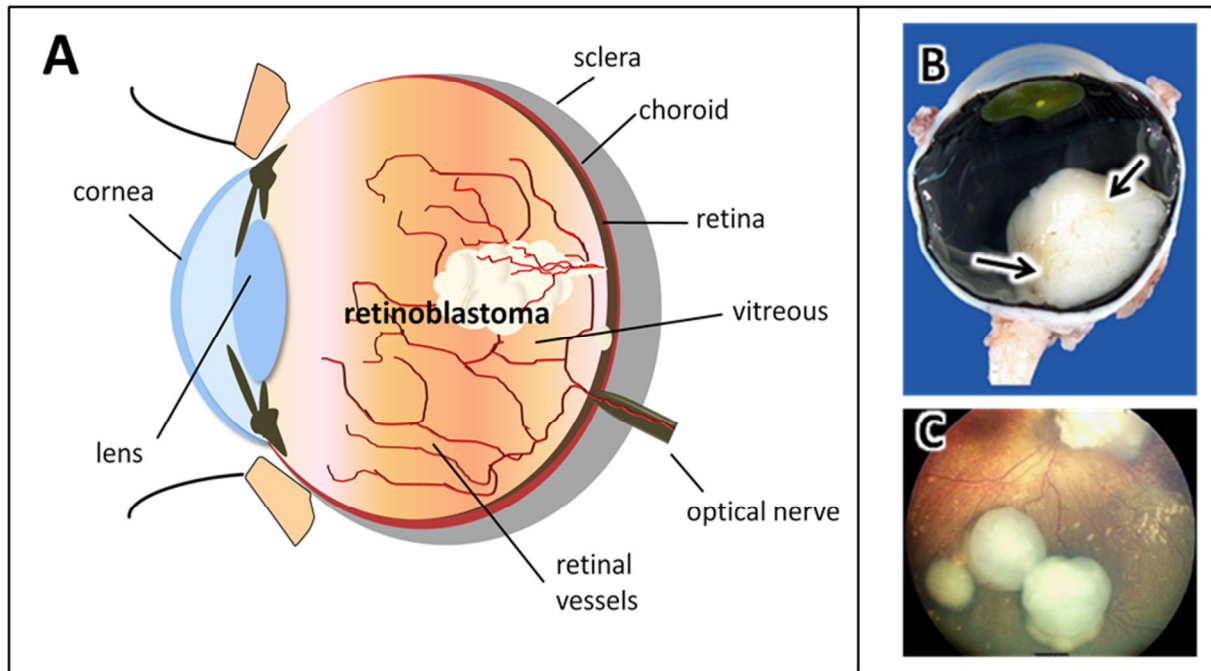


Fig. 2: Illustrations of retinoblastoma. (A): Schematic picture of a human eye with a unifocal Rb tumour with an endophytic growth pattern. The tumour arises from the retina and grows into the vitreous **(B):** Gross photograph of a human eye with a unifocal Rb with an exophytic growth pattern. The tumour arises from the retina (arrows) and grows into the subretinal space (from clinical features, diagnosis, pathology P. Chevez-Barrioz, D.S. Gombos : Rodriguez-Galindo C, Wilson MW, eds. Retinoblastoma. New York: Springer; 2010:32). **(C):** Fundoscopic image of a multifocal Rb (from Bornfeld N, Schüler A., Bölöni R, Jurklies C, Wieland R, Sauerwein W, Lohmann D. (2006) Retinoblastom. *Ophthalmologe* **103**:66)

Rb has an incidence of about 1/20000 live births. It is estimated that Rb affects 7000-8000 new patients worldwide yearly (Broaddus et al., 2009; Seregard et al., 2004). Survival rates vary dramatically worldwide. Untreated, mortality is 100%.

Rb occurs in different forms, depending on the site and direction of growth (fig. 2). Sixty percent of Rb are unilateral, afflicting one eye, with a median age at diagnosis of two years. Rb is bilateral, afflicting both eyes, in about forty percent of cases, with an earlier median age at diagnosis (one year) (Ayari-Jeridi et al., 2015). In very rare cases a trilateral Rb occurs. Here both eyes and the pineal or suprasellar region are afflicted (Antoneli et al., 2007; de Jong et al., 2014).

There is a clear link between the disease and the inactivation of a tumour suppressor gene- the Rb gene (RB1), which was first described by Knudson, who formed the so called “two-hit hypothesis”. According to this theory both alleles of the RB1 tumour suppressor gene must be inactivated to initiate Rb (Knudson, 1971) (fig. 3).

3. Introduction

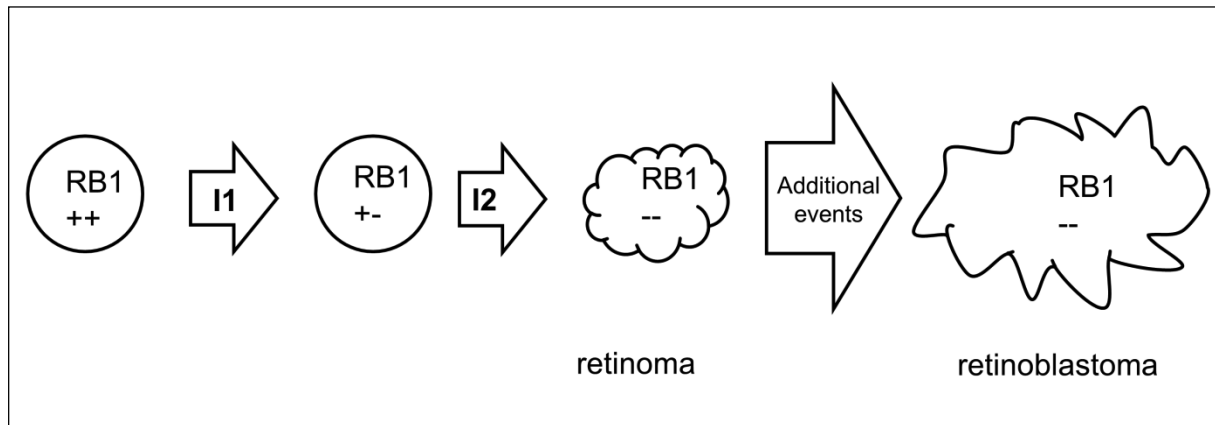


Fig. 3: “**2 hits hypothesis**”. Retinoblastoma is initiated by the inactivation of RB1. The loss of both alleles of RB1 (I1 and I2, inactivation events: mutations, chromosomal loss, methylation of the Rb1 promotor region inactivation on RNA level), are necessary, but not sufficient, for retinoblastoma development. The first inactivation (first hit) can be due to either an inherited or sporadic mutation in a certain retinal cell, the second inactivation (second hit) of the other RB1 allele in that retinal cell, which is always sporadic, predisposes the formation of the benign tumour retinoma, while a number of additional mutational events eventually lead to retinoblastoma. (illustration modified from Genetics of Retinoblastoma and Genetic Counseling H. Dimaras, B. L. Gallie In: Rodriguez-Galindo C, Wilson MW, eds. Retinoblastoma. New York: Springer; 2010:42.)

Rb occurs in two forms, hereditary (40%) and non-hereditary (60%) The hereditary disease is caused by a constitutional mutation in the RB1 gene that predisposes to Rb and other cancers later in life and is transmitted as an autosomal dominant trait with high penetrance (90%). In its non-hereditary form, Rb is initiated by two somatic mutations in the RB1 gene in retinal cells.

All bilateral and multifocal unilateral forms of Rb are hereditary and part of a genetic cancer predisposition syndrome. All children with a bilateral or familial form, and 10 to 15% of children with a unilateral form, constitutionally carry RB1 gene mutations (Ayari-Jeridi et al., 2015; Jehanne et al., 2014).

3.1.4 RB1 gene

The RB1 gene in humans is located on chromosome 13q14. It is the first described tumour suppressor gene (TSG) (Murphree & Benedict, 1984). Various mechanisms have been found which lead to a loss of function of RB1: over 1000 mutations of the Rb1 gene (Richter et al., 2003), loss at chromosome 13 (site of Rb1) (Bunin et al., 1989), silencing by hypermethylation of the promotor of RB1 (Richter et al., 2003) and viral infections (M. Orjuela et al., 2000). These can initiate Rb formation.

3. Introduction

However, the initiation of some very rare forms (3-7%) of Rb without mutations in the RB1 gene is associated with amplifications of the MycN gene (Rushlow et al., 2013).

3.1.5 Rbp interactions and its role in cancer

The product of the RB1 gene, the retinoblastoma protein (Rbp), belongs to the group of the so called “pocket proteins”: This family includes three members, Rbp1/p105, p107 and Rbp2/p130, all of them are involved in cell cycle regulation. (Giacinti & Giordano, 2006).

The Rbp has various functions (fig. 4), it represses gene transcription by directly binding to the transactivation domain of E2F (E transcription factor) and by binding to the promoter of these genes as a complex with E2F. Rbp represses transcription also by remodeling chromatin structure through interaction with proteins such as hBRM ((Brahma homologue) also known as SMARCA2 - SWI/SNF related, matrix associated, actin dependent regulator of chromatin, subfamily a, member 4), BRG1 ((Brahma-related gene 1) also known as SMARCA4), HDAC1 (Histone deacetylase 1) (Luo et al., 1998) and SUV39H1 (Suppressor of variegation 3-9 homolog), which are involved in chromatin remodelling, histone acetylation/deacetylation and methylation respectively, and interacts with different other non-chromatin remodeling proteins like APC/C (anaphase promoting complex/cyclosome), SKP2 (S-phase kinase-associated protein 2) and MDM2 (Mouse double minute 2). Loss of Rbp functions may lead to cell cycle deregulation and tumourigenesis (Burkhart & Sage, 2008).

3. Introduction

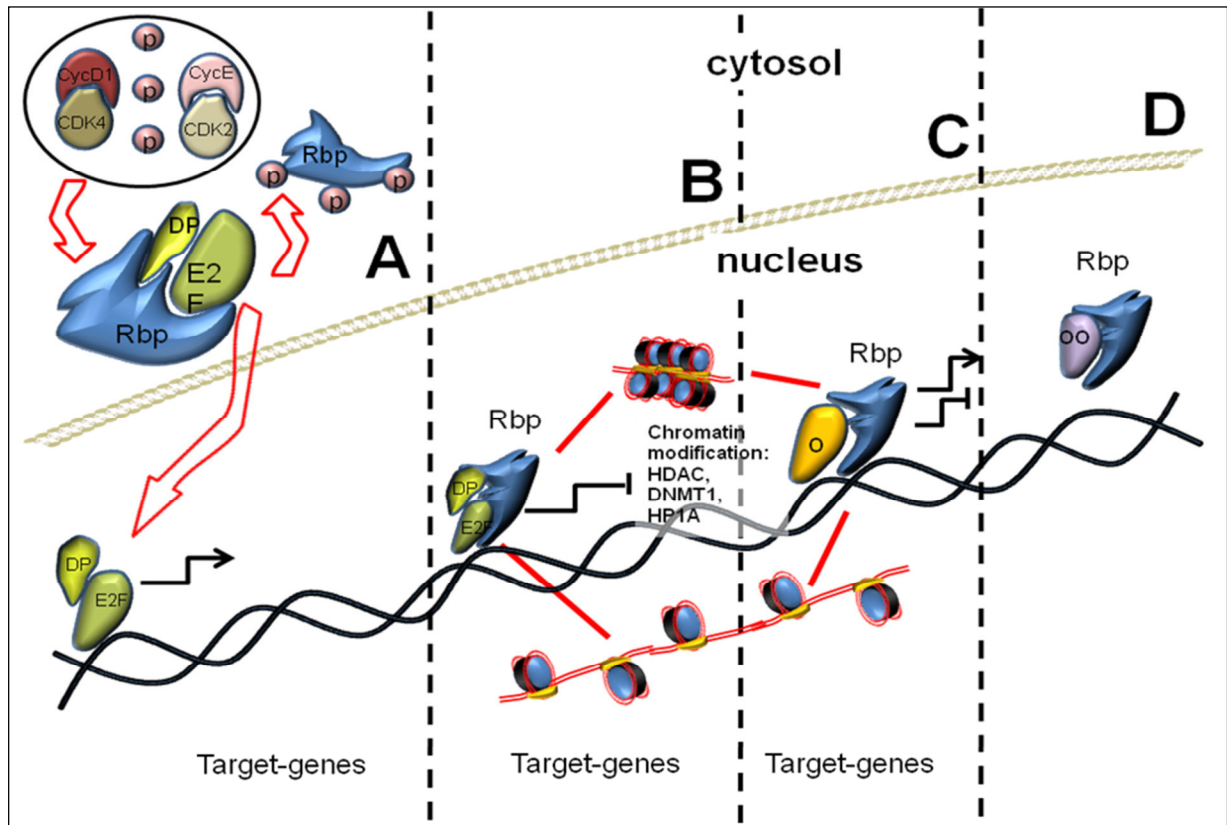


Fig. 4: Interactions of Rbp. **(A):** In the cytosol, Rbp binds to E2F/DP and prevents them from entering the nucleus and activating their target genes, this activity is controlled by the CycD1/CDK4 and CycE/CDK2 complexes, which phosphorylate Rbp, leading to the release of E2F/DP **(B)** Rbp/E2F is recruited to the promoter region of target genes and inhibits their transactivation, additionally this complex interacts with chromatin remodeling complexes (including HDAC (histone deacetylase), DNMT1 (DNA methyltransferase 1), HP1A (heterochromatin protein 1A) and SUV39H1) to repress transcription of target genes. **(C)** Rbp interacting with the chromatin remodelling machinery acts as a transcriptional co-factor for non-E2F transcription factors or other co-factors (o), such as the HIF1 α (hypoxia-induced factor 1 α), MYOD (myogenic factor D) and SP1 (specificity protein 1) transcription factors. **(D)** Rbp serves as a non-chromatin-associated co-factor with other proteins (oo), e.g. Rbp forms a complex with APC/C (anaphase promoting complex/cyclosome) and SKP2 (S-phase kinase-associated protein 2) promoting SKP2 degradation. Rbp binds and inactivates MDM2, an inactivator of p53 (illustration modified from (Burkhart & Sage, 2008))

Additionally, Rbp is involved in various mechanisms of tumour suppression (fig. 5). Rbp can suppress cancer development through its interactions with more than 100 different partners, including lineage-specific transcription factors, DNA-modifying enzymes and members of chromatin remodelling complexes (Chinnam & Goodrich, 2011; Viatour et al., 2003), by inducing differentiation, controlling cell-cycle arrest, maintaining genomic stability and inducing senescence (Takahashi et al., 2007) in response to oncogenic stresses. Furthermore, the absence of Rbp has been associated with increased tumour angiogenesis and metastasis (Gabellini et al., 2006), although the mediators of these functions are less well understood.

3. Introduction

Surprisingly, the presence of Rbp has a partly pro-survival function because of its inhibition of cell death through apoptosis and, potentially, autophagy by interacting with APAF1 (apoptotic peptidase activating factor 1); BNIP3 (BCL2-interacting protein 3); CDH1 (cadherin 1); DNMT1 (DNA methyltransferase 1); HIF1 α , (hypoxia-induced factor 1 α); PCNA (proliferating cell nuclear antigen); VEGF (vascular endothelial growth factor) to mention a few, an overview is presented in (fig. 4). Of particular interest for this thesis was the Rbp/MDM2 (fig. 5, red circled) interaction which is involved in the p53 pathway, which will be discussed further (Burkhart & Sage, 2008).

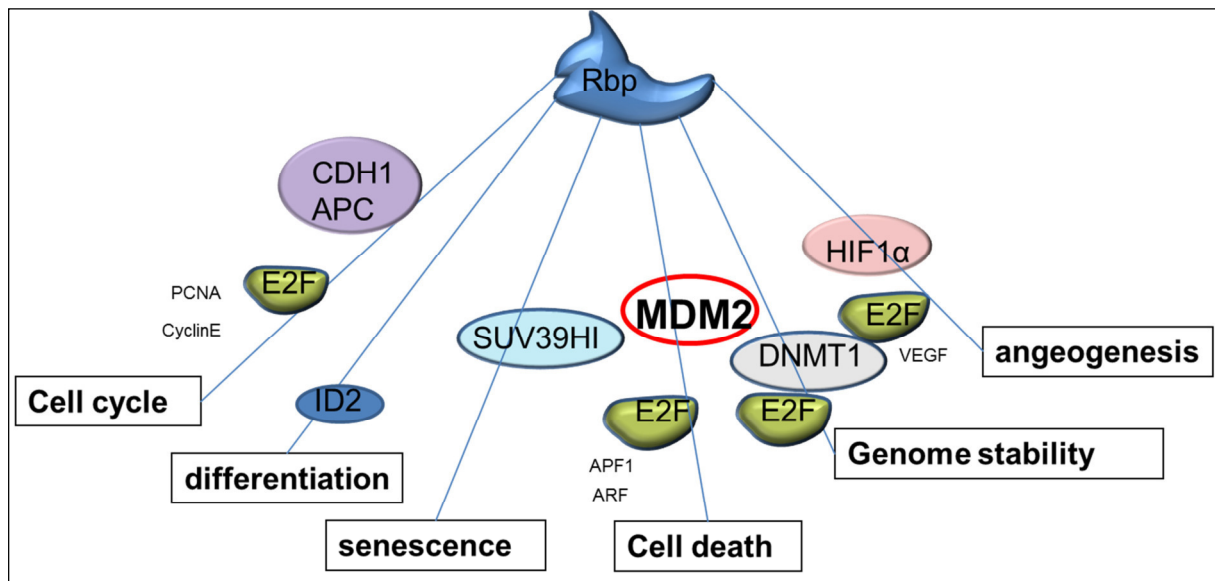


Fig. 5: Overview of the numerous Rbp binding partners and transcriptional targets that might mediate its tumour suppressor ability. Presence of Rbp might prevent tumour formation by inducing differentiation, controlling cell-cycle arrest, maintaining genomic stability and inducing senescence in response to oncogenic stresses. The absence of Rbp has been associated with increased angiogenesis and metastasis. This figure depicts a simplified representation of the potential role of Rbp in tumour suppression. Each function is illustrated with some of the key protein binding partners and transcriptional targets associated with that function, but they are not meant to be comprehensive. APAF1, apoptotic peptidase activating factor 1; BNIP3, BCL2-interacting protein 3; CDH1, cadherin 1; DNMT1, DNA methyltransferase 1; HIF1 α , hypoxia-induced factor 1 α ; PCNA, proliferating cell nuclear antigen; VEGF, vascular endothelial growth factor, MDM2 (red circled) (illustration modified from (Burkhart & Sage, 2008))

3.1.6 Rb research

As confirmed by numerous historical references, Rb was always an object of scientific interest. Innovative surgical, radiotherapy (RT), chemotherapy (ChT) and other therapeutical methods were developed for the treatment of Rb. The biological, genetic and aetiological studies of Rb have widened and deepened our understanding of this tumour and tumours in general. This was the first tumour where a heredity predisposition for a cancer disease due to a genetic alteration was shown (Knudson, 1971).

Knowledge on the tumourigenesis and development of Rb has made a huge step forward with the development of suitable mouse models (Dyer et al., 2005; Macpherson, 2008; Villegas et al., 2013).

For example, using the transgenic LHBETATAG mouse with hereditary Rb, 26% of advanced Rb tumours have been shown to have hypoxic regions (Boutrid et al., 2008). As a result, hypoxic cells may serve as important targets for adjuvant therapies. Treatment with glycolytic inhibitors which decrease hypoxia as an adjuvant to chemotherapy has the potential to increase the efficacy of chemotherapy in advanced Rb (Boutrid et al., 2008). Recently, the chemotherapeutic effect of focal melphalan, a highly potent drug for Rb treatment (Muen et al., 2012; Schaiquevich et al., 2012) was investigated in the LHBETATAG murine model and it has shown a significant effect on reducing tumour burden, hypoxia and vasculature (Shah et al., 2014). The genetic background of the Rb incidence differs in mouse and human. So for the development of a Rb-tumour in a mouse, not only the RB1 gene has to be inactivated, but also another member of the Rb gene group (p107, p130) and/or the tumour suppressor gene p53 (Zhang et al., 2004). The advantage of xenograft models is the usage of human cells (Pacal & Bremner, 2006). These models are especially suitable for studying novel therapeutic approaches.

3.1.7 Diagnosis of Rb

Diagnosis of a retinoblastoma should be made as early as possible. Therefore, if either parent suffered from retinoblastoma, the first examination of the new-born child should already be performed at the age of two weeks.

The first and often decisive leading symptom when diagnosing this condition is leucocoria, a white reflection in the pupil, if this is detected, then the cause should be identified as soon as possible. In addition, if strabismus is present, the child should be examined for Rb.

3. Introduction

The first measure to be taken in the diagnosis of retinoblastoma is inspection of the fundus. However, for a more detailed clarification of the exact shape, size and possible space occupied by the retinoblastoma, additional examinations with (high-resolution) ultrasound and magnet resonance imaging are often used.

Beyond this, well-established techniques like Fundoscopy, Wide-field Photography, Computer Tomography, Magnetic Resonance Imaging, Ultra Sound-based techniques (de Graaf et al., 2012), Scanning Laser Ophthalmoscopy (SLO) and Fluorescein Angiography (FA) were shown to be useful for the study of the tumour's vessel system and its changes after treatment (Bianciotto et al., 2012; Wetzig, 1966): Using Auto-Fluorescence Fundoscopy, clinical features of Rb, especially calcifications, could be effectively analysed (Ramasubramanian et al., 2011).

Recently optical coherence tomography (OCT) is being used for the diagnosis and characterisation of ocular tumours, it is more precise with regard to surface changes to the macula, macular oedema and subfoveal fluid compared to a simple clinical examination or ultrasonography. Within a very short space of time, it has become highly regarded in clinical retinal diagnostics (Shields et al., 2004).

The introduction of OCT in diagnosis and monitoring of Rb patients allows visualization of foveal anatomy and microstructure. This allows a correct assessment and facilitates planning for visual rehabilitation (Rootman et al., 2013). *In vivo* methods like SLO/OCT have also been successfully used for detection and characterisation of tumours in mouse models by our group (Tschulakow et al., 2016) and Wenzel et al. (Wenzel et al., 2015).

For the successful treatment of patients with Rb, an early diagnosis is essential. The various aspects of the disease like grading, size, localisation etc. must be taken into account. The aim is to save the patient's life and to cause as little damage as possible. In cases where the tumour has grown too big and the likelihood of restoring vision is low or there is a danger of metastasising, enucleation is still the only treatment option (Jehanne et al., 2014).

3.1.8 Radiotherapy and other treatment options for Rb treatment

Rb responds very well to radiotherapy (RT) and external beam radiotherapy was the first globe and vision saving therapy for Rb (Albert, 1987). However, in addition to the unavoidable risk of the RT, the genotype of the hereditary Rb patients predisposes the appearance of secondary malignancies. The RT further enhances the risk of RT-induced tumours occurring in the irradiated area (Mayorga et al., 2014). In these patients secondary tumours can already be triggered by exposure to natural

3. Introduction

radioactivity, X-rays or the cosmic radiation on high mountains or on board airplanes or during X-ray exposure for diagnostic purposes. Of course this means a reduction in the quality of life for these patients. The incidence of secondary tumours 50 years after diagnosis due to radiotherapy of retinoblastoma is 38% (Kleinerman et al., 2005). This explains why the trend has been to move away from radiotherapy (Abramson & Frank, 1998; Dommering et al., 2012; Rodjan et al., 2013; Vasudevan et al., 2010). This has favoured the use of other therapeutical approaches like cryo-, thermotherapy as well as systemic, periocular, intra-arterial or intravitreal chemotherapy and combined therapies such as chemosurgery (Ghassemi & Shields, 2012; Schueler et al., 2006; Temming et al., 2012; Yamane et al., 2004).

Although radiotherapy for the treatment of Rb is nowadays avoided as much as possible and is considered only as the last treatment option prior to enucleation, it is still considered necessary for patients with large tumours who are not candidates for chemosurgery, but who have visual potential. Approximately 80% of the Rb patients are still diagnosed at a locally advanced stage, and only 20-25% at an early stage. Additionally chemotherapy fails in more than two-thirds of eyes with advanced stages of Rb, requiring RT or enucleation (Kim & Park, 2015).

Strategies which could reduce the described side effects of RT and make RT safer are currently in the focus of extensive scientific investigations. High-tech RT like proton beam RT (Krengli et al., 2005; Mouw et al., 2014), intensity-modulated and fractionated stereotaxic RT (Combs et al., 2007) enables precise radiation delivery to the tumour while sparing the healthy tissues, improving the efficacy/toxicity ratio. Additionally, the side effects of the RT can be reduced by the usage of radioprotectors before and mitigators after RT (Bourgier et al., 2012). For these pharmacological agents, it is important to be active only in normal tissues and not to interfere with the RT.

3.2 Radioprotectors

There is an intensive search for radioprotectors which can protect the normal tissues from damage of the RT and prevent side effects like induced tumours, but do not interfere with the radiotherapy. Different radioprotective substances are in the focus of scientific interest like natural compounds (Kuntic et al., 2013), ethanol, trimethylglycine, beer (Rodriguez et al., 2013) and DMSO (Ashwood-Smith, 1967) to name but a few. A group of special interest are aminothiols, an important representative of this group is amifostine (WR-2721), which until now is the only radioprotector used for therapy in humans (Yugas, 1970). Most of these substances

3. Introduction

have a radical oxygen species (ROS) scavenging mode of action reducing the cellular damage caused by IR.

Another strategy is the activation of cellular radio resistance mechanisms like DNA repair and - protection (Chang et al., 2014; Sun et al., 2011), changes in the energy supply, downregulation of cellular breathing (Kam & Banati, 2013) or the induction of autophagy (Chaachouay et al., 2011; Y. S. Chen et al., 2011).

Activation of the ATM/ATR-pathway by radiation leads to cell cycle arrest, DNA-PK signalling and enhanced DNA repair. Activation of HER (human epidermal growth factor receptor) by radiation, leads to ERK1/2 and AKT signalling which suppresses apoptosis induction. Additionally, this signalling positively regulates cell cycle checkpoint response and DNA repair (Hein et al., 2014) (fig. 6). Of particular interest for the enhancement of cellular radio resistance is the EGFR (epidermal growth factor receptor) pathway.

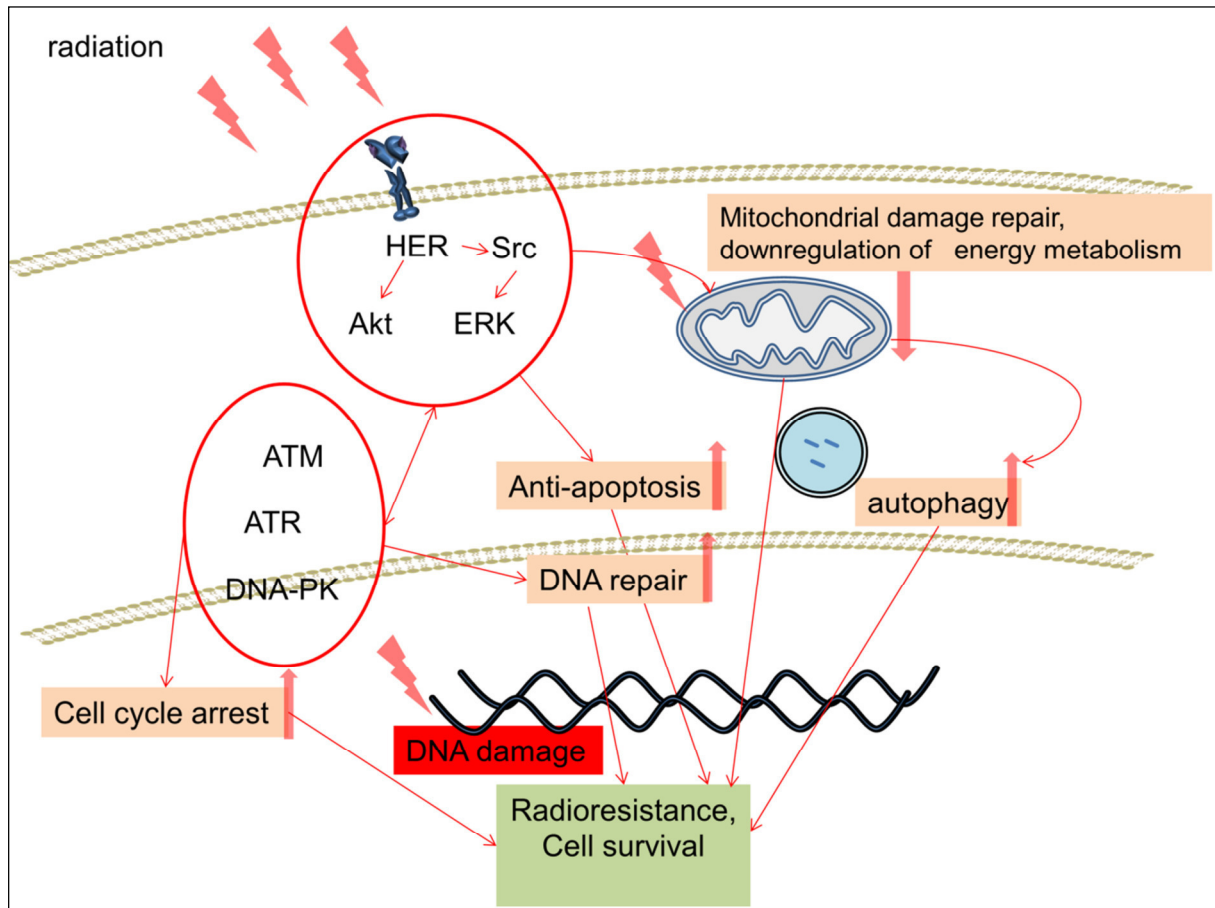


Fig. 6: **Overview of radiation-induced signaling pathways that promote cell survival.** Activation of ATM, ATR and DNA-PK signalling by DNA breaks leads to cell cycle arrest and DNA repair. Activation of HER, ERK1/2 and AKT signalling pathways by radiation suppresses apoptosis induction. HER, ERK1/2 and AKT signalling activation following radiation positively regulate cell cycle checkpoint response and DNA repair. Additionally, the Akt and Src signalling activates the mitochondrial damage repair, suppresses mitochondrial metabolism and enhances autophagy (modified from (Hein et al., 2014)).

3.2.1 Epidermal growth factor receptor (EGFR)

EGFR or human epidermal growth factor receptor 1 (HER1) or erythroblastosis oncogene B (ErbB-1) is a member of the HER family. EGFR is often overexpressed in many human tumours, which leads to their enhanced proliferation aggressiveness and resistance to ChT (chemotherapy) and RT (radiotherapy) (Brand et al., 2011; D. J. Chen & Nirodi, 2007).

The receptor can be phosphorylated after binding of ligands like EGF (epidermal growth factor), TGF α (tumour growth factor alpha), Amphiregulin, Betacellulin, HB-EGF (heparin binding EGF), Epiregulin (Rowinsky, 2004), after transactivation by G-protein coupled receptors (Bhola & Grandis, 2008) and after exposure to oxidative, hyperthermic, hypoxic stresses, UV-radiation and ionizing radiation (K. Dittmann et al., 2008). After phosphorylation, the receptor is internalized and starts the EGFR

3. Introduction

signalling (Rodemann et al., 2007). However, phosphorylated EGFR after having bound to growth factors, dimerizes and is then internalized into coated pits (fig. 7) initiates signalling via the phosphoinositol 3-kinase (PI3K) pathway, the signal transducer and activator of transcription (STAT-1, STAT-3, STAT-5) pathway, the Ras/MAPK (mitogen-activated protein kinase) pathway and activates specific enzymes, such as the phospholipase C-gamma and is then degraded in lysosomes (Alwan et al., 2003). Partly EGFR after EGF stimulation and Src, an activated downstream product of the EGFR pathway, are translocated into mitochondria. There they interfere with the cytochrome c oxidase subunit II (CoxII, MTCO2) which leads to a down-regulation of mitochondrial function. EGFR stabilizes COXII by binding it and prevents the activation of apoptosis (Demory et al., 2009) (fig.7).

Radiation-induced EGFR internalization is realized by caveolae formation and is associated with nuclear translocation (K. Dittmann, Mayer, et al., 2005; K. Dittmann et al., 2008). In the nucleus EGFR activates various mechanisms like DNA-PK driven DNA repair and chromatin relaxation via enhancement of acetylase TIP60 activity and building complexes with Ataxia telangiectasia mutated (ATM), promyelocytic leukemia protein (PML), histone H3 and hetero-chromatin binding protein (HP1) (K. Dittmann et al., 2011) (fig.7).

Partly phosphorylated EGFR after irradiation (IR) is translocated into mitochondria, where the receptor binds COXII and acts in a similar way to EGF stimulated EGFR (Nyati et al., 2006). EGFR and the sodium-dependent glucose transporter, SGLT1, were found in complex after radiation treatment, which was shown to increase the glucose uptake (K. Dittmann et al., 2013) and trigger a metabolic switch to increase lactate production (K. Dittmann et al., 2015) (fig. 7).

3. Introduction

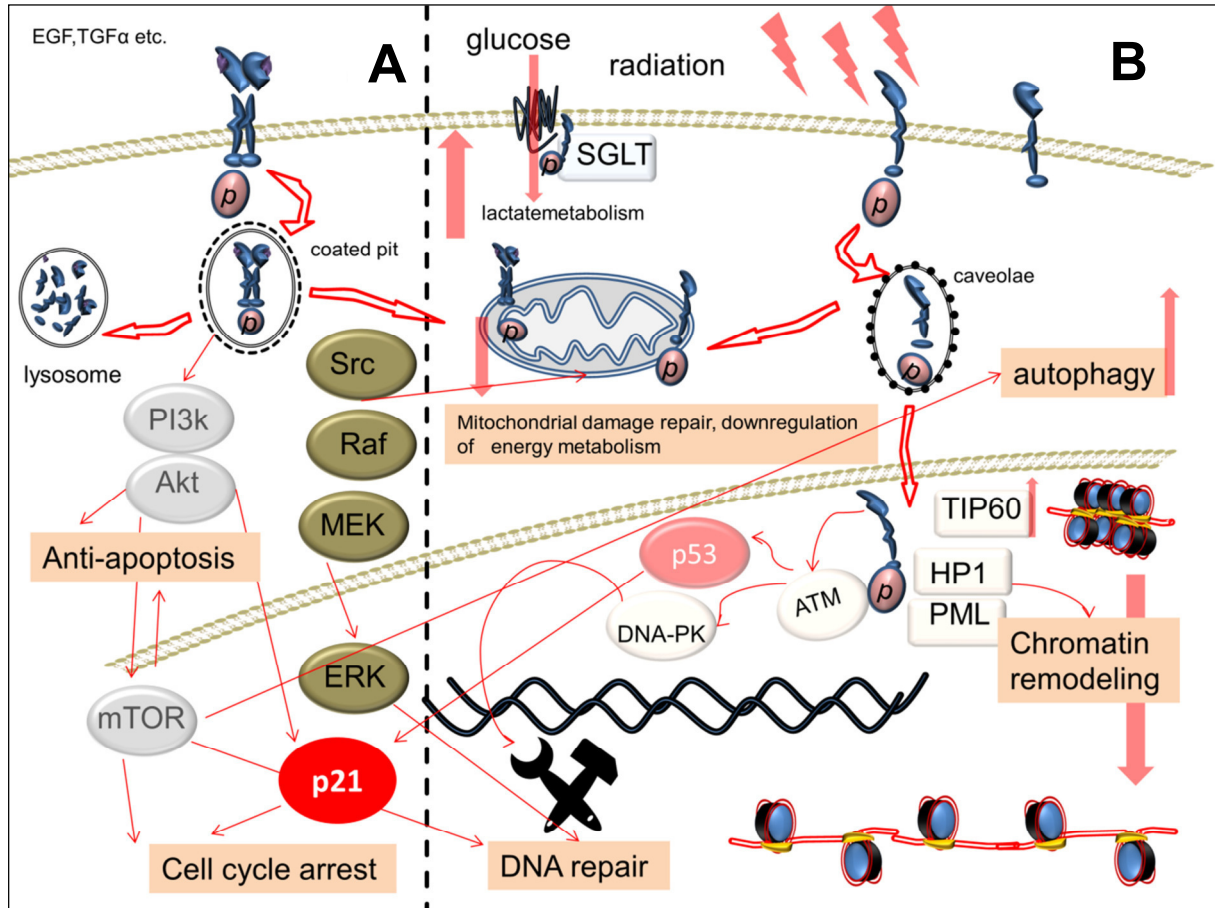


Fig. 7: EGFR signalling. (A): After binding of growth factors like EGF, TGF α etc., the receptor can be phosphorylated and initialized in coated pits and starts signalling via Akt and ERK pathways which leads to the activation of radio resistance by activating anti-apoptotic and DNA-repair mechanisms, activating cell cycle arrest and autophagy. EGFR and Src also have a mitochondria regulating function: binding of COXII leads to the downregulation of the mitochondrial metabolism. After initialization, EGFR is degraded in lysosomes. **(B):** After irradiation, EGFR can be phosphorylated and is then initialized in caveolae which leads to an intranuclear transport. In the nucleus EGFR enhances chromatin remodelling, DNA-repair and autophagy, which leads to radio resistance. EGFR after IR is partly translocated to the mitochondria, where it acts as after stimulation with growth factors. EGFR also binds the SGLT glucose transporter increasing the glucose uptake. (For the illustration numerous sources were used, please refer to Chapter 3.2.1 for reference).

3.2.2 Ortho-phospho-L-tyrosine (pTyr)

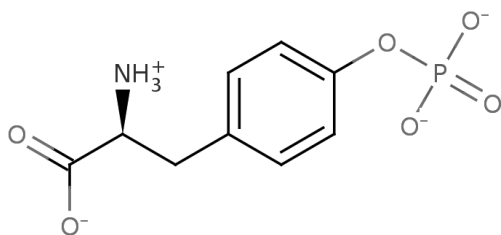


Fig. 8: **Formula: ortho-phospho-L-tyrosine (pTyr)**

The application of the radio protector pTyr results in a multimodal mode of action. pTyr mediates activation of phosphokinase C epsilon (PKC ϵ), which phosphorylates EGFR at the residue No. T654 and triggers nuclear EGFR accumulation (Wanner et al., 2008), which leads to enhanced DNA repair mechanisms (K. Dittmann et al., 2007), chromatin remodelling (K. Dittmann et al., 2013), a higher glucose uptake (K. Dittmann et al., 2013) and a shift from oxidative metabolism to lactate metabolism (K. Dittmann et al., 2015) in normal cells after treatment with radiation (fig. 8 B). Moreover, pTyr was shown to be predominantly radioprotective in cells with a WT (wild type) p53 phenotype (K. H. Dittmann et al., 2001) which indicates p53 stabilisation by pTyr (fig. 9). The p53 gene is a very important tumour suppressor gene, also known by its bynames "the guardian of the genome", "gatekeeper-gene" or "caretaker-gene". It was found to be mutated in about half of all human cancers (Vogelstein et al., 2000). P53 has various tumour suppression functions like cycle arrest and apoptosis, genomic stability, and inhibition of angiogenesis (Harris & Levine, 2005). It is also involved in the internalization of EGFR in coated pits (Endo et al., 2008) and the downregulation of the oxidative phosphorylation, glycolysis and glucose intake by interfering with mitochondrial and glycolysis enzymes and glucose transporters, respectively (Puzio-Kuter, 2011). It can be activated by diverse mediators like ATM, ATR, JNK, p38 after various stimuli like irradiation, DNA damage, viral infections, hypoxia etc. (Harris & Levine, 2005; Sato & Tsurumi, 2013). A greatly simplified schema of EGFR-pTyr-p53 interactions and p53 functions is shown in (fig.9).

3. Introduction

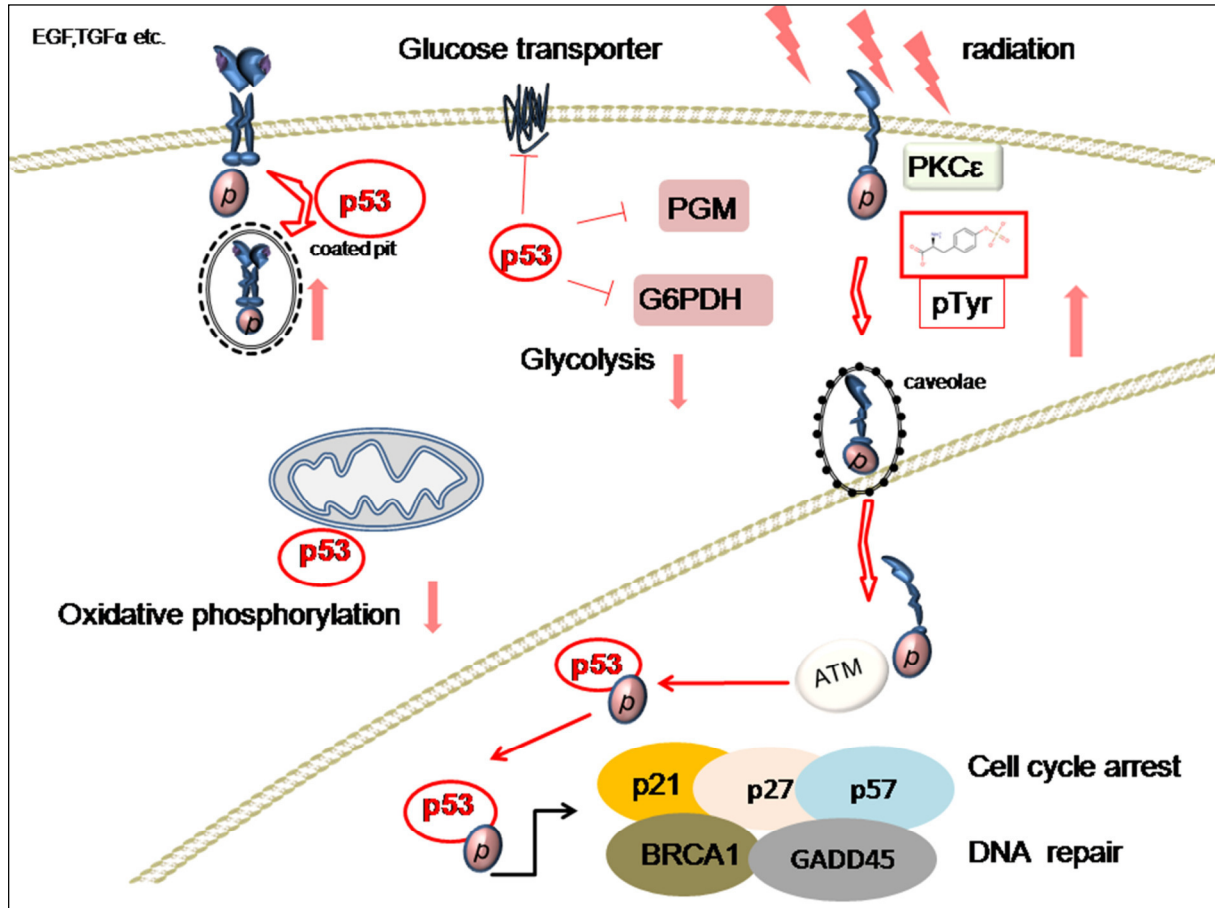


Fig. 9: **pTyr driven activation of p53 and some of its tumour suppressor functions.** pTyr (red framed) leads via PKCε to an enhanced EGFR phosphorylation and its intranuclear transport, where it activates ATM which activates p53, which enhances the transcription of several activators of anti-cancer mechanisms like cell cycle arrest via p21, p27, p57, DNA repair via BRCA1, GADD45 activation and others. p53 suppresses the glucose intake, the glycolysis and oxidative phosphorylation and is involved in the EGFR intake and transport in coated pits. (For the illustration numerous sources were used, please refer to Chapter 3.2.2 for reference).

Although a direct mutation of p53 is not frequent in Rb, the p53 signalling is found to be inactivated in Rb-cells. The Rbp and p53 pathways are directly coupled, Rbp binds to MDM2 an inactivator of p53, which rescues the apoptotic activity of p53 (Hsieh et al., 1999) additionally the MDMX protein, which is another p53 inactivator, is found to be overexpressed in Rb-/- cells (Laurie et al., 2006; Sherr & McCormick, 2002). p53 signalling was also found to be inactivated by hypermethylation of its promoter region in Rb (Livide et al., 2012) (fig.10).

This various inactivation mechanisms of the p53 pathway led to the hypothesis that pTyr, which was shown to be predominantly radioprotective in cells with active p53, is potentially not radio protective in Rb and is therefore usable for radiotherapy of retinoblastoma.

3. Introduction

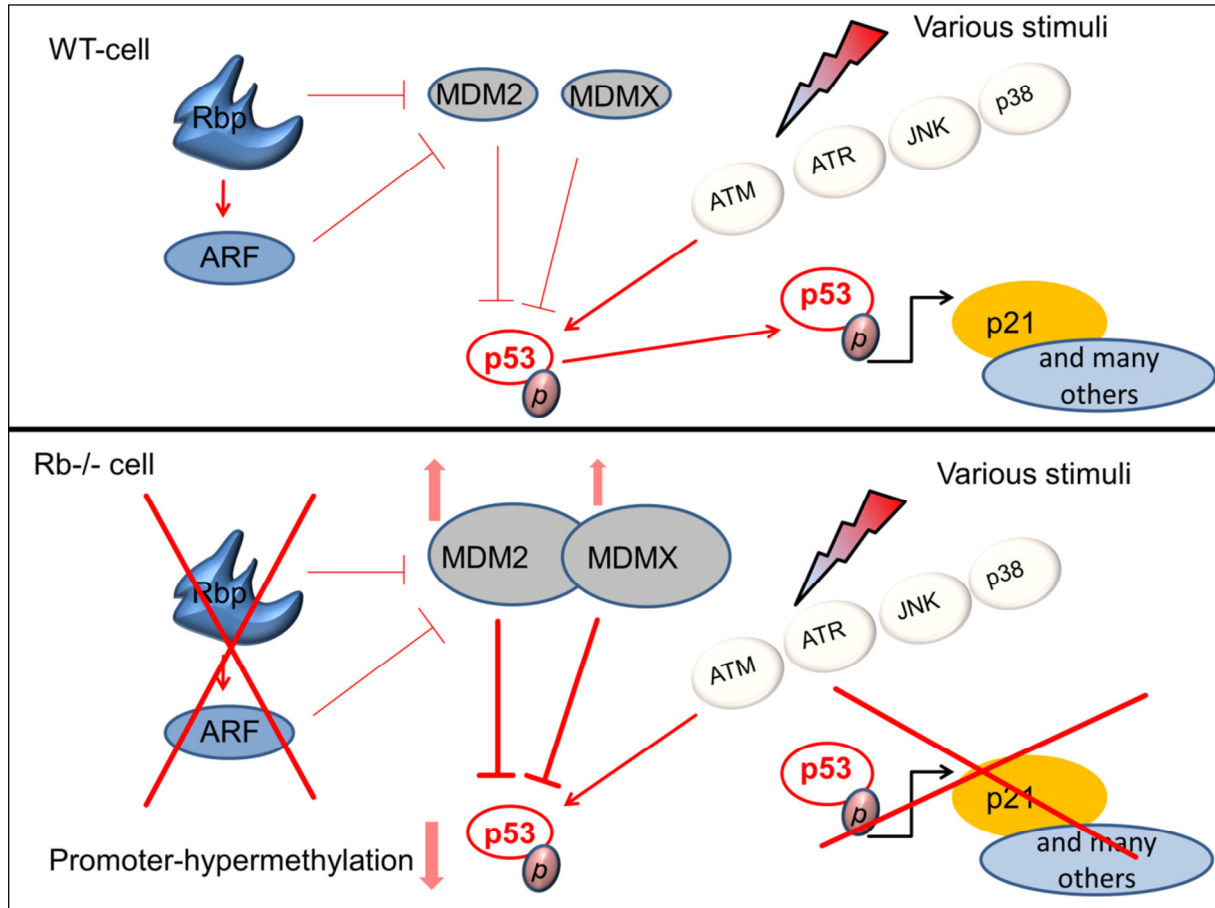


Fig. 10: **p53 inactivation in Rb-/- cells.** (**Upper panel**) In WT cells, the retinoblastoma protein (Rbp) inactivates the inactivator of p53 MDM2 by direct binding and MDM2/MDMX via ARF activation, p53 can be activated by diverse mediators like ATM, ATR, JNK, p38 after various stimuli like irradiation, DNA damage, viral infections, hypoxia etc., which leads to p53 mediated anti-tumour reactions (like cell cycle arrest via p21 activation, metabolic shutdown etc., see fig 9 for reference) (**Lower panel**) In Rb-/- cells, Rbp cannot suppress the p53-inactivators MDM2 and MDMX, additionally p53 expression and functioning is suppressed by other mechanisms like hypermethylation of the p53 promoter-region.

(For the illustration numerous sources were used, please refer to Chapter 3.2.2 for reference).

4. Objectives

The aim of this study was to find a way to increase the effectivity and safety of the radiotherapy of retinoblastoma. In order to develop a strategy to avoid side effects and secondary tumour induction, the radioprotector pTyr was investigated for a possible application before the radiotherapy of retinoblastoma.

Three main questions had to be answered:

1. Is there a relevant mouse model, which can be used for radiotherapeutic approaches?
2. Can the application of pTyr protect tissues that are affected by irradiation during radiotherapy and prevent the induction of secondary tumours?
3. Does the application of pTyr interfere with the radiotherapy?

5. Results

The results of this project are published in the form of two peer-reviewed articles which are presented in this chapter. Furthermore, unpublished additional material and short summaries of the experiments are presented.

5.1 Is there a relevant mouse model, which can be used for radiotherapeutic approaches?

Currently there are two types of retinoblastoma animal models: transgenic- and xenograft models. The advantage of xenograft models is the usage of human cells (Pacal & Bremner, 2006).

The injection of the cells can be performed in various compartments of the eye, in former times the anterior chamber was often preferred because it is more easily accessible for both the implantation and observation (Gallie et al., 1977; Totsuka et al., 1982), (Benedict et al., 1980). However, in patients the tumour starts its growth in the retina and penetrates relatively late into the anterior chamber which is physiologically different to the vitreous body. Thus, a sub-retinal injection of the retinoblastoma cells is a better reflection of the situation in humans (del Cerro et al., 1993; Rowe et al., 1992). Unfortunately, this kind of injection can cause damage to the choroid and retina, which can result in an unnatural spread of the tumour. Another possibility is the intravitreal injection of tumour cells as described by (Chevez-Barrios et al., 2000). After intravitreal injection of Y79 cells in Rag2 KO mice, tumours formed in the eye and gradually spread showing a growth comparable to that in Rb patients. Thus we decided to use the intravitreal route of administration as well. Unfortunately the Rag2 KO model developed by Chevez-Barrioz et al. was never used for radiotherapeutic experiments, but the nude mouse model used by Totsuka (Totsuka et al., 1982) was, therefore we decided to combine the advantages of both models to develop our own model. We established an orthotopic xenograft mouse model by intravitreal injection of human Y79-Rb cells which closely resembles human retinoblastoma tumours and can be used for RT approaches of retinoblastoma treatment (Tschulakow et al., 2016). To see the detailed version, please refer to Chapter 5.1.1.

Briefly: 2×10^4 human retinoblastoma Y79 cells were intravitreally injected in both eyes of immune-deficient nude mice and the growing tumours were analysed *in vivo* using scanning laser ophthalmoscopy (SLO) and optical coherence ophthalmoscopy (OCT), as well as histologically and using electron microscopy (EM).

5. Results

Five weeks after the injection, the eyes began to swell in individual animals. This swelling and tumour-growth was similar to that of tumours in untreated human Rb patients.

Xenograft-tumours grew in 29 of 42 investigated eyes. The *in vivo* as well as the histological and EM analysis showed that the xenograft tumours have similar growth-, cellular- and ultrastructural characteristics to human Rb-tumours (Tschulakow et al., 2016). To see the detailed version, please refer to Chapter 5.1.1.

5.1.1 Establishment of a novel retinoblastoma (Rb) nude mouse model by intravitreal injection of human Rb Y79 cells – Comparison of *in vivo* analysis versus histological follow up

RESEARCH ARTICLE

Establishment of a novel retinoblastoma (Rb) nude mouse model by intravitreal injection of human Rb Y79 cells – comparison of *in vivo* analysis versus histological follow up

Alexander V. Tschulakow¹, Ulrich Schraermeyer¹, H. Peter Rodemann² and Sylvie Julien-Schraermeyer^{1,*}

ABSTRACT

Retinoblastoma (Rb) is the most frequent primary intraocular tumour in children and, if left untreated, can cause death. Preclinical animal models that mimic molecular, genetic, and cellular features of cancers are essential for studying cancer and searching for promising diagnosis and treatment modalities. There are several models described for Rb, but none of them fully meet our requirements. The aim of this study was to create a novel xenograft-nude mouse-model with broad application possibilities, which closely resembles the clinical observations of Rb patients and which could be used to investigate the development and spread of the tumour by using scanning laser ophthalmoscopy/optical coherence tomography (SLO/OCT) as well as histology methods. We injected human retinoblastoma Y79 cells intravitreally in both eyes of immune-deficient nude mice. The incidences of retinoblastoma as well as growth velocity were analysed 3, 6, 9 and 12 weeks after cell injection *in vivo* by SLO/OCT as well as *ex vivo* by electron microscopy (EM) and hematoxylin/eosin (HE) staining. Moreover, internal organs were histologically screened for potentially occurring metastases. Three weeks post-injection, animals developed a retinoblastoma, and after five weeks tumour growth resulted in swelling of the eyes in individual animals, showing a similar phenotype to that of untreated Rb patients at advanced stages of tumour-development. After 12 weeks, 67.5% of all analysed eyes (29 of 42) contained a retinoblastoma. At early stages of Rb development, the SLO/OCT analysis correlated with the histology results. If the tumours were too large, only histological investigations were feasible. The ultrastructural characteristics of the xenograft-tumours were very similar to those described for patient's tumours. In one mouse, brain metastases were observed. Our retinoblastoma mouse model closely resembles the human disease. SLO/OCT can be used for the detection of Rb at early stages of development and could be used for monitoring the success of future therapies.

KEY WORDS: Retinoblastoma, Xenograft, Mouse model, SLO, OCT, Histology

¹Division of Experimental Vitreoretinal Surgery, Center for Ophthalmology, Eberhard Karls University Tuebingen, Tuebingen 72076, Germany. ²Division of Radiobiology & Molecular Environmental Research, Department of Radiation Oncology, Eberhard Karls University Tuebingen Tuebingen 72076, Germany.

*Author for correspondence (sylvie.julien@med.uni-tuebingen.de)

© S.J.-S., 0000-0002-2322-511X

This is an Open Access article distributed under the terms of the Creative Commons Attribution License (<http://creativecommons.org/licenses/by/3.0>), which permits unrestricted use, distribution and reproduction in any medium provided that the original work is properly attributed.

Received 6 June 2016; Accepted 20 September 2016

INTRODUCTION

Retinoblastoma (Rb) is the most common primary intraocular malignancy of infancy with an incidence of 1/15,000 to 1/20,000 births. It is estimated that annually Rb affects 7000-8000 new patients worldwide (Broaddus et al., 2009; Seregard et al., 2004), and survival rates vary dramatically. Untreated, mortality is 100%. In 60% of Rb patients, an unilateral Rb tumour is diagnosed at an average age of two years, and in most cases these tumours are not hereditary. In the other 40% of cases, Rb is bilateral and is diagnosed at an average age of one year. All bilateral and multifocal unilateral forms belong to a genetic cancer predisposition syndrome and are hereditary. RB1 gene mutation can be found in all children with a bilateral or familial form, as well as in 10 to 15% of children with a unilateral form of Rb (Jehanne et al., 2014).

Knowledge on tumour genesis was increased enormously with the development of mouse models for retinoblastoma (Villegas et al., 2013). For example, recently, the chemotherapeutic effect of focal melphalan was investigated in the transgenic LHBETATAG murine model. This treatment mediates a significant reduction with respect to the tumour burden, hypoxia and vasculature (Shah et al., 2014).

Ophthalmic imaging, like wide-field photography and echography, are reliable tools, not only in diagnosis but also for detecting regression or progression patterns of Rb (Villegas et al., 2013; Houston et al., 2011; Shields et al., 2009). Intraocular calcifications have also been shown to be analysed successfully using autofluorescence (Ramasubramanian et al., 2011). The role of optical coherence tomography (OCT) was also investigated in the evaluation of fundus tumours in children, and the use of OCT scans during the management of Rb was approved by the clinicians (Houston et al., 2013; Shields et al., 2004; Mallipatna et al., 2015).

The aim of this study was to generate an animal model for Rb that closely resembles the human disease for the purpose of developing new therapeutic options or comparing the efficacy and side-effects of existing treatments. To this aim, retinoblastoma cells of the human Rb-/- cell line Y79 were intravitreally injected into the eyes of immune-deficient nude mice to induce tumour growth. Development and spread of the tumours were characterized by scanning laser ophthalmoscopy (SLO), fluorescein angiography (FA) and OCT, as well as by histology including an analysis at the ultrastructural level, and the *in vivo* and *ex vivo* follow ups were compared. In addition, ultrastructural analysis of the xenograft Rb tumours was performed in order to assess the relevance of our Rb mouse model.

RESULTS

Morphological analysis

Starting at week five after the injection, the eyes began to swell in individual animals. We determined four stages depending on the tumour progression as shown in Fig. 1: Stage 0 (S0) was

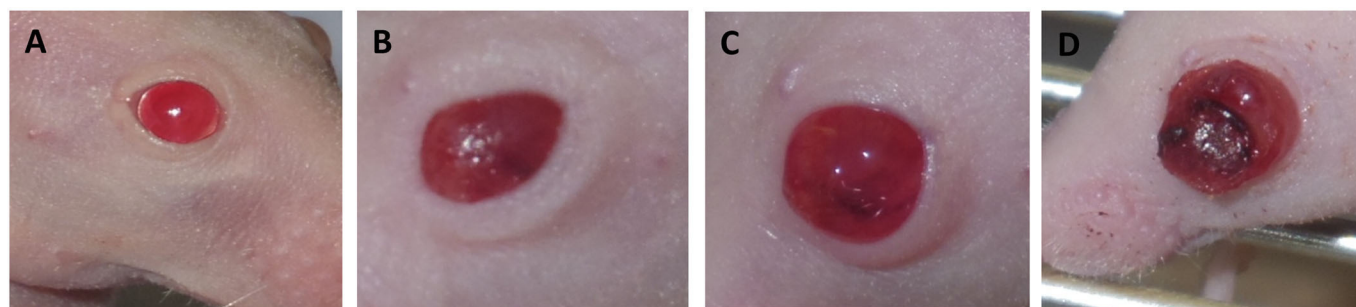


Fig. 1. Results of the morphological analysis. (A-D) the stages S0-SIII of the mouse eyes: (A) stage 0 (S0): eye of an untreated mouse; (B) stage I (SI): the eye is swollen up to 2× of the normal size; (C) stage II (SII): the eye is swollen up to 3× of the normal size, the eye is cloudy; (D) stage III (SIII): the tumour breaks through the cornea.

considered as the morphology of a normal mouse eye. Stage I (SI) was reached after the eye was swollen up to 2× the normal size and showed a cloudy appearance, stage II (SII) was reached after the eye was swollen up to 3× the normal size, stage III (SIII) was reached when the tumour broke through the cornea. Table 1 shows the number of eyes and their corresponding stages at the time points of analysis.

As shown in Fig. 2, there were some intra-individual differences concerning the time point of the start and the progress of the swelling of the eyes. The earliest cases of swelling appeared 34 days after injection, and the latest 70 days after injection. In most cases the swelling started between week five and seven after injection and progressed fast from stage I (on average 39 days after injection) to stage II (on average 43 days after injection) and then to stage III (on average 48 days after injection) (Fig. 2).

In vivo imaging using SLO/OCT

The SLO/OCT analysis could only be performed in stage 0 eyes with tumours at very early stages or in eyes without a tumour. In eyes with tumours at later stages of growth (SI-SIII) no analysis was possible, because the tumour covered the fundus.

In all cases where SLO/OCT analysis was possible, the results showed a good correlation with the results of the histological analysis. Using OCT, not only could we detect the tumour itself, but could also get information about its growth characteristics. The tumour shown in Fig. 3, for example, broke through the retina and began to grow subretinally, which can be clearly seen on the OCT image (Fig. 3A, left panel) and could later be found on the corresponding HE-stained slide Fig. 3B. The results of the angiography analysis with fluorescein gave a good picture of the tumour's vessel structure Fig. 3C.

Histological analysis

In the tumour-bearing eyes tumour cells could be observed in the vitreous, retina and subretinal space. An overview of the exact number of eyes and areas of tumour growth up to the time points of analysis is presented in Table 2.

Table 1. Number and stages of the analysed eyes

| Eye, stage | Week 3 (8 eyes) | Week 6 (10 eyes) | Week 9 (10 eyes) | Week 12 (12 eyes) |
|------------|--------------------|---------------------|---------------------|----------------------|
| S0 | 8 | 5 | 3 | 7 |
| SI | - | - | - | - |
| SII | - | - | 1 | 1 |
| SIII | - | 5 | 6 | 4 |

The table shows the number of the investigated eyes and their corresponding stages at the time points of analysis.

For the initial phase of tumour growth (week 3), eight eyes were analysed. Tumour cells could be seen in the vitreous and on the retina in four of them. In two eyes the tumour grew through the retina, in one of these eyes even subretinal tumour growth could be observed.

In all tumour-bearing eyes which were analysed 6 weeks after injection, the tumour completely replaced the vitreous and grew into the anterior chamber, in seven eyes the tumour invaded or damaged the lens, and in two eyes the tumour did not penetrate the retina (Fig. 4A). In the other eight tumour-bearing eyes, a subretinal growth could be detected (Fig. 4B).

In advanced tumours (week 9 and 12) the tumour replaced most of the eye's structures, like the vitreous, the lens and retina. Here in all six tumour-bearing eyes the sclera was the only part of the eye's tissue remaining (Fig. 4C).

Histologically, the tumours were composed of typical undifferentiated hyperchromatic cells with scanty cytoplasm having a rosette-like growth pattern, as described for the original tumour (Reid et al., 1974). All tumours showed a high mitotic and necrotic activity.

A tumour was found in 67.5% of the analysed eyes (29 of 42) 12 weeks after the injection of the Y79 cells.

Metastases

We screened tissues near the tumour, like the brain and skull, for metastases as well as the kidneys, lung, heart, liver, and spleen for the appearance of distant metastases by analysing HE-stained cross sections of these tissues. Only in one mouse could metastases in the brain be found. The metastases were found in the mouse, which after having reached stage III for one eye was kept for the longest period of time (35 days) before being killed and analysed (Fig. 2, mouse 16). In this eye the tumour broke through the sclera in several areas and grew into the brain (not shown). No distant metastases could be found.

Electron microscopy analysis

The ultrastructural analysis of the xenograft-tumours, shown in Fig. 5, showed very similar characteristics to those described for the original tumour (Reid et al., 1974), such as poor differentiation but still identifiable rosette-like growth, large hyperchromatic nuclei with multiple nucleoli and elaborate convolutions of the nuclei (Fig. 5A), and numerous degraded and necrotic cells (Fig. 5B) (Reid et al., 1974; Green et al., 1979; McFall et al., 1977). These characteristics are also described as typical for patient's Rb tissues (Rodrigues et al., 1986; Allen et al., 1962).

DISCUSSION

Preclinical animal models that mimic molecular, genetic, and cellular features of retinoblastoma are essential for studying this type of cancer.

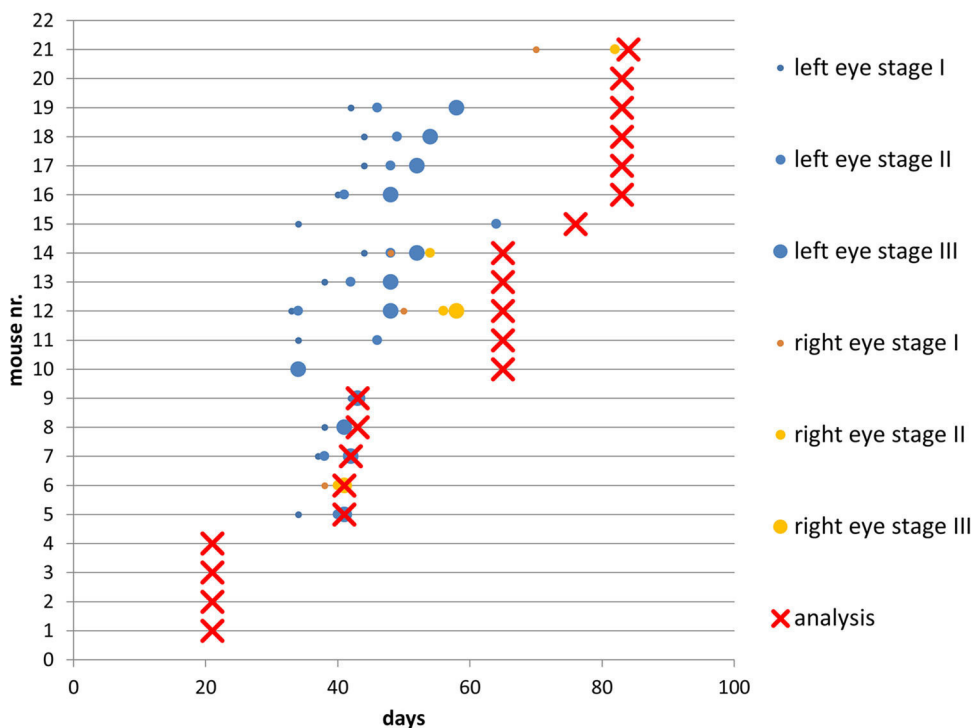


Fig. 2. Overview of the results of the morphological analysis of the mouse eyes during the experiment. Stages shown are: the beginning of the swelling (small circle=S1); the staging of the eye (medium circle=SII and big circle=SIII); and the time point of analysis (red X) of each eye. Mouse 16 had brain metastasis, the mouse was analysed 35 days after the left eye reached stage III.

Currently, two types of retinoblastoma animal models exist: transgenic models and xenograft models. The transgenic models have been developed from LH- β -Tag models to conditional gene knock-out models. There are different types of xenograft models, for example orthotopic models and subcutaneous transplantation models. The two types of Rb models present advantages and disadvantages.

The combination of genetic and xenograft models in retinoblastoma research has already help to better understand tumour biology and to find more effective diagnosis and treatments.

Our aim was to create a xenograft mouse model with close resemblance to human Rb tumours which can be used for broad application possibilities including radio therapeutic approaches of Rb treatment.

Literature research indicates that in addition to the use of transgenic animals as a model system for retinoblastoma, another possibility is the use of a xenograft model which is based on the implantation of human retinoblastoma cells into the eye of immunodeficient animals. Indeed, retinoblastoma xenograft

models are often created using the cell line Y79. This commercially available human retinoblastoma cell line is derived from a two-and-a-half-year-old patient, who had a maternal history of retinoblastoma.

The implantation can be performed in various compartments of the eye; previously the anterior chamber was often preferred because it is more accessible for both the implantation and subsequent observation (Gallie et al., 1977; Totsuka et al., 1982). However, in patients the tumour starts its growth in the retina and penetrates relatively late into the anterior chamber which is physiologically different to the vitreous body, and where the retinoblastoma first encroaches. Thus, a subretinal injection of the retinoblastoma cells is a better reflection of the situation in humans (del Cerro et al., 1993; Rowe et al., 1992). Unfortunately, this kind of injection can cause damage to the choroid and retina, which can result in an unnatural spread of the tumour.

Another possibility is the intravitreal injection of tumour cells as described by (Chevez-Barrios et al., 2000). After the intravitreal implantation of Y79 cells in Rag2 KO mice, tumours formed in the

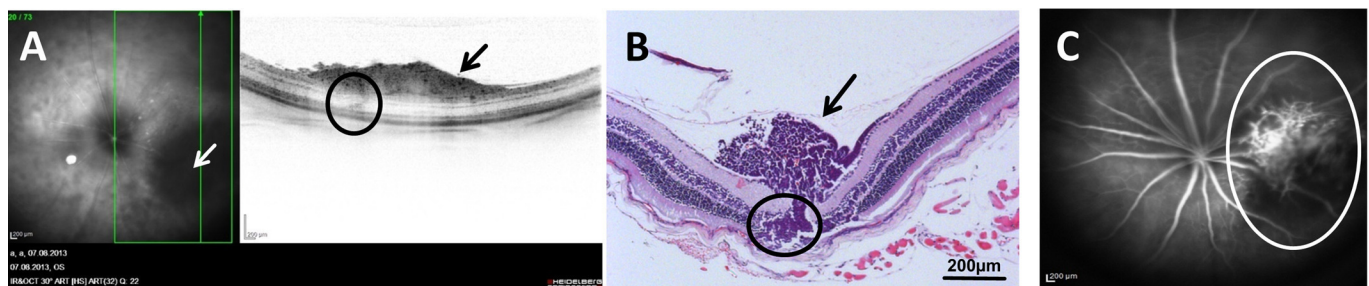


Fig. 3. Results of the *in vivo* and corresponding histological analysis. Panels (A) and (C) show the results from the *in vivo* analysis of the same tumour-bearing eye. The tumour is at an early stage of development, and grew in the vitreous directly on the retina 3 weeks after the injection of the Y79 cells. Left panel in A is the SLO image, the tumour (white arrow) can be seen as a dark region in the lower right corner, the right panel in A shows the OCT image of the green-boxed section in the left panel. (B) The HE-stained sample ($\times 100$) of the right panel in A. In both panels A and B, the tumour is shown with black arrows, and located directly on the retina, the area of the tumour breaking through the retina and the area of subretinal tumour growth are circled. (C) SLO image fluorescein mode (FA) 5 min after fluorescein injection (the tumour vessels are circled).

Table 2. Analysis of the HE-stained eyes: the areas of tumour growth and time-points of analysis are shown

| Area of tumour growth | Week 3 | Week 6 | Week 9 | Week 12 |
|-----------------------|--------|--------|--------|---------|
| Vitreous | 4/8 | 10/10 | 8/10 | 6/12 |
| Retina | 2/8 | 8/10 | 8/10 | 6/12 |
| Subretinal space | 1/8 | 8/10 | 8/10 | 6/12 |
| Lens | 0/8 | 7/10 | 8/10 | 6/12 |
| Anterior chamber | 0/8 | 10/10 | 8/10 | 6/12 |

The data is expressed as the number of eyes that were positive for tumour at each site/total number of eyes examined.

eye and gradually spread, and later could also be found in the brain. Thus we decided to use an intravitreal injection as well.

The Rag2 KO model developed by Chevez-Barrioz was never used for radiotherapeutic experiments, but the nude mouse model used by Totsuka was (Totsuka and Minoda, 1982), therefore we decided to combine the advantages of both models to develop another model.

After the injection of Y79 cells, tumour cells proliferated first in the vitreous and then formed a clearly localised tumour on and through the retina, not exactly consistent with the retinoblastoma tumours observed in children that originate in the retina; however this particularity is common with the retinoblastoma mouse model developed by Chevez-Barrios et al. (2000). In most cases, the tumour broke through the retina and began to grow subretinally. In two cases the tumour did not penetrate the retina at the 6 week time point of analysis (Fig. 4B).

In contrast to the retinoblastoma mouse model developed by Chevez-Barrios et al. (2000) in which the authors observe metastases resulting from migration of tumour cells up the optic nerve, we observed in our model that the sclera seems to be a strong barrier for the tumour. The tumour needs to grow very large and have a long time to break through the sclera. During our experiment the tumour only penetrated the sclera in one mouse eye and formed brain metastases. The metastases were found in the brain of a mouse, which, after having reached stage III for the left eye, was kept alive for the longest period of time (35 days) before being sacrificed and analysed (Fig. 2, mouse 16). However, in the Rag-2 knockout (KO) mice used by Chevez-Barrios et al. (2000), the animals were intravitreally injected with Y79 cells in a similar manner as in our experiment, but the mice already developed metastases 4 weeks after the injection (Chevez-Barrios et al., 2000). These results are consistent with those of other groups, who could show that metastasization metastases in Rag-2 KO mouse models are stronger

than in nude mice for several human cancer xenografts like sarcoma (Nanni et al., 2010), breast cancer (Nanni et al., 2012) or adenocarcinoma (Ye et al., 2015). This should be considered when choosing a model. Despite the mentioned differences of the metastasization process in Rag2 KO and nude mice, Gallie et al., described a metastasization of the optic nerve and brain in cyclophosphamide pre-treated nude mice (Gallie et al., 1977); unfortunately the authors do not make any statement about the time point of analysis. In our experiment we had to kill the animals at the latest 12 weeks after tumour cell injection due to the ethical requirements of local authorities, and we consider it very likely that they might develop metastases at a later time point.

A very important aspect of this work was the use of *in vivo* approaches like SLO/OCT for the detection and characterisation of tumours in the mouse eyes and the comparison of the results with the corresponding results of the histological analysis, which showed a good correlation as shown in Fig. 3. A similar funduscopy/OCT-based approach was used for the analysis of the tumours in the eyes of a TAg-RB mouse model by Wenzel et al. with similar results (Wenzel et al., 2015).

In ophthalmological research, *in vivo* analysis like SLO/OCT allows multiple analysis of dynamic biological processes like tumourigenesis, tumour growth and angiogenesis at certain time points in individual animals and can help to reduce the number of experimental animals used.

In conclusion, we showed that our Rb mouse model mimics the human disease. The xenograft tumour samples from our model showed very similar growth characteristics, cellular appearance and ultrastructural characteristics to those described for Rb patient tumour tissue samples. This makes our model a promising tool for the study of retinoblastoma and its potential therapy approaches.

We also show that SLO/OCT can be used for the detection of tumours at early stages of development and could be used for monitoring the future therapies.

MATERIALS AND METHODS

Cell culture

The Y79 retinoblastoma cell line originates from a primary tumour of a two-and-a-half-year-old Caucasian female with a maternal history of retinoblastoma in 1971 (Reid et al., 1974).

The human retinoblastoma Y79 cell line was purchased at American Type Culture Collection (ATCC, USA). The cells were cultured in RPMI-1640 medium (Gibco®, Darmstadt, Germany) supplemented with 10% fetal

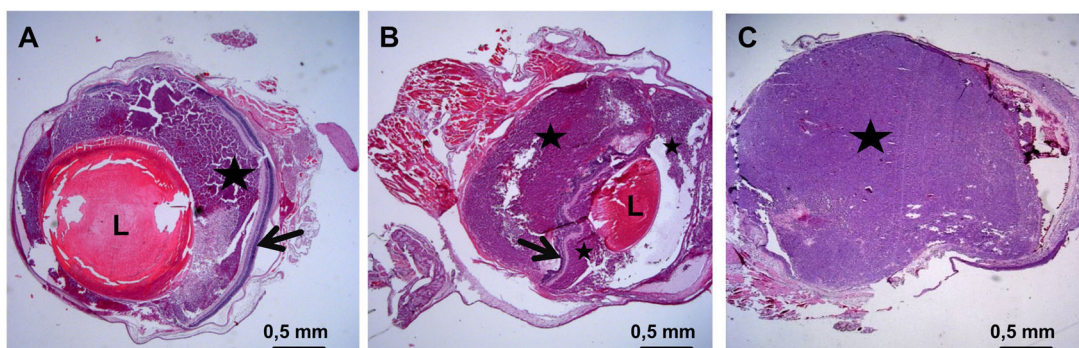


Fig. 4. Results of the histological analysis. (A) Y79 xenograft tumour from a nude mouse eye 6 weeks after injection (25× magnification), the tumour (black star) grows in the vitreous but does not penetrate the retina (black arrow). (B) Y79 xenograft tumour from a nude mouse eye 6 weeks after injection (25× magnification). Here the tumour, after having grown in the vitreous (smaller black star), penetrated the retina and after strong subretinal growth (bigger black star) pressed the retina (black arrow) in direction of the lens (L). (C) Y79 xenograft tumour from a nude mouse eye 9 weeks after injection (25× magnification), the tumour (black star) has replaced all structures of the inner eye, i.e. the vitreous, the retina and the lens and broke through the cornea (out of sight).

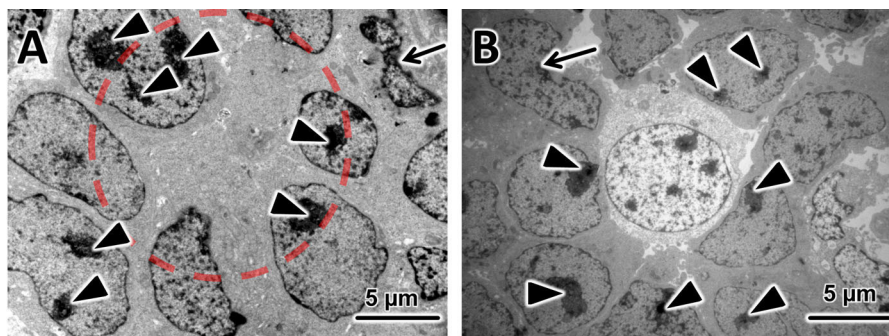


Fig. 5. EM Analysis. In both electron micrographs the tumor cells show typical large hyperchromatic nuclei with multiple nucleoli (black arrowheads) and elaborate convolutions of the nuclei (black arrows point to cells in which this process is very pronounced). (A) A representative electron micrograph (3000× magnification) from a tissue sample from a xenograft tumour which grew in a nude mouse eye 9 weeks after injection of Y79 cells, here the rosette-like growth of the Y79 cells can be clearly recognized (red circle). (B) A representative electron micrograph (3000× magnification) from the same tissue sample. Here in the centre a necrotic Y79 cell is surrounded by other tumour cells. Black arrowheads point to multiple nuclei; black arrows point to cells with very pronounced elaborate convolutions of the nuclei.

bovine serum and 2 mM L-glutamine. The cells grew as a suspension culture and were cultured and passaged as recommended by the ATCC. For the injection, cells from passage 4 were used.

Intravitreal injection

24 BALB/c nude mice [female, 3 months old, purchased at Janvier (Laval, France)] were used for the study. The animals were kept in individually ventilated cages (IVC) in our animal facility.

The mice were handled at all times in accordance with the German Animal Welfare Act and were under the control of the Animal Protection Agency and under supervision of veterinarians of the University of Tuebingen. The experiments were approved by the local authorities (Regierungspräsidium Tuebingen AK 6/12).

Each animal was first anaesthetized with an intraperitoneal injection of a three component narcosis (0.05 mg fentanyl, 5.00 mg midazolam and 0.5 mg of medetomidine/1 kg body weight, prepared by the Animal Protection Agency of the University of Tuebingen).

The pupils were dilated with 1 to 2 drops of Medriaticum drops (Pharmacy of the University of Tuebingen, Germany) and a drop of topical anesthetic Novesine (OmniVision, Puchheim, Germany) was applied. Methocel (OmniVision, Puchheim, Germany) eye drops were used to avoid drying of the eyes. Injections were performed using a surgical microscope. Two microlitres of sterile phosphate buffered saline (Gibco[®], Darmstadt, Germany) containing 2×10^4 Y79 human retinoblastoma cells were injected into the vitreous of each eye through the sclera using a Hamilton syringe with a 26 gauge cannula. Special care was taken to prevent lens damage or posterior retinal punctures. After the injection, the eyes were treated with antibiotic eye drops (Gentamicin-POS[®], Ursapharm, Saarbrücken, Germany). Finally the mice were subcutaneously injected with an antidote (1.2 mg naloxon, 0.5 mg flumazenil, 2.5 mg atipamezol/1 kg body weight, prepared by the Animal Protection Agency of the University of Tuebingen) which neutralized the anaesthetic.

The animals were examined 2, 12 and 24 h after surgery and then daily. Clinical findings regarding the presence of tumour were recorded.

In vivo imaging using SLO/OCT

Three, six, nine and twelve weeks after injection, groups of five mice were formed. Mice which showed tumour-caused phenotypical changes were primarily analysed. For the analysis a Spectralis™ HRA+OCT SLO/OCT device was used (Heidelberg Engineering, Heidelberg, Germany). The whole procedure was performed as described in Huber et al. (2009) and Fischer et al. (2009). Briefly, the Spectralis[®] was remodelled to make it usable for the analysis of small rodents by fixing a 78 dpt double aspheric lens (Volk Optical, Inc., Mentor, OH 44060, USA) directly to the outlet of the device, and an additional custom-made 100 dpt contact lens directly on the eyes of the mice. The mice were anaesthetized by a peritoneal injection of a three component narcosis (as described above), and the pupils were dilated with 1 to 2 drops of Medriaticum (Pharmacy of the University of Tuebingen, Germany). Methocel (OmniVision, Puchheim, Germany) eye

drops were used to avoid drying of the eyes and to ensure the adherence of 100 dpt- lenses on the mice eyes. The mice were put in front of the device on the XYZ-table and positioned for the analysis. The mice were covered with cloth to avoid hypothermia.

After positioning, the SLO images were taken. In cases when a tumour was detected, an angiography analysis was also performed. 25 µl of a 2% solution of Fluorescein[®] 10% (Alcon Freiburg, Germany) was given subcutaneously to the mice to make it possible to visualize the retinal and tumour vessels using the FA (fluorescein angiography) mode of the SLO device. After that the OCT-imaging was performed. A detailed protocol for anaesthesia and imaging is described elsewhere (Huber et al., 2009).

Histological analysis

Directly after the *in vivo* analysis the mice were killed by cervical dislocation. One eye, the brain, lungs, heart, kidney, spleen, and liver of each mouse were immediately fixed in 4.5% formalin containing fixation solution (4.5% Roti Histofix, Carl Roth, Karlsruhe, Germany). The tissues were processed and embedded in paraffin using conventional automated systems. The blocks were cut to obtain serial 4 µm thick sections and stained with conventional hematoxylin-eosin (HE). The slides were examined by the means of a light microscope.

Light and electron microscopy (EM)

The other eye of each mouse was fixed in 5% glutaraldehyde for electron microscopic analysis. After the fixation (min. 3 days) the eyes were screened under a binocular for areas of interest (aoi), especially tumour-containing areas. The samples containing these aoi were cut (1 mm×1 mm). These specimens were post-fixed with 1% OsO₄ at room temperature in 0.1 M cacodylate buffer (pH 7.4), *en bloc* stained with uranyl acetate and lead citrate, and embedded in Epon after dehydration in a graded series of acetones. Semi-thin sections (0.2 µm) were stained with Toluidine Blue and examined by light microscopy (Zeiss Axioplan2 imaging, Zeiss, Jena, Germany). For electron microscopy, the sections were cut ultrathin (0.07 µm) and analysed with a Zeiss 902 A electron microscope (Zeiss, Jena, Germany).

Acknowledgements

The authors thank Monika Rittgarn and Sigrid Schultheiss for their excellent technical assistance (Division of Experimental Vitreoretinal Surgery, Center for Ophthalmology, Eberhard Karls University Tuebingen, Germany) and Dr. Tobias Peters and Norman Rieger (Institute of Ophthalmic Research, Centre for Ophthalmology, University of Tuebingen) for valuable discussions.

Competing interests

The authors declare no competing or financial interests.

Author contributions

S.J.-S. designed the experiments. S.J.-S. and A.V.T. performed the experiments and data analysis and wrote the paper. U.S. and H.P.R. gave valuable suggestions and revised the paper. All authors approved the final version of the manuscript.

Funding

This work was financially supported by the Deutsche Kinderkrebsstiftung [grant no. DKS 2012.08]. We acknowledge support by Deutsche Forschungsgemeinschaft and Open Access Publishing Fund of University of Tübingen.

References

- Allen, R. A., Latta, H. and Straatsma, B. R. (1962). Retinoblastoma. A study of two cases by electron microscopy. *Invest. Ophthalmol.* **1**, 728-744.
- Broadus, E., Topham, A. and Singh, A. D. (2009). Incidence of retinoblastoma in the USA: 1975-2004. *Br. J. Ophthalmol.* **93**, 21-23.
- Chevez-Barrios, P., Hurwitz, M. Y., Louie, K., Marcus, K. T., Holcombe, V. N., Schafer, P., Aguilar-Cordova, C. E. and Hurwitz, R. L. (2000). Metastatic and nonmetastatic models of retinoblastoma. *Am. J. Pathol.* **157**, 1405-1412.
- Del Cerro, M., Seigel, G. M., Lazar, E., Grover, D., Del Cerro, C., Brooks, D. H., Diloreto, D., Jr and Chader, G. (1993). Transplantation of Y79 cells into rat eyes: an in vivo model of human retinoblastomas. *Invest. Ophthalmol. Vis. Sci.* **34**, 3336-3346.
- Fischer, M. D., Huber, G., Beck, S. C., Tanimoto, N., Muehlfriedel, R., Fahl, E., Grimm, C., Wenzel, A., Reme, C. E., Van De Pavert, S. A. et al. (2009). Noninvasive, in vivo assessment of mouse retinal structure using optical coherence tomography. *PLoS ONE* **4**, e7507.
- Gallie, B. L., Albert, D. M., Wong, J. J., Buyukmihci, N. and Pullafito, C. A. (1977). Heterotransplantation of retinoblastoma into the athymic "nude" mouse. *Invest. Ophthalmol. Vis. Sci.* **16**, 256-259.
- Green, A. L. W., Meek, E. S., White, D. W., Stevens, R. H., Ackerman, L. D., Judisch, G. F. and Patil, S. R. (1979). Retinoblastoma Y79 cell line: a study of membrane structures. *Albrecht Von Graefes Arch. Klin. Exp. Ophthalmol.* **211**, 279-287.
- Houston, S. K., Berrocal, A. M. and Murray, T. G. (2011). The future of diagnostic imaging in retinoblastoma. *J. AAPOS* **15**, 125-126.
- Houston, S. K., Lampidis, T. J. and Murray, T. G. (2013). Models and discovery strategies for new therapies of retinoblastoma. *Expert Opin. Drug Discov.* **8**, 383-394.
- Huber, G., Beck, S. C., Grimm, C., Sahaboglu-Tekgoz, A., Paquet-Durand, F., Wenzel, A., Humphries, P., Redmond, T. M., Seeliger, M. W. and Fischer, M. D. (2009). Spectral domain optical coherence tomography in mouse models of retinal degeneration. *Invest. Ophthalmol. Vis. Sci.* **50**, 5888-5895.
- Jehanne, M., Brisse, H., Gauthier-Villars, M., Lumbroso-Le Rouic, L., Freneaux, P. and Aerts, I. (2014). Retinoblastoma: recent advances. *Bull. Cancer* **101**, 380-387.
- Mallipatna, A., Vinekar, A., Jayadev, C., Dabir, S., Sivakumar, M., Krishnan, N., Mehta, P., Berendschof, T. and Yadav, N. K. (2015). The use of handheld spectral domain optical coherence tomography in pediatric ophthalmology practice: our experience of 975 infants and children. *Indian J. Ophthalmol.* **63**, 586-593.
- Mcfall, R. C., Sery, T. W. and Makadon, M. (1977). Characterization of a new continuous cell line derived from a human retinoblastoma. *Cancer Res.* **37**, 1003-1010.
- Nanni, P., Nicoletti, G., Landuzzi, L., Croci, S., Murgo, A., Palladini, A., Antognoli, A., Ianzano, M. L., Stivani, V., Grosso, V. et al. (2010). High metastatic efficiency of human sarcoma cells in Rag2/gammac double knockout mice provides a powerful test system for antimetastatic targeted therapy. *Eur. J. Cancer.* **46**, 659-668.
- Nanni, P., Nicoletti, G., Palladini, A., Croci, S., Murgo, A., Ianzano, M. L., Grosso, V., Stivani, V., Antognoli, A., Lamolinara, A. et al. (2012). Multiorgan metastasis of human HER-2+ breast cancer in Rag2-/-;Il2rg-/- mice and treatment with PI3K inhibitor. *PLoS ONE* **7**, e39626.
- Ramasubramanian, A., Shields, C. L., Mellen, P. L., Haji, S., Harmon, S. A., Vemuganti, G. K. and Shields, J. A. (2011). Autofluorescence of treated retinoblastoma. *J. AAPOS* **15**, 167-172.
- Reid, T. W., Albert, D. M., Rabson, A. S., Russell, P., Craft, J., Chu, E. W., Tralka, T. S. and Wilcox, J. L. (1974). Characteristics of an established cell line of retinoblastoma. *J. Natl. Cancer Inst.* **53**, 347-360.
- Rodrigues, M. M., Wilson, M. E., Wiggert, B., Krishna, G. and Chader, G. J. (1986). Retinoblastoma. A clinical, immunohistochemical, and electron microscopic case report. *Ophthalmology* **93**, 1010-1015.
- Rowe, S. G., Lee, W. H. and Madreperla, S. (1992). Subretinal and vitreal growth of human retinoblastoma cells in the mouse eye. *Invest. Ophthalmol. Vis. Sci.* **33**:875 (abstr.)
- Seregard, S., Lundell, G., Svedberg, H. and Kivela, T. (2004). Incidence of retinoblastoma from 1958 to 1998 in Northern Europe: advantages of birth cohort analysis. *Ophthalmology* **111**, 1228-1232.
- Shah, N. V., Pham, D. G., Murray, T. G., Decatur, C., Hernandez, E., Shah, N. N., Cavalcante, M. and Houston, S. K. (2014). Intravitreal and subconjunctival melphalan for retinoblastoma in transgenic mice. *J. Ophthalmol.* **2014**, 829879.
- Shields, C. L., Mashayekhi, A., Luo, C. K., Materin, M. A. and Shields, J. A. (2004). Optical coherence tomography in children: analysis of 44 eyes with intraocular tumors and simulating conditions. *J. Pediatr. Ophthalmol. Strabismus* **41**, 338-344.
- Shields, C. L., Palamar, M., Sharma, P., Ramasubramanian, A., Leahey, A., Meadows, A. T. and Shields, J. A. (2009). Retinoblastoma regression patterns following chemoreduction and adjuvant therapy in 557 tumors. *Arch. Ophthalmol.* **127**, 282-290.
- Totsuka, S. and Minoda, K. (1982). Radiation effects on retinoblastoma successively transplanted into nude mouse eyes. *Ophthalmologica* **185**, 158-167.
- Totsuka, S., Akazawa, K. and Minoda, K. (1982). [Transplantation of retinoblastoma into nude mouse. 3. Tumor doubling time of retinoblastoma (author's transl)]. *Nihon Ganka Gakkai Zasshi* **86**, 418-425.
- Villegas, V. M., Hess, D. J., Wildner, A., Gold, A. S. and Murray, T. G. (2013). Retinoblastoma. *Curr. Opin. Ophthalmol.* **24**, 581-588.
- Wenzel, A. A., O'hare, M. N., Shadmand, M. and Corson, T. W. (2015). Optical coherence tomography enables imaging of tumor initiation in the TAG-RB mouse model of retinoblastoma. *Mol. Vis* **21**, 515-522.
- Ye, W., Jiang, Z., Li, G.-X., Xiao, Y., Lin, S., Lai, Y., Wang, S., Li, B., Jia, B., Li, Y. et al. (2015). Quantitative evaluation of the immunodeficiency of a mouse strain by tumor engraftments. *J. Hematol. Oncol.* **8**, 59.

5.1.1.1 Additional unpublished material

The SLO/OCT results of tumours at early stages of development could be well correlated with the corresponding histological results. However, at stages where the tumour grew too big and covered the fundus, SLO/OCT could not be performed (fig. 11).



Fig. 11: **Mouse eye with an advanced tumour 6 weeks after injection of Y79 cells.** (Left panel) Photo-image: the eye looks cloudy because of the growing tumour (Right panel) The corresponding SLO-image, as the laser cannot reach the fundus, no imaging is possible.

In one animal a metastasis in the brain was found. It was discovered in the animal which was sacrificed 35 d after the tumour grew so big that it broke through the sclera. In all other cases, due to the suggestions of the veterinarians and the experiments schedule, the animals were sacrificed at an earlier time point. In this animal the tumour had enough time to break through the sclera (fig. 12 A) and to form metastasis in the brain (fig. 12 B).

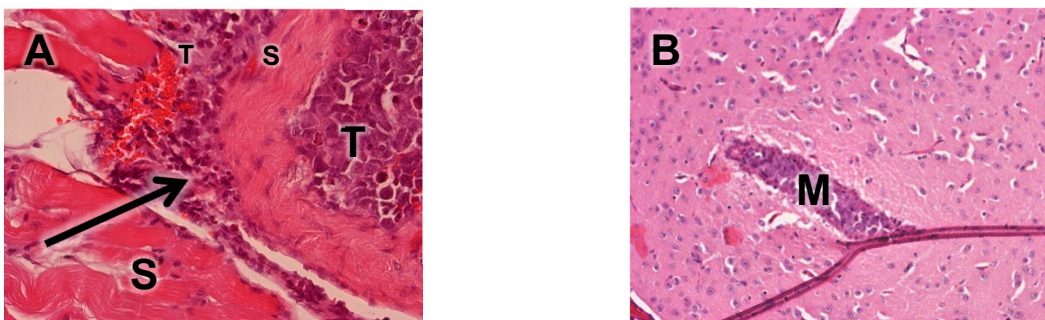


Fig. 12: **Histological analysis of Y79 xenograft tumour metastases:** histological image (x400) of the mouse eye (9 months after Y79 injection). (A) The tumour (T) is breaking (arrow) through the sclera (S). (B) Histological image (x100) of the brain with a metastasis (M).

5.2 Can the application of pTyr protect tissues that are affected by irradiation during radiotherapy and prevent radiotherapy-induced secondary tumours?

To analyse the ability of pTyr to protect tissues that are affected during radiotherapy and to avoid the induction of secondary tumours *in vivo*, B6;129-Rb1tm3Tyj/J Rb^{+/-} mice, which have a mutation in one of the Rb1- gene alleles (Jacks et al., 1992) were irradiated using a radiotherapy simulating irradiation scheme. These mice served as a model for patients with hereditary Rb, who having a genetic defect in the homologue human gene Rb- 1, have a higher risk of secondary malignancies after RT (Abramson & Frank, 1998).

Two pairs of each of a B6;129-Rb1tm3Tyj/J Rb^{+/-} and B6 wild type (WT) mice were purchased at the Jackson laboratory (Bar Harbor, ME, USA). Pairs of each an Rb^{+/-} and WT mouse (Rb^{+/+}) were formed to avoid offspring with a double knockout of the Rb1-gene, because these die *in utero*. The mice were bred in our animal facility. Twenty-four mice with an Rb^{+/-} genotype were needed for our experiment. Thus, the newborn mice had to be genotyped using a polymerase chain reaction (PCR) according to the instructions given by the Jackson laboratory (tab.1).

Briefly: DNA was isolated using a standard isopropanole extraction method from hairs which were plucked from the mouse. This DNA was used for the PCR analysis. We used 2 sets of primers, the same forward primer and one reverse primer for detection of the wildtype allele (tab.1) of the Rb-gen and another reverse primer for the mutated allele (tab.1) were used. The PCR products were run on a gel. When bands for the PCR products with the reverse primer for both the WT- and mutated allele were detected, the mouse genotype was Rb^{+/-} (fig.13).

5. Results

| Reaction Component | Volume (μl) | Final Concentration | Total Volume (μl) |
|----------------------------------|-------------|---------------------|-------------------|
| ddH ₂ O | 5.15 | - | 5.15 |
| 5 X Kapa 2G HS buffer | 2.40 | 1.00 X | 2.40 |
| 25 mM MgCl ₂ | 0.96 | 2.00 mM | 0.96 |
| 10 mM dNTP KAPA | 0.24 | 0.20 mM | 0.24 |
| 20 uM forward primer | 0.30 | 0.50 uM | 0.30 |
| 20 uM reverse primer* | 0.30 | 0.50 uM | 0.30 |
| 2.5 ul Kapa 2G HS taq polymerase | 0.05 | 0.01 ul | 0.05 |
| 20X EvaGreen | 0.60 | 1.00 X | 0.60 |
| DNA | 2.00 | - | 2.00 |

| Step # | Temp °C | Time | Note |
|--------|---------|-------|--------------------------------|
| 1 | 94 | 2 min | - |
| 2 | 94 | 20sec | - |
| 3 | 65 | 15sec | -0.5 C per cycle |
| 4 | 68 | 10sec | - |
| 5 | - | - | repeat steps 2-4 for 10 cycles |
| 6 | 94 | 15sec | - |
| 7 | 60 | 15sec | - |
| 8 | 72 | 10sec | - |
| 9 | - | - | repeat steps 6-8 for 28 cycles |
| 10 | 72 | 1 min | - |
| 11 | 4 | - | hold |

Reaction Components for the PCR analysis.
 Forward primer: AAT TGC GGC CGC ATC TGC ATC TTT ATC GC
 * Reverse primer wildtype: CCC ATG TTC GGT CCC TAG
 * Reverse primer mutated: GAA GAA CGA GAT CAG CAG
 *<http://www.jax.org/index.html>

Cycling protocol for the PCR reactions
<http://www.jax.org/index.html>

Table 1. **Genotyping protocol (Left panel):** Reaction protocol and primers (fig.1), **(Right panel):** Cycling protocol for the PCR for the genotyping of the newborn B6;129-Rb1tm3Tyj/J Rb^{+/-} mice. (Source <https://www.jax.org/strain/008186>).

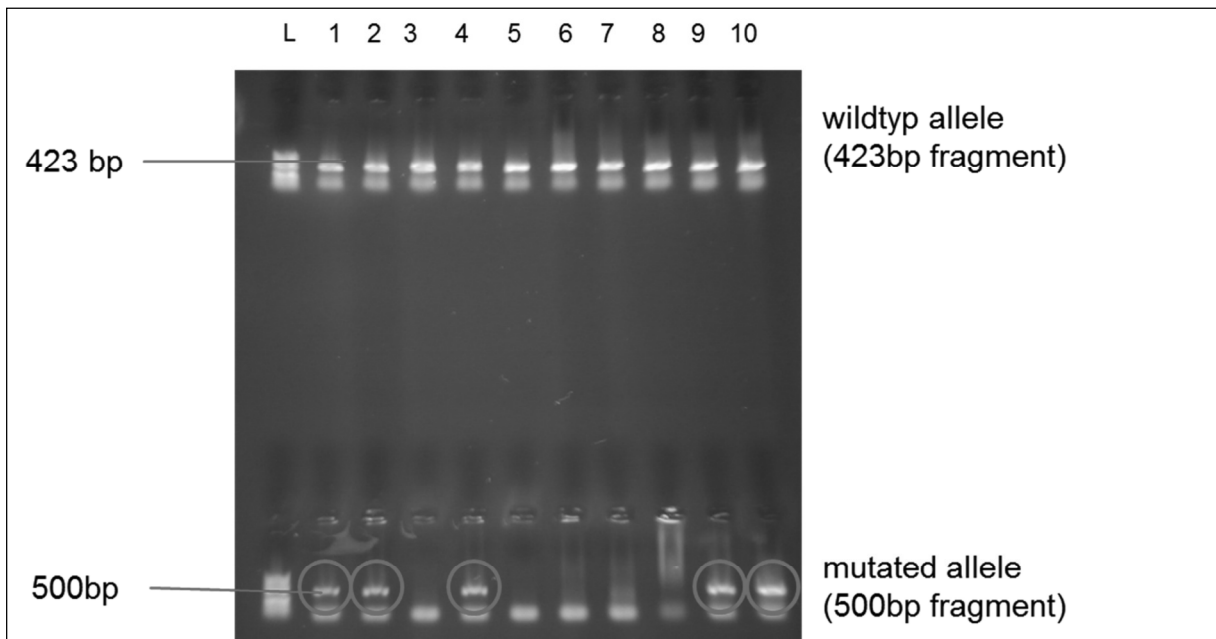


Fig.13: **Genotyping of 10 newborn mice of a B6;129-Rb1tm3Tyj/J Rb^{+/-} and B6 WT mouse pair.** On the gel under L (1000 bp DNA ladder) bands of 100-1000 bp are presented. In the upper part of the gel, bands from the 423 bp fragment of the WT allele can be seen, which is presented in all animals. In the lower part of the gel bands from the 500 bp fragment of the mutated allele can be seen in the samples of the mice with the numbers 1, 2, 4, 9 and 10 (red circled). These mice have an Rb^{+/-} genotype.

5. Results

Twenty four B6; 129-Rb1tm3Tyj/J Rb^{+/-} mice with and without pTyr pretreatment (fig. 14 A) were irradiated in a radiotherapy-simulating way (fig. 14 B) using a linear accelerator Linac-G (fig. 14 C) and a fractionated radiotherapy schedule (fig 14 D).

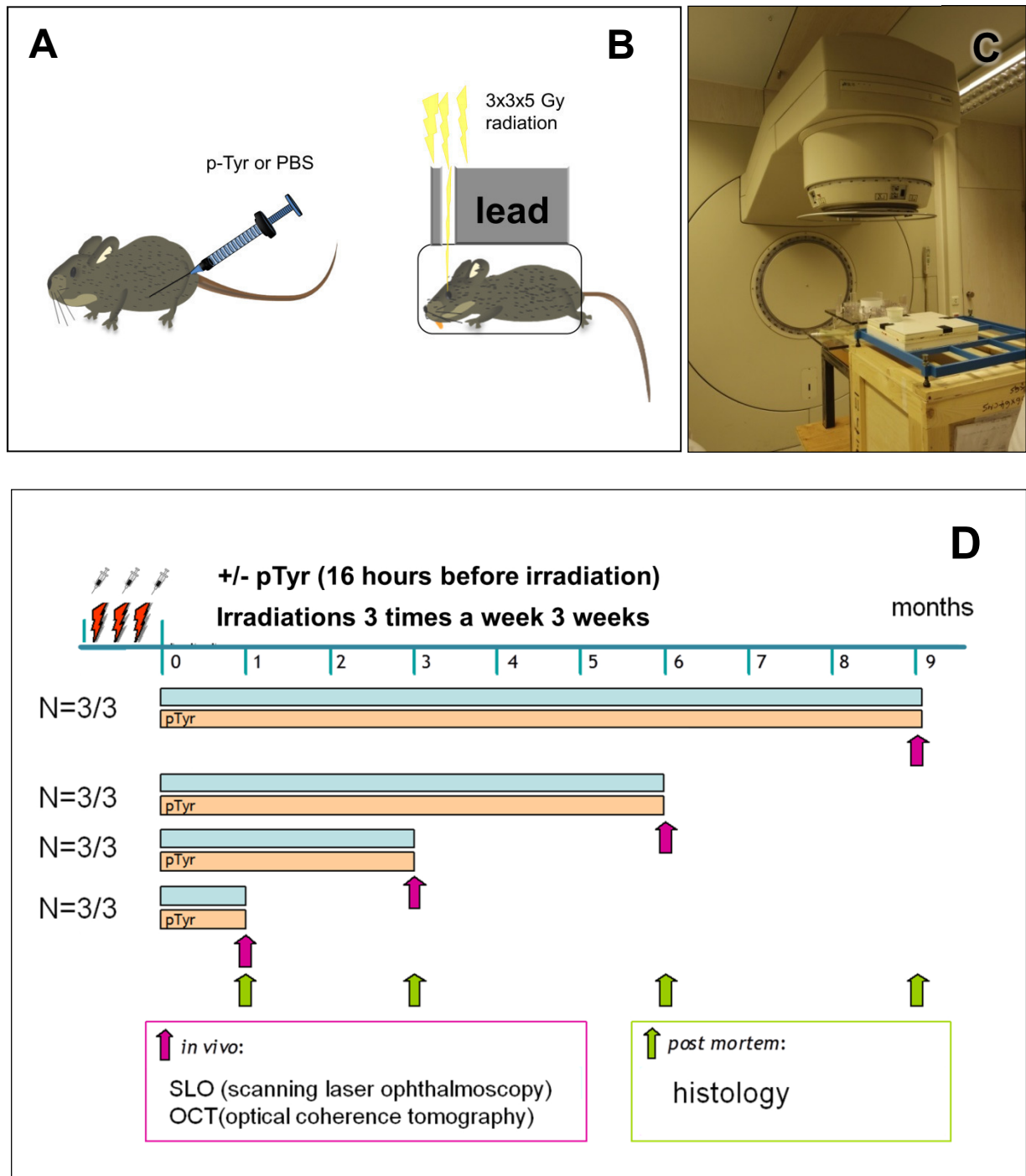


Fig. 14: Irradiation of Rb^{+/-} mice with and without pTyr. **(A):** One group of mice was pre-treated with intraperitoneal injections of pTyr (100 mg/kg body weight) 16 hours before each irradiation. The other group was pre-treated with PBS injections. **(B):** Diagram of the custom-made system where the mice were anaesthetised and their bodies, except for the area of interest, were covered with a lead shield during the irradiations. **(C):** Linear accelerator Linac-G (Philips) in the laboratory of the Experimental Radiooncology Department.

5. Results

(D): Irradiation schedule: Both groups were irradiated over a period of 3 weeks 3 times a week with a dosage of 5 Gy per exposure. The animals were investigated using SLO/OCT and histologically 1, 3, 6 and 9 months after IR. Radiation-induced tumour induction as well as normal tissue radiation toxicity was evaluated as a function of pTyr-treatment.

The most important results of this part of the project are, briefly, as follows:

Five weeks after the last irradiation, a greying of the fur in the irradiated area began in the pTyr untreated mice. The same change in fur pigmentation started eight weeks after irradiation in the pTyr treated mice and was significantly reduced in the pTyr treated mice six and nine months after RT.

The optical coherence tomography (OCT) analysis results showed a stronger reduction of the retina-thickness in the pTyr untreated animals 3, 6 and 9 months after IR and the corresponding histological analysis showed a greater loss of photoreceptors in the pTyr untreated animals 3, 6 and 9 months after IR. No metastases in the irradiated area or distant metastases were found.

Thus pTyr being radioprotective for normal tissues meets one of the requirements to be considered for the radiotherapy of Rb (Tschulakow et al., 2017). To see the detailed version, please refer to Chapter 5.4.

5.3 Does the application of pTyr interfere with the radiotherapy of retinoblastoma?

To examine whether pTyr can radioprotect retinoblastoma cells and thus counteracts the effectiveness of the radiotherapy, *in vitro* irradiation experiments with Y79 cells and *in vivo* radiotherapeutic experiments using our Y79 xenograft nude mouse model were performed.

5.3.1 *In vitro* studies

The Y79 retinoblastoma cells grew as a suspension culture and were cultured and passaged as recommended by the American Type Culture Collection (ATTC). The cell cultures were treated and irradiated according to the corresponding protocols (Tschulakow et al., 2017), to see the detailed version please refer to chapter 5.4. and used for western blot and limited dilution assay analysis (fig 15).

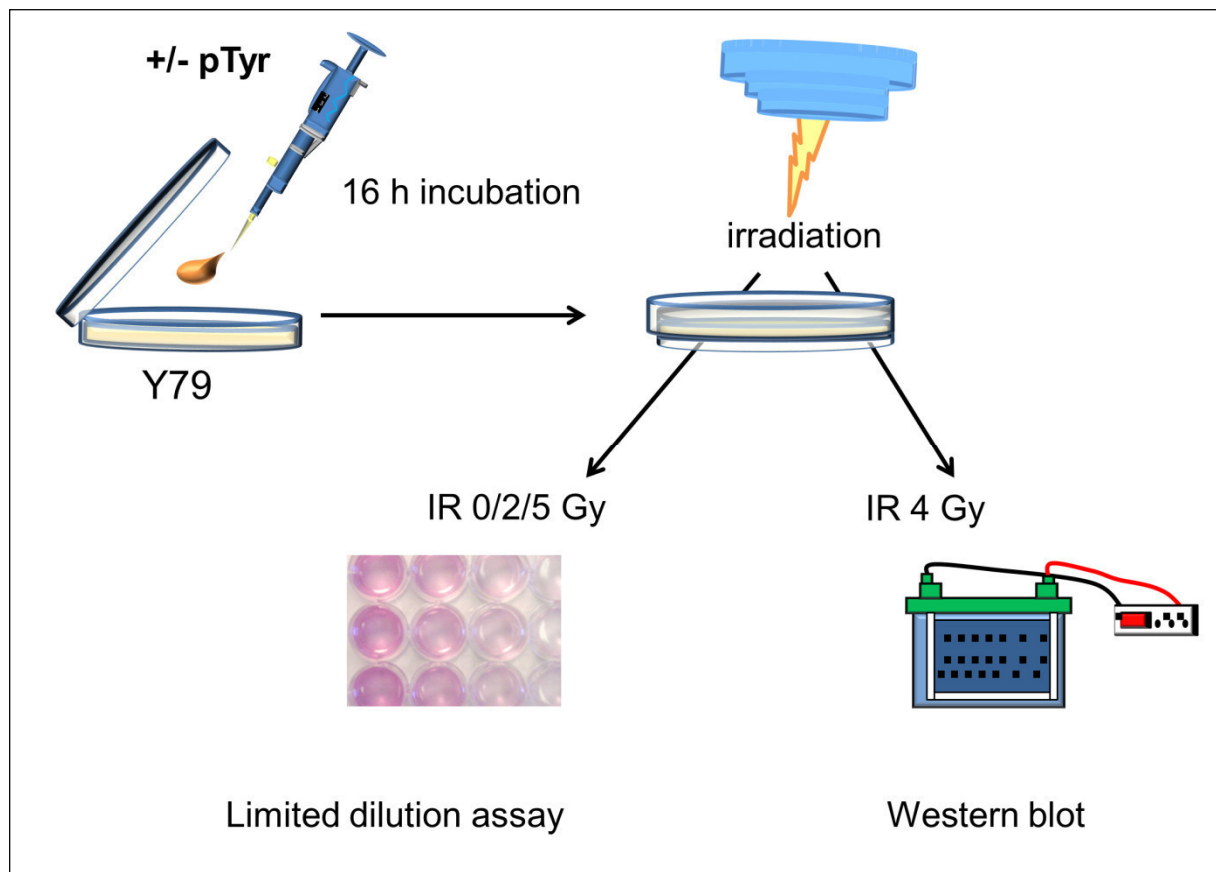


Fig. 15: ***In vitro* analysis of irradiated 79 cell cultures with and without pTyr-pretreatment.** The Y79 cells were pre-treated with pTyr (10 μ M) or vehicle (PBS) 16 hours before IR. The irradiations were performed using a linear accelerator Linac-G (Phillips). For the analysis of the ability of pTyr to radioprotect Y79 cells *in vitro* a “pre- and delayed plating limited dilution assay” was performed after IR with 0 Gy,

5. Results

2 Gy and 5 Gy. For the analysis of the p53 protein expression in Y79 cells after the IR with 4 Gy, a **western blot analysis** was performed. For the analysis of the p53 protein activity, we also measured the amount of its phosphorylated (at Ser-residue-15) form and the amount of p21 (a downstream p53 pathway-member).

5.3.1.1. Western blot

pTyr was shown to radioprotect predominantly p53 WT cells (K. H. Dittmann et al., 2001). Y79 cells have a p53 WT and if pTyr would radioprotect them, it wouldn't be suitable for a RT of Rb. But for other Rb- and particularly for Y79 cells different mechanisms were described which interfere with the p53-pathway or inactivate p53. To test this hypothesis western-blot analysis was used. We analysed the impact of irradiation with and without pTyr pretreatment on the p53-, phosphorylated p53 and the p53 pathway downstream-member p21 status of Y79 cells (fig.15). As a result, irradiation of Y79 cells resulted in stabilization of p53 and up regulation of the p53 target p21. Moreover, pTyr was capable to stabilize p53 in unirradiated Y79 cells and facilitating radiation-induced p21 up-regulation, confirming a modulation of p53 activity by pTyr (Tschulakow et al., 2017), (Chapter 5.4, supplementary fig. 4). As the p53 inactivation in Y79 could not be shown, we decided to test the capability of pTyr to radioprotect Y79 cells directly *in vitro*.

5.3.1.2 Pre-plating and delayed plating limited dilution assay- studies with Y79 cells

To test if pTyr (10mM) will radioprotect Y79 cells *in vitro*, we performed a pre-plating and a delayed plating limited dilution assay after irradiation of Y79 cell cultures with 0 Gy-, 2 Gy- and 5 Gy. No significant radioprotective effect of pTyr could be observed (Chapter 5.4, supplementary fig. 3). Therefore pTyr seemed to fulfill another requirement to be considered for use in radiotherapy of retinoblastoma.

5.3.2 Irradiation studies in our Rb Y79-xenograft nude mouse model

To analyse the possible interference of the application of pTyr with radio therapy *in vivo* we used our newly established Y79 xenograft nude mouse model. We performed radiotherapies of the xenograft-tumours with and without pTyr pretreatment of the mice. We used the same irradiation-schedule as for the irradiations of the Rb+/- mice (fig. 12 C).

5. Results

Twenty seven to 64 days after the radiotherapy, 80% of the eyes of the pTyr pretreated animals started to swell. In the pTyr untreated group only 18% of the eyes were swollen on days 51 to 89. During histological analysis tumours were found in all swollen and unswollen eyes of pTyr pretreated animals (100%) as well as in the swollen eyes of the irradiated but pTyr untreated animals (18%) indicating pTyr-mediated failure of the radiotherapy of the retinoblastoma. These results show that in contrast to the *in vitro* studies pTyr radioprotected the xenograft-Y79 tumours *in vivo* (Tschulakow et al., 2017). To see the detailed version please refer to Chapter 5.4.

5.4 The radioprotector ortho-phospho-L-tyrosine (pTyr) attenuates the side effects of fractionated irradiation in retinoblastoma mouse models but also decreases the local tumour control



Experimental radiobiology

The radioprotector ortho-phospho-L-tyrosine (pTyr) attenuates the side effects of fractionated irradiation in retinoblastoma mouse models but also decreases the local tumour control



Alexander V. Tschulakow^a, Klaus Dittmann^b, Stephan M. Huber^c, Dominik Klumpp^c, Benjamin Stegen^c, Ulrich Schraermeyer^a, H. Peter Rodemann^b, Sylvie Julien-Schraermeyer^{a,*}

^a Division of Experimental Vitreoretinal Surgery, Centre for Ophthalmology; ^b Division of Radiobiology & Molecular Environmental Research, Department of Radiation Oncology; and ^c Department of Radiation Oncology, University of Tuebingen, Germany

ARTICLE INFO

Article history:

Received 6 July 2016

Received in revised form 20 June 2017

Accepted 22 June 2017

Available online 12 July 2017

Keywords:

Retinoblastoma

Radiotherapy

Radioprotector pTyr

Mouse model

In vivo imaging

Histology

ABSTRACT

Background: Radiotherapy (RT) is used to treat retinoblastoma (Rb), the most frequent ocular tumour in children. Besides eradicating the tumour, RT can cause severe side effects including secondary malignancies. This study aimed to define whether the radioprotector ortho-phospho-L-tyrosine (pTyr) prevents RT-induced side effects and affects local tumour control in a *xenograft* and a genetic orthotopic Rb mouse model.

Methods: B6;129-Rb1tm3Tyj/J (Rb^{+/-}) and Y79-Rb cell-*xenografted* nude mice were fractionated external beam irradiated (15 fractions of 5 Gy 6 MV photons during 3 weeks) with or without pTyr pre-treatment (100 mg/kg BW, 16 h prior to each irradiation). One, three, six and nine months after RT, tumour control and RT toxicity were evaluated using *in vivo* imaging and histology. We also analysed pTyr dependant post irradiation cell survival and p53 activity *in vitro*.

Results: *In vitro* pTyr pre-treatment showed no radioprotection on Y79 cells, but led to p53 stabilisation in unirradiated Y79 cells and to a facilitation of radiation-induced p21 up-regulation, confirming a modulation of p53 activity by pTyr. In both mouse models, secondary tumours were undetectable. In Rb^{+/-} mice, pTyr significantly lowered RT-induced greying of the fur, retinal thickness reduction and photoreceptor loss. However, in the *xenografted* Rb model, pTyr considerably decreased RT-mediated tumour control, which was observed in 16 out of 22 control eyes but in none of the 24 pTyr treated eyes.

Conclusions: In Rb^{+/-} mice pTyr significantly prevents RT-induced greying of the fur as well as retinal degeneration. However, since non-irradiated control mice were not used in our study, a formal possibility exists that the effect shown in the retina of Rb^{+/-} mice may be due to ageing of the animals and/or actions of pTyr alone. Unfortunately, as tested in a *xenograft* model, pTyr treatment reduced the control of Rb tumours.

© 2017 Elsevier B.V. All rights reserved. Radiotherapy and Oncology 124 (2017) 462–467

Retinoblastoma (Rb) is the most common intraocular neoplasm of childhood originating in progenitor cells of the developing retina with an estimated incidence of 1/20,000 births [1]. Untreated Rb always leads to death. Rb is closely linked to the inactivation of the retinoblastoma tumour suppressor gene *Rb1*. According to the two-hit hypothesis, both alleles of the *Rb1* tumour suppressor gene must be inactivated to initiate Rb [2].

Deciphering the molecular mechanisms of tumorigenesis allowed the development of genetic Rb mouse models [3–5]. In addition, a BALB nude mouse Rb *xenograft* model has been established by our group [6].

* Corresponding author at: Division of Experimental Vitreoretinal Surgery, Centre for Ophthalmology, Schleichstrasse 12/1, 72076 Tuebingen, Germany.

E-mail address: Sylvie.Julien@med.uni-tuebingen.de (S. Julien-Schraermeyer).

New imaging techniques have improved diagnosis, understanding and management of Rb [7–9]. Moreover, the introduction of optical coherence tomography (OCT) in diagnosis and monitoring of the therapy of Rb patients allows a detailed monitoring of tumour-growth in all tissues of the eye [10]. *In vivo* methods like scanning laser ophthalmoscopy combined with OCT (SLO/OCT) have been successfully adapted for detection and characterisation of tumours in mouse models by our group [6] and others [11].

For advanced Rb with high risk of metastasis and low probability of vision preservation, enucleation is still the only treatment [12]. Rb responds very well to radiotherapy (RT) and external beam RT was the first established Rb therapy preserving globe and vision. However, it enhances the risk of secondary malignancies, in particular in patients with hereditary Rb [13]. The incidence of secondary

tumours 50 years after Rb radiotherapy is 38% [14]. Therefore, other therapy approaches like cryo-, thermo-, chemotherapy and chemosurgery meanwhile have been established as first line treatments [15,16]. Nevertheless, RT is considered as the last option prior to enucleation for patients with large tumours or as second line treatment for patients with recurrent Rb. Approximately 80% of the Rb patients are diagnosed at a locally advanced stage, and local control by chemotherapy fails in more than two-thirds of advanced Rb [17].

Strategies which could reduce the side effects of RT are currently the focus of extensive scientific investigations. High-tech RT like proton beam RT [18], intensity-modulated and fractionated stereotactic RT [19] enable precise radiation delivery to the tumour and spare the healthy tissue, thereby improving the efficacy/toxicity ratio. The use of radioprotectors before and mitigators after RT is a further approach to reduce side effects of the RT [20]. The specificity for the non-tumoural tissues is a prerequisite for the use of such drugs during RT of Rb.

In vitro and *in vivo* studies on the radioprotective effect of ortho-phospho-L-tyrosine (pTyr) showed significant differences between non-tumoural and tumoural cells with p 53 dysfunction [21–23].

The present study aimed by using a genetic knock out- and a xenograft Rb mouse model to analyse the potency of pTyr to prevent normal tissue damage and to define whether pTyr interferes with the local Rb control mediated by fractionated RT.

Materials and methods

For our *in vitro* studies Y79 cells were cultured as recommended by the American Type Culture Collection (ATCC), where the cells were purchased. 16 h before IR pTyr (10 μ M) or vehicle was added to the culture medium.

Limited dilution assays

For the preplating assay the cells were put directly in 96 wells plates for IR, incubation and readout for the delayed plating assay the cells were irradiated in the culture-flasks and put in 96 wells plates for incubation and readout after IR. The cells were irradiated with 0 Gy, 2 Gy and 5 Gy. The readout was performed after two weeks of incubation using a microplate spectrophotometer.

Western blot

A sample of unirradiated cells was analysed immediately after 16 h of pTyr treatment (co). The other samples were irradiated with 4 Gy. 1, 6, 24 h after IR cells were lysed, and proteins were resolved by SDS-PAGE. Western blotting was performed according to standard procedures. All primary antibodies were diluted 1:1000 and purchased from the following sources: anti-TP53 (Cell Signaling, clone 7F5), anti-phospho-TP53 (Ser15) (Cell Signaling, clone 16G8), anti-p21 Waf1/Cip1 (Cell Signaling, clone 12D1) and anti-Actin (Sigma, A2066). Quantification was performed with the LI-COR detection system (LI-COR, Odyssey Fc).

Mouse models

B6;129-Rb1tm3Tyj/J Rb^{+/-} mice ($n = 24$, 5–6 weeks old, Jackson's lab, Bar Harbor, USA, having a mutation in one of the Rb1-gene alleles [24] were used as a model for patients with hereditary Rb, who having a genetic defect in the homologue human gene Rb-1 have a higher risk of secondary malignancies after RT [13]. In addition, BALB nude mice ($n = 24$, 6 weeks old, Janvier Labs, Le Genest-Saint-Isle, France) were xenotransplanted intravitreally with human Y79 Rb tumour cells as described in [6]. All animal experiments were performed in accordance with the German Ani-

mal Protection Law and approved by the local authorities (Regierungspraesidium Tuebingen AK 6/12).

Radiation protocol

Fractionated external beam radiation (IR) of the eyes was performed under isoflurane anaesthesia applying 9 fractions of 5 Gy within 3 weeks (Fig. 1) by the use of a linear accelerator (LINAC SL25, Phillips, dose rate of 4 Gy/min). The IR- and the pTyr administration schedule were chosen in consideration of the results of our group [21]. In particular, both eyes were irradiated simultaneously with a single field technique by the use of 6 MV photons that were directed from lateral to an area of about 4×4 mm (50% isodose) [25] supplementary appendix Fig. 1A, B). The dose distribution as determined in a mouse phantom by film dosimetry is shown in (supplementary appendix Fig. 1C). Prior to each radiation fraction (16 h) mice received i.p. injections of vehicle or pTyr (0 or 100 mg/kg BW in PBS).

The animals were examined at 2, 12 and 24 h after RT and then daily. Clinical findings regarding the presence of secondary tumours or other side effects were recorded.

In vivo and *ex vivo* analysis of the mice after IR

The eyes of each 3 of pTyr pre-treated and 3 pTyr untreated mice of the immune-compromised mice carrying retinoblastoma xenografts and of the Rb^{+/-} mice were assessed in dependence of pTyr treatment 1, 3, 6 and 9 months after irradiation for radiation toxicity and tumour development by SLO/OCT and histology (Fig. 1).

Analysis of the fur of Rb^{+/-} mice

Directly after SLO/OCT analysis and similar to the method described in [26], hairs were plucked from the area between the eyes/forehead (supplementary appendix Fig. 2A). Using a binocular microscope (EXACTA+OPTECH, Muenchen, Germany), the hairs were manually sorted into three categories: black, white, and grey. A total of 100 to 150 hairs were counted for each mouse.

In vivo analysis using SLO/OCT

One, three, six and nine months after irradiation, groups of three pTyr pre-treated and -untreated mice were analysed using a Spectralis™ HRA+OCT (Heidelberg Engineering, Heidelberg, Germany) SLO/OCT device. The whole procedure was performed as described in [27] and the mice were anaesthetized and prepared as described in [6].

For a detailed analysis of the changes of the retinal thickness a custom-made program (multimodalmapper) was used which automatically measures the retina thickness on the OCT images (supplementary appendix Fig. 2B).

Histological analysis

Upon sacrifice of the mice by cervical dislocation, eyes, brain, lungs, heart, kidney, spleen, and liver were resected and histologically analysed as described in [6]. As a measure of photoreceptor damage, photoreceptor nuclei were counted at 15 distinct areas near to the optical nerve in each eye (supplementary appendix Fig. 2C).

Statistics

Data are mean \pm SD. Statistical analysis was performed using Student's *t*-test or log rank test where appropriate.

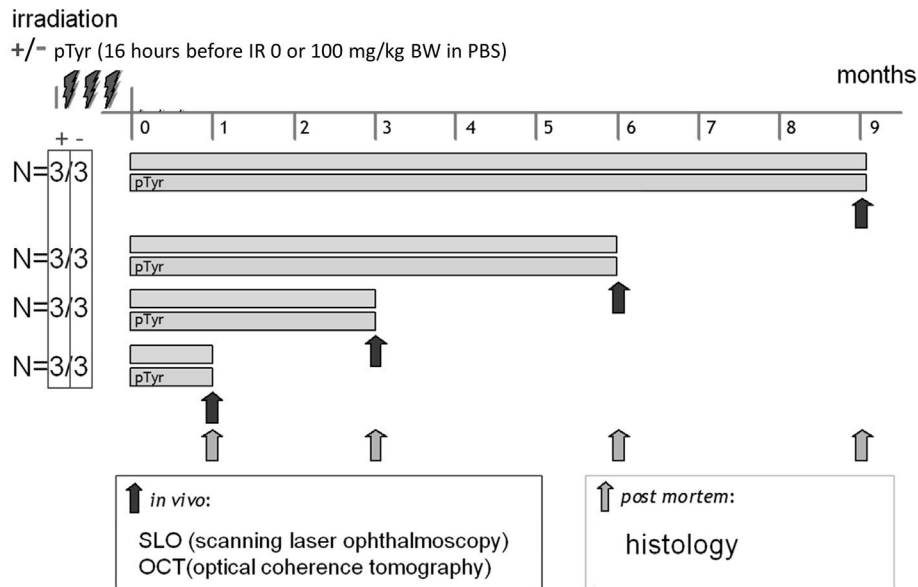


Fig. 1. Time schedule of the irradiation and pTyr treatment protocol and the *in vivo* and *ex vivo* analysis. All eyes of the immune-compromised mice carrying retinoblastoma xenografts and of the $Rb^{+/-}$ mice were irradiated over a period of 3 weeks 3 times a week with a dose of 5 Gy per fraction with (+) or without (-) pTyr pre-treatment (16 h before IR 0 or 100 mg/kg BW in PBS). Radiation toxicity and tumour development were assessed in dependence of pTyr treatment 1, 3, 6 and 9 months after irradiation in 3 mice per group by SLO/OCT and histology.

Results

Post irradiation cell survival and p53 activity *in vitro*

Under *in vitro* conditions pTyr treated and irradiated Y79 cells showed no significant radioprotection when tested in pre- and delayed plating limited dilution assays (supplementary appendix Fig. 3). However, when compared to vehicle-treated cells, in non-irradiated and irradiated Y79 cells, pre-treatment with pTyr resulted in an increased stabilisation of the p53 protein (TP53) and its phosphorylation at Ser-residue-15. As a consequence of p53 activity in irradiated cells, the expression of p21 as downstream target of p53 was substantially stimulated by pTyr treatment (supplementary appendix Fig. 4).

$Rb^{+/-}$ mice

Five weeks after the last irradiation, a greying of the fur in the irradiated area began in the pTyr untreated mice. The same change in fur-pigmentation started eight weeks after irradiation in the pTyr treated mice and was significantly reduced in the pTyr treated mice six and nine months after RT (Fig. 2A).

Nine months after the end of the irradiation procedure, all mice developed a cataract but the opacity of the lenses was still slight enough to allow an OCT-analysis. As a result, 3, 6 and 9 months after irradiation retinal thickness was significantly reduced in the pTyr untreated group compared to the pTyr treated one ($p < 0.05$ 3 months, $p < 0.001$ 6 months and $p < 0.0001$ 9 months after irradiation) (Fig. 2B).

Histological analysis of the retina showed a significantly increased photoreceptor loss in the pTyr untreated group vs. the pTyr treated one ($p < 0.001$, 3 months and $p < 0.0001$ 6 and 9 months after irradiation) (Fig. 2C). Furthermore, we screened tissues in and near the irradiated area, like skull, skin, brain for induced tumours and metastasis. In kidneys, lung, heart, liver and spleen the appearance of distant metastasis was evaluated by analysing haematoxylin and eosin stained cross sections of these tissues. No RT-induced tumours or metastasis were found in any of the analysed organs.

Xenografted mice

Three weeks after intravitreal Y79 tumour challenge, 38 of 42 analysed eyes developed tumours at an early stage as detected by SLO/OCT. Four tumour-developing eyes were swollen. These eyes could not be analysed *in vivo* (Table 1). Initial swelling of the four eyes disappeared during the first two weeks of RT suggestive of a RT-mediated tumour down-sizing. Importantly, in the pTyr treated group swelling of 12 eyes newly occurred on days 27 to 64 after RT while in the pTyr untreated group only three mice developed a swollen eye on days 51 to 89 (Table 2) strongly suggesting radioprotection of the Y79 Rb tumour cells by pTyr (Table 2). Three months after RT, all other eyes developed a severe cataract making further *in vivo* analysis impossible.

During histological analysis tumours were found in all swollen and unswollen eyes of pTyr treated animals as well as in the three swollen eyes but in non of the unswollen eyes of the irradiated control animals (Table 2 and Fig. 3) indicating pTyr-mediated failure of Rb tumour eradication by RT. In all investigated animals, no distant metastases were found.

Discussion

Most radioprotectors are reactive oxygen species scavengers reducing the cellular damage caused by irradiation [28–31]. pTyr, in contrast, induces in irradiated cells [21] accumulation of EGFR in the nucleus [32] which has been proposed to enhance DNA repair and chromatin remodelling [33] and to induce a metabolic switch from oxidative respiration to lactic acid fermentation [34].

Importantly, pTyr has been shown to radioprotect predominantly normal cells with wild type p53 genotype [21]. Mutations in the p53 gene are infrequent in Rb and Y79 cells have been demonstrated to express p53 protein [35,36]. On the other hand Y79 cells do not express functional RB1 protein, which reportedly prevents E3 ubiquitin-protein ligase MDM2 from targeting p53 [37] which, e.g., rescues the apoptotic activity of p53. However, Y79 cells have been shown to overexpress the p53 inhibitors MDMX [38] and MDM2 [39]. Additionally in $Rb^{-/-}$ cells a downreg-

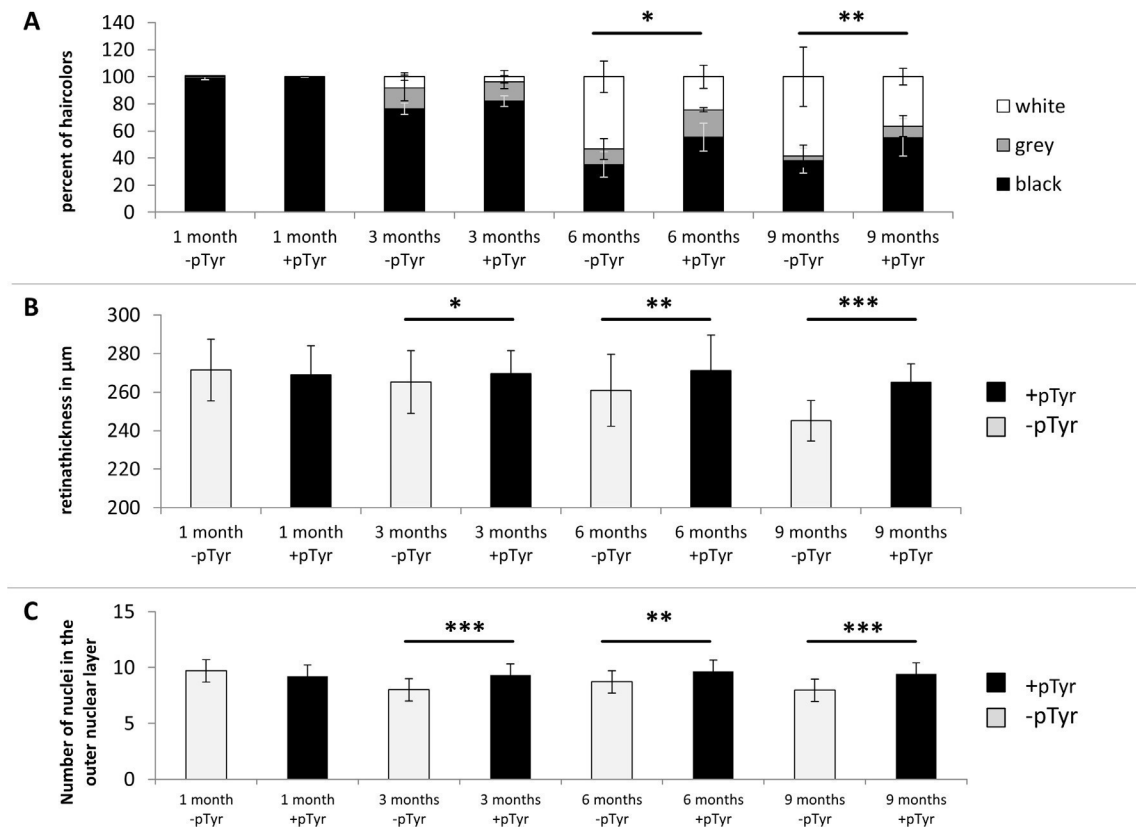


Fig. 2. pTyr effect on the radiation-associated toxicity in normal tissue. (A) Mean percentage (\pm SD, $n = 24$) of black, grey and white hairs of the irradiated skin of pTyr or vehicle-treated $Rb^{+/-}$ mice before (control), 1, 3, and 9 month after irradiation. * and ** indicate $p \leq 0.05$ and $p \leq 0.001$, respectively (Student's *t*-test). For the classification of hair colours hairs were plucked from the area between the eyes/forehead directly after the SLO/OCT analysis and were manually sorted into three categories: black, white, and grey. A total of 100 to 150 hairs were counted per mouse. (B) Mean (\pm SD, $n = 24$) retinal thickness as analysed by OCT applying 30 automatised measurements using multimodal mapper-software. Retinal thickness was determined 1, 3, and 9 months after irradiation in pTyr- or vehicle treated $Rb^{+/-}$ mice. *, **, and *** indicate $p \leq 0.05$, $p \leq 0.001$, and $p \leq 0.0001$, respectively (Student's *t*-test). (C) Mean (\pm SD, $n = 24$) number of nuclei outer nuclear layer of the retina. For this histological analysis, photoreceptor nuclei rows of pTyr- or vehicle-treated $Rb^{+/-}$ mice were manually counted 1, 3, and 9 months after irradiation. ** and *** indicate $p \leq 0.001$ and $p \leq 0.0001$, respectively (Student's *t*-test).

Table 1

Shows the number of swollen eyes, eyes with tumours at an early stage of development and eyes where no tumour was detected three weeks after the injection of the human Y79 Rb cells. The table shows as well how the eyes were split into the groups, which were irradiated with pTyr pre-treatment (group 1: +pTyr-group, $n = 12$ mice (24 eyes)) and without pTyr pre-treatment (group 2: -pTyr, $n = 11$ mice (22 eyes)).

| Eyes | No tumour detected | Tumour at early stage of development | Swollen eye |
|---------------|--------------------|--------------------------------------|-------------|
| +pTyr group 1 | 2/24 | 20/24 | 2/24 |
| -pTyr group 2 | 2/22 | 18/22 | 2/22 |

ulation of the MDM2 inactivator p14 ARF [40] and hypermethylation in the p53 promoter-region [41] were found, suggesting that Rb and particularly Y79 cells might have an impaired p53 function [42].

Despite functional Rb1 deficiency and MDM2/MDMX overexpression and downregulated p14 ARF expression, irradiation of

Y79 cells resulted in the present study in stabilization of p53 and upregulation of the p53 target p21 as demonstrated by Western blotting (supplementary appendix Fig. 3A). Moreover, pTyr was capable to stabilize p53 in unirradiated Y79 cells and to facilitate radiation-induced p21 up-regulation confirming a modulation of p53 activity by pTyr (supplementary appendix Fig. 3A). Since in some p53 wild type cells, such as FSAll sarcoma, pTyr has been demonstrated, not to act radioprotective [21–23] we tested the effect of pTyr (10 μ M) in 0 Gy-, 2 Gy- and 5 Gy-irradiated Y79 cells *in vitro* by pre-plating and delayed plating limited dilution assays. No radioprotective effect by pTyr could be observed (supplementary appendix Fig. 3).

In the present study, the radiosensitivity of the eyes differed between the two mouse models. Cataract formation started much earlier in the xenograft nude mice as compared to the $Rb^{+/-}$ mice. Three months after RT, all nude mice already have developed severe cataract, which made *in vivo* OCT analysis impossible. In the $Rb^{+/-}$ mice, in contrast, the cataract formation did not start earlier than six months after IR and the opacity of the lenses, even nine months after IR, was still slight enough to allow an OCT analysis.

Table 2

shows the results of the histological analysis of the Rb xenograft nude mouse eyes after RT (group 1: +pTyr-group; $n = 12$ mice (24 eyes)) and without pTyr pre-treatment (group 2: -pTyr, $n = 11$ mice (22 eyes)).

| Eyes | Not analysable | No tumour detected | Tumour at early stage of development | Tumour in swollen eye |
|-------|----------------|--------------------|--------------------------------------|-----------------------|
| +pTyr | 5/24 | 0 | 3/24 | 16/24 |
| -pTyr | 2/22 | 16/22 | 1/22 | 3/22 |

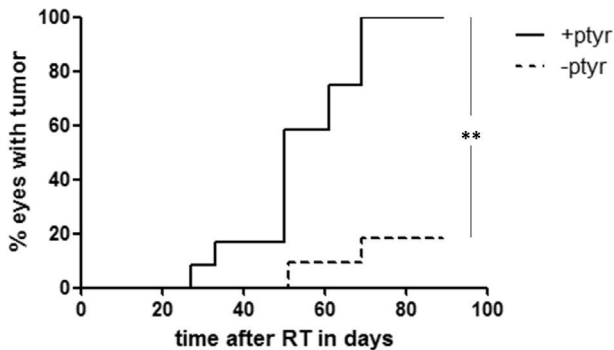


Fig. 3. Effect of pTyr on tumour recurrence after irradiation in Rb-*xenografted* eyes. Cumulative percentage of irradiated eyes with Rb recurrence in pTyr (solid line) and vehicle treated (dashed line) mice. Data represent 46 Rb-*xenografted* eyes of 23 mice. ** indicates $p < 0.001$ (log rank test).

Radiation irreversibly impairs the self-renewal capacity of follicular melanocyte stem cells resulting in hair greying of black mice [26,43]. In our study, pTyr reduced the greying of the fur in Rb^{+/-} mice after IR. Moreover, in the rodent retina, photoreceptors are the most radiosensitive cells [44]. The inverted heterochromatin organization, containing a single large chromocentre in the middle of the nucleus, impairs double-strand break repair in the photoreceptors [45]. In our Rb^{+/-} mouse model, pTyr significantly reduced the photoreceptor loss observed after IR. pTyr, in contrast, failed to protect in both mouse models the lenses which are assumed to be the most radiosensitive tissue of the eye [46]. However, there was a clear difference between the two mouse models used. The cataract formation started much earlier in the nude *xenograft* mice. Indeed, three months after RT all mice already had severe cataracts. In the Rb^{+/-} mice, the cataract formation started not earlier than six months after RT and the opacity of the lenses, even nine months after IR, was still slight enough to allow an OCT analysis.

Combined, our data indicate a radioprotective function of pTyr *in vivo* in follicular melanocyte stem cells of the hair follicles and photoreceptors of the retina.

Unexpectedly, pTyr *in vivo* also radioprotected the Rb Y79 *xenograft* contraindicating its use for radioprotection of the eyes during RT of Rb patients, although in our *in vitro* studies pTyr did not show a significant radioprotection of Y79 cells based on the results of the limited dilution assay. The reason for the different outcome for the *in vitro/vivo* studies might be of technical nature. For the limited dilution assays, a single cell solution is needed, but normally the Y79 cells in solution grow in clusters and even show some differentiation. Therefore, the behaviour of Y79 cells might be different concerning micromilieu and grow conditions in single cell solution, in clusters or as a solid tumour-mass, causing the different outcome.

In neither mouse model, radiation-associated secondary tumours were observed in pTyr treated as well as pTyr untreated animals. RT-induced secondary tumours in Rb patients are reported in most cases not to appear earlier than 30 years after treatment [47]. In the present study, the maximum life-span of the used mouse models is about 18 months; therefore, we cannot exclude that this life-span is too short for analyses of RT-induced secondary tumours. In addition, Rb^{+/-} mice did not develop Rb, suggesting that further knockouts of other genes of the Rb gene family like p107 or p130 or an additional knockout of p53 are required to establish a genetic Rb model [3–5]. Moreover, to our knowledge, studies investigating the occurrence of second cancers were not performed in this mouse model yet. Since non-irradiated control mice were not used in our study, a formal possibility exists

that the effect shown in the retina of Rb^{+/-} mice may be due to ageing of the animals and/or actions of pTyr alone.

To conclude, pTyr acts as a potent radioprotector preventing radiation-induced normal tissue toxicity/alterations in Rb^{+/-} mice. However, based on the tumour control data presented here for Y79 Rb tumour *xenografts*, pTyr treatment seems to be contraindicated for RT, at least of Rb p53 wt tumours, but it could be interesting for RT of other tumour types presenting a p53 dysfunction.

Conflict of interest

None.

Acknowledgments

This work was financially supported by the Deutsche Kinderkrebsstiftung – Germany (Project No. DKS 2012.08).

The authors thank Monika Rittgarn for technical assistance and Judith Birch for proofreading of the manuscript.

Appendix A. Supplementary data

Supplementary data associated with this article can be found, in the online version, at <http://dx.doi.org/10.1016/j.radonc.2017.06.023>.

References

- [1] Aerts I, Lumbroso-Le Rouic L, Gauthier-Villars M, Brisse H, Doz F, Desjardins L. Retinoblastoma. *Orphanet J Rare Dis* 2006;1:31.
- [2] Knudson Jr AG. Mutation and cancer: statistical study of retinoblastoma. *Proc Natl Acad Sci U S A* 1971;68:820–3.
- [3] Villegas VM, Hess DJ, Wildner A, Gold AS, Murray TG. Retinoblastoma. *Curr Opin Ophthalmol* 2013;24:581–8.
- [4] Dyer MA, Rodriguez-Galindo C, Wilson MW. Use of preclinical models to improve treatment of retinoblastoma. *PLoS Med* 2005;2:e332.
- [5] Macpherson D. Insights from mouse models into human retinoblastoma. *Cell Div* 2008;3:9.
- [6] Tschulakow AV, Schraermeyer U, Rodemann HP, Julien-Schraermeyer S. Establishment of a novel retinoblastoma (Rb) nude mouse model by intravitreal injection of human Rb Y79 cells – comparison of *in vivo* analysis versus histological follow up. *Biol Open* 2016;5:1625–30.
- [7] de Graaf P, Goricke S, Rodjan F, Galluzzi P, Maeder P, Castelijns JA, et al. Guidelines for imaging retinoblastoma: imaging principles and MRI standardization. *Pediatr Radiol* 2012;42:2–14.
- [8] Bianciotto C, Shields CL, Iturralde JC, Sarici A, Jabbour P, Shields JA. Fluorescein angiographic findings after intra-arterial chemotherapy for retinoblastoma. *Ophthalmology* 2012;119:843–9.
- [9] Ramasubramanian A, Shields CL, Mellen PL, Haji S, Harmon SA, Vemuganti GK, et al. Autofluorescence of treated retinoblastoma. *J AAPOS* 2011;15:167–72.
- [10] Rootman DB, Gonzalez E, Mallipatna A, Vandenhoven C, Hampton L, Dimaras H, et al. Hand-held high-resolution spectral domain optical coherence tomography in retinoblastoma: clinical and morphologic considerations. *Br J Ophthalmol* 2013;97:59–65.
- [11] Wenzel AA, O'Hare MN, Shadmand M, Corson TW. Optical coherence tomography enables imaging of tumor initiation in the TAG-RB mouse model of retinoblastoma. *Mol Vis* 2015;21:515–22.
- [12] Jehanne M, Brisse H, Gauthier-Villars M, Lumbroso-Le Rouic L, Freneaux P, Aerts I. Retinoblastoma: recent advances. *Bull Cancer* 2014;101:380–7.
- [13] Abramson DH, Frank CM. Second nonocular tumors in survivors of bilateral retinoblastoma: a possible age effect on radiation-related risk. *Ophthalmology* 1998;105:573–9 [discussion 9–80].
- [14] Kleinerman RA, Tucker MA, Tarone RE, Abramson DH, Seddon JM, Stovall M, et al. Risk of new cancers after radiotherapy in long-term survivors of retinoblastoma: an extended follow-up. *J Clin Oncol* 2005;23:2272–9.
- [15] Ghassemi F, Shields CL. Intravitreal melphalan for refractory or recurrent vitreous seeding from retinoblastoma. *Arch Ophthalmol* 2012;130:1268–71.
- [16] Temming P, Lohmann D, Bornfeld N, Sauerwein W, Goericke SL, Eggert A. Current concepts for diagnosis and treatment of retinoblastoma in Germany: aiming for safe tumor control and vision preservation. *Klin Padiatr* 2012;224:339–47.
- [17] Kim JY, Park Y. Treatment of retinoblastoma: the role of external beam radiotherapy. *Yonsei Med J* 2015;56:1478–91.
- [18] Mouw KW, Sethi RV, Yeap BY, MacDonald SM, Chen YL, Tarbell NJ, et al. Proton radiation therapy for the treatment of retinoblastoma. *Int J Radiat Oncol Biol Phys* 2014;90:863–9.

- [19] Combs SE, Behnisch W, Kulozik AE, Huber PE, Debus J, Schulz-Ertner D. Intensity Modulated Radiotherapy (IMRT) and Fractionated Stereotactic Radiotherapy (FSRT) for children with head-and-neck-rhabdomyosarcoma. *BMC Cancer* 2007;7:177.
- [20] Bourcier C, Levy A, Vozenin MC, Deutsch E. Pharmacological strategies to spare normal tissues from radiation damage: useless or overlooked therapeutics? *Cancer Metastasis Rev* 2012;31:699–712.
- [21] Dittmann KH, Mayer C, Rodemann HP. O-phospho-L-tyrosine protects TP53 wild-type cells against ionizing radiation. *Int J Cancer* 2001;96(Suppl.):1–6.
- [22] Dittmann KH, Gueven N, Mayer C, Rodemann H-P. Characterization of the amino acids essential for the photo- and radioprotective effects of a Bowman-Birk protease inhibitor-derived nonapeptide. *Protein Eng* 2001;14:157–60.
- [23] Dittmann K, Toulany M, Classen J, Heinrich V, Milas L, Rodemann HP. Selective radioprotection of normal tissues by Bowman-birk proteinase inhibitor (BBI) in mice. *Strahlentherapie und Onkologie: Organ der Deutschen Rontgengesellschaft [et al.]*. 2005;181:191–6.
- [24] Jacks T, Fazeli A, Schmitt EM, Bronson RT, Goodell MA, Weinberg RA. Effects of an Rb mutation in the mouse. *Nature* 1992;359:295–300.
- [25] Edalat L, Stegen B, Klumpp L, Haehl E, Schilbach K, Lukowski R, et al. BK K + channel blockade inhibits radiation-induced migration/brain infiltration of glioblastoma cells. *Oncotarget* 2016;7:14259–78.
- [26] Aoki H, Hara A, Motohashi T, Kunisada T. Protective effect of Kit signaling for melanocyte stem cells against radiation-induced genotoxic stress. *J Investigat Dermatol* 2011;131:1906–15.
- [27] Huber G, Beck SC, Grimm C, Sahaboglu-Tekgoz A, Paquet-Durand F, Wenzel A, et al. Spectral domain optical coherence tomography in mouse models of retinal degeneration. *Investigat Ophthalmol Visual Sci* 2009;50:5888–95.
- [28] Kuntic VS, Stankovic MB, Vujic ZB, Brboric JS, Uskokovic-Markovic SM. Radioprotectors – the evergreen topic. *Chem Biodiver* 2013;10:1791–803.
- [29] Rodriguez SD, Brar RK, Drake LL, Drumm HE, Price DP, Hammond JI, et al. The effect of the radio-protective agents ethanol, trimethylglycine, and beer on survival of X-ray-sterilized male *Aedes aegypti*. *Parasites Vectors* 2013;6:211.
- [30] Ashwood-Smith MJ. Radioprotective and cryoprotective properties of dimethyl sulfoxide in cellular systems. *Ann N Y Acad Sci* 1967;141:45–62.
- [31] Yuhas JM. Biological factors affecting the radioprotective efficiency of S-2-[2-aminopropylamino] ethylphosphorothioic acid (WR-2721). LD50(3)) doses. *Radiat Res* 1970;44:621–8.
- [32] Dittmann K, Mayer C, Wanner G, Kehlbach R, Rodemann HP. The radioprotector O-phospho-tyrosine stimulates DNA-repair via epidermal growth factor receptor- and DNA-dependent kinase phosphorylation. *Radiotherap Oncol* 2007;84:328–34.
- [33] Dittmann K, Mayer C, Rodemann HP, Huber SM. EGFR cooperates with glucose transporter SGLT1 to enable chromatin remodeling in response to ionizing radiation. *Radiotherap Oncol* 2013;107:247–51.
- [34] Dittmann K, Mayer C, Paasch A, Huber S, Fehrenbacher B, Schaller M, et al. Nuclear EGFR renders cells radio-resistant by binding mRNA species and triggering a metabolic switch to increase lactate production. *Radiotherap Oncol* 2015;116:431–7.
- [35] Kondo Y, Kondo S, Liu J, Haqqi T, Barnett GH, Barna BP. Involvement of p53 and WAF1/CIP1 in gamma-irradiation-induced apoptosis of retinoblastoma cells. *Exp Cell Res* 1997;236:51–6.
- [36] Lee BJ, Kim JH, Jo DH, Kim KW, Yu YS, Kim JH. Nuclear expression of p53 in mature tumor endothelium of retinoblastoma. *Oncol Rep* 2014;32:801–7.
- [37] Hsieh JK, Chan FS, O'Connor DJ, Mittnacht S, Zhong S, Lu X. RB regulates the stability and the apoptotic function of p53 via MDM2. *Mol Cell* 1999;3:181–93.
- [38] Sherr CJ, McCormick F. The RB and p53 pathways in cancer. *Cancer Cell* 2002;2:103–12.
- [39] Hu B, Gilkes DM, Chen J. Efficient p53 activation and apoptosis by simultaneous disruption of binding to MDM2 and MDMX. *Cancer Res* 2007;67:8810–7.
- [40] To KH, Pajovic S, Gallie BL, Theriault BL. Regulation of p14ARF expression by miR-24: a potential mechanism compromising the p53 response during retinoblastoma development. *BMC Cancer* 2012;12:69.
- [41] Livide G, Epistolato MC, Amenduni M, Disciglio V, Marozza A, Mencarelli MA, et al. Epigenetic and copy number variation analysis in retinoblastoma by MS-MLPA. *Pathol Oncol Res: POR* 2012;18:703–12.
- [42] Laurie NA, Donovan SL, Shih CS, Zhang J, Mills N, Fuller C, et al. Inactivation of the p53 pathway in retinoblastoma. *Nature* 2006;444:61–6.
- [43] Boyland E, Sargent S. The local greying of hair in mice treated with x rays and radiomimetic drugs. *Br J Cancer* 1951;5:433–40.
- [44] Amoaku WM, Mahon GJ, Gardiner TA, Frew L, Archer DB. Late ultrastructural changes in the retina of the rat following low-dose X-irradiation. *Graefes archive for clinical and experimental ophthalmology = Albrecht von Graefes Archiv fur klinische und experimentelle Ophthalmologie*. 1992;230:569–74.
- [45] Frohns A, Frohns F, Naumann SC, Layer PG, Loblrich M. Inefficient double-strand break repair in murine rod photoreceptors with inverted heterochromatin organization. *Curr Biol: CB* 2014;24:1080–90.
- [46] Brown NP. The lens is more sensitive to radiation than we had believed. *Br J Ophthalmol* 1997;81:257.
- [47] Marees T, van Leeuwen FE, de Boer MR, Imhof SM, Ringens PJ, Moll AC. Cancer mortality in long-term survivors of retinoblastoma. *Eur J Cancer* 2009;45:3245–53.

SUPPLEMENTARY APPENDIX

FIGURES

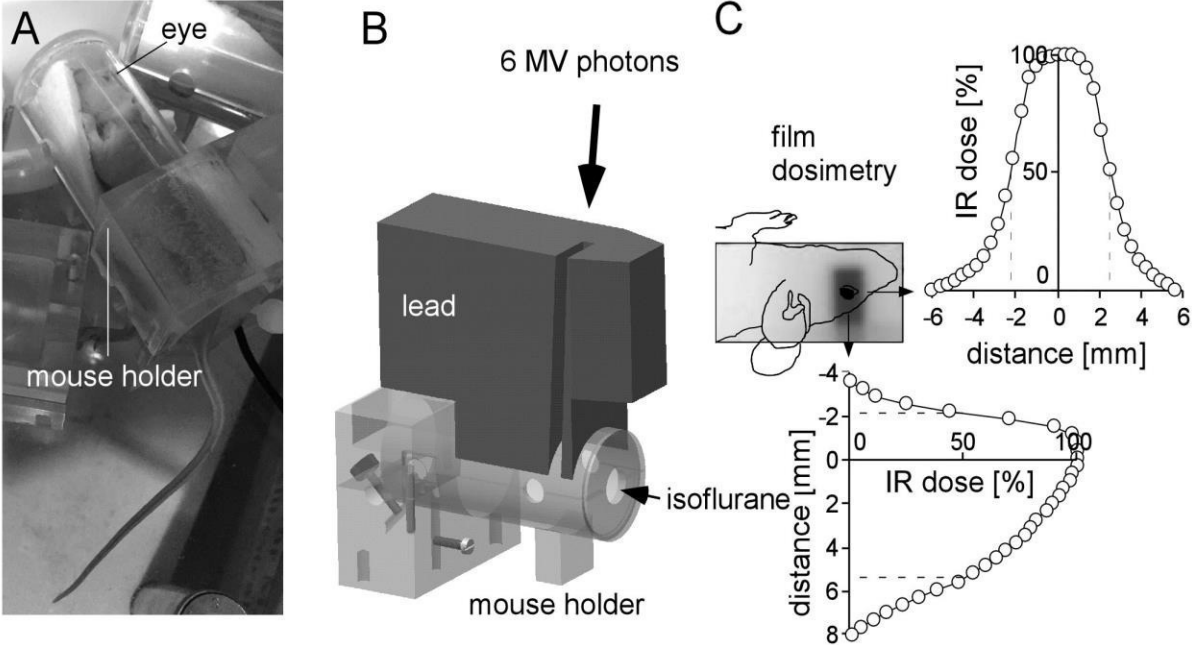
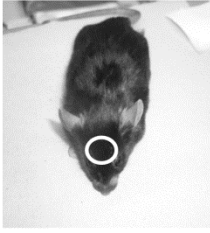


Figure 1:(A) mouse in the mouse fixation unit (B) scheme of the mouse holder with the lead shield s, (C) IR dose distribution as determined in a mouse phantom by film dosimetry [25].

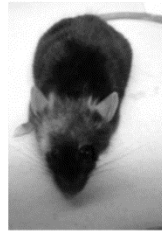
-p-Tyr



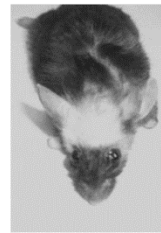
Not irradiated
Rb+/-
mouse: circle
- area of
hair-
sampling



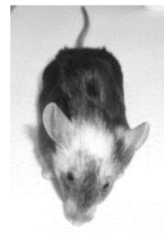
1 month after IR



3 months after IR

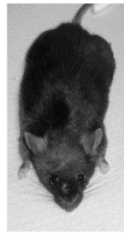


6 months after IR

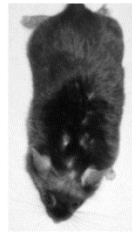


9 months after IR

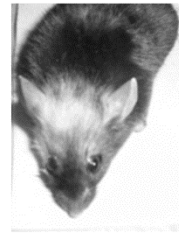
+p-Tyr



1 month after IR



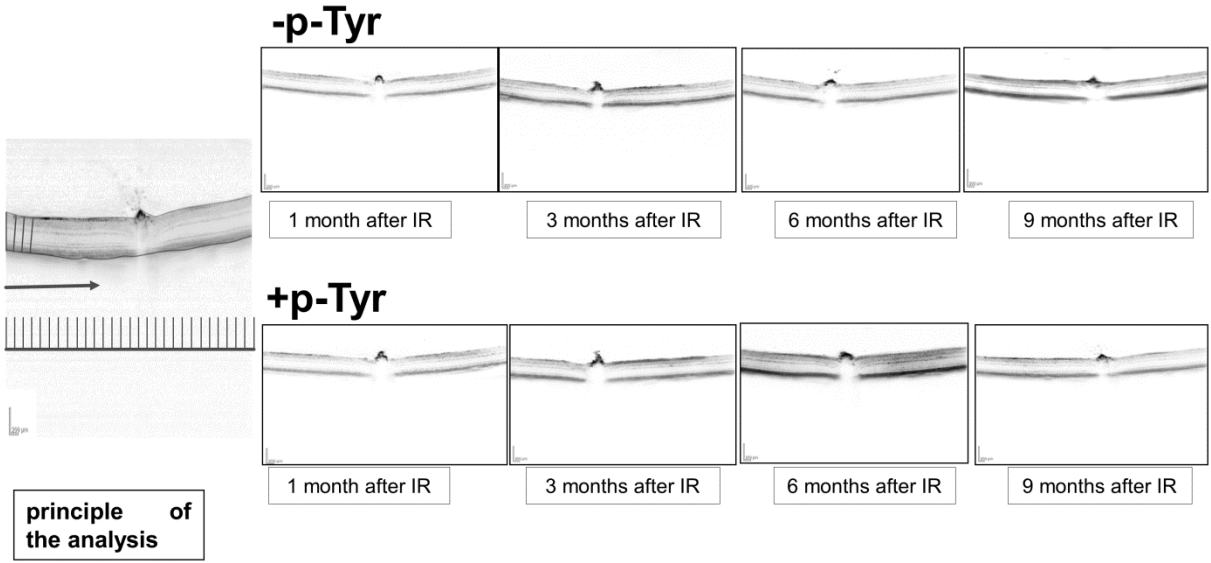
3 months after IR



6 months after IR



9 months after IR



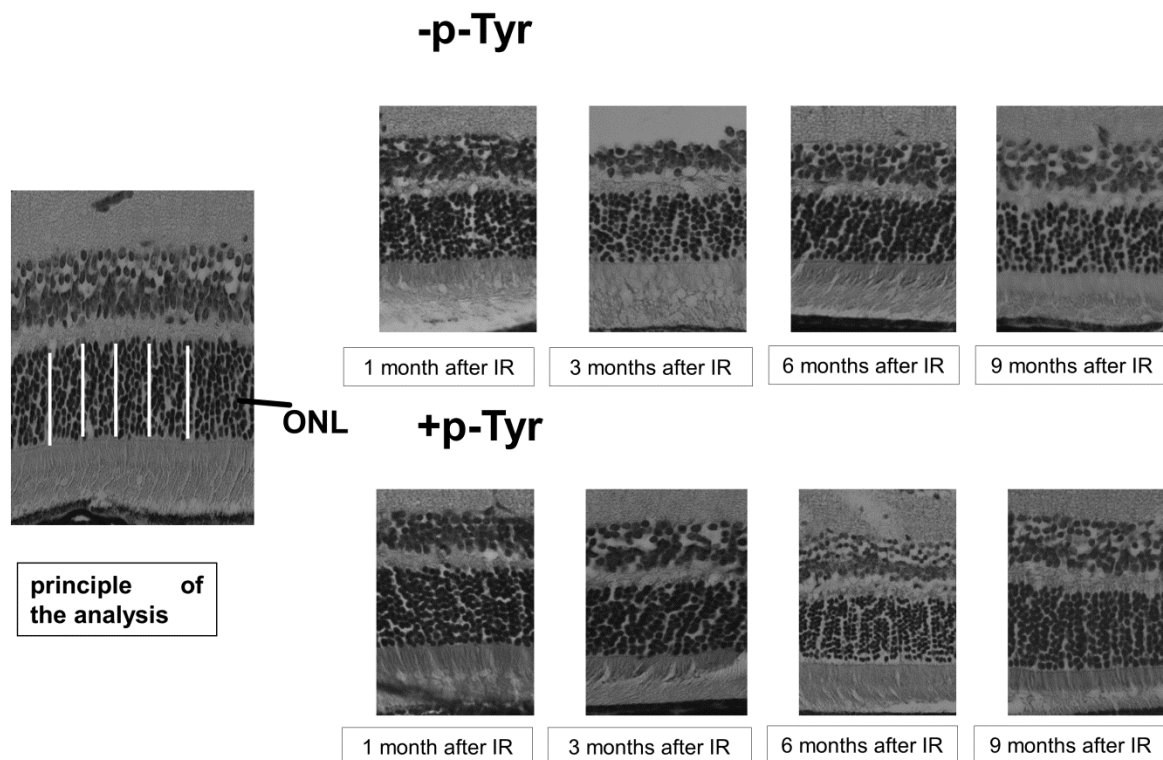


Figure 2: (A) For the classification of hair colors, the hairs were plucked from the area between the eyes/forehead (circle) after the SLO/OCT analysis and were manually sorted into three categories: black, white, and gray. A total of 100 to 150 hairs were counted in each tested mouse. Representative images of pTyr pretreated and not pTyr pretreated mice for each time point of analysis are presented. (B) principle of the analysis of the OCT images of the retina with the MultiModalMapper-software: the retina thickness was automatically measured at each of the 30 points shown on the scale at the bottom of the image, here shown on an image of a not irradiated Rb^{+/-} mouse. Representative OCT scans of the retina of pTyr pretreated and not pTyr pretreated mice for each time point of analysis are presented. (C) principle of the analysis of the histological slices of the retina: the outer nuclei-layers (ONL) were manually counted on representative slides, here shown on an image of a not irradiated Rb^{+/-} mouse. The mean/standard deviation of 45 counts for each time point and condition were used for statistical analysis. Representative images of histological slides of the retina of pTyr pretreated and not pTyr pretreated mice for each time point of analysis are presented.

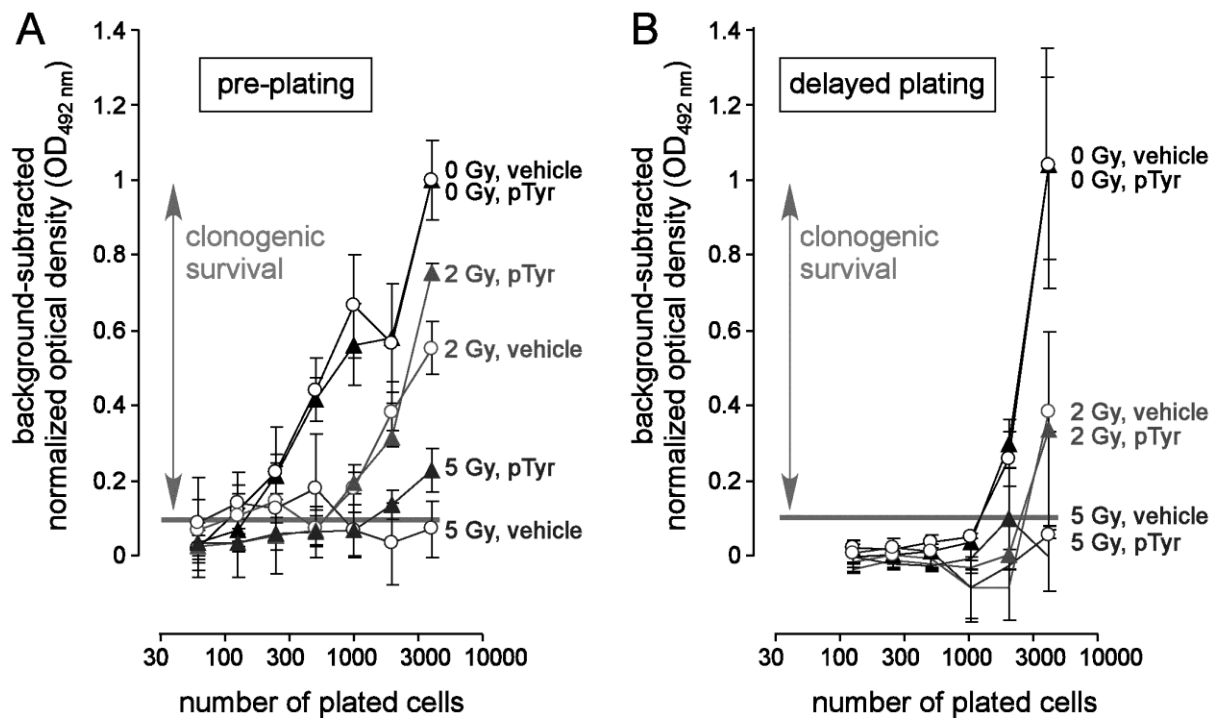


Figure 3: Results of a preplating (A) and delayed plating (B) limited dilution assay of pTyr pre-treated (16 hours before IR, 10 μ M) (\blacktriangle) and untreated (o) Y79 cells after irradiation with 0 Gy, 2 Gy and 5 Gy. No significant differences between pTyr treated and untreated cells were found.

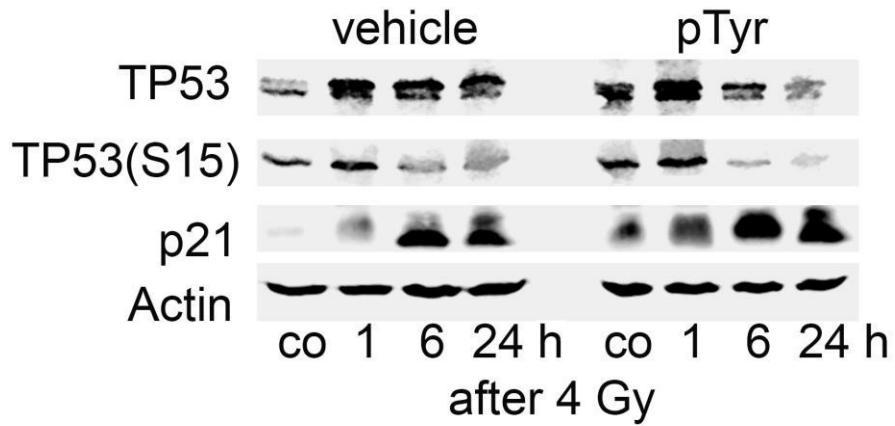


Figure 4: Western blot analysis: Y79 cells were pretreated with pTyr (10 μ M) or vehicle 16 hours before IR (4 Gy). Unirradiated cells in absence of pTyr express TP53 and it is phosphorylated, p21 is not expressed. After pTyr administration and after IR TP53 was stabilised, phosphorylated and p21 was expressed. pTyr treatment led to TP53 stabilization and p21 expression in unirradiated cells and increased p21 expression after IR compared to untreated cells, confirming a modulation of TP53 activity by pTyr.

6. Discussion

6.1 Is there a relevant mouse model, which can be used for radiotherapeutic approaches?

For the development of effective and safe radiotherapy of retinoblastoma studies with suitable models are needed. A good model should have as many characteristics of the original tumour as possible. To implement this, we used cultured human Y79 Rb cells and injected them into the vitreous of nude mouse eyes, the area the tumour grows into in most cases (orthotopic). Indeed, the growth characteristics of the xenograft-tumours of our model were similar to those of Rb-tumours in patients. The histological and ultrastructural analysis of the xenograft-tumours showed very similar characteristics to those described for the tumour the Y79 cells originate from (Reid et al., 1974) and Rb-tumours of other patients in general such as multiple degraded and necrotic cells, poor differentiation but still identifiable rosette-like growth, large hyperchromatical nuclei with multiple nucleoli and elaborate convolutions of the nuclei (Green et al., 1979; McFall et al., 1977; Reid et al., 1974), (Allen et al., 1962; Rodrigues et al., 1986).

Interestingly, typical metastasation via the optic nerve, ciliary body or blood vessels of the eye (Rodriguez-Galindo et al., 2003) was not observed in our model and the sclera forms a strong barrier for the growing xenograft-tumour, thus the tumour needs to grow very large and to have long time to break through the sclera. During our experiment, a tumour only penetrated the sclera in one mouse eye and formed brain metastases. The metastases were found in the brain of the animal (fig. 12), which after its tumour broke through the cornea, was kept alive for the longest period of time (35 days) of all analysed mice before sacrifice. However, in the Rag-2 knockout mice, which were used by Chevez-Barrios et al., the animals were intravitreally injected with Y79 cells in a similar manner as in our experiment, the mice already developed metastasis 4 weeks after the injection (Chevez-Barrios et al., 2000). These results are consistent with that of other groups, who showed, that metastasising in Rag-2 knockout based mouse models is superior to that in nude mice for several human cancer xenografts like sarcoma (Nanni et al., 2010), breast cancer (Nanni et al., 2012) or adenocarcinoma (Ye et al., 2015). This different metastasising behaviour should be taken into account when choosing a model.

In conclusion, we showed that our retinoblastoma mouse model mimics the symptoms observed in Rb patients. The xenograft tumours from our model showed very similar growth characteristics, cellular appearance and ultrastructural

6. Discussion

characteristics to that of retinoblastoma tumour tissue samples of Rb patients. This makes our model a promising tool for the study of retinoblastoma and its potential therapeutic approaches.

A very important aspect of this thesis was the use of SLO/OCT for the detection and characterization of tumours in the mouse eyes and the comparison of these results with those of the corresponding histological analysis.

SLO/OCT can be used for the detection of tumours at early stages of development and might be used for monitoring of the success of the potential therapy approaches. Unfortunately the method is limited to tumours at early stages of development. If the tumour covers most of the fundus no analysis is possible (fig. 11).

A similar funduscopy/OCT based approach was used for the analysis of the tumours in the eyes of a TAg-RB mouse model by Wenzel et al. Using OCT the group was able to characterise developing retinoblastomas in mice two weeks after birth. Their results showed, similar to our findings, that their OCT-data could also be correlated with the funduscopy- and corresponding histology-results (Wenzel et al., 2015). In ophthalmological research, *in vivo* analysis like SLO/OCT allows multiple analysis of dynamic biological processes like tumourigenesis, tumour growth and - angiogenesis at certain time points in individual animals and can help to reduce the number of experimental animals used according to the 3 rules in animal welfare (replace, reduce, refine).

6.2 Can the application of pTyr protect tissues that are affected by irradiation during radiotherapy and prevent the induction of secondary tumours?

In the rodent retina the photoreceptors are the most radiosensitive cells (Amoaku et al., 1992). It was shown that the double-strand break repair in the photoreceptors is weaker than in all other cells of the retina because of their inverted heterochromatin organization, containing a single large chromocentre in the middle of the nucleus (Frohns et al., 2014). The fractionated, therapy simulating irradiations of 5 Gy used for each single irradiation were administered at such low rates to avoid cell damage and to give the tissues enough time to regenerate with the help of cellular repair mechanisms. It was shown, that radiation-effects on a mouse retina are characterized by a non-linear dose-response curve. After irradiation with intensities up to 14 Gy, no morphological destruction was observed after a period of 30 days, indicating that retinal repair mechanisms took place (Tronov et al., 2015; Vinogradova lu et al., 2014). We were interested in long-term side effects of RT. We

6. Discussion

analysed the animals 3, 6 and 9 months after nine irradiations with 5 Gy. In the non-pTyr pretreated animals the reduction of the retina thickness and photoreceptor loss did not differ from the pTyr pretreated animals one month after IR. However, 3, 6 and 9 months after IR the retina thickness reduction and photoreceptor loss we measured in the non-pTyr pretreated mice was about 10% compared to the corresponding pretreated groups and results one month after IR, and thus comparatively low but statistically significant. The retinal thickness and photoreceptor number 1, 3, 6 and 9 months after IR did not significantly differ in the pTyr pretreated animals, indicating pTyr effectivity.

Radiation-induced hair greying in black mice is a known IR-induced side effect. It is caused by irreversible defects in the self-renewal of melanocyte stem cells in the hair follicles (Aoki et al., 2011; Boyland & Sargent, 1951). Thus during our experiment in the Rb^{+/-} mice this effect could also be observed in the irradiated area. Our results showed that pTyr-administration can reduce this side effect, which was a clear indication for radioprotection by pTyr.

The question as to whether pTyr can prevent the induction of secondary tumours after IR unfortunately could not be answered. During the period of investigation no induced tumours were detected. Actually, in Rb patients, radiotherapy-induced secondary tumours in most cases were not diagnosed any earlier than 30 years after treatment (Marees et al., 2009). In our study we used mouse models which unfortunately are not able to live longer than one and a half years. Thus the period of investigation seems to be too short for the tumours to appear, which probably explains the absence of IR-induced tumours in the mice.

6.3. Does the application of pTyr interfere with the radiotherapy of retinoblastoma?

The results of former experiments suggested that pTyr is predominantly radioprotective in cells with a p53 wild type (WT) (K. H. Dittmann et al., 2001). The results of our western blot analysis showed that Y79 cells express p53. Irradiation of the cells resulted in the stabilization of p53 and upregulation of the p53 target p21. Moreover, pTyr was capable of stabilising p53 in unirradiated Y79 cells and facilitating radiation-induced p21 up-regulation confirming a modulation of p53 activity by pTyr.

However, because of the mentioned inactivation mechanisms of the p53 pathway in Y79 cells like MDM2-activity increase (Hsieh et al., 1999), overexpression of MDMX (Laurie et al., 2006; Sherr & McCormick, 2002) and hypermethylation of the p53 promotor region (Livide et al., 2012), we decided to test the ability of pTyr to radio-

7. Final conclusions

protect Y79 cell cultures directly in *in vitro* irradiation experiments. We discovered that pTyr did indeed fail to protect the cell cultures after irradiation.

Unexpectedly and in contrast to our *in vitro* irradiation studies, pTyr showed radioprotection *in vivo* of Rb Y79 xenografts in the nude mouse eyes. The reason for the different outcome of the *in vitro/vivo* studies might be of a technical nature. For the limited dilution assays, a single cell solution was prepared, but normally the Y79 cells in solution grow in clusters and even show some differentiation (Reid et al., 1974). Therefore, the behaviour of Y79 cells might be different with regard to the micromilieu and growing conditions in a single cell solution, in clusters or as a solid tumour-mass, causing the different outcome. A similar effect was, for example, shown for the variation of the radioprotection of WR-2721 on tumours which depended on the tumour size (Milas et al., 1984).

Additionally in FSAll sarcoma cells, which have a p53 WT, pTyr has been demonstrated not to act radioprotectively due to possible additional mutations which interfere with the p53 function (K. Dittmann, Toulany, et al., 2005). Thus, the p53 status does not seem to be an exclusive criterion for pTyr to be radioprotective in a certain cell type.

6.4 Additional finding

The lens is the most radiosensitive tissue of the whole rodent eye (Brown, 1997). In our study we did not detect a radioprotective effect of pTyr on the lens, but there was a clear difference between the two mouse models used. The cataract formation started much earlier in the nude mice, as three months after RT all the mice already had severe cataracts. In the Rb^{+/-} mice the cataract formation did not start earlier than 6 months after IR and even 9 months after IR the opacity of the lenses was slight enough to enable an OCT analysis. The nude mice we used are historically on a BALB/c mouse genetic background. Thus the finding that BALB/c mice are more sensitive to radiation-induced cataractogenesis than pigmented mice (Sayama et al., 1991) is consistent with our results. Of course the mutation in the FOXP1 gene in the nude mice can also have an influence on their cataractogenesis.

7. Final conclusions

The application of pTyr before irradiation significantly reduced the negative effects of radiation on the retina and hair coat of Rb^{+/-} mice 3, 6 and 9 months after irradiation.

8. Perspectives

A fractionated radiotherapy can eliminate Y79-retinoblastoma-tumours in nude mice eyes if the treatment is started at an early time point of tumour growth, and the mice can remain tumour-free up to 9 months after radiotherapy. pTyr is a potent radioprotector for human Y79 xenograft tumours and is consequently contraindicated for the radiotherapy of retinoblastoma. The appearance of secondary tumours which is an often seen side effect of radiotherapy in patients was not observed in our mouse-models at the investigated time points. The development of irradiation-induced tumours might take a longer period of time.

Although pTyr is contraindicated for the radiotherapy for retinoblastoma, its radioprotective abilities might make it interesting for the radiotherapy of other cancers, which are not protected by pTyr, especially those with p53 mutations. The radioprotective effects on the retina might also make pTyr interesting for the reduction of occupational risks in areas where humans are exposed to irradiation, for example in space and aviation sectors (Cucinotta et al., 2014; Moreno-Villanueva et al., 2017).

8. Perspectives

It can be assumed that radiotherapy will continue to play a role in the therapy of retinoblastoma, and a search for possibilities, which could help to make the radiotherapy of retinoblastoma more efficient and safe, will also continue.

Currently chemotherapies with vincristine, etoposide, carboplatin, melphalan, or combined chemotherapies are the state of the art treatment of retinoblastoma (Yanik et al., 2015). Depending on the size and location of the tumour, the chemotherapeutic agents are administrated via the intra-arterial, intra-venous or intra-vitreous route. Although being successful in over 90% of the cases for tumours at an early stage of development, if they are confined to the retina with no seeding, (Fabian et al., 2018), the therapy is far from being optimal, especially for tumours at advanced stages, with seeds or metastasis. Here the treatment success is only 48% (Mendoza & Grossniklaus, 2016).

To conclude, my vision about future retinoblastoma treatment could be the use of a very promising method of therapeutics administration to the eye via a catheter in the retrobulbar space that I am currently developing. This approach will help to reduce the number of traumatic operative interventions in young children and prevent systemic side effects. Moreover, it will allow a better local bioavailability and

8. Perspectives

importantly the fast supply of a therapeutic dose in case of tumour recurrence ensuring a better tumour control.

9. Appendix

9.1 List of references

- Abramson, D. H., & Frank, C. M. (1998). Second nonocular tumors in survivors of bilateral retinoblastoma: a possible age effect on radiation-related risk. *Ophthalmology*, *105*(4), 573-579; discussion 579-580. doi:10.1016/S0161-6420(98)94006-4
- Aerts, I., Lumbroso-Le Rouic, L., Gauthier-Villars, M., Brisse, H., & Doz, F. (2016). [Retinoblastoma update]. *Arch Pediatr*, *23*(1), 112-116. doi:10.1016/j.arcped.2015.09.025
- Aerts, I., Lumbroso-Le Rouic, L., Gauthier-Villars, M., Brisse, H., Doz, F., & Desjardins, L. (2006). Retinoblastoma. *Orphanet J Rare Dis*, *1*, 31. doi:10.1186/1750-1172-1-31
- Ajioka, I., Martins, R. A., Bayazitov, I. T., Donovan, S., Johnson, D. A., Frase, S., Dyer, M. A. (2007). Differentiated horizontal interneurons clonally expand to form metastatic retinoblastoma in mice. *Cell*, *131*(2), 378-390. doi:10.1016/j.cell.2007.09.036
- Albert, D. M. (1987). Historic review of retinoblastoma. *Ophthalmology*, *94*(6), 654-662.
- Allen, R. A., Latta, H., & Straatsma, B. R. (1962). Retinoblastoma. A study of two cases by electron microscopy. *Invest Ophthalmol*, *1*, 728-744.
- Alwan, H. A., van Zoelen, E. J., & van Leeuwen, J. E. (2003). Ligand-induced lysosomal epidermal growth factor receptor (EGFR) degradation is preceded by proteasome-dependent EGFR de-ubiquitination. *J Biol Chem*, *278*(37), 35781-35790. doi:10.1074/jbc.M301326200
- Amoaku, W. M., Mahon, G. J., Gardiner, T. A., Frew, L., & Archer, D. B. (1992). Late ultrastructural changes in the retina of the rat following low-dose X-irradiation. *Graefes Arch Clin Exp Ophthalmol*, *230*(6), 569-574.
- Antoneli, C. B., Ribeiro Kde, C., Sakamoto, L. H., Chojniak, M. M., Novaes, P. E., & Arias, V. E. (2007). Trilateral retinoblastoma. *Pediatr Blood Cancer*, *48*(3), 306-310. doi:10.1002/pbc.20793
- Aoki, H., Hara, A., Motohashi, T., & Kunisada, T. (2011). Protective effect of Kit signaling for melanocyte stem cells against radiation-induced genotoxic stress. *J Invest Dermatol*, *131*(9), 1906-1915. doi:10.1038/jid.2011.148
- Ashwood-Smith, M. J. (1967). Radioprotective and cryoprotective properties of dimethyl sulfoxide in cellular systems. *Ann N Y Acad Sci*, *141*(1), 45-62.
- Ayari-Jeridi, H., Moran, K., Chebbi, A., Bouguila, H., Abbes, I., Charradi, K., Ganguly, A. (2015). Mutation spectrum of RB1 gene in unilateral retinoblastoma cases from Tunisia and correlations with clinical features. *PLoS One*, *10*(1), e0116615. doi:10.1371/journal.pone.0116615
- Balmer, A., Zografos, L., & Munier, F. (2006). Diagnosis and current management of retinoblastoma. *Oncogene*, *25*(38), 5341-5349. doi:10.1038/sj.onc.1209622
- Benedict, W. F., Dawson, J. A., Banerjee, A., & Murphree, A. L. (1980). The nude mouse model for human retinoblastoma: a system for evaluation of retinoblastoma therapy. *Med Pediatr Oncol*, *8*(4), 391-395.
- Bhola, N. E., & Grandis, J. R. (2008). Crosstalk between G-protein-coupled receptors and epidermal growth factor receptor in cancer. *Front Biosci*, *13*, 1857-1865.

9. Appendix

- Bhuvaneshwari, A., Pallavi, V. R., Jayshree, R. S., & Kumar, R. V. (2012). Maternal transmission of human papillomavirus in retinoblastoma: A possible route of transfer. *Indian J Med Paediatr Oncol*, 33(4), 210-215. doi:10.4103/0971-5851.107080
- Bianciotto, C., Shields, C. L., Iturralde, J. C., Sarici, A., Jabbour, P., & Shields, J. A. (2012). Fluorescein angiographic findings after intra-arterial chemotherapy for retinoblastoma. *Ophthalmology*, 119(4), 843-849. doi:10.1016/j.ophtha.2011.09.040
- Bourgier, C., Levy, A., Vozenin, M. C., & Deutsch, E. (2012). Pharmacological strategies to spare normal tissues from radiation damage: useless or overlooked therapeutics? *Cancer Metastasis Rev*, 31(3-4), 699-712. doi:10.1007/s10555-012-9381-9
- Boutrid, H., Jockovich, M. E., Murray, T. G., Pina, Y., Feuer, W. J., Lampidis, T. J., & Cebulla, C. M. (2008). Targeting hypoxia, a novel treatment for advanced retinoblastoma. *Invest Ophthalmol Vis Sci*, 49(7), 2799-2805. doi:10.1167/iovs.08-1751
- Boyer, S. N., Wazer, D. E., & Band, V. (1996). E7 protein of human papilloma virus-16 induces degradation of retinoblastoma protein through the ubiquitin-proteasome pathway. *Cancer Res*, 56(20), 4620-4624.
- Boylard, E., & Sargent, S. (1951). The local greying of hair in mice treated with x rays and radiomimetic drugs. *Br J Cancer*, 5(4), 433-440.
- Brand, T. M., Iida, M., Li, C., & Wheeler, D. L. (2011). The nuclear epidermal growth factor receptor signaling network and its role in cancer. *Discov Med*, 12(66), 419-432.
- Broadus, E., Topham, A., & Singh, A. D. (2009). Incidence of retinoblastoma in the USA: 1975-2004. *Br J Ophthalmol*, 93(1), 21-23. doi:10.1136/bjo.2008.138750
- Brown, N. P. (1997). The lens is more sensitive to radiation than we had believed. *Br J Ophthalmol*, 81(4), 257.
- Bunin, G. R., Emanuel, B. S., Meadows, A. T., Buckley, J. D., Woods, W. G., & Hammond, G. D. (1989). Frequency of 13q abnormalities among 203 patients with retinoblastoma. *J Natl Cancer Inst*, 81(5), 370-374.
- Burkhardt, D. L., & Sage, J. (2008). Cellular mechanisms of tumour suppression by the retinoblastoma gene. *Nat Rev Cancer*, 8(9), 671-682. doi:10.1038/nrc2399
- Chaachouay, H., Ohneseit, P., Toulany, M., Kehlbach, R., Multhoff, G., & Rodemann, H. P. (2011). Autophagy contributes to resistance of tumor cells to ionizing radiation. *Radiother Oncol*, 99(3), 287-292. doi:10.1016/j.radonc.2011.06.002
- Chang, L., Graham, P. H., Hao, J., Ni, J., Bucci, J., Cozzi, P. J., Li, Y. (2014). PI3K/Akt/mTOR pathway inhibitors enhance radiosensitivity in radioresistant prostate cancer cells through inducing apoptosis, reducing autophagy, suppressing NHEJ and HR repair pathways. *Cell Death Dis*, 5, e1437. doi:10.1038/cddis.2014.415
- Chen, D. J., & Nirodi, C. S. (2007). The epidermal growth factor receptor: a role in repair of radiation-induced DNA damage. *Clin Cancer Res*, 13(22 Pt 1), 6555-6560. doi:10.1158/1078-0432.CCR-07-1610
- Chen, Y. S., Song, H. X., Lu, Y., Li, X., Chen, T., Zhang, Y., Fu, T. (2011). Autophagy inhibition contributes to radiation sensitization of esophageal squamous carcinoma cells. *Dis Esophagus*, 24(6), 437-443. doi:10.1111/j.1442-2050.2010.01156.x
- Chevez-Barrios, P., Hurwitz, M. Y., Louie, K., Marcus, K. T., Holcombe, V. N., Schafer, P., Hurwitz, R. L. (2000). Metastatic and nonmetastatic models of retinoblastoma. *Am J Pathol*, 157(4), 1405-1412. doi:10.1016/S0002-9440(10)64653-6
- Chinnam, M., & Goodrich, D. W. (2011). RB1, development, and cancer. *Curr Top Dev Biol*, 94, 129-169. doi:10.1016/B978-0-12-380916-2.00005-X

9. Appendix

- Combs, S. E., Behnisch, W., Kulozik, A. E., Huber, P. E., Debus, J., & Schulz-Ertner, D. (2007). Intensity Modulated Radiotherapy (IMRT) and Fractionated Stereotactic Radiotherapy (FSRT) for children with head-and-neck-rhabdomyosarcoma. *BMC Cancer*, *7*, 177. doi:10.1186/1471-2407-7-177
- Cucinotta, F. A., Alp, M., Sulzman, F. M., & Wang, M. (2014). Space radiation risks to the central nervous system. *Life Sciences in Space Research*, *2*(Supplement C), 54-69. doi:https://doi.org/10.1016/j.lssr.2014.06.003
- de Graaf, P., Goricke, S., Rodjan, F., Galluzzi, P., Maeder, P., Castelijns, J. A., European Retinoblastoma Imaging, C. (2012). Guidelines for imaging retinoblastoma: imaging principles and MRI standardization. *Pediatr Radiol*, *42*(1), 2-14. doi:10.1007/s00247-011-2201-5
- de Jong, M. C., Kors, W. A., de Graaf, P., Castelijns, J. A., Kivela, T., & Moll, A. C. (2014). Trilateral retinoblastoma: a systematic review and meta-analysis. *Lancet Oncol*, *15*(10), 1157-1167. doi:10.1016/S1470-2045(14)70336-5
- del Cerro, M., Seigel, G. M., Lazar, E., Grover, D., del Cerro, C., Brooks, D. H., Chader, G. (1993). Transplantation of Y79 cells into rat eyes: an in vivo model of human retinoblastomas. *Invest Ophthalmol Vis Sci*, *34*(12), 3336-3346.
- Demory, M. L., Boerner, J. L., Davidson, R., Faust, W., Miyake, T., Lee, I., Parsons, S. J. (2009). Epidermal growth factor receptor translocation to the mitochondria: regulation and effect. *J Biol Chem*, *284*(52), 36592-36604. doi:10.1074/jbc.M109.000760
- Dittmann, K., Mayer, C., Fehrenbacher, B., Schaller, M., Kehlbach, R., & Rodemann, H. P. (2011). Nuclear epidermal growth factor receptor modulates cellular radio-sensitivity by regulation of chromatin access. *Radiother Oncol*, *99*(3), 317-322. doi:10.1016/j.radonc.2011.06.001
- Dittmann, K., Mayer, C., Fehrenbacher, B., Schaller, M., Raju, U., Milas, L., Rodemann, H. P. (2005). Radiation-induced epidermal growth factor receptor nuclear import is linked to activation of DNA-dependent protein kinase. *J Biol Chem*, *280*(35), 31182-31189. doi:10.1074/jbc.M506591200
- Dittmann, K., Mayer, C., Kehlbach, R., & Rodemann, H. P. (2008). Radiation-induced caveolin-1 associated EGFR internalization is linked with nuclear EGFR transport and activation of DNA-PK. *Mol Cancer*, *7*, 69. doi:10.1186/1476-4598-7-69
- Dittmann, K., Mayer, C., Paasch, A., Huber, S., Fehrenbacher, B., Schaller, M., & Rodemann, H. P. (2015). Nuclear EGFR renders cells radio-resistant by binding mRNA species and triggering a metabolic switch to increase lactate production. *Radiother Oncol*, *116*(3), 431-437. doi:10.1016/j.radonc.2015.08.016
- Dittmann, K., Mayer, C., Rodemann, H. P., & Huber, S. M. (2013). EGFR cooperates with glucose transporter SGLT1 to enable chromatin remodeling in response to ionizing radiation. *Radiother Oncol*, *107*(2), 247-251. doi:10.1016/j.radonc.2013.03.016
- Dittmann, K., Mayer, C., Wanner, G., Kehlbach, R., & Rodemann, H. P. (2007). The radioprotector O-phospho-tyrosine stimulates DNA-repair via epidermal growth factor receptor- and DNA-dependent kinase phosphorylation. *Radiother Oncol*, *84*(3), 328-334. doi:10.1016/j.radonc.2007.07.006
- Dittmann, K., Toulany, M., Classen, J., Heinrich, V., Milas, L., & Rodemann, H. P. (2005). Selective radioprotection of normal tissues by Bowman-birk proteinase inhibitor (BBI) in mice. *Strahlenther Onkol*, *181*(3), 191-196. doi:10.1007/s00066-005-1358-y
- Dittmann, K. H., Mayer, C., & Rodemann, H. P. (2001). O-phospho-L-tyrosine protects TP53 wild-type cells against ionizing radiation. *Int J Cancer*, *96 Suppl*, 1-6. doi:10.1002/ijc.10340
- Dommering, C. J., Marees, T., van der Hout, A. H., Imhof, S. M., Meijers-Heijboer, H., Ringens, P. J., Moll, A. C. (2012). RB1 mutations and second primary

9. Appendix

- malignancies after hereditary retinoblastoma. *Fam Cancer*, 11(2), 225-233. doi:10.1007/s10689-011-9505-3
- Dyer, M. A., Rodriguez-Galindo, C., & Wilson, M. W. (2005). Use of preclinical models to improve treatment of retinoblastoma. *PLoS Med*, 2(10), e332. doi:10.1371/journal.pmed.0020332
- Endo, Y., Sugiyama, A., Li, S. A., Ohmori, K., Ohata, H., Yoshida, Y., Taya, Y. (2008). Regulation of clathrin-mediated endocytosis by p53. *Genes Cells*, 13(4), 375-386. doi:10.1111/j.1365-2443.2008.01172.x
- Fabian, I. D., Onadim, Z., Karaa, E., Duncan, C., Chowdhury, T., Scheimberg, I., Sagoo, M. S. (2018). The management of retinoblastoma. *Oncogene*. doi:10.1038/s41388-017-0050-x
- Frohns, A., Frohns, F., Naumann, S. C., Layer, P. G., & Lohrich, M. (2014). Inefficient double-strand break repair in murine rod photoreceptors with inverted heterochromatin organization. *Curr Biol*, 24(10), 1080-1090. doi:10.1016/j.cub.2014.03.061
- Gabellini, C., Del Bufalo, D., & Zupi, G. (2006). Involvement of RB gene family in tumor angiogenesis. *Oncogene*, 25(38), 5326-5332. doi:10.1038/sj.onc.1209631
- Gaitan-Yanguas, M. (1978). Retinoblastoma: analysis of 235 cases. *Int J Radiat Oncol Biol Phys*, 4(5-6), 359-365.
- Gallie, B. L., Albert, D. M., Wong, J. J., Buyukmihci, N., & Pullafito, C. A. (1977). Heterotransplantation of retinoblastoma into the athymic "nude" mouse. *Invest Ophthalmol Vis Sci*, 16(3), 256-259.
- Ghassemi, F., & Shields, C. L. (2012). Intravitreal melphalan for refractory or recurrent vitreous seeding from retinoblastoma. *Arch Ophthalmol*, 130(10), 1268-1271. doi:10.1001/archophthalmol.2012.1983
- Giacinti, C., & Giordano, A. (2006). RB and cell cycle progression. *Oncogene*, 25(38), 5220-5227. doi:10.1038/sj.onc.1209615
- Green, A. L., Meek, E. S., White, D. W., Stevens, R. H., Ackerman, L. D., Judisch, G. F., & Patil, S. R. (1979). Retinoblastoma Y79 cell line: a study of membrane structures. *Albrecht Von Graefes Arch Klin Exp Ophthalmol*, 211(4), 279-287.
- Grossniklaus, H. E. (2014). Retinoblastoma. Fifty years of progress. The LXXI Edward Jackson Memorial Lecture. *Am J Ophthalmol*, 158(5), 875-891. doi:10.1016/j.ajo.2014.07.025
- Harris, S. L., & Levine, A. J. (2005). The p53 pathway: positive and negative feedback loops. *Oncogene*, 24(17), 2899-2908. doi:10.1038/sj.onc.1208615
- Hein, A. L., Ouellette, M. M., & Yan, Y. (2014). Radiation-induced signaling pathways that promote cancer cell survival (review). *Int J Oncol*, 45(5), 1813-1819. doi:10.3892/ijco.2014.2614
- Hooper, M. L. (1999). Is sunlight an aetiological agent in the genesis of retinoblastoma? *Br J Cancer*, 79(7-8), 1273-1276. doi:10.1038/sj.bjc.6690204
- Hsieh, J. K., Chan, F. S., O'Connor, D. J., Mitnacht, S., Zhong, S., & Lu, X. (1999). RB regulates the stability and the apoptotic function of p53 via MDM2. *Mol Cell*, 3(2), 181-193.
- Jacks, T., Fazeli, A., Schmitt, E. M., Bronson, R. T., Goodell, M. A., & Weinberg, R. A. (1992). Effects of an Rb mutation in the mouse. *Nature*, 359(6393), 295-300. doi:10.1038/359295a0
- Jehanne, M., Brisse, H., Gauthier-Villars, M., Lumbroso-le Rouic, L., Freneaux, P., & Aerts, I. (2014). Retinoblastoma: Recent advances. *Bull Cancer*, 101(4), 380-387. doi:10.1684/bdc.2014.1931
- Jemal, A., Devesa, S. S., Fears, T. R., & Fraumeni, J. F., Jr. (2000). Retinoblastoma incidence and sunlight exposure. *Br J Cancer*, 82(11), 1875-1878. doi:10.1054/bjoc.2000.1215
- Kam, W. W., & Banati, R. B. (2013). Effects of ionizing radiation on mitochondria. *Free Radic Biol Med*, 65, 607-619. doi:10.1016/j.freeradbiomed.2013.07.024

9. Appendix

- Kim, J. Y., & Park, Y. (2015). Treatment of Retinoblastoma: The Role of External Beam Radiotherapy. *Yonsei Med J*, 56(6), 1478-1491. doi:10.3349/ymj.2015.56.6.1478
- Kivela, T., & Polkunen, M. L. (2003). Pieter Pauw's tumor oculorum: reappraisal of the presumed first description of retinoblastoma in 1597. *Arch Ophthalmol*, 121(6), 881-886. doi:10.1001/archophth.121.6.881
- Kleinerman, R. A., Tucker, M. A., Tarone, R. E., Abramson, D. H., Seddon, J. M., Stovall, M., Fraumeni, J. F., Jr. (2005). Risk of new cancers after radiotherapy in long-term survivors of retinoblastoma: an extended follow-up. *J Clin Oncol*, 23(10), 2272-2279. doi:10.1200/JCO.2005.05.054
- Knudson, A. G., Jr. (1971). Mutation and cancer: statistical study of retinoblastoma. *Proc Natl Acad Sci U S A*, 68(4), 820-823.
- Krengli, M., Hug, E. B., Adams, J. A., Smith, A. R., Tarbell, N. J., & Munzenrider, J. E. (2005). Proton radiation therapy for retinoblastoma: comparison of various intraocular tumor locations and beam arrangements. *Int J Radiat Oncol Biol Phys*, 61(2), 583-593. doi:10.1016/j.ijrobp.2004.06.003
- Kristensen, P., Andersen, A., Irgens, L. M., Bye, A. S., & Sundheim, L. (1996). Cancer in offspring of parents engaged in agricultural activities in Norway: incidence and risk factors in the farm environment. *Int J Cancer*, 65(1), 39-50. doi:10.1002/(SICI)1097-0215(19960103)65:1<39::AID-IJC8>3.0.CO;2-2
- Kuntic, V. S., Stankovic, M. B., Vujic, Z. B., Brboric, J. S., & Uskokovic-Markovic, S. M. (2013). Radioprotectors - the evergreen topic. *Chem Biodivers*, 10(10), 1791-1803. doi:10.1002/cbdv.201300054
- Laurie, N. A., Donovan, S. L., Shih, C. S., Zhang, J., Mills, N., Fuller, C., Dyer, M. A. (2006). Inactivation of the p53 pathway in retinoblastoma. *Nature*, 444(7115), 61-66. doi:10.1038/nature05194
- Livide, G., Epistolato, M. C., Amenduni, M., Disciglio, V., Marozza, A., Mencarelli, M. A., Ariani, F. (2012). Epigenetic and copy number variation analysis in retinoblastoma by MS-MLPA. *Pathol Oncol Res*, 18(3), 703-712. doi:10.1007/s12253-012-9498-8
- Luo, R. X., Postigo, A. A., & Dean, D. C. (1998). Rb interacts with histone deacetylase to repress transcription. *Cell*, 92(4), 463-473.
- Macpherson, D. (2008). Insights from mouse models into human retinoblastoma. *Cell Div*, 3, 9. doi:10.1186/1747-1028-3-9
- Marees, T., van Leeuwen, F. E., de Boer, M. R., Imhof, S. M., Ringens, P. J., & Moll, A. C. (2009). Cancer mortality in long-term survivors of retinoblastoma. *Eur J Cancer*, 45(18), 3245-3253. doi:10.1016/j.ejca.2009.05.011
- Mayorga, P. A., Brualla, L., Sauerwein, W., & Lallena, A. M. (2014). Monte Carlo study for designing a dedicated "D"-shaped collimator used in the external beam radiotherapy of retinoblastoma patients. *Med Phys*, 41(1), 011714. doi:10.1118/1.4855855
- McFall, R. C., Sery, T. W., & Makadon, M. (1977). Characterization of a new continuous cell line derived from a human retinoblastoma. *Cancer Res*, 37(4), 1003-1010.
- Mendoza, P. R., & Grossniklaus, H. E. (2016). Therapeutic Options for Retinoblastoma. *Cancer Control*, 23(2), 99-109. doi:10.1177/107327481602300203
- Milas, L., Hunter, N., Ito, H., & Peters, L. J. (1984). Effect of tumor type, size, and endpoint on tumor radioprotection by WR-2721. *Int J Radiat Oncol Biol Phys*, 10(1), 41-48.
- Moll, A. C., Imhof, S. M., Cruysberg, J. R., Schouten-van Meeteren, A. Y., Boers, M., & van Leeuwen, F. E. (2003). Incidence of retinoblastoma in children born after in-vitro fertilisation. *Lancet*, 361(9354), 309-310. doi:10.1016/S0140-6736(03)12332-X

9. Appendix

- Moll, A. C., Imhof, S. M., Kuik, D. J., Bouter, L. M., Den Otter, W., Bezemer, P. D., Tan, K. E. (1996). High parental age is associated with sporadic hereditary retinoblastoma: the Dutch retinoblastoma register 1862-1994. *Hum Genet*, 98(1), 109-112.
- Moreno-Villanueva, M., Wong, M., Lu, T., Zhang, Y., & Wu, H. (2017). Interplay of space radiation and microgravity in DNA damage and DNA damage response. *NPJ Microgravity*, 3, 14. doi:10.1038/s41526-017-0019-7
- Mouw, K. W., Sethi, R. V., Yeap, B. Y., MacDonald, S. M., Chen, Y. L., Tarbell, N. J., Shih, H. A. (2014). Proton radiation therapy for the treatment of retinoblastoma. *Int J Radiat Oncol Biol Phys*, 90(4), 863-869. doi:10.1016/j.ijrobp.2014.07.031
- Muen, W. J., Kingston, J. E., Robertson, F., Brew, S., Sagoo, M. S., & Reddy, M. A. (2012). Efficacy and complications of super-selective intra-ophthalmic artery melphalan for the treatment of refractory retinoblastoma. *Ophthalmology*, 119(3), 611-616. doi:10.1016/j.ophtha.2011.08.045
- Munakata, T., Nakamura, M., Liang, Y., Li, K., & Lemon, S. M. (2005). Down-regulation of the retinoblastoma tumor suppressor by the hepatitis C virus NS5B RNA-dependent RNA polymerase. *Proc Natl Acad Sci U S A*, 102(50), 18159-18164. doi:10.1073/pnas.0505605102
- Murphree, A. L., & Benedict, W. F. (1984). Retinoblastoma: clues to human oncogenesis. *Science*, 223(4640), 1028-1033.
- Nanni, P., Nicoletti, G., Landuzzi, L., Croci, S., Murgo, A., Palladini, A., Lollini, P. L. (2010). High metastatic efficiency of human sarcoma cells in Rag2/gammac double knockout mice provides a powerful test system for antimetastatic targeted therapy. *Eur J Cancer*, 46(3), 659-668. doi:10.1016/j.ejca.2009.11.018
- Nanni, P., Nicoletti, G., Palladini, A., Croci, S., Murgo, A., Ianzano, M. L., Lollini, P. L. (2012). Multiorgan metastasis of human HER-2+ breast cancer in Rag2/-;Il2rg/- mice and treatment with PI3K inhibitor. *PLoS One*, 7(6), e39626. doi:10.1371/journal.pone.0039626
- Nyati, M. K., Morgan, M. A., Feng, F. Y., & Lawrence, T. S. (2006). Integration of EGFR inhibitors with radiochemotherapy. *Nat Rev Cancer*, 6(11), 876-885. doi:10.1038/nrc1953
- Orjuela, M., Castaneda, V. P., Ridaura, C., Lecona, E., Leal, C., Abramson, D. H., Cordon-Cardo, C. (2000). Presence of human papilloma virus in tumor tissue from children with retinoblastoma: an alternative mechanism for tumor development. *Clin Cancer Res*, 6(10), 4010-4016.
- Orjuela, M. A., Titievsky, L., Liu, X., Ramirez-Ortiz, M., Ponce-Castaneda, V., Lecona, E., Mueller, N. E. (2005). Fruit and vegetable intake during pregnancy and risk for development of sporadic retinoblastoma. *Cancer Epidemiol Biomarkers Prev*, 14(6), 1433-1440. doi:10.1158/1055-9965.EPI-04-0427
- Pacal, M., & Bremner, R. (2006). Insights from animal models on the origins and progression of retinoblastoma. *Curr Mol Med*, 6(7), 759-781.
- Pandey, A. N. (2014). Retinoblastoma: An overview. *Saudi J Ophthalmol*, 28(4), 310-315. doi:10.1016/j.sjopt.2013.11.001
- Parkin, D. M., Stiller, C. A., Draper, G. J., & Bieber, C. A. (1988). The international incidence of childhood cancer. *Int J Cancer*, 42(4), 511-520.
- Puzio-Kuter, A. M. (2011). The Role of p53 in Metabolic Regulation. *Genes Cancer*, 2(4), 385-391. doi:10.1177/1947601911409738
- Ramasubramanian, A., Shields, C. L., Mellen, P. L., Haji, S., Harmon, S. A., Vemuganti, G. K., & Shields, J. A. (2011). Autofluorescence of treated retinoblastoma. *J AAPOS*, 15(2), 167-172. doi:10.1016/j.jaapos.2010.12.011
- Reid, T. W., Albert, D. M., Rabson, A. S., Russell, P., Craft, J., Chu, E. W., Wilcox, J. L. (1974). Characteristics of an established cell line of retinoblastoma. *J Natl Cancer Inst*, 53(2), 347-360.

9. Appendix

- Richter, S., Vandezande, K., Chen, N., Zhang, K., Sutherland, J., Anderson, J., Gallie, B. (2003). Sensitive and efficient detection of RB1 gene mutations enhances care for families with retinoblastoma. *Am J Hum Genet*, 72(2), 253-269. doi:10.1086/345651
- Rodemann, H. P., Dittmann, K., & Toulany, M. (2007). Radiation-induced EGFR-signaling and control of DNA-damage repair. *Int J Radiat Biol*, 83(11-12), 781-791. doi:10.1080/09553000701769970
- Rodjan, F., Graaf, P., Brisse, H. J., Verbeke, J. I., Sanchez, E., Galluzzi, P., Castelijns, J. A. (2013). Second cranio-facial malignancies in hereditary retinoblastoma survivors previously treated with radiation therapy: clinic and radiologic characteristics and survival outcomes. *Eur J Cancer*, 49(8), 1939-1947. doi:10.1016/j.ejca.2013.01.010
- Rodrigues, M. M., Wilson, M. E., Wiggert, B., Krishna, G., & Chader, G. J. (1986). Retinoblastoma. A clinical, immunohistochemical, and electron microscopic case report. *Ophthalmology*, 93(8), 1010-1015.
- Rodriguez-Galindo, C., Wilson, M. W., Haik, B. G., Lipson, M. J., Cain, A., Merchant, T. E., Pratt, C. B. (2003). Treatment of metastatic retinoblastoma. *Ophthalmology*, 110(6), 1237-1240. doi:10.1016/S0161-6420(03)00258-6
- Rodriguez, S. D., Brar, R. K., Drake, L. L., Drumm, H. E., Price, D. P., Hammond, J. I., Hansen, I. A. (2013). The effect of the radio-protective agents ethanol, trimethylglycine, and beer on survival of X-ray-sterilized male *Aedes aegypti*. *Parasit Vectors*, 6, 211. doi:10.1186/1756-3305-6-211
- Rootman, D. B., Gonzalez, E., Mallipatna, A., Vandenhoven, C., Hampton, L., Dimaras, H., Heon, E. (2013). Hand-held high-resolution spectral domain optical coherence tomography in retinoblastoma: clinical and morphologic considerations. *Br J Ophthalmol*, 97(1), 59-65. doi:10.1136/bjophthalmol-2012-302133
- Rowe, S. G., Lee, W. H., & Madreperla, S. (1992). *Subretinal and vitreal growth of human retinoblastoma cells in the mouse eye*. Paper presented at the Invest Ophthalmol Vis Sci.
- Rowinsky, E. K. (2004). The erbB family: targets for therapeutic development against cancer and therapeutic strategies using monoclonal antibodies and tyrosine kinase inhibitors. *Annu Rev Med*, 55, 433-457. doi:10.1146/annurev.med.55.091902.104433
- Rushlow, D. E., Mol, B. M., Kennett, J. Y., Yee, S., Pajovic, S., Theriault, B. L., Gallie, B. L. (2013). Characterisation of retinoblastomas without RB1 mutations: genomic, gene expression, and clinical studies. *Lancet Oncol*, 14(4), 327-334. doi:10.1016/S1470-2045(13)70045-7
- Sato, Y., & Tsurumi, T. (2013). Genome guardian p53 and viral infections. *Rev Med Virol*, 23(4), 213-220. doi:10.1002/rmv.1738
- Sayama, K., Moriyama, T., & Matsuzawa, A. (1991). [Marked difference in sensitivity to gamma-ray-induced cataract between BALB/c and CBA-C3H strain mice]. *Jikken Dobutsu*, 40(4), 541-543.
- Schaiquevich, P., Buitrago, E., Taich, P., Torbidoni, A., Ceciliano, A., Fandino, A., Chantada, G. L. (2012). Pharmacokinetic analysis of melphalan after superselective ophthalmic artery infusion in preclinical models and retinoblastoma patients. *Invest Ophthalmol Vis Sci*, 53(7), 4205-4212. doi:10.1167/iovs.12-9501
- Schueler, A. O., Fluhs, D., Anastassiou, G., Jurklies, C., Neuhauser, M., Schilling, H., Sauerwein, W. (2006). Beta-ray brachytherapy with 106Ru plaques for retinoblastoma. *Int J Radiat Oncol Biol Phys*, 65(4), 1212-1221. doi:10.1016/j.ijrobp.2006.02.002
- Seregard, S., Lundell, G., Svedberg, H., & Kivela, T. (2004). Incidence of retinoblastoma from 1958 to 1998 in Northern Europe: advantages of birth

9. Appendix

- cohort analysis. *Ophthalmology*, 111(6), 1228-1232. doi:10.1016/j.ophtha.2003.10.023
- Shah, N. V., Pham, D. G., Murray, T. G., Decatur, C., Hernandez, E., Shah, N. N., Houston, S. K. (2014). Intravitreal and subconjunctival melphalan for retinoblastoma in transgenic mice. *J Ophthalmol*, 2014, 829879. doi:10.1155/2014/829879
- Sherr, C. J., & McCormick, F. (2002). The RB and p53 pathways in cancer. *Cancer Cell*, 2(2), 103-112.
- Shields, C. L., Mashayekhi, A., Luo, C. K., Materin, M. A., & Shields, J. A. (2004). Optical coherence tomography in children: analysis of 44 eyes with intraocular tumors and simulating conditions. *J Pediatr Ophthalmol Strabismus*, 41(6), 338-344.
- Sun, C. H., Chang, Y. H., & Pan, C. C. (2011). Activation of the PI3K/Akt/mTOR pathway correlates with tumour progression and reduced survival in patients with urothelial carcinoma of the urinary bladder. *Histopathology*, 58(7), 1054-1063. doi:10.1111/j.1365-2559.2011.03856.x
- Takahashi, A., Ohtani, N., & Hara, E. (2007). Irreversibility of cellular senescence: dual roles of p16INK4a/Rb-pathway in cell cycle control. *Cell Div*, 2, 10. doi:10.1186/1747-1028-2-10
- Temming, P., Lohmann, D., Bornfeld, N., Sauerwein, W., Goericke, S. L., & Eggert, A. (2012). Current concepts for diagnosis and treatment of retinoblastoma in Germany: aiming for safe tumor control and vision preservation. *Klin Padiatr*, 224(6), 339-347. doi:10.1055/s-0032-1327563
- Totsuka, S., Akazawa, K., & Minoda, K. (1982). [Transplantation of retinoblastoma into nude mouse. 3. Tumor doubling time of retinoblastoma (author's transl)]. *Nihon Ganka Gakkai Zasshi*, 86(4), 418-425.
- Tronov, V. A., Vinogradova, Y. V., Poplinskaya, V. A., Nekrasova, E. I., & Ostrovsky, M. A. (2015). [Radiation preconditioning of mouse retina results in tolerance to MNU-induced degeneration and stimulates retinal recovery]. *Tsitologiya*, 57(2), 119-128.
- Tschulakow, A. V., Dittmann, K., Huber, S. M., Klumpp, D., Stegen, B., Schraermeyer, U., Julien-Schraermeyer, S. (2017). The radioprotector ortho-phospho-L-tyrosine (pTyr) attenuates the side effects of fractionated irradiation in retinoblastoma mouse models but also decreases the local tumour control. *Radiother Oncol*, 124(3), 462-467. doi:10.1016/j.radonc.2017.06.023
- Tschulakow, A. V., Schraermeyer, U., Rodemann, H. P., & Julien-Schraermeyer, S. (2016). Establishment of a novel retinoblastoma (Rb) nude mouse model by intravitreal injection of human Rb Y79 cells - comparison of in vivo analysis versus histological follow up. *Biol Open*, 5(11), 1625-1630. doi:10.1242/bio.019976
- Vasudevan, V., Cheung, M. C., Yang, R., Zhuge, Y., Fischer, A. C., Koniaris, L. G., & Sola, J. E. (2010). Pediatric solid tumors and second malignancies: characteristics and survival outcomes. *J Surg Res*, 160(2), 184-189. doi:10.1016/j.jss.2009.05.030
- Verhoeff, F. H. (1921). Glioma Retinae Treated by X-Rays, with Apparent Destruction of the Tumor and Preservation of Normal Vision. *Trans Am Ophthalmol Soc*, 19, 209-216.
- Verhoeff, F. H. (1952). Retinoblastoma successfully treated with x-rays: normal vision retained after thirty-four years; second report on a case. *AMA Arch Ophthalmol*, 48(6), 720-722.
- Viatour, P., Bentires-Alj, M., Chariot, A., Deregowski, V., de Leval, L., Merville, M. P., & Bours, V. (2003). NF- kappa B2/p100 induces Bcl-2 expression. *Leukemia*, 17(7), 1349-1356. doi:10.1038/sj.leu.2402982

9. Appendix

- Villegas, V. M., Hess, D. J., Wildner, A., Gold, A. S., & Murray, T. G. (2013). Retinoblastoma. *Curr Opin Ophthalmol*, 24(6), 581-588. doi:10.1097/ICU.0000000000000002
- Vinogradova Iu, V., Tronov, V. A., Liakhova, K. N., Poplinskaia, V. A., & Ostrovskii, M. A. (2014). [Damage and functional recovery of the mouse retina after exposure to ionizing radiation and methylnitrosourea]. *Radiats Biol Radioecol*, 54(4), 385-392.
- Vogelstein, B., Lane, D., & Levine, A. J. (2000). Surfing the p53 network. *Nature*, 408(6810), 307-310. doi:10.1038/35042675
- Wanner, G., Mayer, C., Kehlbach, R., Rodemann, H. P., & Dittmann, K. (2008). Activation of protein kinase Cepsilon stimulates DNA-repair via epidermal growth factor receptor nuclear accumulation. *Radiother Oncol*, 86(3), 383-390. doi:10.1016/j.radonc.2007.10.041
- Wenzel, A. A., O'Hare, M. N., Shadmand, M., & Corson, T. W. (2015). Optical coherence tomography enables imaging of tumor initiation in the TAG-RB mouse model of retinoblastoma. *Mol Vis*, 21, 515-522.
- Wetzig, P. C. (1966). Fluorescein photography. In the differential diagnosis of retinoblastoma. *Am J Ophthalmol*, 61(2), 341-343.
- Yamane, T., Kaneko, A., & Mohri, M. (2004). The technique of ophthalmic arterial infusion therapy for patients with intraocular retinoblastoma. *Int J Clin Oncol*, 9(2), 69-73. doi:10.1007/s10147-004-0392-6
- Yanik, O., Gunduz, K., Yavuz, K., Tacyildiz, N., & Unal, E. (2015). Chemotherapy in Retinoblastoma: Current Approaches. *Turk J Ophthalmol*, 45(6), 259-267. doi:10.4274/tjo.06888
- Ye, W., Jiang, Z., Li, G. X., Xiao, Y., Lin, S., Lai, Y., Li, P. (2015). Quantitative evaluation of the immunodeficiency of a mouse strain by tumor engraftments. *J Hematol Oncol*, 8, 59. doi:10.1186/s13045-015-0156-y
- Yuhas, J. M. (1970). Biological factors affecting the radioprotective efficiency of S-2-[2-aminopropylamino] ethylphosphorothioic acid (WR-2721). LD50(3)) doses. *Radiat Res*, 44(3), 621-628.
- Zhang, J., Schweers, B., & Dyer, M. A. (2004). The first knockout mouse model of retinoblastoma. *Cell Cycle*, 3(7), 952-959.

9.2 Declaration according to § 5 Abs. 2 No. 8 of the PromO of the Faculty of Science - Share in publications done in team work

Name: Tschulakow Alexander Viktor

List of Publications

1. Establishment of a novel retinoblastoma (Rb) nude mouse model by intravitreal injection of human Rb Y79 cells - comparison of *in vivo* analysis versus histological follow up.

Tschulakow AV, Schraermeyer U, Rodemann HP, Julien-Schraermeyer S

Biol Open. 2016 Nov 15; 5(11):1625-1630. doi: 10.1242/bio.019976.

2. The radioprotector ortho-phospho-L-tyrosine (pTyr) attenuates the side effects of fractionated irradiation in retinoblastoma mouse models but also decreases the local tumour control.

Tschulakow AV, Dittmann K, Huber SM, Klumpp D, Stegen B, Schraermeyer U, Rodemann HP, Julien-Schraermeyer S

Radiother Oncol. 2017 Jul 12; pii: S0167-8140(17)30434-6. doi: 10.1016/j.radonc.2017.06.023.

| Nr. | Accepted for publication yes/no | Number of all authors | Position of the candidate in list of authors | Scientific ideas of candidate (%) | Data generation by candidate (%) | Analysis and Interpretation by candidate (%) | Paper writing by candidate (%) |
|-----|---------------------------------|-----------------------|---|-----------------------------------|----------------------------------|--|--------------------------------|
| | | | <i>Optional, the declaration of the own share can also be done in words, please add an extra sheet.</i> | | | | |
| 1 | yes | 4 | 1 | 30 | 80 | 90 | 80 |
| 2 | yes | 8 | 1 | 50 | 80 | 90 | 80 |

I certify that the above statement is correct.

Date, Signature of the candidate

9.3 List of publications

Peer-reviewed journal articles:

1. The anatomy of the foveola reinvestigated.

Tschulakow AV, Oltrup T, Bende T, Schmelzle S, Schraermeyer U.

PeerJ 2018 Mar 12, 6, e4482. doi:10.7717/peerj.4482

2. The radioprotector ortho-phospho-L-tyrosine (pTyr) attenuates the side effects of fractionated irradiation in retinoblastoma mouse models but also decreases the local tumour control.

Tschulakow AV, Dittmann K, Huber SM, Klumpp D, Stegen B, Schraermeyer U, Rodemann HP, Julien-Schraermeyer S.

Radiother Oncol. 2017 Jul 12; pii: S0167-8140(17)30434-6. doi: 10.1016/j.radonc.2017.06.023.

3. Effects of intravitreally injected Fc fragment on rat eyes.

Taubitz T, Steinbrenner LP, **Tschulakow AV**, Biesemeier A, Julien-Schraermeyer S, Schraermeyer U.

Graefes Arch Clin Exp Ophthalmol. 2016 Dec 25; 4(12):2401-2409. doi: 10.1007/s00417-016-3511-y.

4. Establishment of a novel retinoblastoma (Rb) nude mouse model by intravitreal injection of human Rb Y79 cells - comparison of *in vivo* analysis versus histological follow up.

Tschulakow AV, Schraermeyer U, Rodemann HP, Julien-Schraermeyer S.

Biol Open. 2016 Nov 15; 5(11):1625-1630. doi: 10.1242/bio.019976.

5. The Effects of VEGF-A-inhibitors aflibercept and ranibizumab on the ciliary body and iris of monkeys.

Ludinsky M; Christner S; Su N; Taubitz T; **Tschulakow AV**; Antje Biesemeier A; Julien S; Schraermeyer U.

Graefes Arch Clin Exp Ophthalmol. 2016 Jun 25; 4(6):1117-25. doi: 10.1007/s00417-016-3344-8.

9. Appendix

6. Effects of a single intravitreal injection of aflibercept and ranibizumab on glomeruli of monkeys.

Tschulakow AV, Christner S, Julien S., Ludinsky M, van der Giet M, Schraermeyer U.

PLoS One. 2014 Nov 21; 9(11):e113701. doi: 10.1371/journal.pone.0113701.

7. First study of oral Arteminol-R in advanced cervical cancer: clinical benefit, tolerability and tumour markers.

Jansen FH, Adoubi I, Kouassi Comoe JC, De Cnodder T, Jansen N, **Tschulakow AV**, Efferth T.

Anticancer Res. 2011 Nov 31; 4417-4422. doi: -

8. Sleep and circadian rhythm regulate circulating complement factors and immunoregulatory properties of C5a.

Reis ES, Lange T, Köhl G, Herrmann A, **Tschulakow AV**, Naujoks J, Born J, Köhl J.

Brain Behav Immun. 2011 Oct 25; (7):1416-26. doi: 10.1016/j.bbi.2011.04.011.

9. A new approach to the memory of water.

Tschulakow AV, Yan Y & Klimek W.

Homeopathy. 2005 Oct 9; 4, 241-247. doi: 10.1016/j.homp.2005.07.003.

Submitted articles:

1. Data showing the shapes of cones and Müller cells within the fovea of monkeys reconstructed from serial sections and focused ion beam analysis.

Schraermeyer U; Schmelzle S; **Tschulakow AV**.

Submitted in Data in Brief 02.03.2018

2. Ultrastructural alterations in the retinal pigment epithelium and photoreceptors of a Stargardt patient and Stargardt mouse models: evidence for the central role of RPE melanin in oxidative stress.

Taubitz T, **Tschulakow AV**, Tikhonovich M, Illing B, Fang Y, Biesemeier AK, Julien-Schraermeyer S, Schraermeyer U.

Submitted in PeerJ 24.02.2018

Citable abstracts, posters, presentations and lectures at congresses:

1. Effect of the pre-treatment with the radioprotector ortho-phospho-L-tyrosine (pTyr) in a xenograft retinoblastoma mouse model.

Tschulakow AV; H. Peter Rodemann H-P; Huber SM; Rittgarn M; Klumpp D; Steegen B; Schraermeyer U; Julien-Schraermeyer S.

Invest. Ophthalmol. Vis. Sci. 2017; 58(8): ARVO E-Abstract 1775.

ARVO (Association for Research in Vision and Ophthalmology) meeting, in Baltimore Maryland (2017)

2. Unravelling the mystery of the Stiles Crawford Effect.

Schraermeyer U; Schultheiss S; Oltrup T; Bende T; Schmelzle S; **Tschulakow AV**

Invest. Ophthalmol. Vis. Sci. 2017; 58(8): ARVO E-Abstract 5603.

ARVO (Association for Research in Vision and Ophthalmology) meeting, in Baltimore Maryland (2017)

(A.V. Tschulakow gave the talk on behalf of Prof. U Schraermeyer)

3. Preclinical results of a new pharmacological therapy approach for Stargardt disease and dry age-related macular degeneration.

Fang Y; **Tschulakow AV**; Tikhonovich M; Taubitz T; Illing B; Schultheiss S; Schraermeyer U; Julien-Schraermeyer S.

Invest. Ophthalmol. Vis. Sci. 2017; 58(8): ARVO E-Abstract 256.

ARVO (Association for Research in Vision and Ophthalmology) meeting, in Baltimore Maryland (2017)

9. Appendix

4. A valid ultrastructural rat choroidal neovascularization model developed by overexpression of VEGF.

Shan Liu; **Tschulakow AV**; Julien-Schraermeyer S; Schraermeyer U; Biesemeier AK.

Invest. Ophthalmol. Vis. Sci. 2017; 58(8): ARVO E-Abstract 2269.

ARVO (Association for Research in Vision and Ophthalmology) meeting, in Baltimore Maryland (2017)

5. Effects of pretreatment with the radioprotector ortho-phospho-L-tyrosine (pTyr) on Rb+/- mice after radiation exposure - Implication for the treatment of retinoblastoma patients with radiotherapy.

Tschulakow AV; Rodemann H-P; Huber SM; Rittgarn M; Schraermeyer U; Julien-Schraermeyer S.

Invest. Ophthalmol. Vis. Sci. 2015; 56(7): ARVO E-Abstract 72

ARVO (Association for Research in Vision and Ophthalmology) meeting, in Denver Colorado (2015)

6. Removal of lipofuscin from the RPE of Abca4 -/- mice with THPE: quantitative and toxicity studies.

Taubitz T; Peters T; Pöschel S; **Tschulakow AV**; Rittgarn M; Schultheiss S; Schenke-Layland K; Burnet M; Julien S; Schraermeyer U.

Invest. Ophthalmol. Vis. Sci. 2015; 56(7): ARVO E-Abstract 4199

ARVO (Association for Research in Vision and Ophthalmology) meeting, in Denver Colorado (2015)

7. Intravitreal injection of Fc-fragments has multiple adverse effects on retina and choroid.

Ulrich Schraermeyer; Tatjana Taubitz; Laura-Pia Steinbrenner; Tobias Peters; Antje Kristina Biesemeier; Monika Rittgarn; Sigrid Schultheiss; **Tschulakow AV**; Julien S .

Invest. Ophthalmol. Vis. Sci. 2015; 56(7): ARVO E-Abstract 1511

ARVO (Association for Research in Vision and Ophthalmology) meeting, in Denver Colorado (2015)

9. Appendix

8/9. Establishment of a new retinoblastoma mouse model by intravitreal injection of human retinoblastoma Y79 cells into nude mice eyes - Comparison of SLO/OCT vs. histological follow up.

Tschulakow AV; Rodemann H-P; Schraermeyer U; Julien S.

Invest. Ophthalmol. Vis. Sci. 2014; 55(13): ARVO E-Abstract 3074.

Annual meeting of the German Society for Radiation Research (GBS) in Tuebingen, 2014 and ARVO (Association for Research in Vision and Ophthalmology) meeting , in Orlando Florida (2014)

10. Effects of a single intravitreal injection of aflibercept and ranibizumab on glomeruli of monkeys.

Julien S; **Tschulakow AV**; Christner S; Schraermeyer U.

Invest. Ophthalmol. Vis. Sci. 2014; 55(13): ARVO E-Abstract 1946.

ARVO (Association for Research in Vision and Ophthalmology) meeting, in Orlando Florida (2014)

11. A Role for the Mineralocorticoid Receptor in the Redistribution of naive T Cells during Sleep in Humans.

Besedovsky L, **Tschulakow AV**, Linz B, Born J, Lange T.

NeuroImmunoModulation Jan 2011 18, 6, 364-364

12/13. The triterpenoid saponins of *Gynostemma pentaphyllum* exert anti-cancer effects in nasopharyngeal carcinoma cell lines and xenograft mouse model.

Tschulakow AV, TAI W, HSIAO W.

7th International Postgraduate Symposium on Chinese Medicine, Hong Kong (2011) and 10th meeting of the Consortium for Globalization of Chinese Medicine, in Shanghai (2011)

9.4 Articles from other projects published during PhD study

9.4.1 The anatomy of the foveola reinvestigated

The anatomy of the foveola reinvestigated

Alexander V. Tschulakow¹, Theo Oltrup², Thomas Bende², Sebastian Schmelzle³ and Ulrich Schraermeyer^{1,4}

¹ Division of Experimental Vitreoretinal Surgery, Centre for Ophthalmology, University Hospital Tübingen, Tübingen, Germany

² Division of Experimental Ophthalmic Surgery, Centre for Ophthalmology, University Hospital Tübingen, Tübingen, Germany

³ Ecological Networks, Department of Biology, Technische Universität Darmstadt, Darmstadt, Germany

⁴ Ocutox (www.ocutox.com), Hechingen, Germany

ABSTRACT

Objective. In the foveola of the eye, photoreceptors and Müller cells with a unique morphology have been described, but little is known about their 3D structure and orientation. Considering that there is an angle-dependent change in the foveolar photoreceptor response for the same light beam, known as the Stiles Crawford Effect of the first kind (SCE I), which is still not fully understood, a detailed analysis of the anatomy of the foveolar cells might help to clarify this phenomenon.

Methods. Serial semithin and ultrathin sections, and focused ion beam (FIB) tomography were prepared from 32 foveolae from monkeys (*Macaca fascicularis*) and humans. Foveolae were also analyzed under the electron microscope. Serial sections and FIB analysis were then used to construct 3D models of central Müller and photoreceptor cells. In addition, we measured the transmission of collimated light under the light microscope at different angles after it had passed through human foveae from flat mounted isolated retinae.

Results. In monkeys, outer segments of central foveolar cones are twice as long as those from parafoveal cones and do not run completely parallel to the incident light. Unique Müller cells are present in the central foveolae (area of 200 μm in diameter) of humans and monkeys. Light entering the fovea center, which is composed only of cones and Müller cells, at an angle of 0° causes a very bright spot after passing through this area. However, when the angle of the light beam is changed to 10°, less light is measured after transpassing through the retina, the foveolar center becomes darker and the SCE-like phenomenon is directly visible. Measurements of the intensities of light transmission through the central foveola for the incident angles 0 and 10° resemble the relative luminance efficiency for narrow light bundles as a function of the location where the beam enters the pupil as reported by Stiles and Crawford. The effect persisted after carefully brushing away the outer segments.

Conclusion. We show that unique cones and Müller cells with light fibre-like properties are present in the center of the fovea. These unique Müller cells cause an angle dependent, SCE-like drop in the intensity of light guided through the foveola. Outer segments from the foveolar cones of monkeys are not straight.

Subjects Biophysics, Cell Biology, Anatomy and Physiology, Ophthalmology, Histology

Keywords Foveola, Fovea, Müller glial cells, Cone receptors, 3D model, Stiles–Crawford effect

Submitted 11 January 2018
Accepted 20 February 2018
Published 12 March 2018

Corresponding author
Ulrich Schraermeyer,
u.schraermeyer@gmail.com,
Ulrich.Schraermeyer@med.uni-tuebingen.de

Academic editor
Juan Riesgo-Escovar

Additional Information and
Declarations can be found on
page 13

DOI 10.7717/peerj.4482

© Copyright
2018 Tschulakow et al.

Distributed under
Creative Commons CC-BY 4.0

OPEN ACCESS

INTRODUCTION

The primate retina contains two types of photoreceptors, rods for night vision and cones for daylight vision. Cones are predominately located in the macula lutea. This has a diameter of around 5.5 mm in humans and is subdivided into the fovea and parafovea with diameters of 1.8 mm and 2.3 mm, respectively (Hogan, Alvarado & Weddell, 1971).

The fovea is a small pit in the retina which contains the largest concentration of cones and is responsible for sharp central vision. The central part of the fovea is called the foveola (Hogan, Alvarado & Weddell, 1971) and has been regarded as being 350 μm in diameter since 1941 (Polyak, 1941). Only in the foveola does visual acuity reach 100 percent (Trauzettel-Klosinski, 2010).

The original discovery by Stiles and Crawford described that the apparent brightness of an object is not proportional to the pupil area because light rays entering the pupil distant from the axis are not so visually effective as rays entering along or near to the central axis (Stiles & Crawford, 1933).

Stiles also showed that monochromatic light will differ in hue between on- and off-axis even after the light beams are equated for brightness. This was described as the Stiles–Crawford effect of the second kind (SCE 2).

The Stiles Crawford Effect of the first kind (SCE I) was regarded as one of the most important discoveries in visual science of the last century (Westheimer, 2008). The explanation of the SCE has so far been handled in abstract models involving specific photoreceptor orientation, subtle morphological differences in rods and cones, anchoring of photo-pigment molecules in membranes or possible phototropism of retinal cells (Laties, 1969). But none of these models could be proven and a full explanation of the SCE continues to provide challenges (Westheimer, 2008).

Since the first report of Stiles and Crawford, a large body of histological and psychophysical evidence has accumulated (for review see Westheimer, 2008) showing that cones in different retinal regions are directionally sensitive.

It was speculated that a change in the shape or the orientation of foveal cones was probably responsible for the SCE (Westheimer, 1967). But until now, no morphologic evidence for this assumption has been found, and in contrast a different orientation of foveal and parafoveal cones in monkeys and humans (Hogan, Alvarado & Weddell, 1971) was ruled out by histologic examinations more than four decades ago (Laties, 1969; Westheimer, 2008). To study the SCE I, monkey eyes are suitable because human and monkey foveae are very similar (Krebs & Krebs, 1991) and the existence of the SCE I has also been demonstrated for monkeys (Matsumoto et al., 2012).

The most renowned publication about the histology of the human eye (Hogan, Alvarado & Weddell, 1971) states that in meridional sections of the foveolar region, the cones are perfectly straight and oriented vertically with respect to the retinal surface, and their axes are parallel to each other. Thus, the view that foveal cones lack directional morphology has remained valid right up to the present day.

Clinically the SCE I is used for diagnosis of macular telangiectasia type 2 (Charbel Issa et al., 2016) which is a poorly understood condition of the retina that may result in blindness (Charbel Issa et al., 2013).

The SCE is absent in rod photoreceptors (Lu et al., 2013) leading to the speculation that differences in photo-pigment structure and anchoring of cones and rods may be involved in SCE (Enoch & Stiles, 1961; Walraven & Bouman, 1960; Westheimer, 2008). Despite its pivotal role for sharp central vision the definite anatomy of the fovea at high resolution is not known (Yamada, 1969).

The aim of our study was to investigate the 3D anatomy of foveolar cells (Fig. 1) and whether it can help to explain the SCE I.

MATERIALS AND METHODS

Light and electron microscopy from monkey eyes

Twenty-four monkey eyes (*Macaca fascicularis*, 14 males, 10 females) were collected after sacrificing the animals under general anesthesia, i.e., intramuscular injection of ketamine hydrochloride followed by an intravenous sodium pentobarbitone (Lethabarb[®], Virbac, Australia) overdose. Monkeys were kept at Covance Laboratories GmbH (Münster, Germany study numbers 0382055, 8260977, 8274007) or SILABE-ADUEIS (Niederhausbergen, France). The Covance Laboratories GmbH test facility is fully accredited by the Association for Assessment and Accreditation of Laboratory Animal Care (AAALAC). This study was approved by the local Institutional Animal Care and Use Committee (IACUC), headed by Dr. Jörg Luft and the work was carried out in accordance with the Code of Ethics of the World Medical Association (Declaration of Helsinki). The monkeys from SILABE-ADUEIS were euthanized due to veterinarian reasons. Since they had not been included in a study before, they do not have a study number. The age of the monkeys varied between four to eight years. The eyes were enucleated 5 min post-mortem, cleaned of orbital tissue, and were slit carefully at the limbus without damaging the ora serata. Then, 200 μ l of the fixative (5% glutaraldehyde) were carefully injected into the center of the vitreous. The intraocular pressure was balanced because vitreous could leak out from the opening thereby compensating the volume of the fixative. This protocol has been shown to minimize fixation artefacts according to our own experience. The eyes were then fixed at 4 °C by immersion into 5% glutaraldehyde in 0.1 M cacodylate buffer (pH 7.4; Sigma, St. Louis, MO, USA) overnight for electron microscopy. Glutaraldehyde fixed specimens were post-fixed with 1% OsO₄ at room temperature in 0.1 M cacodylate buffer (pH 7.4), stained with uranyl acetate, and the maculae were excised and embedded in Epon after dehydration in a graded series of ethanol and propylene oxide. Semi-thin sections were stained with toluidine blue and examined by light microscopy (Zeiss Axioplan 2 imaging; Zeiss, Jena, Germany). For electron microscopy, ultrathin sections were made and analyzed with a Zeiss 900 electron microscope (Zeiss, Jena, Germany). The foveae from 24 eyes were sectioned in a sagittal plane until the center of 21 foveolae was found. In three eyes, the foveal centers were missed. The center of the foveola was defined as the site where the cell fiber layers at the bottom of the foveal pit were free of nuclei and were 10 μ m thin or less.

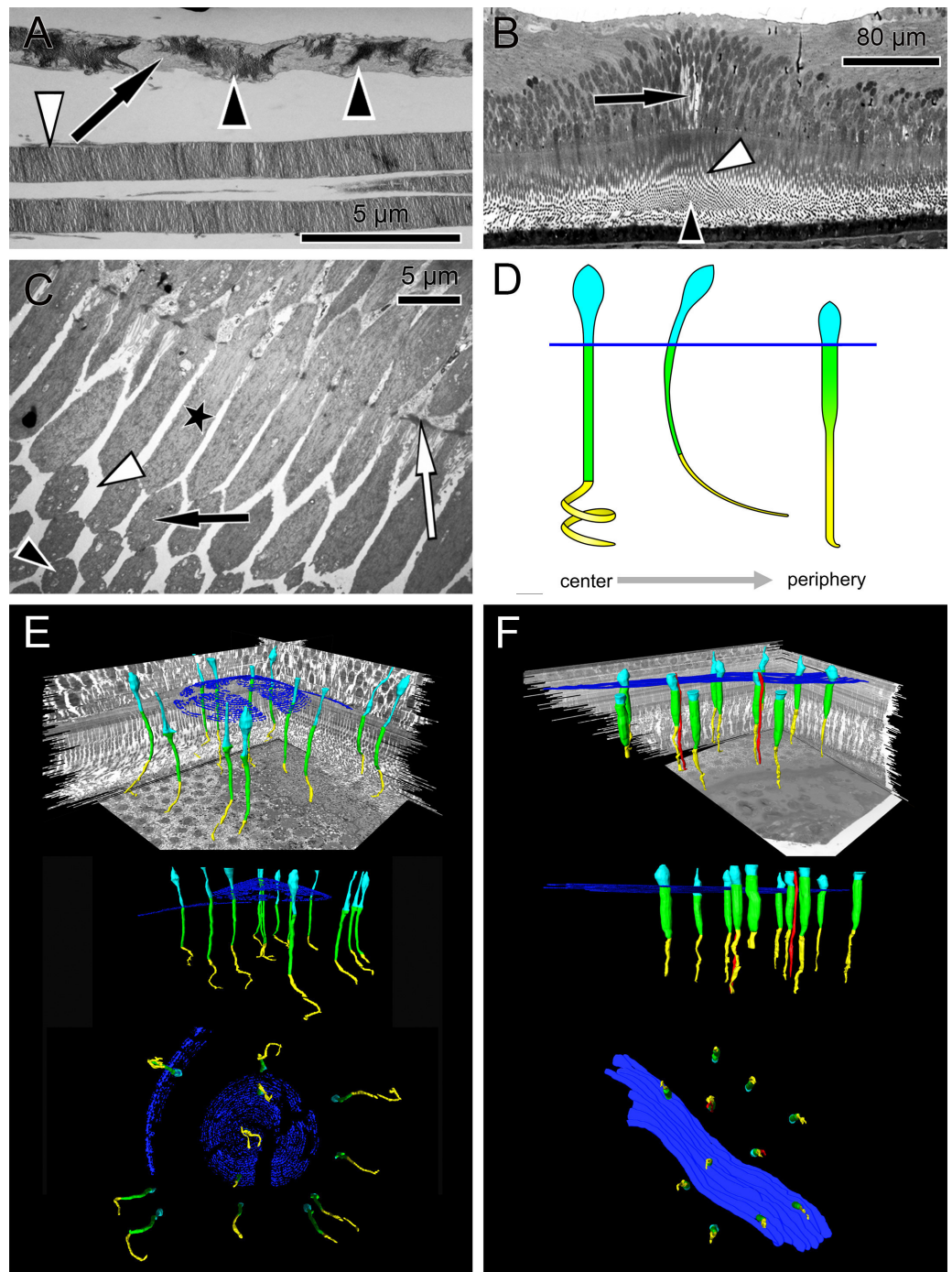


Figure 1 Anatomical findings in monkey foveae and cones. (A) In an electron micrograph, an extra foveal cone contains irregularly ordered stacks of photoreceptor disc membranes (black arrowheads) and spaces free of photoreceptor membranes (white arrowhead). In contrast, the disk membranes in rods are highly ordered (white arrowhead). (B) In a semi-thin transverse section of the central fovea, the prominent Müller cells are present (arrow). Inner segments are curved and are (continued on next page...)

Full-size DOI: 10.7717/peerj.4482/fig-1

Figure 1 (...continued)

cut transversely in the plane of section. Spaces between the curved inner segments form symmetrical patterns (white arrowhead) (see also C and the model in D). Also in the middle of the subretinal space the outer segments are cut transversely (black arrowhead). (C) In an electron micrograph sectioned parallel to the optical axis through the central fovea, the inner segments of the cones are cut longitudinally (asterisk), diagonally (black arrow) and transversely (black arrowhead) in the same plane of section indicating their curved nature. The spaces between the curved inner segments shown in (B) are marked (white arrowhead). The white arrow marks the outer limiting membrane. (D) Different shapes of cones are presented schematically from the central fovea to the parafovea. (E + F) Central cones (E) and parafoveal cones (F) are shown in different views integrated into the retinal environment (top), from the front (middle) or from the RPE towards the vitreous (bottom). Parafoveal rods are marked in red, inner segments in green, outer segments in yellow and the outer limiting membrane in blue.

Light and electron microscopy from human eyes

Three human eyes from a 57 and 81-year-old male, and a 68-year-old female were fixed 8 and 12 h postmortem at 4 °C by immersion into 5% glutaraldehyde in 0.1 M cacodylate buffer (pH 7.4; Sigma, St. Louis, MO, USA) for half an hour. Then the cornea was removed and fixation continued overnight for electron microscopy. The human eyes were gifts from the Clinical Anatomy of the University of Tuebingen (ethical number for scientific issues 237/2007B01), and taken from full body donors, who had previously given informed consent. Embedding and sectioning was done as described for the monkey eyes.

Evaluation of serial sections through the fovea of monkey and humans

For 3D model reconstruction, semi-thin (700 nm) serial sections were performed from 6 monkey foveae.

Series 1 and 2 comprised 21 sections which correspond after mounting to a foveal tissue piece with a thickness of 14.7 µm. Unexpectedly, due to their curved shape, a foveal cone did not completely fit into such a tissue block. Therefore series 3 and 4 were sectioned in sagittal planes with 41 and 160 sections respectively. Additionally, series 5 and 6 were cut as transverse sections with 450 and 195 sections respectively. Sagittal sections run within or parallel to the optical axis, while transverse sections were made perpendicular to it.

Serial transverse sections were performed from two human foveae. Series 7 from a 68-year-old female and series 8 from an 81-year-old male contained 250 and 460 sections, respectively. From each section, the fovea was photographed at a 600-fold magnification.

3D modelling

The 3D reconstructions of the presented figures and measurements were performed with Amira® software (version 5.6; FEI, Hillsboro, OR, USA). Using previous embedded fixed marker, the images of the sections were aligned manually following digitization by comparing superimposed slices, translating, and rotating adjacent slides with respect to one another. Additionally, the border of each slide and the regular structures and patterns were used as markers for alignment.

Once the aligned sections were imported into Amira, the structures of interest were labeled using the software segmentation tools. The structures of interest were cone nuclei, inner and outer segments, the outer limiting membrane, and Müller cells. The length of the

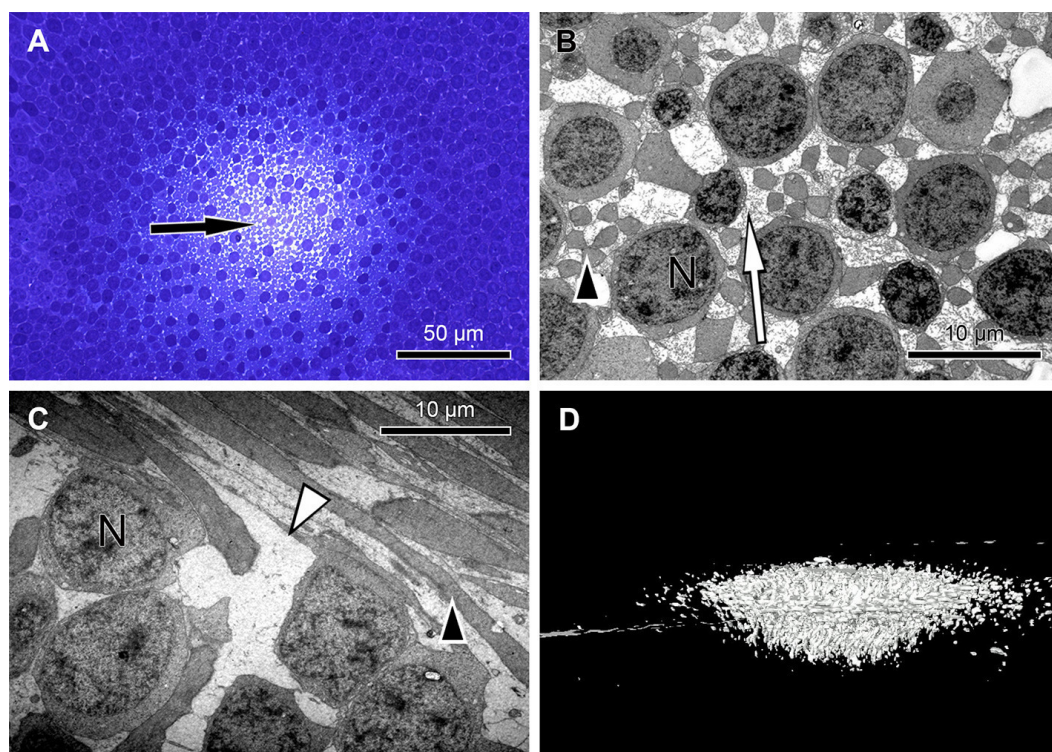


Figure 2 Unique central foveolar Müller cells from monkeys. In the fovea there are only two types of cells. Müller cells appear white or electron-lucent and cone photoreceptors appear blue or electron-opaque. Thus they can be easily distinguished. (A) In a semi-thin section perpendicular to the optical axis the central Müller cells are translucent (arrow). (B) The Müller cells (arrow) are shown in the same orientation as in (A) at high magnification. They do not contain cell organelles at this topographic site and appear white or electron-lucent. The arrowhead marks a Henle fibre. (C) The plateau zone of a Müller cell is indicated by a white arrowhead in a section parallel to the optic axis. Henle fibers are indicated by a black arrowhead and cone nuclei by (N). (D) A 3D model shows the main part of the central Müller cells of a monkey.

Full-size  DOI: [10.7717/peerj.4482/fig-2](https://doi.org/10.7717/peerj.4482/fig-2)

inner and outer segments of cones from the parafovea and the central fovea were measured using the “Amira-3D length—measurement-tool”. For Fig. 2D and Video S1, areas of interest were selected by visually adjusting the grey value threshold of the volumetric dataset.

Focused ion beam/scanning electron microscopy

Focused ion beam/scanning electron microscopy (FIB/ SEM) tomography data were acquired using a Zeiss Auriga CrossBeam instrument at the Natural and Medical Sciences Institute at the University of Tuebingen (NMI, Reutlingen, Germany) as described (Steinmann *et al.*, 2013). For FIB/SEM analysis, the block of the embedded sample was sputter coated with gold palladium and mounted on an appropriate SEM sample holder. A semi-thin section of the embedded sample was imaged with the light microscope and correlated with the SEM image of the ultramicrotome block face to define the region of interest for three-dimensional analysis. Using a Crossbeam instrument (Zeiss) equipped

with a gallium FIB and a low voltage SEM, FIB/SEM serial sectioning tomography was accomplished. The gallium FIB produces thereby a series of cross-sections containing the region of interest. Each of these cross-sections is imaged by the low keV SEM using the energy-selected backscattered (EsB) electron detector for image acquisition. The following parameters were used for SEM: Primary energy of 1.8 keV with the aperture 60 μm : for image acquisition the EsB detector was used with a grid voltage of $-1,500$ V, i.e., only backscattered electrons with a maximum energy loss of 300 V were used for image acquisition. The resolution was $2,048 \times 1,535$ pixels with a pixel size of 42.41 nm.

For FIB, the following parameters were used: Primary energy of 30 keV, slicing was performed with a probe current of 2 nA, the slice thickness was 42 nm. In this way cubic voxels were obtained, i.e., the same resolution in x, y , and z , which is good for the reconstruction. The resulting stack of two-dimensional images was utilized for three-dimensional reconstruction using appropriate software.

Wholemout preparations from human retinae

The maculae of five eyes from three donors were excised using a trephine with 1 cm diameter. The donors were two females of 74 and 90 years old, and one male of age 18. Three maculae were fixed in formalin transferred into phosphate buffered saline and mounted on slides covered with a cover glass on wax feet to prevent squeezing of the retinae. Another two eyes were treated identically but fixation was omitted. Finally, the maculae were observed under the light microscope having the condenser replaced by a modification with adjustable mirror (Fig. 3C).

Illumination optics for measuring angle dependent light transmission through Müller cells

The optical fiber homogenizes the light of the light-emitting diode (LED). The light cone at the end of the fibre is collimated with an aspherical lens. With the focal length f_{col} , the core diameter D_{fiber} defines the divergence angle θ_{div} and the opening angle θ_{NA} defines the diameter D_{spot} of the light spot on the sample. The mirror can be tilted and slid. The angle of incidence of light on the sample is α_{slide} .

To homogenize the intensity distribution of the light spot to be projected, the light from a light emitting diode (high power white LED, type: OSOLON SSL, LCW CP7P.PC) is coupled to an optical fibre with the core diameter $D_{\text{core}} = 200$ μm (Fig. 3C). Through the principle of total reflection, the incident light in this optical conductor is reflected on the wall several times. In this way, the light is mixed and emerges homogeneously from the conductor. The light cone emitted in the opening angle θ_{NA} is collimated by an aspheric lens of focal length $f_{\text{col}} = 35$ mm. Since the light is not a point source, the rays diverge slightly. The divergence angle is in paraxial approximation $\theta_{\text{div}} = D_{\text{core}}/f_{\text{col}} = 0.2$ mm/35 mm = 5.7 mrad (0,3°). The diameter D_{spot} of the projected light spots is given as $\text{NA} = 0.16$ through the focal length f_{col} of the lens and the numerical aperture of the optical fibre. With $\text{NA} = \theta_{\text{NA}}/2$, $D_{\text{spot}} = 2 \cdot f_{\text{col}} \cdot \text{NA} = 2 \cdot 35$ mm \cdot 0,16 = 11,2 mm. The light striking the slide at an angle α_{slides} is partially reflected according to the Fresnel equations and should be taken into account when measuring the intensity on the microscope. In normal incidence, $\alpha_{\text{slide}} = 0^\circ$,

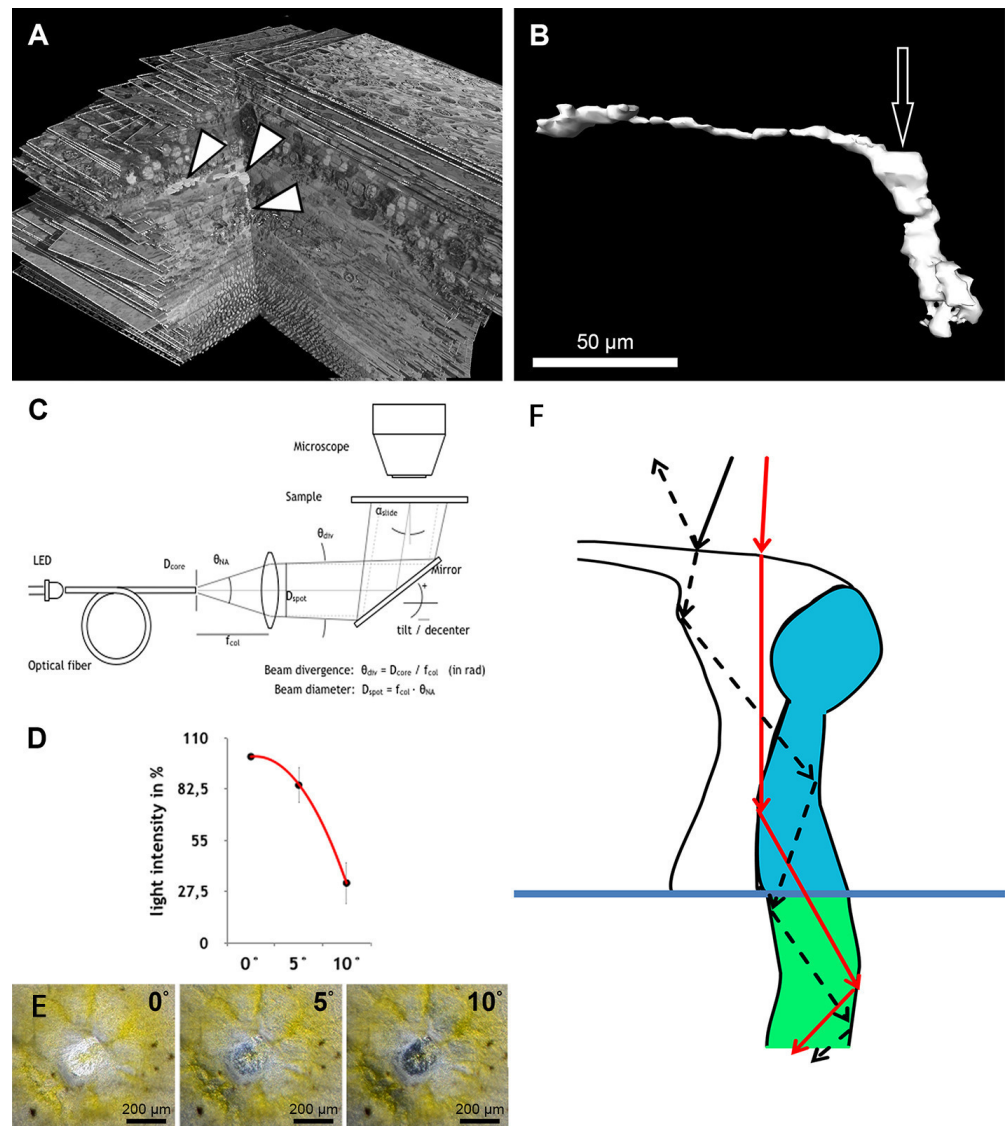


Figure 3 Measurement of light intensity after transpassing human foveolae. (A) The central Müller cell (arrowheads) is shown integrated into a stack mounted from serial sections. (B) A human foveolar Müller cell 3D model is shown and its plateau zone marked by an arrow. (C) Schematic drawing of the measurement equipment is shown. Illumination optics for angle measurement at the Müller cells. The optical fiber homogenizes the emitted light of the light-emitting diode (LED). The light cone at the fiber end is collimated with an aspherical lens. With the focal length f_{col} , the core diameter D_{core} defines the divergence angle θ_{div} and the aperture angle θ_{NA} defines the diameter D_{spot} of the light spot on the sample. The mirror is rotatable and movable. The angle of light incidence on the sample is α_{slide} . (For more details, see Methods.) (D) Measurements of light intensities of translucent light in the foveolar centre entering at different angles are shown. The mean loss of intensity + standard deviation at an angle of 5 and 10° was calculated as a percentage of the 0°'s value and was 15,3% + 9,6% and 67,8% + 11,3% respectively. (E) A human foveolar center is shown in translucent light entering at 0, 5 and 10° respectively. These images correspond to the measurements in (D). (F) Hypothetical explanation of the SCE-like drop of light intensity: light hitting the Müller cell at an angle is partly reflected (black dashed line) at the surface when entering the watery cytoplasm and reduces the transmission of light into the cones. Light not entering at an angle is fully transmitted into the cones (red line).

Full-size DOI: 10.7717/peerj.4482/fig-3

the transmitted light intensity is about 96% of the incident intensity, depending on the refractive index of the slide when $n_{\text{slide}} = 1.5255$ ($\lambda = 546$ nm, borosilicate glass/Schott). The intensity declines by about 4% when light incidence is under $\alpha_{\text{slide}} = 20^\circ$. The angle $\alpha_{\text{müller}}$ of a light beam to a Müller cell can be distinguished from the angle of incidence on the slide through the multiple refractions of previous optical layers (glass material etc.). This angle is determined by the refractive index n_{front} of the substrate before the Müller cell and the angle of incidence $\alpha_{\text{müller}} = \alpha_{\text{slide}}/n_{\text{front}}$.

The maximum acceptance angle (half angle) under which a light beam can penetrate the cell is

$$\Theta_{\text{max}} = \sin^{-1} \left(\frac{1}{n_{\text{front}}} \sqrt{n_{\text{core}}^2 - n_{\text{gladding}}^2} \right), \quad (1)$$

with the refractive indices n_{core} of the substrate within the cell and $n_{\text{gladding}} < n_{\text{core}}$ of the cell edge.

The acceptance angle of the Müller cells *in vivo* is estimated with the refractive indices according to Franze *et al.* (2007) whereby $n_{\text{front}} = 1.358$ (neuron), when the light coupling of a cell does not connect to the vitreous body of the eye, and $n_{\text{core}} = 1.359$ (end foot). The refractive index of the cell edge is not known and is set as $n_{\text{gladding}} = n_{\text{front}}$. According to Eq. (1), the acceptance angle *in vivo* is $\theta_{\text{max}} = 2,2^\circ$. When fixing the sample with phosphate buffered saline (PBS—buffer, $n_{\text{PBS}} = 1.33$) it can be assumed that the substrate surrounding the Müller cells has the index value $n_{\text{gladding}} = n_{\text{PBS}}$. The acceptance angle is then $\theta_{\text{max}} = 12,0^\circ$ and is measured in the experiment with $\alpha_{\text{slide}} = n_{\text{front}} \cdot \theta_{\text{max}} = 16^\circ$.

Quantification of angle dependent foveal light transmission

Light micrographs with 100-fold magnification from the foveae and parafoveae of the three donors were taken under equal conditions with collimated light hitting the sample at a 0° , 5° , and 10° angle. The photos were processed using ImageJ 1.48v. The mean pixel intensity of the fovea or parafovea area was measured. The value of the image taken at the angle of 0° was set as 100% for each fovea. The mean loss of intensity \pm standard deviation at an angle of 5° and 10° was calculated as a percentage of the 0° 's value.

RESULTS

The first interesting finding was that the arrangement of disk membranes is more regular in rods compared to cones (Fig. 1A).

In semi- and ultrathin cross sections of fixed monkey foveolae, inner and outer segments of the cone photoreceptors were arranged in a highly ordered pattern (Fig. 1B). In the same plane of section, the inner segments were hit longitudinally, diagonally, and transversely in subsequent underlying rows (Figs. 1C and 4). These results indicate that the inner segments of the cones in the central foveola area are curved. We detected curved inner segments in 18 out of 21 monkey foveae. There were substantial differences in the shape of individual foveae, which corresponds to the variance among individuals observed in psychophysical measurements (He, Marcos & Burns, 1999). The diameter of the area containing curved inner segments was $267 \mu\text{m} \pm 132 \mu\text{m}$. A calculation of cone numbers in the central part

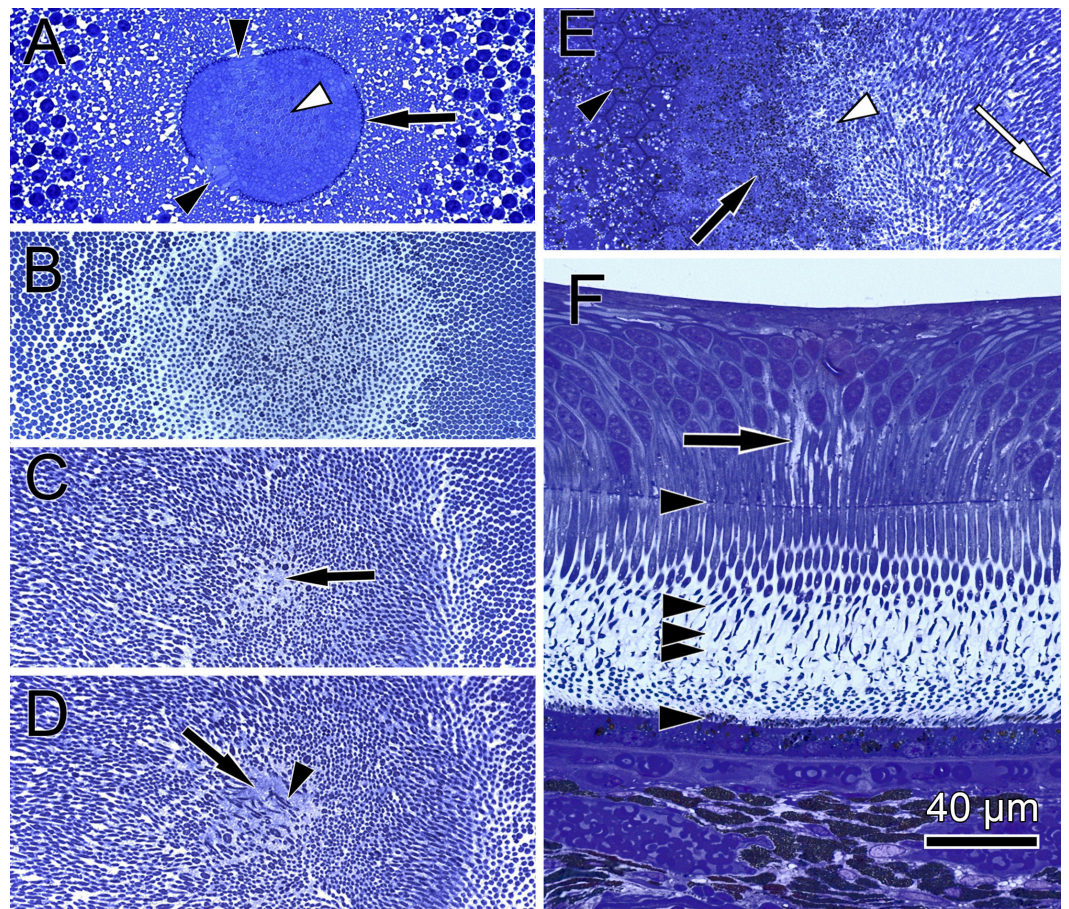


Figure 4 Distribution of central cone orientation in serial sections of the monkey fovea. (A) At the level of the outer limiting membrane (arrow) inner segments are hit in different directions (arrowheads) in the same plane of section. (B) Cones are thin and separated. (C) The foveolar center is kept open (arrow). (D) Cone outer segments run perpendicularly (arrowhead) within the open center (arrow). (E) The tips of central cones (white arrowhead) reach the RPE (black arrowhead). Close to the RPE, cone outer segments run parallel (white arrow). The black arrow points to melanosomes of the RPE. (F) Arrowheads show the planes of section in (A–E). The arrow indicates central Müller cells.

Full-size DOI: [10.7717/peerj.4482/fig-4](https://doi.org/10.7717/peerj.4482/fig-4)

of the foveola with a diameter of 200 μm results in approximately 6,500 cells. Of these cones, 75% of the inner segments are curved. These cones are located in the ring—like area between the central part of the foveola with a diameter of 100 μm . The remaining 25% of cone inner segments within the area of the central 100 μm diameter are straight. The pattern formed by the outer segments was of an even higher complexity but they were not straight in the central foveola (diameter of 200 μm).

The precise form of foveal fundus cells, however, can only be judged by three-dimensional (3D) reconstruction. To unravel the form and shape of foveal cells (Fig. 1D), we performed serial horizontal and vertical semi-thin sections through monkey foveae and constructed 3D models of foveal cones. The outer segments of cones within the central foveolae were indeed curved or even spirally twisted (Fig. 1E and Video S2). In addition,

the central foveolar cone outer segments ($52 \mu\text{m} \pm 5.8 \mu\text{m}$) were twice as long as the cone outer segments in the parafovea ($26 \mu\text{m} \pm 1.6 \mu\text{m}$) (Fig. 1F).

To understand the three-dimensional shape of the central Müller cells, we formed 3D models of human and monkey retinæ (Fig. 2D, Videos S3 and S4) from light and electron microscopic serial sections. The cross-section of individual Müller cells was often triangular (Video S5, bottom left). Focused ion beam (FIB) analysis shows that the Müller cells adapt to the shape of the cone nuclei and cross the retina in a wavy manner (Video S4). We found that individual foveolar Müller cells have a plateau zone at the site where their processes bend horizontally (Figs. 2C and 3B). Our model resembled the one described earlier (Bringmann *et al.*, 2006).

We found that when the light enters the fovea of human retinæ at an angle of 0° , the transmitted light forms a very bright spot in the center of the foveola (approximately $200 \mu\text{m}$ in diameter) (Fig. 3C). This area corresponds exactly to the area composed only of cones and Müller cells (Bodis-Wollner, Glazman & Yerram, 2013). However, when the angle of the transmitted light was changed to 10° , the bright spot in the foveolar center became dark (Fig. 3D, bottom right) and the SCE-like drop in light intensity became directly visible (Video S6). Measurements of the intensities of light transmission in the central foveola for incident angles of 0 , 5 , and 10° (Fig. 3F) resemble the relative luminance efficiency for narrow light bundles as a function of the location where the beam enters the pupil as reported by Stiles & Crawford (1933). The effect was observed in all human foveae and persisted after carefully brushing away the outer segments. The 3D structure of human foveolar Müller cells is shown in Video S7.

DISCUSSION

Already in 1907 the unique central cones were described and called the “bouquet of central cones” (Rochon-Duvigneaud, 1907). The fact that the form and outer segment lengths of the central cones differ from that of the peripheral ones also was described in Greeff & Graefe, (1900) but their spatial organization remained unclear. In the present study we performed 3D modeling of central- and para-foveolar cones to investigate their exact anatomical shape, orientation and spatial arrangement.

The lengths of inner and outer segments and numbers of cones in our study correspond to reported measurements from monkey and human cones (Borwein *et al.*, 1980; Packer, Hendrickson & Curcio, 1989; Yuodelis & Hendrickson, 1986). The 3D model of the central foveolar cones shows that outer segments do not run parallel to the incident light as reported earlier (Hogan, Alvarado & Weddell, 1971; Laties, 1969) but are curved or even coiled (Video S2) and proceed collaterally to the retinal pigment epithelium (RPE) (Fig. 1E). Our serial sections through the inner and outer segment layer of foveal cones clearly show that in the foveal center ($100 \mu\text{m}$) cones have unique shapes, directionalities, and distances from each other (Fig. 4). However, using these findings no convincing hypothesis for the origin of the SCE I could be proposed.

Thus, we searched for the origin of the SCE within the neural retina and performed sagittal and transverse serial sections through the foveolae of humans and monkeys to

construct 3D models and investigate its three-dimensional structure. Unexpectedly, we found extremely large Müller cells in the central foveola of monkeys (Fig. 2A and Video S1) and humans (Fig. 3A, Videos S7 and S4) in which cell organelles are rarely present (Figs. 2B, 2C and Video S5). These Müller cells were already described 47 years ago (Yamada, 1969) in human eyes as having an unusual watery cytoplasm but have been neglected (Gass, 1999).

As light propagation by Müller cells through the retina (Franze *et al.*, 2007) has been shown to be important and increases photon absorption specifically by cones (Labin *et al.*, 2014), we hypothesize that light hitting the Müller cell plateau at an angle of 0° is effectively transmitted into the photoreceptors whereas light hitting the Müller cell plateau at a different angle is partly reflected accordingly, which reduces the amount of light guided through the Müller cells (Fig. 3F). This is in accordance with the finding that retinal foveal structures reflect light entering at an angle different from 0° (Gao *et al.*, 2008; Van de Kraats & Van Norren, 2008).

To test this hypothesis, we used human foveae from flat mounted isolated retinæ and measured the transmission of collimated light under the light microscope at different angles. We could indeed measure a SCE-like decrease in the transmitted light intensity when the angle of the lightbeam was deflected from 0° . We do not completely exclude that the Henle fibres and the shape of the foveal pit are also involved in light reflection. It is also not ruled out that the specific shape of the cone outer segments plays an additional role in causing the SCE by possible angle dependent sensitivity of conopsins for photons.

The spatial resolution of human vision decreases by 50% when a subject in the view is deviated 2.3° from the foveation point (Zhang *et al.*, 2010). The present findings may be physiologically involved in foveation, which is a process of bringing eccentric targets to the direct sight line by saccadic eye movements. This process may be accelerated by reflection of photons entering at an angle different from the direct sight line.

This study might also add a new piece to the puzzle of the pathogenesis of macular telangiectasia type 2 which is characterized by a loss of Müller cells and a reduction of SCE (Powner *et al.*, 2013; Zhao *et al.*, 2015).

CONCLUSIONS

This paper shows the 3D anatomy of primate foveolar Müller cells and cones for the first time. Outer and inner segments of foveolar cones in monkey eyes have directionality and are not arranged in a perfectly straight manner in the axis of the straight entering light. Unique Müller cells with optical fibre characteristics are present in the center of the foveola. These findings may be involved in the foveation process.

In addition, our findings could be of interest for the understanding of the pathogenesis of macular telangiectasia type 2. Finally a new hypothesis for foveal Müller cells, causing the SCE by angle-dependent light reflection, is presented.

ACKNOWLEDGEMENTS

We thank Prof. Susanne Trauzettel-Klosinski and Prof. Brian Vohnsen for constructive discussion, Hanna Janicki and Sigrid Schultheiss for technical support, Dr. Birgit Schröppel for FIB analysis and Judith Birch for editorial assistance.

ADDITIONAL INFORMATION AND DECLARATIONS

Funding

We received support from the Deutsche Forschungsgemeinschaft and the Open Access Publishing Fund of the University of Tübingen. The funders had no role in study design, data collection and analysis, decision to publish, or preparation of the manuscript.

Grant Disclosures

The following grant information was disclosed by the authors:
Deutsche Forschungsgemeinschaft.
Open Access Publishing Fund of the University of Tübingen.

Competing Interests

The authors declare there are no competing interests.

Author Contributions

- Alexander V. Tschulakow and Ulrich Schraermeyer conceived and designed the experiments, performed the experiments, analyzed the data, contributed reagents/materials/analysis tools, prepared figures and/or tables, authored or reviewed drafts of the paper, approved the final draft.
- Theo Oltrup performed the experiments, analyzed the data, contributed reagents/materials/analysis tools, prepared figures and/or tables, authored or reviewed drafts of the paper, approved the final draft.
- Thomas Bende analyzed the data, authored or reviewed drafts of the paper, approved the final draft.
- Sebastian Schmelzle contributed reagents/materials/analysis tools, prepared figures and/or tables, authored or reviewed drafts of the paper, approved the final draft.

Human Ethics

The following information was supplied relating to ethical approvals (i.e., approving body and any reference numbers):

The human eyes were gifts from the Clinical Anatomy of the University of Tübingen (ethical number for scientific issues 237/2007B01).

Animal Ethics

The following information was supplied relating to ethical approvals (i.e., approving body and any reference numbers):

Monkeys were kept at Covance Laboratories GmbH (Münster, Germany study numbers 0382055, 8260977, 8274007) or SILABE-ADUEIS (Niederhausbergen, France). The

Covance Laboratories GmbH test facility is fully accredited by the Association for Assessment and Accreditation of Laboratory Animal Care (AAALAC). This study was approved by the local Institutional Animal Care and Use Committee (IACUC), headed by Dr. Jörg Luft and the work was carried out in accordance with the Code of Ethics of the World Medical Association (Declaration of Helsinki). The monkeys from SILABE-ADUEIS were euthanized due to veterinarian reasons. Since they had not been included in a study before, they do not have a study number.

Data Availability

The following information was supplied regarding data availability:

Figshare

<https://doi.org/10.6084/m9.figshare.5769507>
<https://doi.org/10.6084/m9.figshare.5769501>
<https://doi.org/10.6084/m9.figshare.5769444>
<https://doi.org/10.6084/m9.figshare.5769447>
<https://doi.org/10.6084/m9.figshare.5769450>
<https://doi.org/10.6084/m9.figshare.5769420>
<https://doi.org/10.6084/m9.figshare.5769399>
<https://doi.org/10.6084/m9.figshare.5769372>
<https://doi.org/10.6084/m9.figshare.5769366>.

Supplemental Information

Supplemental information for this article can be found online at <http://dx.doi.org/10.7717/peerj.4482#supplemental-information>.

REFERENCES

- Bodis-Wollner I, Glazman S, Yerram S. 2013.** Fovea and foveation in Parkinson's disease. *Behavioral Neuroscience* **127**:139–150 DOI 10.1037/a0031225.
- Borwein B, Borwein D, Medeiros J, McGowan JW. 1980.** The ultrastructure of monkey foveal photoreceptors, with special reference to the structure, shape, size, and spacing of the foveal cones. *The American Journal of Anatomy* **159**:125–146 DOI 10.1002/aja.1001590202.
- Bringmann A, Pannicke T, Grosche J, Francke M, Wiedemann P, Skatchkov SN, Osborne NN, Reichenbach A. 2006.** Muller cells in the healthy and diseased retina. *Progress in Retina and Eye Research* **25**:397–424 DOI 10.1016/j.preteyeres.2006.05.003.
- Charbel Issa P, Gillies MC, Chew EY, Bird AC, Heeren TF, Peto T, Holz FG, Scholl HP. 2013.** Macular telangiectasia type 2. *Progress in Retina and Eye Research* **34**:49–77 DOI 10.1016/j.preteyeres.2012.11.002.
- Charbel Issa P, Heeren TF, Kupitz EH, Holz FG, Berendschot TT. 2016.** Very early disease manifestations of macular telangiectasia type 2. *Retina* **36**:524–534 DOI 10.1097/IAE.0000000000000863.
- Enoch JM, Stiles WS. 1961.** The colour change of monochromatic light with retinal angle of incidence. *Optica Acta* **8**:329–358 DOI 10.1080/713826396.

- Franze K, Grosche J, Skatchkov SN, Schinkinger S, Foja C, Schild D, Uckermann O, Travis K, Reichenbach A, Guck J. 2007.** Muller cells are living optical fibers in the vertebrate retina. *Proceedings of the National Academy of Sciences of the United States of America* **104**:8287–8292 DOI 10.1073/pnas.0611180104.
- Gao W, Cense B, Zhang Y, Jonnal RS, Miller DT. 2008.** Measuring retinal contributions to the optical Stiles-Crawford effect with optical coherence tomography. *Optics Express* **16**:6486–6501 DOI 10.1364/OE.16.006486.
- Gass JD. 1999.** Muller cell cone, an overlooked part of the anatomy of the fovea centralis: hypotheses concerning its role in the pathogenesis of macular hole and foveomacular retinoschisis. *Archives of Ophthalmology* **117**:821–823 DOI 10.1001/archophth.117.6.821.
- Greeff R, Graefe A. 1900.** Die mikroskopische anatomie des sehnerven und der netzhaut. In: *Graefe-Saemisch handbuch der gesamten augenheilkunde*. Leipzig: Wilhelm Engelmann.
- He JC, Marcos S, Burns SA. 1999.** Comparison of cone directionality determined by psychophysical and reflectometric techniques. *Journal of the Optical Society of America. A, Optics, Image Science, and Vision* **16**:2363–2369 DOI 10.1364/JOSAA.16.002363.
- Hogan MJ, Alvarado JA, Weddell JE. 1971.** *Histology of the human eye*. Philadelphia: W.B. Saunders Company.
- Krebs W, Krebs I. 1991.** *Primate retina and choroid atlas of fine structure in man and monkey*. New York: Springer Verlag.
- Labin AM, Safuri SK, Ribak EN, Perlman I. 2014.** Muller cells separate between wavelengths to improve day vision with minimal effect upon night vision. *Nature Communications* **5**:4319 DOI 10.1038/ncomms5319.
- Laties AM. 1969.** Histological techniques for study of photoreceptor orientation. *Tissue and Cell* **1**:63–81 DOI 10.1016/S0040-8166(69)80006-6.
- Lu R, Levy AM, Zhang Q, Pittler SJ, Yao X. 2013.** Dynamic near-infrared imaging reveals transient phototropic change in retinal rod photoreceptors. *Journal of Biomedical Optics* **18**:106013 DOI 10.1117/1.JBO.18.10.106013.
- Matsumoto CS, Shinoda K, Matsumoto H, Satofuka S, Mizota A, Nakatsuka K, Miyake Y. 2012.** Stiles-Crawford effect in focal macular ERGs from macaque monkey. *Journal of Vision* **12** DOI 10.1167/12.3.6.
- Packer O, Hendrickson AE, Curcio CA. 1989.** Photoreceptor topography of the retina in the adult pigtail macaque (*Macaca nemestrina*). *Journal of Comparative Neurology* **288**:165–183 DOI 10.1002/cne.902880113.
- Polyak SL. 1941.** *The retina*. Chicago: The University of Chicago Press.
- Powner MB, Gillies MC, Zhu M, Vevis K, Hunyor AP, Fruttiger M. 2013.** Loss of Muller's cells and photoreceptors in macular telangiectasia type 2. *Ophthalmology* **120**:2344–2352 DOI 10.1016/j.ophtha.2013.04.013.
- Rochon-Duvigneaud A. 1907.** Recherches sur la fovea de la rétine humaine et particulièrement sur le bouquet des cônes centraux. *Archives d'Anatomie Microscopique* **9**:315–342.

- Steinmann U, Borkowski J, Wolburg H, Schroppe B, Findeisen P, Weiss C, Ishikawa H, Schwerk C, Schrotten H, Tenenbaum T. 2013.** Transmigration of polymorphonuclear neutrophils and monocytes through the human blood-cerebrospinal fluid barrier after bacterial infection *in vitro*. *Journal of Neuroinflammation* **10**:31 DOI 10.1186/1742-2094-10-31.
- Stiles WS, Crawford BH. 1933.** The luminous efficiency of rays entering the eye pupil at different points. *Proceedings of the Royal Society of London B: Biological Sciences* **112(778)**:428–450.
- Trauzettel-Klosinski S. 2010.** Rehabilitation for visual disorders. *Journal of Neuroinflammation* **30**:73–84 DOI 10.1097/WNO.0b013e3181ce7e8f.
- Van de Kraats J, Van Norren D. 2008.** Directional and nondirectional spectral reflection from the human fovea. *Journal of Biomedical Optics* **13**:024010 DOI 10.1117/1.2899151.
- Walraven PL, Bouman MA. 1960.** Relation between directional sensitivity and spectral response curves in human cone vision. *Journal of the Optical Society of America* **50**:780–784 DOI 10.1364/JOSA.50.000780.
- Westheimer G. 1967.** Dependence of the magnitude of the Stiles-Crawford effect on retinal location. *Journal de Physiologie* **192**:309–315 DOI 10.1113/jphysiol.1967.sp008301.
- Westheimer G. 2008.** Directional sensitivity of the retina: 75 years of Stiles-Crawford effect. *Proceedings of the Royal Society B: Biological Sciences* **275**:2777–2786 DOI 10.1098/rspb.2008.0712.
- Yamada E. 1969.** Some structural features of the fovea centralis in the human retina. *Archives of Ophthalmology* **82**:151–159 DOI 10.1001/archophth.1969.00990020153002.
- Yuodelis C, Hendrickson A. 1986.** A qualitative and quantitative analysis of the human fovea during development. *Vision Research* **26**:847–855 DOI 10.1016/0042-6989(86)90143-4.
- Zhang X, Wang Z, Wang R, Yang Z, Chen W, Peng Q. 2010.** Real-time foveation filtering using nonlinear Mipmap interpolation. *Visual Computer* **26**:923–932 DOI 10.1007/s00371-010-0432-3.
- Zhao M, Andrieu-Soler C, Kowalczyk L, Paz Cortes M, Berdugo M, Dernigoghossian M, Halili F, Jeanny JC, Goldenberg B, Savoldelli M, El Sanharawi M, Naud MC, Van Ijcken W, Pescini-Gobert R, Martinet D, Maass A, Wijnholds J, Crisanti P, Rivolta C, Behar-Cohen F. 2015.** A new CRB1 rat mutation links Muller glial cells to retinal telangiectasia. *Journal of Neuroscience* **35**:6093–6106 DOI 10.1523/JNEUROSCI.3412-14.2015.

9.4.2 Effects of intravitreally injected Fc fragment on rat eyes

According to the copyrights, here only the last accepted manuscript version of this article can be shown.

To see the published version please visit [Graefe's Archive for Clinical and Experimental Ophthalmology](#).

Effects of intravitreally injected Fc fragment on rat eyes

Tatjana Taubitz¹, Laura-Pia Steinbrenner¹, Alexander V. Tschulakow¹, Antje Bieseimer^{1*}, Sylvie Julien-Schraermeyer¹, Ulrich Schraermeyer^{1,2}

¹Centre for Ophthalmology, Division of Experimental Vitreoretinal Surgery,
Schleichstrasse 12/1, Tuebingen, Germany

²STZ OcuTox Preclinical Drug Assessment, Hechingen, Germany, www.ocutox.com

*Corresponding author: Antje Bieseimer; Centre for Ophthalmology, Division of Experimental Vitreoretinal Surgery, Schleichstrasse 12/1, Tuebingen, Germany; Phone: +49 7071 29 84774; Fax: +49 7071 4554; antje.bieseimer@med.uni-tuebingen.de

Acknowledgements

We thank Monika Rittgarn and Sigrid Schultheiss for technical assistance and Judith Birch for proof reading. This study was supported by Novartis.

Abstract

Purpose: Anti-VEGF drugs are used to treat neovascular eye diseases. Some of these drugs contain Fc fragments (Fc), but it is unknown how their mode of action is influenced by Fc. Therefore, Fc effects were investigated on rat eyes after intravitreal injection.

Methods: 18 Long Evans rats were intravitreally injected with sterile, biotin-labelled rat Fc (9.1 µg in 5 µl PBS). For control, 5 µl PBS were injected in another nine rats. Animals were sacrificed between 1-3 days (group 1), 7 (group 2) and 14 days (group 3) after injection. Right eyes were examined by electron microscopy (EM). Left eyes were stained for distribution of Fc and presence of macrophages by immunohistochemistry.

Results: After one day, Fc had penetrated into the anterior chamber and the retina up to the inner nuclear layer and was located especially in retinal vessels. High amounts of infiltrating cells within the vitreous, around the ciliary body, anterior chamber and inside the retina were present 1-3 days after Fc injection ($p < 0.02$ group 1 vs. control). Immunohistochemistry and EM showed that they were macrophages or granulocytes in close association with Fc. Ultrastructurally, there were effects on the blood vessels such as thrombocyte activation and fibrin formation.

Conclusions: Biotin-labelling is ideal for investigating the distribution of intravitreally injected proteins in ocular tissue. Fc fragments at a dose corresponding to their concentration in standard AMD treatments induced inflammation, particularly the attraction of immune competent cells. This might be associated with the risk of inflammation or endophthalmitis after anti-VEGF treatment and needs further investigation.

Keywords: Fc fragment, anti-VEGF therapy, intravitreal injection, endophthalmitis

Introduction

The eye is an immune-privileged organ, which means that immune responses are usually suppressed [1, 2]. Nevertheless, side effects including inflammation or sterile endophthalmitis were observed after intravitreal application of full length antibodies [3, 4].

Fc receptors (Fc stands for fragment crystallisable) are present in more or less all parts of the eye, e.g. the outer nuclear layer, Müller cells, nerve fiber and photoreceptor layer and the pigment epithelium (RPE) of the retina, but also in the ciliary body, cornea, trabecular meshwork, choroid and iris [5]. In humans, age-related decrease in Fcγ receptor expression was shown [5] and could play a role in the pathogenesis of age-related macular degeneration (AMD) and its treatment. Indeed, Fc-containing anti-VEGF therapeutics (bevacizumab (Avastin®, Genentech/Roche), aflibercept (Eylea®, Regeneron/Bayer)) are used as a standard therapy in AMD and could affect treatment outcome [6-11].

Bevacizumab is a humanized monoclonal antibody that inhibits all isoforms of VEGF-A [12, 13], while aflibercept is a recombinant fusion protein containing VEGF receptor sequences (VEGFR1 and VEGFR2) fused to an IgG backbone [14]. Aflibercept binds to all VEGF-A isoforms, VEGF-B and placental growth factor [13]. Both drugs contain the human Fc fragment. A third anti-VEGF drug is ranibizumab (Lucentis®, Genentech/Novartis), a humanized monoclonal antibody fragment (Fab) [15]. Ranibizumab inhibits all VEGF-A isoforms [13], but in contrast to bevacizumab, lacks the Fc fragment.

Fc-containing anti-VEGF therapeutics have been reported to induce protein complexes [6] and platelet activation [16] *in vitro*, while ranibizumab did not [6, 16]. Additionally, it was found that bevacizumab can induce platelet aggregation, degranulation and thrombosis via complex formation with VEGF, heparin and activation of the platelet FcγRIIa receptor [17]. Bevacizumab accumulates *in vitro* in RPE cells, whereas ranibizumab does not [18]. It was shown that this difference in pharmacokinetics is due to bevacizumab being recognized by the neonatal Fc receptor and thus transported into the RPE cells [19, 20]. Whether intravitreally administered anti-VEGF therapeutics with an Fc fragment really cause more ocular and/or systemic adverse effects is still under debate since study results are divergent [21-24].

Therefore, the present study was performed to investigate the effects of intravitreally administered isolated Fc fragment on rat eyes. Since, in the therapeutic context, injection of human Fc fragment containing anti-VEGF drugs is of interest for patient treatment, we performed our study in rats with their respective rat Fc fragment.

Methods

Animals

6 week-old Long Evans rats (n=27) were purchased from Janvier Labs, Le Genest-Saint-Isle, France. Animals were kept under 12-h on-off cyclic lighting and provided with water and food *ad libitum*. All procedures involving animals were in accordance with the German laws governing the use of experimental animals and were previously approved by the local authorities (Regierungspraesidium Tuebingen; AK02/14). All efforts were made to minimize suffering.

Biotinylation of Fc fragment

Fc fragment from rat IgG (ChromPure Rat IgG, Fc Fragment, Jackson ImmunoResearch, Baltimore, PA, USA) was obtained as a 2.4 mg/ml solution in a 0.25M saline solution buffered with 0.01M sodium phosphate (pH 7.6). The solution was concentrated to approximately 100 μ l by ultrafiltration using a Pierce[®] Concentrator 9k MWCO (Thermo Scientific, Waltham, MA, USA). Biotinylation was done with the BiotinTag[™] Micro Biotinylation Kit (Sigma-Aldrich, St. Louis, MO, USA) according to the manufacturer's instructions. Briefly, the biotinylation reagent (BAC-SulfoNHS) was reconstituted with sodium phosphate buffer, pH 7.2 and 10 μ l of the biotinylation reagent solution was added to the Fc fragment and incubated for 30 minutes at room temperature. Excess biotinylation reagent was removed by loading the reaction mixture onto micro-spin G-50 columns and eluting the labeled protein with PBS. The concentration of the labeled protein was determined with the Bicinchoninic Acid Protein Assay Kit (Sigma-Aldrich, St. Louis, MO, USA) according to the manufacturer's instructions. In brief, the biotinylated Fc Fragment and a diluted series of BSA as a standard were mixed with freshly prepared working solution

5

containing copper sulfate and biconchonic acid and incubated in a 96-well plate at room temperature for 2 hours. Absorption was measured at 562 nm with a microplate reader (Synergy HT, Biotek). Before injection into the eyes the Fc fragment solution was sterile-filtered.

Intravitreal injection

18 rats were anaesthetized using a mixture of ketamine and xylazine (WDT, Garbsen, Germany). They were intravitreally injected in both eyes with sterile, 9.1 μ g biotin-labelled Fc from rats in 5 μ l PBS using an UltraMicroPump III microsyringe injector with Micro4 controller. The pump was equipped with a NanoFil 100 μ L syringe loaded with the labeled Fc fragment. A 34 gauge beveled needle was connected to the syringe with a SiFlex tubing and a needle holder. All instruments were obtained from World Precision Instruments, Berlin, Germany. The advantage of this system is accurate and repetitive injection. Injection volume was 5 μ l per eye and injection rate was 2 μ l per second. For control, 5 μ l sterile PBS was injected in another 9 rats. Eleven Fc fragment and six PBS treated animals were sacrificed 1-3 days (group 1) after injection and another five / three animals 7 days (group 2) after injection, respectively. Two rats were killed 14 days after Fc fragment injection (group 3).

Tissue preparation

On days 1-3 (group 1), 7 (group 2) and 14 (group 3) after intravitreal injection, the animals were sacrificed by cervical dislocation under general anesthesia using a mixture of ketamine and xylazine (WDT, Garbsen, Germany). The eyes were enucleated immediately post-mortem and cleaned of orbital tissue. Right eyes were fixed for electron microscopy in 5 % glutaraldehyde in 0.1 M cacodylate buffer (pH

6

7.4, Sigma, St. Louis, MO, USA). Left eyes were fixed for immunohistochemistry in 4.5 % formalin (Carl Roth, Karlsruhe, Germany).

Immunohistochemistry

Eyes were fixed in formalin, embedded in paraffin wax, cut into 5- μ m sections and deparaffinized according to standard procedures.

Biotinylated Fc fragments were detected using a streptavidin alkaline – phosphatase detection kit (RED Rabbit/Mouse K5005 Dako, Glostrup, Denmark) or a Cy3-conjugated AffiniPure Goat Anti-Rat IgG (H+L) antibody (112-165-143, Jackson ImmunoResearch, Baltimore, PA, USA, 1:250) according to the manufacturer's protocol. Sections were counterstained with hematoxylin solution modified according to Gill III for microscopy (Merck, Darmstadt, Germany).

For detection of macrophages, sections were incubated for 1 hour with mouse anti-rat CD-68 antibodies (SeroTec MCA 341R, Kidlington, Oxford, UK) 1:100 and stained with Goat Anti-Mouse IgG (H+L) Cy3 Conjugate (Invitrogen 81-6515, Carlsbad, CA, USA) 1:100 diluted 30 min at room temperature. Dilution was performed with antibody diluent with background reducing components (Dako S3022) at room temperature.

Sections were mounted on SuperFrost Plus slides (Langenbrinck, Emmendingen, Germany) using FluoroSave (Calbiochem, La Jolla, CA, USA) and inspected with a fluorescence microscope (Axioplan2; Carl Zeiss, Oberkochen, Germany).

Light and electron microscopy

After fixation in glutaraldehyde for 30 minutes, the corneas were carefully removed from the bulbi and the fixation was continued overnight. Specimens were post-fixed with 1% OsO₄ at room temperature in 0.1 M cacodylate buffer (pH 7.4), stained with

uranyl acetate, and embedded in Epon after dehydration in a graded series of ethanol and propylene oxide. Semi-thin sections were stained with toluidine blue and examined by light microscopy (Zeiss Axioplan2 imaging, Zeiss, Jena, Germany). For electron microscopy, the sections were cut ultrathin and analyzed with a Zeiss 900 electron microscope (Zeiss, Jena, Germany).

Quantification of infiltrating cells in the vitreous-retinal interface

Cells that were present within the vitreous close to the retina were counted in semi-thin sections.

Quantification of macrophages in the vitreous and retina

CD68 positive cells that were present within the vitreous close to the retina were counted in paraffin sections.

Statistical analysis

Statistical significance for the evaluation of the occurrence of macrophages in the vitreous was determined by using the Dunnett's test and the JMP11.0 statistical program (SAS, Heidelberg, Germany). The null hypothesis was that the treated samples were histologically not different from the PBS controls. All p-values < 0.05 were stated significantly different (error probability 5%).

Results

Detection of Fc fragments and macrophages by immunohistochemistry

Between one and three days after injection, Fc fragments were detected within the vitreous, often associated with fibrous material (Fig. 1 a). Fc fragments were also present in infiltrating cells within the vitreous (Fig. 1 b, e), around the ciliary body (Fig. 1 c) and the anterior chamber (Fig. 1 c). One day after injection, the Fc fragments were localized in infiltrating cells (Fig. 1 e) and the inner retina (Fig. 1b). However, two and three days after injection, Fc fragments permeated into the retina and were taken up by ganglion cells and cells of the inner nuclear layer (Fig. 1 a). Also within retinal vessels Fc fragments were clearly detectable (Fig. 1 a). Infiltrating cells were very prominent between one and three days after injection of Fc fragments (Fig. 1 a, b, c, e). By CD68 labelling many of them were identified as macrophages (Fig. 1 f). These macrophages also infiltrated the retina (Fig. 1 f). After 7 and 14 days of injection, the Fc fragments disappeared from the vitreous (not shown) but were still detectable in the RPE (Fig. 1 d). In PBS injected rats, staining for biotin was completely negative in sections from all eyes (Supplementary Figure 1).

Light microscopy of semi-thin sections

After Fc fragment injection, all three groups showed infiltrating cells within the vitreous and thrombocyte activation in the retinal vessels (Fig. 2). Infiltrating cells were most frequent in treated group 1.

Electron microscopy

At electron microscopical level, the loosely aggregating thrombocytes (Fig. 3 a, c), unknown fibrous material, fibrin (Fig. 3 b) and granulocytes fixed in the state of

degranulation (Fig. 3 c) were regularly seen in retinal veins of all groups after Fc fragment treatment. After the injection of PBS, these findings were only infrequently observed. Also microparticles were observed after Fc injection in all groups (Fig. 3b), but also in the respective PBS injected controls in retinal and choroidal vessels (not significant). In untreated LE rats we never noticed such an accumulation of microparticles (not shown).

In a few cases of groups 2 and 3, unusual electron-dense material accumulated within the subretinal space and the vitreous, as shown in an examples from group 3 (Fig. 4). This electron-dense material penetrated the retina and was localized close to the retinal veins (Fig. 4 b). At higher magnification vesicular transport (transcytosis) of this material through smooth muscle cells and endothelium into the lumen of the veins was clearly seen (not shown). As this phenomenon was only infrequently observed, it was not further investigated.

The most prominent finding after Fc fragment treatment was cellular infiltration of the vitreous and retina (Fig. 5). The cells were frequently seen within damaged retinal cells close to the inner limiting membrane (Fig. 5 a, c). Some of them were clearly identified as granulocytes by the morphology of their nuclei (Fig. 5 a). Also eosinophil granulocytes were detected infiltrating the retina. These cells can be clearly recognized by the typical morphology of their granules, as shown in Fig. 3 c. Others resembled macrophages judged by the U-shape of their nuclei (Fig. 5 c, d). Macrophages within the vitreous were highly activated which was indicated by the formation of microvilli (Fig. 5 b, d). Infiltrating cells were only infrequently seen after PBS injection. The number of these cells is quantified in figure 6.

14 days after Fc treatment, cells attached to the inner limiting membrane and collagen fibers were seen within the vitreous (Fig. 5 e).

Quantification of infiltrating cells in the vitreous-retinal interface

Cells that were present within the vitreous close to the retina were counted in semi-thin sections. Fc fragment injection significantly ($p < 0.02$) enhanced the number of infiltrating cells in group 1 (Fig. 6). The type of infiltrating cell was not distinguished ($n = 6$ eyes/group).

Quantification of macrophages in the vitreous

To identify the number of CD68 positive macrophages within the group of infiltrating cells observed in the Fc-treated rats, all CD68 positive and negative cells were counted along the vitreo-retinal interface in central paraffin sections of whole eyes of each two to three rats per group. Both, CD68 positive and negative infiltrating cells were most prominent in the Fc treated group1 (both $p < 0.05$ as compared to PBS control in group 1, Fig. 7). Note, that the majority of infiltrating cells were found to be CD68 positive (ratio 2.88 in group1; 7.67 in group 2).

Discussion

To our knowledge this is the first study that has investigated the role of isolated Fc fragments after intravitreal injection. There is clear evidence that Fc fragments have multiple effects on eye tissues that are not yet understood in detail. It is, however, well known that Fc receptors are involved in pharmacokinetics of therapeutic IgG in eye tissues and play an important role in eliminating intravitreally administered full-length IgGs across the blood-retinal barrier into the systemic blood system [19].

Previous work showed that Fc-containing anti-VEGF drugs preferentially accumulate in endothelial and RPE cells with prolonged treatment time. This implies potential side effects in the treatment of AMD and diabetic retinopathy which both are to be applied over several years [10, 11]. Indeed, Fc fragments induce platelet aggregation, degranulation and thrombosis through complex formation with VEGF and activation of the platelet Fc γ R1a receptor, and this can provide an explanation for the thrombotic events observed in vivo after bevacizumab [8, 9, 17, 25] and aflibercept [7] treatment of AMD patients.

Also endothelial cells in mammals express the endocytic Fc γ receptor IIb2 [26] and the neonatal Fc receptor [27]. Fc fragment binding stimulates phagocytosis of waste material [26]. In this manner, endothelial cells can directly communicate with Fc fragments yielding the clearance of the drugs from the eye [19]. Additionally, the RPE has been shown to express Fc receptors and to take up Fc-containing drugs like bevacizumab and aflibercept *via* membrane-standing Fc γ and the intracellular neonatal Fc receptors [20].

The present findings are in accordance with the common knowledge about the interaction of Fc fragments and Fc receptors. Stimulation and modulation of cellular immune reactivity is the natural function of Fc fragments and phagocytes, including epithelial cells, are also known to express Fc γ receptors [28]. Thus, it is not

surprising that Fc fragments induced cellular activation of macrophages and granulocytes in the vitreous and retina.

This study demonstrates uptake of Fc fragments into the retina and the blood stream of retinal vessels within the first 3 days after injection. Alteration of the serum composition in general and by Fc fragments in particular can activate platelets and induce fibrin formation and were frequently observed in this study. Microparticles are also strongly correlated to thrombotic events, but whether they are risk factors or results of thrombosis is under discussion [29]. Thus, the alterations in the retinal veins i.e. activation of platelets, fibrin formation and degranulation of granulocytes is not surprising. These observations are also in accordance with our previous findings in monkey studies [7-9].

Exclusively after Fc fragment injection, immune cells infiltrated the retina and vitreous and were found associated to damaged retinal cells (Fig. 5 a, c). At least two thirds of the infiltrating cells in the vitreous were CD68 positive monocytes/macrophages. The remnant CD68 negative infiltrating cells are supposed to be lymphocytes or granulocytes, as shown in Figure 5a and d. Infiltrating cells, both CD68 positive and negative, were most prominent on day 1, and diminished over time.

The present study also shows that biotinylation is a suitable method to investigate the transport and turnover of intravitreal injected proteins and excludes cross reactions with endogenous immune globulins in the eye.

In conclusion, intravitreal injection of Fc fragments at a dose corresponding to Fc fragment portion in standard treatments in AMD patients induced multiple reactions in rats within the first days particularly the attraction of immune competent cells which might be associated with the risk of inflammation or endophthalmitis and needs further investigation.

Compliance with ethical standards

Funding

Novartis provided financial support in the form of research grant funding. The sponsor had no role in the design or conduct of this research.

Conflict of interest

All authors certify that they have no affiliations with or involvement in any organization or entity with any financial interest (such as honoraria; educational grants; participation in speakers' bureaus; membership, employment, consultancies, stock ownership, or other equity interest; and expert testimony or patent-licensing arrangements), or non-financial interest (such as personal or professional relationships, affiliations, knowledge or beliefs) in the subject matter or materials discussed in this manuscript. The work was financially supported by Novartis.

Ethical approval

All applicable international, national, and institutional guidelines for the care and use of animals were followed. All procedures performed in studies involving animals were in accordance with the ethical standards of the institution at which the studies were conducted.

References

1. Ferguson TA, Griffith TS (2006) A vision of cell death: Fas ligand and immune privilege 10 years later. *Immunol Rev* 213:228-238. DOI 10.1111/j.1600-065X.2006.00430.x
2. Taylor AW (2009) Ocular immune privilege. *Eye (Lond)* 23:1885-1889. DOI 10.1038/eye.2008.382
3. Agrawal S, Joshi M, Christoforidis JB (2013) Vitreous inflammation associated with intravitreal anti-VEGF pharmacotherapy. *Mediators Inflamm* 2013:943409. DOI 10.1155/2013/943409
4. Hahn P, Yashkin AP, Sloan FA (2016) Effect of Prior Anti-VEGF Injections on the Risk of Retained Lens Fragments and Endophthalmitis after Cataract Surgery in the Elderly. *Ophthalmology* 123:309-315. DOI 10.1016/j.ophtha.2015.06.040
5. Tripathi RC, Borisuth NS, Tripathi BJ (1991) Mapping of Fc gamma receptors in the human and porcine eye. *Experimental eye research* 53:647-656
6. Julien S, Biesemeier A, Schraermeyer U (2012) In vitro induction of protein complexes between bevacizumab, VEGF-A165 and heparin: explanation for deposits observed on endothelial veins in monkey eyes. *Br J Ophthalmol*. DOI 10.1136/bjophthalmol-2012-302308 [pii]10.1136/bjophthalmol-2012-302308
7. Julien S, Biesemeier A, Taubitz T, Schraermeyer U (2014) Different effects of intravitreally injected ranibizumab and aflibercept on retinal and choroidal tissues of monkey eyes. *Br J Ophthalmol* 98:813-825. DOI 10.1136/bjophthalmol-2013-304019
8. Schraermeyer U, Julien S (2013) Effects of bevacizumab in retina and choroid after intravitreal injection into monkey eyes. *Expert Opin Biol Ther* 13:157-167. DOI 10.1517/14712598.2012.748741
9. Schraermeyer U, Julien S (2012) Formation of immune complexes and thrombotic microangiopathy after intravitreal injection of bevacizumab in the primate eye. *Graefes Arch Clin Exp Ophthalmol* 250:1303-1313. DOI 10.1007/s00417-012-2055-z
10. Lang GE, Lang GK, Deissler HL (2015) [Basic in vitro studies on VEGF inhibition with aflibercept: similarities and differences to other VEGF-binding therapeutic proteins]. *Klin Monbl Augenheilkd* 232:295-302. DOI 10.1055/s-0034-1383142
11. Deissler HL, Lang GK, Lang GE (2016) Internalization of bevacizumab by retinal endothelial cells and its intracellular fate: Evidence for an involvement of the neonatal Fc receptor. *Experimental eye research* 143:49-59. DOI 10.1016/j.exer.2015.10.007
12. Presta LG, Chen H, O'Connor SJ, Chisholm V, Meng YG, Krummen L, Winkler M, Ferrara N (1997) Humanization of an anti-vascular endothelial growth factor monoclonal antibody for the therapy of solid tumors and other disorders. *Cancer Res* 57:4593-4599
13. Papadopoulos N, Martin J, Ruan Q, Rafique A, Rosconi MP, Shi E, Pyles EA, Yancopoulos GD, Stahl N, Wiegand SJ (2012) Binding and neutralization of vascular endothelial growth factor (VEGF) and related ligands by VEGF Trap, ranibizumab and bevacizumab. *Angiogenesis* 15:171-185. DOI 10.1007/s10456-011-9249-6
14. Ohr M, Kaiser PK (2012) Aflibercept in wet age-related macular degeneration: a perspective review. *Ther Adv Chronic Dis* 3:153-161. DOI 10.1177/2040622312446007
15. Ferrara N, Damico L, Shams N, Lowman H, Kim R (2006) Development of ranibizumab, an anti-vascular endothelial growth factor antigen binding fragment, as therapy for neovascular age-related macular degeneration. *Retina* 26:859-870. DOI 10.1097/01.iae.0000242842.14624.e7
16. Nomura Y, Kaneko M, Miyata K, Yatomi Y, Yanagi Y (2015) Bevacizumab and Aflibercept Activate Platelets via Fc gamma R1a. *Invest Ophthalmol Vis Sci* 56:8075-8082. DOI 10.1167/iov.15-17814
17. Meyer T, Robles-Carrillo L, Robson T, Langer F, Desai H, Davila M, Amaya M, Francis JL, Amirkhosravi A (2009) Bevacizumab immune complexes activate platelets and induce thrombosis in FCGR2A transgenic mice. *J Thromb Haemost* 7:171-181. DOI 10.1111/j.1538-7836.2008.03212.x
18. Klettner AK, Kruse ML, Meyer T, Wesch D, Kabelitz D, Roeder J (2009) Different properties of VEGF-antagonists: Bevacizumab but not Ranibizumab accumulates in RPE cells. *Graefes Arch Clin Exp Ophthalmol* 247:1601-1608. DOI 10.1007/s00417-009-1136-0
19. Kim H, Robinson SB, Csaky KG (2009) FcRn receptor-mediated pharmacokinetics of therapeutic IgG in the eye. *Molecular vision* 15:2803-2812
20. Dithmer M, Hattermann K, Pomarius P, Aboul Naga SH, Meyer T, Mentlein R, Roeder J, Klettner A (2016) The role of Fc-receptors in the uptake and transport of therapeutic antibodies in the retinal pigment epithelium. *Experimental eye research* 145:187-205. DOI 10.1016/j.exer.2015.12.013
21. Tolentino M (2011) Systemic and ocular safety of intravitreal anti-VEGF therapies for ocular neovascular disease. *Surv Ophthalmol* 56:95-113. DOI 10.1016/j.survophthal.2010.08.006
22. Schmucker C, Ehlken C, Agostini HT, Antes G, Ruecker G, Leigemann M, Loke YK (2012) A safety review and meta-analyses of bevacizumab and ranibizumab: off-label versus goldstandard. *PLoS One* 7:e42701. DOI 10.1371/journal.pone.0042701
23. van der Reis MI, La Heij EC, De Jong-Hesse Y, Ringens PJ, Hendrikse F, Schouten JS (2011) A systematic review of the adverse events of intravitreal anti-vascular endothelial growth factor injections. *Retina* 31:1449-1469. DOI 10.1097/IAE.0b013e3182278ab4
24. Modi YS, Tanchon C, Ehlers JP (2015) Comparative safety and tolerability of anti-VEGF therapy in age-related macular degeneration. *Drug Saf* 38:279-293. DOI 10.1007/s40264-015-0273-0
25. Schraermeyer U, Julien S, Biesemeier A, Bartz-Schmidt KU, Wolburg H (2015) A new kind of labyrinth-like capillary is responsible for leakage from human choroidal neovascular endothelium, as investigated by high-resolution electron microscopy. *Graefes Arch Clin Exp Ophthalmol* 253:681-689. DOI 10.1007/s00417-014-2733-0
26. Sorensen KK, McCourt P, Berg T, Crossley C, Le Couteur D, Wake K, Smedsrod B (2012) The scavenger endothelial cell: a new player in homeostasis and immunity. *Am J Physiol Regul Integr Comp Physiol* 303:R1217-1230. DOI 10.1152/ajpregu.00686.2011
27. Niu N, Zhang J, Sun Y, Wang S, Sun Y, Korteweg C, Gao W, Gu J (2011) Expression and distribution of immunoglobulin G and its receptors in an immune privileged site: the eye. *Cellular and molecular life sciences : CMLS* 68:2481-2492. DOI 10.1007/s0018-010-0572-7
28. Joshi T, Butchar JP, Tridandapani S (2006) Fc gamma receptor signaling in phagocytes. *Int J Hematol* 84:210-216. DOI 10.1532/IJH97.06140
29. Nomura S, Shimizu M (2015) Clinical significance of procoagulant microparticles. *J Intensive Care* 3:2. DOI 10.1186/s40560-014-0066-z

Figure legends

Fig. 1 Distribution of Fc fragments and infiltrating cells by light and fluorescence microscopy

(a) Three days after injection, biotinylated Fc fragments (red) can be detected within the vitreous often associated with fibrous material as visualized with streptavidin alkaline-phosphatase stain. Fc fragments are present in infiltrating cells within the vitreous (black arrowhead). Fc fragment penetrated through the retina up to the inner nuclear layer (white arrowhead). The photoreceptor nuclei (asterisk) are not reached by permeating Fc fragments. The lumen of a retinal vessel (arrow) contains Fc fragments. The same is true for ganglion cells to the left and right of this vessel. (b) One day after injection, the Fc fragments were localized to the inner limiting membrane (white arrowhead) and cells infiltrating the vitreous (black arrowhead). (c) One day after injection, red labelled Fc fragments are seen within the space between lens (L) and ciliary body (C) in the anterior chamber (asterisk). Around the ciliary body and attached to the iris (I) many infiltrating cells (arrowheads) can be seen. (d) After 7 days of injection, the Fc fragments disappeared from the vitreous (not shown), but were still detectable in the retinal pigment epithelium (white arrowhead). (e) A fluorescent light micrograph one day after injection shows cells infiltrating the vitreous (arrow) that have taken up anti-rat IgG-labeled Fc fragments and are associated with fibers. Fc fragments are also seen in the central vitreous (asterisk). The inner limiting membrane is marked by an arrowhead. (f) By CD68 labelling, these infiltrating cells (1 day after infection) were identified as macrophages. The macrophages also infiltrated the retina (arrows). The inner limiting membrane (ILM) is marked by arrowheads and macrophages are seen on both sides of the ILM within the retina and within the vitreous

17

Fig. 2 Light microscopy of the distribution of infiltrating cells and thrombocytes in the inner retina

(a) Infiltrating cells within the vitreous are shown one day after Fc fragment injection (black arrowheads). Loosely aggregating thrombocytes are marked by an arrow within the central vein (higher magnification in b). The central artery is marked by a white arrowhead. For more details see EM image in Fig. 3 a. (c) One day after injection, fibrin fibers (arrowheads) can already be detected by light microscopy within the central vein. The diameter of the central vein appears enlarged

Fig. 3 Electron microscopy of thrombotic events and inflammation within retinal vessels

(a) Loosely aggregating thrombocytes are marked by an arrow within the central vein, one day after Fc fragment injection. (b) Unknown fibrous material (arrow), thrombocytes (white T) and microparticles (black arrow heads), 14 days after injection. The endothelium has unusual projections (white arrowhead) towards the vessel lumen. (c) An eosinophil granulocyte has been fixed in the state of degranulation in a retinal vein, 14 days after Fc fragment injection. The plasma membrane is partly missing (black arrowhead). Eosinophilic granules are seen free in the cytoplasm (arrow) but also within the cell (white arrow head). Activated thrombocytes (T) are also present

Fig. 4 Electron microscopy of electron-dense material in the vitreous and retina 14 days after intravitreal injection of Fc fragment

(a) An electron micrograph shows unusual electron-dense material which accumulated within the vitreous (black asterisk) from an Fc treated rat. This material is probably transported into the vessel lumen (white asterisk) but cannot be

18

recognized at this magnification. The ILM (black arrow) is well preserved but a damaged cell (white arrow) is attached to it. (b) Electron-dense particles are localized in the vitreous (black asterisk) and in the space around the central retinal vein (white asterisk). The ILM (black arrow) is well preserved. (c) Very unusual electron-dense particles of unknown origin are shown in the subretinal space between outer segments (ROS) and attached to the microvilli of the RPE (black arrowheads). The nucleus of this RPE cell is marked by an N and a melanosome by a white arrowhead. The outer segments appear healthy

Fig. 5 Electron microscopy of infiltrating cells

(a) The most prominent finding one day after Fc fragment treatment is cellular infiltration of the vitreous and retina as shown here in an electron micrograph. The cell in the ganglion cell layer can be clearly identified as a granulocyte (G) by the morphology of the nucleus. Microvilli (arrow) of this granulocyte are within a damaged retinal cell close to the inner limiting membrane (arrowhead). (b) A macrophage within the vitreous is highly activated which is indicated by the formation of microvilli (arrow), one day after injection. (c) This micrograph reveals a cell with microvillar (arrow) projections within a retinal cell one day after Fc treatment. The cell probably is a macrophage (M) infiltrating the retina close to the inner limiting membrane (arrowhead). (d) An activated macrophage (M) with a U-shaped nucleus and a granulocyte (G) and a third cell (arrow) are infiltrating the vitreous close to the ILM (arrowhead), two days after injection. (e) 14 days after Fc treatment, cells (arrow) are attached to the inner limiting membrane (black arrowhead) and newly formed collagen fibers (white arrowhead) are seen within the vitreous

Fig. 6 Quantification of infiltrating cells in the vitreous-retinal interface

19

Cells that were present within the vitreous close to the retina were counted in semithin sections and their number is given per mm inner limiting membrane length. The type of cell was not distinguished. Fc fragment injection significantly ($p < 0.02$) enhanced the number of infiltrating cells in group 1 ($n = 6$ eyes/group)

Fig. 7 Quantification of macrophages in the vitreous

CD68 positive and CD68 negative infiltrating cells were counted along the vitreous-retinal interface in paraffin sections. In group 1, Fc treatment yielded accumulation of CD68 positive macrophages as compared to PBS treatment (* $p < 0.05$). The ratio between stained and unstained infiltrating cells was 2.88 for Fc group 1, and 7.67 for Fc group 2, respectively

20

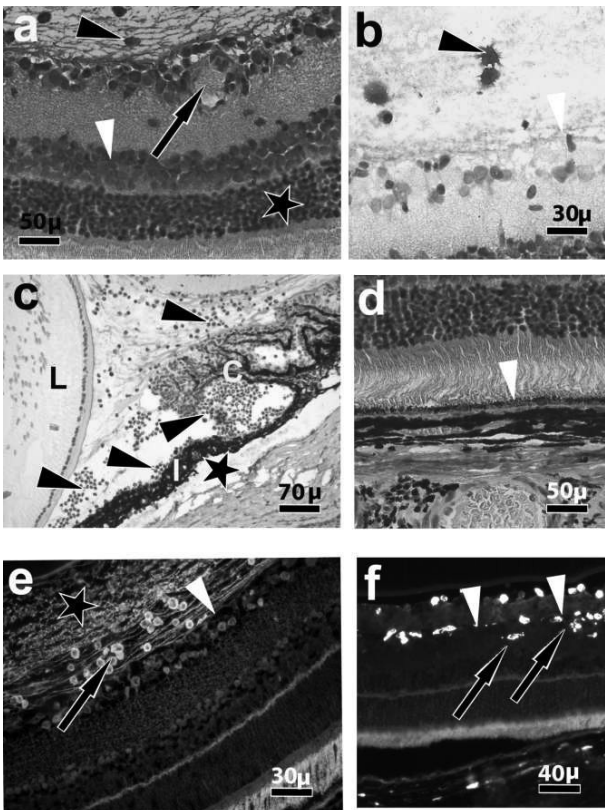


Fig.1

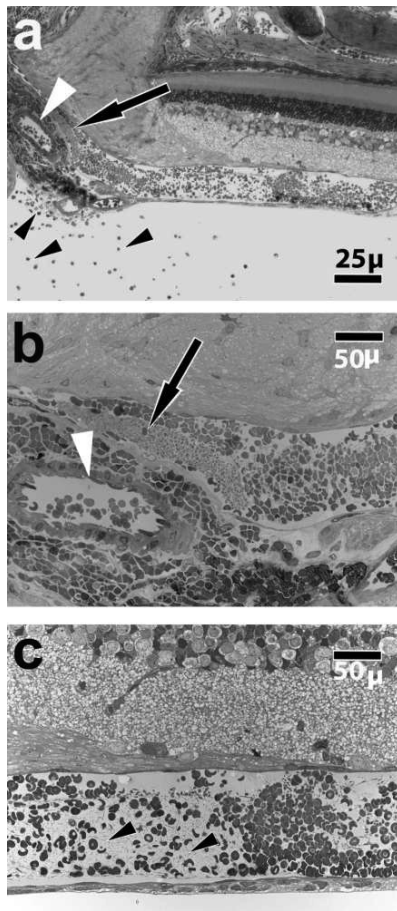


Fig.2

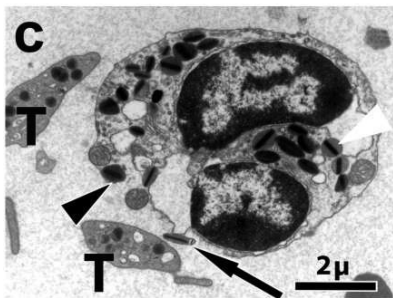
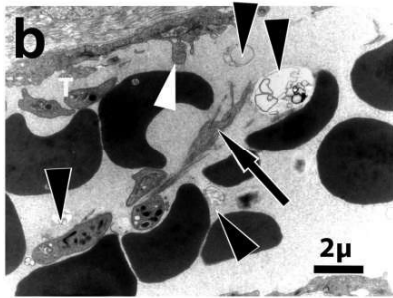
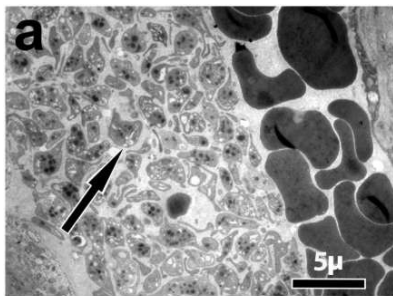


Fig.3

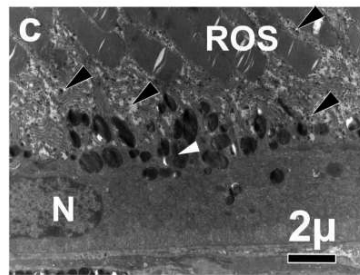
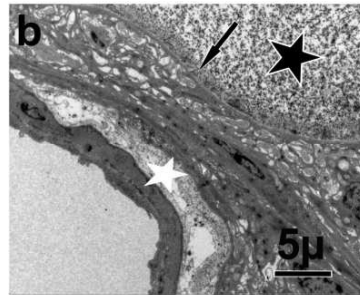
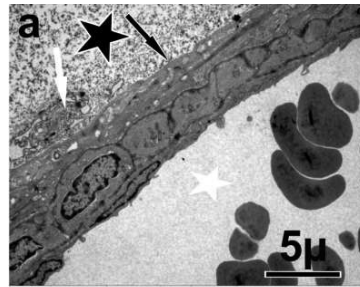


Fig.4

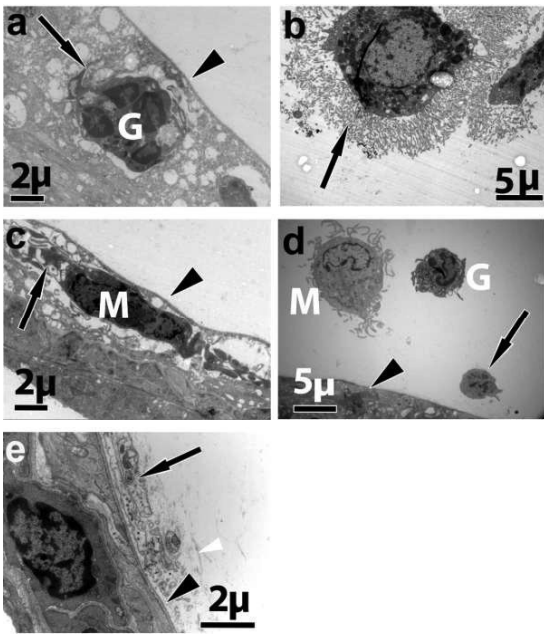


Fig.5

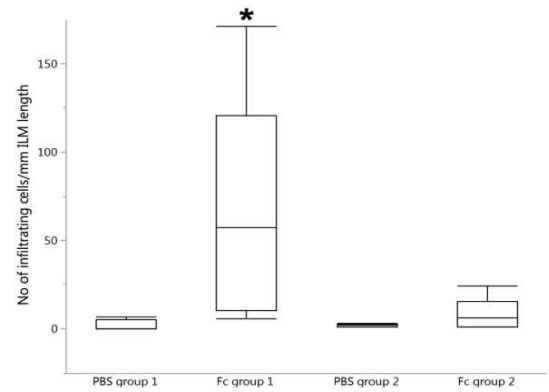


Fig.6

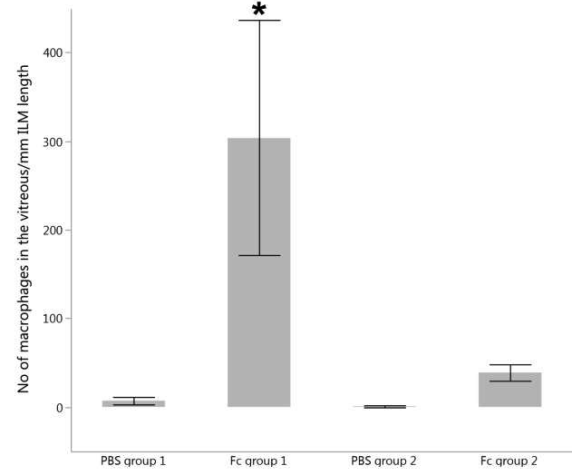


Fig.7

9.4.3 The effects of VEGF-A-inhibitors aflibercept and ranibizumab on the ciliary body and iris of monkeys

According to the copyrights, here only the last accepted manuscript version of this article can be shown.

To see the published version please visit Graefe's Archive for Clinical and Experimental Ophthalmology.

The Effects of VEGF-A-inhibitors aflibercept and ranibizumab on the ciliary body and iris of monkeys

Maximilian Ludinsky^{1#}, Sarah Christner^{1#}, Nan Su¹, Tatjana Taubitz¹, Alexander Tschulakow¹, Antje Biesemeier¹, Sylvie Julien-Schraermeyer¹, Ulrich Schraermeyer^{1,2*}

¹Section of Experimental Vitreoretinal Surgery, Centre for Ophthalmology, Tuebingen, Germany

²STZ OcuTox Preclinical Drug Assessment, Hechingen, Germany, www.ocutox.de

*Corresponding author: Prof. Dr. Ulrich Schraermeyer, Section of Experimental Vitreoretinal Surgery, Centre for Ophthalmology, Schleichstrasse 12/1, 72076 Tuebingen, Germany.

Email: Ulrich.Schraermeyer@med.uni-tuebingen.de

Tel.: +49 7071 29 80715, Fax: +49 7071 29 4554

Both authors are first authors.

Abstract

Purpose:

To investigate the effects of intravitreal ranibizumab (Lucentis®) and aflibercept (Eylea®) on the ciliary body and the iris of 12 cynomolgus monkeys regarding the fenestrations of its blood vessels.

Materials and Methods:

Structural changes in the ciliary body and in the iris were investigated with light, fluorescent and transmission electron microscopy (TEM). The latter was used to specifically quantify fenestrations of the endothelium of blood vessels after treatment with aflibercept and ranibizumab. Each of the two ciliary bodies treated with aflibercept and the two treated with ranibizumab and their controls were examined after 1 and 7 days, respectively. Ophthalmological investigations including funduscopy and intraocular pressure measurements were also applied.

Results:

Ophthalmological investigations did not reveal any changes within the groups. Both drugs reduced the VEGF concentration in the ciliary body pigmented epithelium. The structure of the ciliary body was not influenced, while the posterior pigmented epithelium of the iris showed vacuoles after aflibercept treatment. Ranibizumab was mainly concentrated on the surface layer of the ciliary epithelium, in the blood vessel walls, the lumen of some of the blood vessels and in the cells of the epithelium of the ciliary body. Aflibercept was more concentrated in the stroma and not in the cells of the epithelium, but as with ranibizumab, also in the blood vessel walls and some of their lumina, and again on the surface layer of the epithelium. Both aflibercept and ranibizumab treated eyes showed a decreased number of fenestrations of the capillaries in the ciliary body compared to the untreated controls. On day 1 and day 7, aflibercept had fewer fenestrations than the ranibizumab samples of the same day.

Conclusions:

Both aflibercept and ranibizumab were found to reach the blood vessel walls of the ciliary body and effectively reduced their fenestrations. Aflibercept might eliminate VEGF to a greater extent, possibly due to a higher elimination of fenestrations in a shorter time. Moreover, the vacuoles found in the iris need further research, in order to evaluate whether

they carry a possible pathological potential.

Keywords: aflibercept, ranibizumab, anti-VEGF therapy, ciliary body, iris, fenestration, blood vessels, electron microscopy

Introduction:

Anti-vascular endothelial growth factor (VEGF) therapy is currently used to treat uncontrolled neovascularisation in the eye, e.g. with age-related macular degeneration (AMD), diabetic macular oedema or retinal vein occlusion [1], glaucoma [2], iris rubosis [3] and others [4, 5]. Especially for the treatment of wet AMD, four different VEGF inhibitors are available and delivered by intravitreal injections: ranibizumab (Lucentis®), aflibercept (Eylea®), pegaptanib (Macugen®) and for off-label use, bevacizumab (Avastin®) [6]. The effects of these therapies on the retina have meanwhile been studied quite thoroughly. Remarkable was the decrease of fenestrations in the choriocapillaris [7-9] of monkeys treated with ranibizumab, bevacizumab or aflibercept, respectively. However, the effects of intravitreal ranibizumab and aflibercept on other ocular tissues like the ciliary body have not yet been studied, and will be presented in this work.

The ciliary body is located right behind the iris and is nourished by the same blood vessels which also nourish the iris. It consists of smooth muscle fibers and the ciliary processes, which are connected by zonular fibers to the crystalline lens, and are thus able to change the latter's shape for the purpose of focusing, a process known as accommodation [10]. The ciliary processes epithelium consists of a pigmented outside layer and a non-pigmented inside layer connected by gap-junctions. It is this structure which releases a transparent liquid into the eye called the aqueous humour, whose in and outflow maintains the intraocular eye pressure (IOP). In the ciliary processes there are lots of fenestrated capillaries whose fenestrations are permeable for water and smaller hydrophilic structures [11]. It already has been shown that VEGF blockade can also reduce the number of fenestrations in the ciliary body [12].

The VEGF-family is important for lymphangiogenesis, vasculogenesis and angiogenesis [13]. The mammalian VEGF-family presently contains five members: VEGF-A, placenta growth factor (PlGF), VEGF-B, VEGF-C, and VEGF-D (reviewed by [14]). VEGF-A plays an important role in vascular development and in diseases involving abnormal growth of blood vessels. Clinical studies have shown the significance of VEGF-A in ocular neovascularization, such as diabetic retinopathy and age-related macular degeneration, with the use of VEGF-A neutralizing antibodies [15]. VEGF is a glycosylated, multifunctional cytokine which consists of dimeric polypeptides and executes its effects through receptors

mainly expressed on the vascular endothelium. It also stimulates lymphocyte activation, chemotaxis and increases microvascular permeability [16].

In previous studies, our group investigated the effects of bevacizumab [17], ranibizumab and aflibercept [8] on the retina-choroid interface of cynomolgus monkeys. Systemical effects of aflibercept and ranibizumab were studied by analysing the kidneys of these animals in addition [18]. The same monkeys were used in this work to investigate the effects of aflibercept and ranibizumab on the ciliary body and in particular on the fenestrations of the capillaries of the same individuals.

Materials and Methods:

1. Animals and study protocol

In this study, we used new tissue samples taken from the same monkeys we had used in a previous study to investigate the effects of intravitreal ranibizumab and aflibercept on the retina-choroid complex [8]. The materials and methods applied *in vivo* are thus repeated here as follows.

Twelve Cynomolgus monkeys (*Macaca fascicularis*, aged 3 to 10 years) were raised at the Covance Laboratories (Muenster, Germany) under standard conditions. The monkeys in this study were an average of 5.5 years old for the aflibercept group and an average of 6.5 years old for the ranibizumab group. Animals were housed and handled in strict accordance with good animal practice under supervision of veterinarians and were monitored for evidence of disease and changes in attitude, appetite or behaviour suggestive of illness. Handling and housing of the animals at Covance Laboratories GmbH was done in accordance with the German Animal Welfare Act. For the notice of approval by the appropriate institutional animal care and use committee, please see Covance Studies 8260977 and 8274007.

2. Intravitreal injection of ranibizumab, aflibercept and aflibercept's vehicle

The animals were sedated by intramuscular injection of medetomidine (Domitor) and ketamine hydrochloride. Before injection, the eyes were examined for any signs of inflammation. Pupils were dilated (Mydriasis with 1% tropicamide) and anesthetized (proxymetacaine; Proparacain-pos 0.5 %; Ursapharm). The conjunctival and corneal surface was disinfected (povidone iodine 10%). After sterile coating and insertion of a lid speculum,

50 µl of ranibizumab (10 mg/mL), aflibercept (40 mg/mL) and aflibercept's vehicle (10mM sodium phosphate, 40mM sodium chloride, 0.03% polysorbate 20, and 5% sucrose, pH 6.2) were intravitreally injected using a 27-gauge canula. When removing the syringe, the injection site was compressed with forceps to prevent reflux. A topical antibiotic (gentamicin) was administered. Animals were monitored for signs of inflammation until sacrificed.

3. Ophthalmic examinations

For all ophthalmic examinations, a mydriatic agent (tropicamide) and a local ophthalmic anaesthetic (proxymetacaine) were instilled in the eyes of the sedated animals before examination.

3.1 Funduscopy and fluorescein angiography (FA)

Fundus photographs and FA were obtained for all animals once during the pre-dose phase and on the day of necropsy. For FA, an indwelling catheter was inserted and fluorescein was injected intravenously. A series of images immediately after injection and 10 min thereafter was performed. The equipment used was a digital stationary fundus camera (TRC-50 ex; Topcon, Tokyo, Japan).

3.2 Spectral-domain-optical coherence tomography (SD-OCT)

SD-OCT was obtained for all animals once during the pre-dose phase, directly after injection (only for aflibercept and its vehicle) and on the day of necropsy. The equipment used was Spectralis™ HRA+OCT (Heidelberg Engineering, Heidelberg, Germany).

3.3 Intraocular pressure (IOP)

Measurement of IOP was performed in all animals once during the pre-dose phase, before administration of the drugs, directly after administration, 10 min after administration and on the day of necropsy by using TonoVet® (Kruuse, Langeskov Denmark). Two readings were obtained per eye for each time point, and the mean IOP value was calculated and reported in millimetre of mercury (mm Hg).

4. Enucleation and post mortem analyses

On days 1 and 7 after intravitreal injection, the animals were sacrificed under general anaesthesia, i.e., intramuscular injection of ketamine hydrochloride followed by an intravenous sodium pentobarbitone (Lethobarb®, Virbac, Australia) overdose. The eyes were

enucleated five minutes post-mortem and cleaned of orbital tissue, and were slit carefully at the limbus without damaging the ora serrata. Then 25 µl of the fixative were carefully injected into the vitreous before the eyes were fixed at 4 °C by immersion into 5 % glutaraldehyde in 0.1 M cacodylate buffer (pH 7.4, Sigma, St. Louis, MO, USA) overnight for electron microscopy or into 4% formalin in PBS (Carl Roth, Karlsruhe, Germany) for immunohistochemistry. The eyes of three healthy monkeys without treatment, or with aflibercept's vehicle injection, were handled in the same manner.

5. Immunohistochemistry with paraffin embedded sections

Enucleated eyes were fixed in formalin, embedded in paraffin wax, cut into 4-µm sections and deparaffinised according to standard procedures.

a) Localisation of drug in the ciliary body (fluorescence microscopy)

Ranibizumab and aflibercept were detected respectively using a goat antiserum to human Fab of IgG (GAHu/Fab/7S, dilution 1:250; Nordic Immunological Laboratories, Tilburg, The Netherlands) and a goat anti-human IgG-Fc antibody (NB7446, dilution 1:200, Novus Biologicals Europe, Cambridge, UK), each with a cy3-rabbit anti-goat antibody as a secondary antibody (305-167-003, dilution 1:400, Jackson ImmunoResearch Europe, Suffolk, UK). Stained sections were embedded (FluorSave; Calbiochem, La Jolla, CA, USA) and inspected with a fluorescence microscope (Axioplan2; Carl Zeiss, Oberkochen, Germany).

b) Localisation of VEGF in the ciliary body (light microscopy)

Monoclonal Mouse Anti-Human Vascular Growth Factor, Clone VG1, which labels the VEGF-165, VEGF-121 and VEGF-189 isoforms of vascular endothelial growth factor (DakoCytomation Denmark, Code No.M7273), dilution 1:150, was used as a first antibody and detected with REAL™ Detection System, Alkaline Phosphatase/RED, Rabbit/Mouse(Code k5005,Dako), dilution 1:25 and inspected with a light microscope (Axioskop; Carl Zeiss, Oberkochen, Germany).

6. Light and electron microscopy (LM and EM) of plastic sections from the ciliary body

Glutaraldehyde fixed specimens were post-fixed with 1% OsO₄ at room temperature in 0.1 M

cacodylate buffer (pH 7.4), stained with uranyl acetate, and embedded in Epon after dehydration in a graded series of ethanol and propylene oxide. Semi-thin sections were stained with toluidine blue and examined by light microscopy (Zeiss Axioplan2 imaging, Zeiss, Jena, Germany). For electron microscopy, the sections were cut ultrathin and analysed with a Zeiss 900 electron microscope (Zeiss, Jena, Germany). For every eye at each time point (days 1 to 7 and control), two different regions of interest were chosen. One piece of tissue was taken in which both ciliary body and iris were visible.

7. Quantification of the endothelial fenestration in the ciliary body

A transmission electron microscope was used for counting the fenestrations per μm of endothelium in the ciliary body. The ciliary bodies were investigated for blood vessels, which were photographed. Depending on the size of the blood vessels, lower magnifications from 1100x up to 7000x were used so that the whole blood vessel could be seen on the image and the length of its endothelium could be measured (Fig. 1). For counting the fenestrations, images of the fenestrated parts of the endothelium were taken at 20000 x magnification (Fig. 2). For quantification of the length of endothelium and of fenestrae, image analysis software (iTEM, Olympus Soft Imaging Solutions, Muenster, Germany) was used.

8. Semi-quantification of VEGF staining in the ciliary body

From each specimen, one eye was investigated for VEGF analysis (2 samples per time point). One section was analysed for each eye. Each section was photographed at 630-fold magnification, using a Zeiss Axioscope light microscope with AxioVision software. For each section, 4 photos were taken, that almost covered the whole pigmented epithelium of the ciliary body. So for every sample, 8 photos were analysed.

9. Statistical analysis

Whole blood vessels were investigated for endothelial length and number fenestrations. As vessels always show a fenestrated area and a non-fenestrated area, fenestrations were normalized to fenestrations/10 μm of fenestrated endothelium. Statistical significance for the comparison of aflibercept and ranibizumab to the controls was determined by using the

Dunnett's test and the JMP10 statistical program (SAS, Heidelberg, Germany). $P < 0.05$ was considered statistically significant.

To quantify the staining in the pigmented epithelium of the ciliary body we used the "colour cube based" function in the Image-Pro Plus software. Statistical testing was performed using JMP10 software as described above.

Results:

Ophthalmic examinations (FA, SD-OCT, IOP)

The results from the in vivo ophthalmological examinations have already been published [8]. In brief, FA and SD-OCT analyses did not show any drug-related changes. The intraocular pressure (IOP), baseline 10 -20 mm Hg, was raised immediately after intravitreal injection up to 31 ± 14 mm Hg in the ranibizumab treated group, and up to 50 ± 12 mm Hg in the aflibercept treated group. Both regained normal levels after 10 minutes (ranibizumab 19 ± 6 mm Hg, aflibercept 14 ± 3 mm Hg) and further stabilized after day 1 (ranibizumab 10 ± 1 mm Hg, aflibercept 11 ± 7 mm Hg) and day 7 (ranibizumab 19 ± 4 mm Hg, aflibercept 10 ± 3 mm Hg).

Localisation of drug in the ciliary body (fluorescence immunohistochemistry)

The distribution of aflibercept and ranibizumab within the different structures of the ciliary body were not different, however the staining of aflibercept was a bit stronger (data not shown). The aflibercept treated ciliary bodies were intensively stained in the walls of blood vessels also including the lumen of some, but not all, of these blood vessels. Further staining was detectable on the surface layer of the epithelium and in the connective tissues surrounding the vascular plexus. The ciliary muscle tissue was more weakly stained, as was the cytoplasm of the epithelium, but not their nuclei. The ranibizumab treated ciliary bodies showed a staining similar to the aflibercept ciliary bodies, on the surface layer of the epithelium and the walls of blood vessels including some of their lumina. The ciliary muscle and the vascular layer were also stained more weakly. We did also not find any significant changes in the distribution of staining between day 1 and day 7 samples.

Localisation of VEGF in the ciliary body (light microscopical immunohistochemistry)

In the paraffin embedded samples, no histological changes were detected in the ciliary body after intravitreal aflibercept and ranibizumab as compared to the controls.

Within the pigmented epithelium of the ciliary body, all samples were checked for their amount of VEGF using immunohistochemistry. The pigmented epithelium of the ciliary body of untreated monkeys was intensely stained, while both aflibercept and ranibizumab treated groups showed less VEGF immunoreactivity at all time points (Fig. 3; all p values <0.0001).

11

VEGF levels of samples treated with ranibizumab or aflibercept did not change after day 1 or 7, respectively.

Structural changes in ciliary body and iris (LM and EM of plastic sections)

Investigating the semi-thin sections of whole eye preparations in the light microscope did not show any significant changes in the ciliary body. However, since the iris was shown in the same sections and did show differences between aflibercept and ranibizumab treated samples, it was analysed as well using both light and electron microscopy (Fig. 4). In all aflibercept treated samples, clearly visible vacuoles showed up throughout the posterior pigmented epithelium of the iris as shown in Figs. 4b and 4c. Neither the controls, nor the ranibizumab treated samples showed these vacuoles in either light or electron microscopical evaluations. The vacuoles in the iris in the aflibercept group showed up on day 1 and did not appear to change in the samples taken at day 7.

The transition zone between the pigmented iris epithelium and the unpigmented ciliary epithelium was evaluated as well and didn't show pathological changes in any of the samples. We also couldn't find any other ultrastructural alterations in the area covering the iris and ciliary body.

Quantification of fenestrations in blood vessels of the ciliary body (EM)

The fenestrations of the endothelium decreased in all aflibercept as well as in all ranibizumab treated samples compared to controls. On day 1, the aflibercept samples had an average fenestration rate of 2.7 per $10\mu\text{m}$ of endothelium and on day 7 lower 2.5 fenestrations per $10\mu\text{m}$. The ranibizumab treated samples had an average of 2.9 fenestrations per $10\mu\text{m}$ on day 1 and an average of 2.6 fenestrations per $10\mu\text{m}$ on day 7. Both ranibizumab values are higher than the aflibercept values of the same day. Compared to the control's average of 3.8 fenestrations per $10\mu\text{m}$, the samples with VEGF-inhibitors showed a significant decrease of fenestrations in aflibercept on day 1 and 7 and in ranibizumab on day 7. Exemplary images of the clear differences in fenestrations before and after treatment can be seen in Fig 5. The box plot shows the statistical analysis. The ranibizumab-treated group of day 1 is not significantly different as compared to the controls ($p=0.1$), whereas the other groups (ranibizumab day 7, $p=0.0003$; aflibercept day 1, $p=0.007$; aflibercept day 7, $p=0.053$) had a lower p-value than 0.05, thus showed significant changes.

12

Discussion:

It has been shown before that VEGF-A inhibition leads to a degeneration of blood vessels [19, 20], and since an unusual growth of new blood vessels is characteristic for neovascular age-related macular degeneration (wet AMD) [21], this effect was identified as being an adequate way to treat this disease [22]. Apart from wet AMD, VEGF-dependant ischemic retinopathies going along with pathological neovascularization of the anterior segment of the eye have been described. This is for example the case in rubeosis iridis, which is characterized by a neovascularization of the iris and represents a complication of diabetic retinopathy or central vein occlusion. In the following, neovascular glaucoma may occur. In a previous study, our group has shown that intravitreally injected bevacizumab penetrates quickly not only into the posterior segment of the eye but also into the iris, anterior chamber angle and ciliary body and accumulates particularly in blood-vessel walls [23]. Bevacizumab has already been used intracamerally and intravitreally for the adjuvant treatment of rubeosis iridis and neovascular glaucoma with promising results [3][24, 25][26]. Recently, also ranibizumab injections for the treatment of these diseases have been published [27, 28], but to our knowledge, no trials have yet been performed with aflibercept. Our results show that the VEGF-A inhibitors ranibizumab and aflibercept both reduce the amount of VEGF in the ciliary pigmented epithelium and also reduce the number of fenestrations in the blood vessels of the ciliary body without significant changes in the ultrastructure. We further demonstrate that aflibercept administration resulted in a lower number of fenestrations both after day 1 and day 7 compared to ranibizumab. Since fenestrations can be induced by VEGF-A in vitro and in vivo [29, 30], and an inhibition of VEGF eliminates fenestrations in the choriocapillaris, the ciliary body and even in endothelial cells of the glomeruli of the kidney [7, 9, 12, 18, 31], the loss of them here can be seen as a proof of activity of the drugs in the ciliary body.

All morphological changes observed in the eye and other tissues always have been related to not only the physiological situation but also the age of the subject. For example in the retina it is known that physiological aging processes include steady loss of photoreceptors, thickening of Bruch's membrane, thinning of the choroid and forming of hard drusen in the periphery[32]. For the iris and ciliary body increased pigmentation of the trabecular meshwork, an increase in the resistance to the outflow of aqueous humour with an increased risk of glaucoma are described. Moreover, the iris tends to become less reactive with age and

loses pigment and also the shape and tone of ciliary body changes with age [33]. Taken into account that the average life expectancy of humans in the developed countries is about 77 years [34] and that the average life span of *Macaca fascicularis* is 31 years [35], then the human equivalent age of the study subjects with an average of 5.5 years for aflibercept- and an average of 6.5 years for ranibizumab-treated monkeys is 13.8 and 16 years, respectively. Thus, none of the described aging changes have been observed in our study and the vacuoles found in the iris of aflibercept samples cannot be related to the age of the monkeys. However, the loss of fenestrations in the ciliary body can have negative effects on the function of the ciliary body, e.g. defects of the pigmented epithelial layer, as observed by others after VEGF-A neutralization [12]. A greater loss of fenestrations, as we saw it in the aflibercept treated ciliary bodies, might thus not be desirable, as irreversible damage of the ciliary body can cause prolonged ocular hypotony and phthisis bulbi [36]. By contrast, we did not find a significant amount of microthrombi in the blood vessels after VEGF-A inhibition, as our group previously observed in the choriocapillaris and choroidal vessels after intravitreal bevacizumab injection [37]. Another clinical complication has been documented before, when a 65-year-old patient with unilateral exudative age-related macular degeneration showed a focal atrophic area in the ciliary body corresponding to the site of the intravitreal bevacizumab injection [38]. Another group found a decrease in retrobulbar blood flow after intravitreal bevacizumab injections [39]. VEGF inhibitors also lead to several other defects in various other cell types, for example signs of thrombotic microangiopathy in the glomerular endothelium [40], a decreased vascular perfusion in the choroid plexus of the brain [41], and an increased apoptosis in the neuronal retina of the eye [42]. However, in the retina-choroid complex, there were indications that the fenestrations in the choriocapillaris recovered from the VEGF blockade after day 14 [7]. In a different study, where VEGF-A inhibition led to blood vessel degeneration in pancreas, thyroid, adrenal cortex, pituitary, choroid plexus, small-intestinal villi and epididymal adipose tissue, the vessels also recovered 14 days after the inhibition was stopped [43]. On the other hand- as described above- a higher effectivity in eliminating fenestrations in the ciliary body can be a desirable effect in the treatment of iris neovascularization and neovascular glaucoma and in lowering IOP.

Furthermore, we found vacuoles in the posterior pigmented epithelium of the iris in the aflibercept treated samples, but not in the ranibizumab treated ones. To our knowledge, this is

the first time this has been found in the iris after intravitreal injection with aflibercept or other VEGF-A inhibitors. Vacuolization of the iris pigmented epithelium has been found before in 40% of enucleated eyes of patients with diabetic diseases, and it was also discovered that the material in the vacuoles was glycogen [44]. The vacuoles can also be called microcysts of the iris pigmented epithelium (MIPE) and have been found in enucleated eyes of patients with several different diseases, not necessarily associated with the eye, like alveolar cell carcinoma of the lung, prostatic adenocarcinoma or acute lymphocytic leukemia [45]. The material inside the vacuoles was not identified in this study, but microcysts were found in other compartments of the eye, like the non-pigmented epithelium of the ciliary body [45], which was not the case in our samples of the ciliary body. Microcysts have been identified as a common pathological feature associated with many disorders and in patients who have been on high dosage corticosteroids and the speculative conclusion was drawn that neoplasms might alter the body's metabolism and lead to fluid accumulation in the pigmented epithelium of the iris [45]. Oedema have been found in the macula as a result of branch retinal vein occlusion, which is the second most common major retinal vascular disease, causing decreased visual acuity [46]. Interestingly, the VEGF-A inhibitor bevacizumab showed beneficial effects on macular oedema caused by branch retinal vein occlusion [47] as well as ranibizumab, which can also be used for macular oedema caused by diabetes [48]. In contrast, in our study, the VEGF-A inhibitor aflibercept might cause oedema in the iris. Macular oedema have also been found as a result of retinitis pigmentosa, where changes in the retinal pigmented epithelium take place, endangering the blood-retinal-barrier, causing a subretinal leakage and therefore macular oedema [49]. However, new research in this area might be indicated to get more insight into the influence of the vacuoles in the iris after intravitreal aflibercept injection.

Our immunohistochemical localisation of aflibercept and ranibizumab showed no histological changes compared to the controls, which is in agreement with other studies with bevacizumab where this also did not occur [50]. However, we already saw an intense staining after the first day, showing that both intravitreally injected drugs penetrate the ciliary body well and fast. In all our samples, ranibizumab and aflibercept could be mostly located in the walls of blood vessels, being the place of secretion and binding of VEGF to its receptors on the vascular endothelial cells. This seems to be the optimal place for the best effect of the VEGF-inhibitors

[51]. Despite this, we found staining in other compartments of the ciliary body, where their impact remains theoretical. For example, the immunoreactivity of aflibercept and ranibizumab in the lumen of the blood vessels could lead to the conclusion, that there is a quick distribution, but also a quick elimination of the intravascular drugs. But since there are aggregations of this type only in some, but not all, blood vessels, circulation might not be disturbed in these vessels. The same effect in the ciliary body has been shown before, with intravitreal bevacizumab injection [23]. The effects and distribution of the intravascular drugs throughout the whole body, especially on other structures with fenestrations like the glomerular endothelium of the kidney is an interesting topic for further research. Our group recently published a study in which the kidneys of the animals studied in this work were analysed. Interestingly, both drugs could be detected within the capillaries of the glomeruli and fenestration changes in the glomerular endothelium differed from those observed in the walls of blood vessels in the ciliary body as described above [18]. The drug staining on the surface of the epithelium might indicate the penetration through these tissues and even the stroma, as seen after intravitreal injections with bevacizumab [23].

In conclusion, aflibercept might eliminate more fenestrations than ranibizumab. Whether this is desirable or not remains subject to discussion and will depend on the treated ocular disease and its desired effect. Moreover, the role of the vacuoles in the iris should be clarified, as well as some other effects, where VEGF-A plays some other important roles, such as in photoreceptors and Müller cells. There, increased apoptosis was noticed after VEGF-A inhibition, which in an experiment with mice led to a degraded retinal function [42]. Another experiment where VEGF-A inhibition was paired with ischemia led to retinal ganglion cell death [52]. Furthermore VEGF improved the survival of retinal pigmented epithelium cells under oxidative stress [53] and provided neuroprotection [54]. A more effective VEGF neutralization, as provided by aflibercept, might be beneficial for treating the wet form of AMD or rubeosis iridis/neovascular glaucoma, but regarding all of the preceding aspects, further research is needed to rule out any unexpected side effects.

Funding: Novartis provided financial support in the form of a honorary for author US.

The sponsor had no role in the design or conduct of this research.

Conflict of Interest: All authors certify that they have no affiliations with or involvement in any organization or entity with any financial interest (such as honoraria; educational grants; participation in speakers' bureaus; membership, employment, consultancies, stock ownership, or other equity interest; and expert testimony or patent-licensing arrangements) other than stated below, or non-financial interest (such as personal or professional relationships, affiliations, knowledge or beliefs) in the subject matter or materials discussed in this manuscript. STZ OcuTox Preclinical Drug Assessment provided support in the form of an honorarium for author US, but did not have any additional role in the study design, data collection and analysis, decision to publish, or preparation of the manuscript.

Animal Experiments: Ethical approval: All applicable international, national, and/or institutional guidelines for the care and use of animals were followed.

All procedures performed in studies involving animals were in accordance with the ethical standards of the institution at which the studies were conducted (Covance Studies 8260977 and 8274007).

Figure Legends:

Fig. 1 Overview of a blood vessel (black arrow indicates vessel wall) in the ciliary body treated with aflibercept on day 1; TEM, magnification x3000; CPE ciliary pigmented epithelium

Fig. 2 Detail of endothelium with fenestrations (black arrows), aflibercept day 1
TEM, magnification x20000; e erythrocyte, en endothelium, l lumen

Fig. 3 Reduction of VEGF staining (red) after treatment with ranibizumab and aflibercept. Light micrographs of (a) untreated control eye (b) eye treated with ranibizumab on day 1 (c) eye treated with aflibercept on day 1; CE ciliary unpigmented epithelium, CPE ciliary pigmented epithelium

Fig. 4 Effect of ranibizumab (a) and aflibercept (b, c) on the iris pigmented epithelium. (a) Ranibizumab treated iris day 7 without vacuoles. Semi-thin section, light microscope, magnification x100. (b) Aflibercept treated iris day 1 showing vacuoles between the pigment cells (black arrows); Semi-thin section, light microscope, magnification x100. (c) Aflibercept treated iris day 1 with vacuoles (black arrows); TEM, magnification x7000; IPEa anterior iris pigment epithelium, IPEi interior iris pigment epithelium

Fig. 5 Fenestration in ciliary blood vessels (a) Endothelium with a lot of fenestrations (black arrows) in an untreated blood vessel of the ciliary body. (b) Endothelium with significantly less fenestrations (black arrow) in a ranibizumab treated sample after day 7; TEM, magnification x12000. (c) Box-plot of average fenestrations per 10 μ m. Lines extending vertically from the boxes (*whiskers*) indicate the variability outside the upper and lower quartiles and individual points marking outliers. * statistically significant to control group ($p < 0.05$). CPE ciliary pigmented epithelium, en endothelium, l lumen

References

1. Tah V, Orlans HO, Hyer J, Casswell E, Din N, Sri Shanmuganathan V, Ramskold L, Pasu S (2015) Anti-VEGF Therapy and the Retina: An Update. *Journal of ophthalmology*: 627674 DOI 10.1155/2015/627674
2. Bikbov MM, Babushkin AE, Orenburkina OI (2012) [Anti-VEGF-agents in treatment of neovascular glaucoma]. *Vestnik oftalmologii* 128: 50-53
3. Grisanti S, Biester S, Peters S, Tatar O, Ziemssen F, Bartz-Schmidt KU, Tuebingen Bevacizumab Study G (2006) Intracameral bevacizumab for iris rubeosis. *Am J Ophthalmol* 142: 158-160 DOI 10.1016/j.ajo.2006.02.045
4. Tolentino M (2011) Systemic and ocular safety of intravitreal anti-VEGF therapies for ocular neovascular disease. *Survey of ophthalmology* 56: 95-113 DOI 10.1016/j.survophthal.2010.08.006
5. Barkmeier AJ, Akduman L (2009) Bevacizumab (avastin) in ocular processes other than choroidal neovascularization. *Ocular immunology and inflammation* 17: 109-117 DOI 10.1080/09273940802596534
6. Cheung LK, Eaton A (2013) Age-related macular degeneration. *Pharmacotherapy* 33: 838-855 DOI 10.1002/phar.1264
7. Peters S, Heiduschka P, Julien S, Ziemssen F, Fietz H, Bartz-Schmidt KU, Tubingen Bevacizumab Study G, Schraermeyer U (2007) Ultrastructural findings in the primate eye after intravitreal injection of bevacizumab. *Am J Ophthalmol* 143: 995-1002 DOI 10.1016/j.ajo.2007.03.007
8. Julien S, Biesemeier A, Taubitz T, Schraermeyer U (2014) Different effects of intravitreally injected ranibizumab and aflibercept on retinal and choroidal tissues of monkey eyes. *The British journal of ophthalmology* 98: 813-825 DOI 10.1136/bjophthalmol-2013-304019
9. Ford KM, Saint-Geniez M, Walshe T, Zahr A, D'Amore PA (2011) Expression and role of VEGF in the adult retinal pigment epithelium. *Investigative ophthalmology & visual science* 52: 9478-9487 DOI 10.1167/iovs.11-8353
10. Helmholtz H (1855) Ueber die Accommodation des Auges. *Graefes Archive for Clinical and Experimental Ophthalmology* 1: 1-74 DOI 10.1007/BF02720789
11. Welsch U, Deller T (2010) *Lehrbuch Histologie*. Urban & Fischer Verlag/Elsevier GmbH, Munich, pp. 210, 504.
12. Ford KM, Saint-Geniez M, Walshe TE, D'Amore PA (2012) Expression and role of VEGF-a in the ciliary body. *Investigative ophthalmology & visual science* 53: 7520-7527 DOI 10.1167/iovs.12-10098
13. Shibuya M, Claesson-Welsh L (2006) Signal transduction by VEGF receptors in regulation of angiogenesis and lymphangiogenesis. *Experimental cell research* 312: 549-560 DOI 10.1016/j.yexcr.2005.11.012
14. Ferrara N (2009) Vascular endothelial growth factor. *Arteriosclerosis, thrombosis, and vascular biology* 29: 789-791 DOI 10.1161/ATVBAHA.108.179663
15. Wolf S (2008) Current status of anti-vascular endothelial growth factor therapy in Europe. *Japanese journal of ophthalmology* 52: 433-439 DOI 10.1007/s10384-008-0580-4
16. Schlingemann RO, van Hinsbergh VW (1997) Role of vascular permeability factor/vascular endothelial growth factor in eye disease. *The British journal of ophthalmology* 81: 501-512
17. Schraermeyer U, Julien S (2013) Effects of bevacizumab in retina and choroid after intravitreal injection into monkey eyes. *Expert Opin Biol Ther* 13: 157-167 DOI 10.1517/14712598.2012.748741
18. Tschulakow A, Christner S, Julien S, Ludinsky M, van der Giet M, Schraermeyer U (2014) Effects of a single intravitreal injection of aflibercept and ranibizumab on glomeruli of monkeys. *PloS one* 9: e113701 DOI 10.1371/journal.pone.0113701
19. Folkman J (1971) Tumor angiogenesis: therapeutic implications. *The New England journal of medicine* 285: 1182-1186 DOI 10.1056/NEJM197111182852108
20. Folkman J (1992) Angiogenesis--retrospect and outlook. *Exs* 61: 4-13
21. Fine SL, Berger JW, Maguire MG, Ho AC (2000) Age-related macular degeneration. *The New England journal of medicine* 342: 483-492 DOI 10.1056/NEJM200002173420707
22. Nguyen DH, Luo J, Zhang K, Zhang M (2013) Current therapeutic approaches in neovascular age-related macular degeneration. *Discovery medicine* 15: 343-348
23. Peters S, Heiduschka P, Julien S, Bartz-Schmidt KU, Schraermeyer U (2008) Immunohistochemical localisation of intravitreally injected bevacizumab in the anterior chamber angle, iris and ciliary body of the primate eye. *The British journal of ophthalmology* 92: 541-544 DOI 10.1136/bjo.2007.133496
24. Yazdani S, Hendi K, Pakravan M (2007) Intravitreal bevacizumab (Avastin) injection for neovascular glaucoma. *Journal of glaucoma* 16: 437-439 DOI 10.1097/IJG.0b013e3180457c47
25. Wolf A, von Jagow B, Ulbig M, Haritoglou C (2011) Intracameral injection of bevacizumab for the treatment of neovascular glaucoma. *Ophthalmologica Journal international d'ophtalmologie International journal of ophthalmology Zeitschrift fur Augenheilkunde* 226: 51-56 DOI 10.1159/000327364
26. Ghanem AA, El-Kannishy AM, El-Wehidy AS, El-Agamy AF (2009) Intravitreal bevacizumab (avastin) as an adjuvant treatment in cases of neovascular glaucoma. *Middle East African journal of ophthalmology* 16: 75-79 DOI 10.4103/0974-9233.53865
27. Luke J, Nassar K, Luke M, Grisanti S (2013) Ranibizumab as adjuvant in the treatment of rubeosis iridis and neovascular glaucoma--results from a prospective interventional case series. *Graefes archive for clinical and experimental ophthalmology = Albrecht von Graefes Archiv fur klinische und experimentelle Ophthalmologie* 251: 2403-2413 DOI 10.1007/s00417-013-2428-y
28. Tu Y, Fay C, Guo S, Zarkin MA, Marcus E, Bhagat N (2012) Ranibizumab in patients with dense cataract and proliferative diabetic retinopathy with rubeosis. *Oman journal of ophthalmology* 5: 161-165 DOI 10.4103/0974-620X.106099
29. Esser S, Wolburg K, Wolburg H, Breier G, Kurzchalia T, Risau W (1998) Vascular endothelial growth factor induces endothelial fenestrations in vitro. *The Journal of cell biology* 140: 947-959
30. Roberts WG, Palade GE (1995) Increased microvascular permeability and endothelial fenestration induced by vascular endothelial growth factor. *Journal of cell science* 108 (Pt 6): 2369-2379
31. Inai T, Mancuso M, Hashizume H, Baffert F, Haskell A, Baluk P, Hu-Lowe DD, Shalinsky DR, Thurston G, Yancopoulos GD, McDonald DM (2004) Inhibition of vascular endothelial growth factor (VEGF) signaling in cancer causes loss of endothelial fenestrations, regression of tumor vessels, and appearance of basement

- membrane ghosts. *The American journal of pathology* 165: 35-52 DOI 10.1016/S0002-9440(10)63273-7
32. Ardeljan D, Chan CC (2013) Aging is not a disease: distinguishing age-related macular degeneration from aging. *Progress in retinal and eye research* 37: 68-89 DOI 10.1016/j.preteyeres.2013.07.003
 33. Salvi SM, Akhtar S, Currie Z (2006) Ageing changes in the eye. *Postgraduate medical journal* 82: 581-587 DOI 10.1136/pgmj.2005.040857
 34. Roser M (2016) Life Expectancy. <http://ourworldindata.org/data/population-growth-vital-statistics/life-expectancy/> Accessed 25 Mar 2016
 35. Cawthon Lang K (2006) Primate Factsheets: Long-tailed macaque (*Macaca fascicularis*). Taxonomy, Morphology, & Ecology. <http://pin.primate.wisc.edu/factsheets/entry/long-tailed_macaque>. Accessed 2016 March 21. Wisconsin Primate Research Center (WPRC) Library at the University of Wisconsin-Madison.
 36. Jovanovic-Pandova L, Watson PG, Liu C, Chan WY, de Wolff-Rouendaal D, Barthen ER, Emmanouilidis-van der Spek K, Jager MJ (2006) Ciliary tissue transplantation in the rabbit. *Experimental eye research* 82: 247-257 DOI 10.1016/j.exer.2005.06.019
 37. Schraermeyer U, Julien S (2012) Formation of immune complexes and thrombotic microangiopathy after intravitreal injection of bevacizumab in the primate eye. Graefes archive for clinical and experimental ophthalmology = Albrecht von Graefes Archiv fur klinische und experimentelle Ophthalmologie 250: 1303-1313 DOI 10.1007/s00417-012-2055-z
 38. Martel JN, Han Y, Lin SC (2011) Severe intraocular pressure fluctuation after intravitreal anti-vascular endothelial growth factor injection. *Ophthalmic surgery, lasers & imaging : the official journal of the International Society for Imaging in the Eye* 42 Online: e100-102 DOI 10.3928/15428877-20111006-02
 39. Mete A, Saygili O, Mete A, Bayram M, Bekir N (2010) Effects of intravitreal bevacizumab (Avastin) therapy on retrolubar blood flow parameters in patients with neovascular age-related macular degeneration. *Journal of clinical ultrasound : JCU* 38: 66-70 DOI 10.1002/jcu.20650
 40. Eremina V, Jefferson JA, Kowalewska J, Hochster H, Haas M, Weisstuch J, Richardson C, Kopp JB, Kabir MG, Backx PH, Gerber HP, Ferrara N, Barisoni L, Alpers CE, Quaggin SE (2008) VEGF inhibition and renal thrombotic microangiopathy. *The New England journal of medicine* 358: 1129-1136 DOI 10.1056/NEJMoa0707330
 41. Maharaj AS, Walshe TE, Saint-Geniez M, Venkatesha S, Maldonado AE, Himes NC, Matharu KS, Karumanchi SA, D'Amore PA (2008) VEGF and TGF-beta are required for the maintenance of the choroid plexus and ependyma. *J Exp Med* 205: 491-501 DOI 10.1084/jem.20072041
 42. Saint-Geniez M, Maharaj AS, Walshe TE, Tucker BA, Sekiyama E, Kurihara T, Darland DC, Young MJ, D'Amore PA (2008) Endogenous VEGF is required for visual function: evidence for a survival role on muller cells and photoreceptors. *PLoS one* 3: e3554 DOI 10.1371/journal.pone.0003554
 43. Kamba T, Tam BY, Hashizume H, Haskell A, Sennino B, Mancuso MR, Norberg SM, O'Brien SM, Davis RB, Gowen LC, Anderson KD, Thurston G, Joho S, Springer ML, Kuo CJ, McDonald DM (2006) VEGF-dependent plasticity of fenestrated capillaries in the normal adult microvasculature. *Am J Physiol Heart Circ Physiol* 290: H560-576 DOI 10.1152/ajpheart.00133.2005
 44. Yanoff M, Fine BS, Berkow JW (1970) Diabetic lacy vacuolation of iris pigment epithelium; a histopathologic report. *Am J Ophthalmol* 69: 201-210
 45. Fischer R, Henkind P, Gartner S (1979) Microcysts of the human iris pigment epithelium. *The British journal of ophthalmology* 63: 750-753
 46. Aref AA, Scott IU (2011) Management of macular edema secondary to branch retinal vein occlusion: an evidence-based update. *Advances in therapy* 28: 28-39 DOI 10.1007/s12325-010-0089-3
 47. Lee K, Jung H, Sohn J (2014) Comparison of injection of intravitreal drugs with standard care in macular edema secondary to branch retinal vein occlusion. *Korean journal of ophthalmology : KJO* 28: 19-25 DOI 10.3341/kjo.2014.28.1.19
 48. Schmidt-Erfurth U, Lang GE, Holz FG, Schlingemann RO, Lanzetta P, Massin P, Gerstner O, Bouazza AS, Shen H, Osborne A, Mitchell P, Group RES (2014) Three-year outcomes of individualized ranibizumab treatment in patients with diabetic macular edema: the RESTORE extension study. *Ophthalmology* 121: 1045-1053 DOI 10.1016/j.ophtha.2013.11.041
 49. Barge S, Rothwell R, Sepulveda P, Agrelos L (2013) Intravitreal and subtenon depot triamcinolone as treatment of retinitis pigmentosa associated cystoid macular edema. *Case reports in ophthalmological medicine* 2013: 591681 DOI 10.1155/2013/591681
 50. Sugimoto Y, Mochizuki H, Miyagi H, Kawamata S, Kiuchi Y (2013) Histological findings of uveal capillaries in rabbit eyes after multiple intravitreal injections of bevacizumab. *Current eye research* 38: 487-496 DOI 10.3109/02713683.2013.763990
 51. Simorre-Pinatel V, Guerrin M, Chollet P, Penary M, Clamens S, Malecaze F, Plouet J (1994) Vasculotropin-VEGF stimulates retinal capillary endothelial cells through an autocrine pathway. *Investigative ophthalmology & visual science* 35: 3393-3400
 52. Nishijima K, Ng YS, Zhong L, Bradley J, Schubert W, Jo N, Akita J, Samuelsson SJ, Robinson GS, Adams AP, Shima DT (2007) Vascular endothelial growth factor-A is a survival factor for retinal neurons and a critical neuroprotectant during the adaptive response to ischemic injury. *The American journal of pathology* 171: 53-67 DOI 10.2353/ajpath.2007.061237
 53. Byeon SH, Lee SC, Choi SH, Lee HK, Lee JH, Chu YK, Kwon OW (2010) Vascular endothelial growth factor as an autocrine survival factor for retinal pigment epithelial cells under oxidative stress via the VEGF-R2/P13K/Akt. *Investigative ophthalmology & visual science* 51: 1190-1197 DOI 10.1167/iov.09-4144
 54. Beazley-Long N, Hua J, Jehle T, Hulse RP, Dersch R, Lehrling C, Bevan H, Qiu Y, Lagreze WA, Wynn D, Churchill AJ, Kehoe P, Harper SJ, Bates DO, Donaldson LF (2013) VEGF-A165b is an endogenous neuroprotective splice isoform of vascular endothelial growth factor A in vivo and in vitro. *The American journal of pathology* 183: 918-929 DOI 10.1016/j.ajpath.2013.05.031



Figure 1

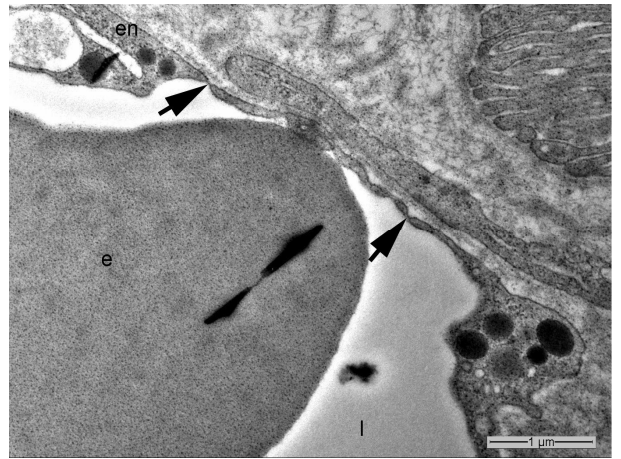


Figure 2

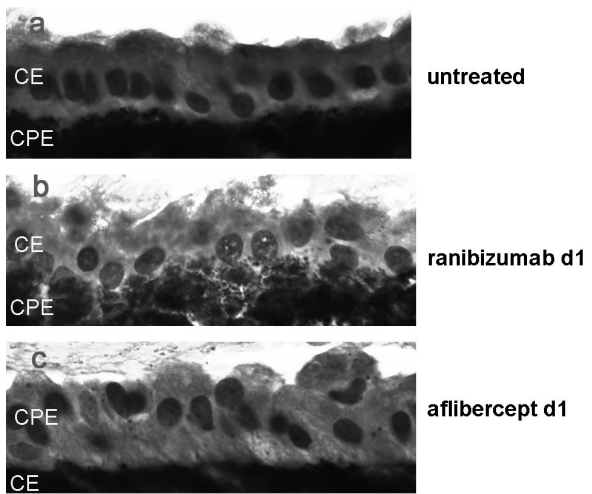


Figure 3

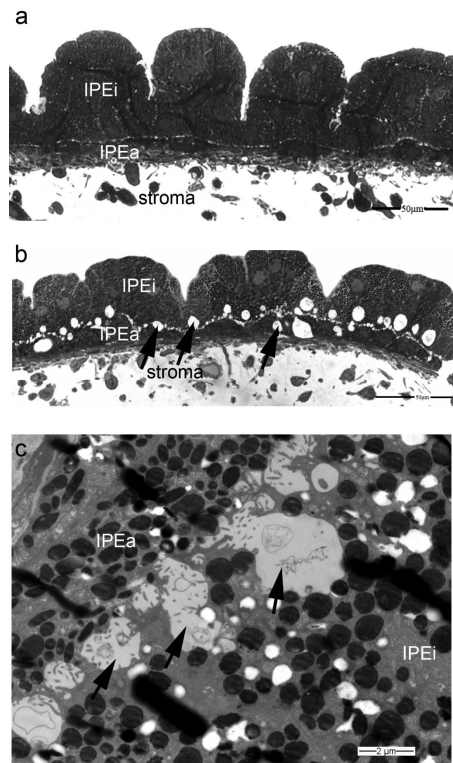


Figure 4

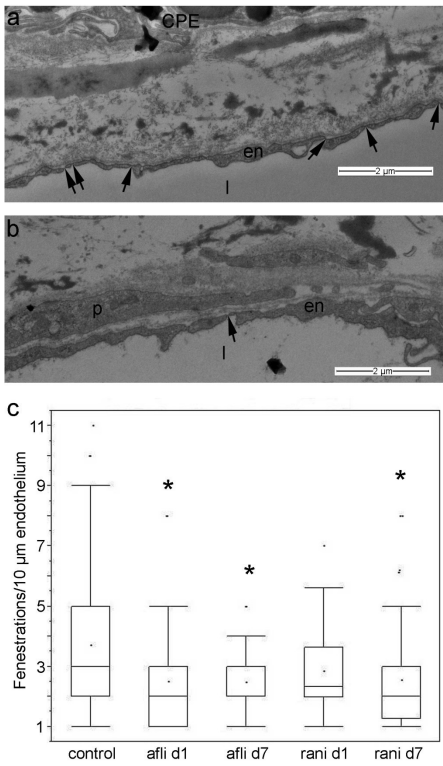


Figure 5

9.4.4 Effects of a Single Intravitreal Injection of Aflibercept and Ranibizumab on Glomeruli of Monkeys



OPEN ACCESS

Citation: Tschulakow A, Christner S, Julien S, Ludinsky M, van der Giet M, et al. (2014) Effects of a Single Intravitreal Injection of Aflibercept and Ranibizumab on Glomeruli of Monkeys. PLoS ONE 9(11): e113701. doi:10.1371/journal.pone.0113701

Editor: Stuart E. Dryer, University of Houston, United States of America

Received: August 1, 2014

Accepted: October 28, 2014

Published: November 21, 2014

Copyright: © 2014 Tschulakow et al. This is an open-access article distributed under the terms of the Creative Commons Attribution License, which permits unrestricted use, distribution, and reproduction in any medium, provided the original author and source are credited.

Data Availability: The authors confirm that all data underlying the findings are fully available without restriction. All relevant data are within the paper.

Funding: The study was financially supported by Novartis Pharma AG. The funders had no role in study design, data collection and analysis, decision to publish, or preparation of the manuscript. STZ OcuTox Preclinical Drug Assessment provided support in the form of an honorarium for author US, but did not have any additional role in the study design, data collection and analysis, decision to publish, or preparation of the manuscript. The specific roles of these authors are articulated in the 'author contributions' section.

Competing Interests: This study was financially supported by Novartis Pharma AG. Ranibizumab is marketed by Novartis and Ulrich Schraermeyer is a consultant on ocular toxicity to Novartis Pharma AG. SZT Ocutox is a Steinbeis transfer centre. Ulrich Schraermeyer and Sylvie Julien work as freelancers for STZ OcuTox, and Ulrich Schraermeyer is the managing director. The Steinbeis Foundation is an institute headquartered in Stuttgart, Germany dedicated to the transfer of academic findings and knowledge into the field of business. The transfer centres operate as stand-alone profit centres. There are no further patents, products in development or marketed products to declare. This does not alter the authors' adherence to all the PLOS ONE policies on sharing data and materials, as detailed online in the guide for authors.

RESEARCH ARTICLE

Effects of a Single Intravitreal Injection of Aflibercept and Ranibizumab on Glomeruli of Monkeys

Alexander Tschulakow¹, Sarah Christner¹, Sylvie Julien^{1,2}, Maximilian Ludinsky¹, Markus van der Giet³, Ulrich Schraermeyer^{1,2*}

1. Section of Experimental Vitreoretinal Surgery, Centre for Ophthalmology, Tuebingen, Germany, **2.** STZ OcuTox Preclinical Drug Assessment, Hechingen, Germany, **3.** Division of Nephrology, Charité University Medicine, Charité Campus Benjamin Franklin, Berlin, Germany

*Ulrich.Schraermeyer@med.uni-tuebingen.de

These authors contributed equally to this work.

Abstract

Purpose: It is known that endothelial cells in the kidney are also strongly VEGF-dependent. Whether intravitreal drugs can be detected within the glomeruli or affect VEGF in glomerular podocytes is not known. Therefore, the aim of this pilot study was to investigate the effects of a single intravitreal injection of aflibercept and ranibizumab on glomeruli of monkeys.

Methods: The kidneys of eight cynomolgus monkeys, which were intravitreally injected either with 2 mg of aflibercept or with 0.5 mg of ranibizumab, were investigated one and seven days after injection. Two animals served as controls. The distribution of aflibercept, ranibizumab and VEGF was evaluated using anti-Fc- or anti-F(ab)-fragment and anti-VEGF antibodies respectively. The ratio of stained area/nuclei was calculated using a semi-quantitative computer assisted method. Glomerular endothelial cell fenestration was quantified in electron microscopy using a systematic uniform random sampling protocol and estimating the ratio of fenestrae per μm .

Results: Compared to the controls, the anti-VEGF stained area/nuclei ratio of the ranibizumab-treated animals showed no significant changes whereas the stained areas of the aflibercept-treated monkeys showed a significant decrease post-treatment. Immune reactivity (IR) against aflibercept or ranibizumab was detected in aflibercept- or ranibizumab treated animals respectively. The number of fenestrations of the glomerular endothelial cells has shown no significant differences except one day after aflibercept injection in which the number was increased.

Conclusion: Surprisingly, both drugs could be detected within the capillaries of the glomeruli. After a single intravitreal injection of aflibercept, VEGF IR in the podocytes was significantly reduced compared to controls. Ranibizumab injection had no significant effect on the glomeruli's VEGF level. Whether this is caused by aflibercept's higher affinity to VEGF or because it is used in a higher stoichiometric concentration compared to ranibizumab remains to be investigated.

Introduction

Vascular endothelial growth factor (VEGF) is a 43- to 46-kd glycoprotein and a major regulator of physiological and pathological angiogenesis [1]. It increases vascular permeability and plays a vital role in endothelial cell migration, proliferation and survival. In the kidney, VEGF is highly expressed in presumptive as well as in mature podocytes and plays a critical role in glomerular development and function i.e. to establish the glomerular filtration barrier [2].

Anti-VEGF-agents were first used in cancer treatment with some severe side effects in consequence of systemic administration. Concerning the kidneys, proteinuria and hypertension have been reported [3–5]. In addition, thrombotic microangiopathy, nephrotic syndrome, bowel perforation, haemorrhages, stroke, myocardial infarction, decreased pulmonary surfactant and delayed wound healing may occur [6–9].

Also in ophthalmology, excessive angiogenesis is a pathogenic factor in many diseases. These include diabetic proliferative retinopathy and age-related macular degeneration (AMD) in adults and retinopathy of prematurity in infants. In the pathogenesis of wet AMD, VEGF plays an outstanding role as it appears to be sufficient and essential in both physiological and pathological angiogenesis [10, 11]. Bevacizumab (Avastin, Genentech/Roche), used in an off-label manner in ophthalmology, is a full length antibody, as such carries the Fc-fragment and is therefore kept in circulation by the binding to the neonatal Fc receptor (FcR) [12]. The importance of the FcR for pharmacokinetics of agents containing the Fc domain was also shown in animal models [13]. Besides good clinical results in ophthalmologic treatment, adverse effects like arterial thromboembolic events, hypertension and renal thrombotic microangiopathy were observed [14–17]. Our group has extensively described the effects of intravitreally injected bevacizumab on monkey eyes [18–21]. Local ocular effects like reductions in choriocapillaris fenestrations, alteration of choroidal blood flow [19], formation of immune complexes and thrombotic microangiopathy [20, 21] have been reported.

Ranibizumab (Lucentis, Genentech/Novartis) was approved in 2006 by the food and drug administration (FDA) for the treatment of wet AMD after the first off-label uses of bevacizumab. As a cleavage product of bevacizumab, it only consists of a Fab fragment and similarly to bevacizumab it blocks the receptor binding domain of all isoforms of VEGF-A. In contrast to the latter, its modified

molecular structure aims to avoid immunological reactions. Aflibercept (VEGF Trap-Eye/Eylea, Regeneron/Bayer) is the latest FDA approved agent for ophthalmic use. It possesses binding sequences for VEGFR-1 and VEGFR-2 that were fused to the Fc segment of human IgG1 antibody with a binding affinity that was 140 times greater than that of ranibizumab and binds to all VEGF-A isoforms, VEGF-B and PlGF [22].

After intravitreal injection of anti-angiogenic agents, Csaky et al., detected these substances in the systemic circulation [16] and there is evidence that anti-VEGF drugs reach the systemic circulation sufficiently to decrease serum VEGF concentrations [10, 23, 24]. Heiduschka et al. have shown in monkeys that some 2% to 5% of bevacizumab is already in the blood stream one and four days after intravitreal injection [18]. Bevacizumab with its long serum half-life of 20 days can lower blood VEGF levels even when intravitreally administered in an amount comparable to that achieved with intravenous therapy [10, 25, 26]. This finding raises the possibility that intravitreally administered bevacizumab may suppress baseline physiologic VEGF activity. Ranibizumab, in contrast, has a much shorter serum half-life of 6 hours and its serum levels remain low. Although renal complications have been reported in only rare cases after intravitreal injections of ranibizumab or bevacizumab [14, 17, 27–29], the possibility of systemic complications after intravitreal injections of anti-VEGF agents has to be considered. Regarding aflibercept, little data concerning systemic effects after intravitreal injection is available although a clearance from the eye into the systemic circulation has been shown [30]. Therefore, it is vital to investigate the effects of anti-VEGF agents in nonhuman primates to establish biologic activity and adverse effects relevant to humans. This *in vivo* study was performed in monkeys as antibody molecules and their interaction with Fc receptors in monkeys mimic those present in humans [31]. To this aim, we investigated the effects of a single intravitreal injection of ranibizumab and aflibercept on the kidneys of eight monkeys on days one and seven after injection. The distribution of aflibercept and ranibizumab in renal glomeruli was analysed, VEGF levels in glomeruli and the glomerular endothelial cell fenestrations were quantified.

Note that due to the high costs of experiments, this pilot study only consists of a small number of animals and the study design does not allow the evaluation of a great variety of time points.

Materials and Methods

1. Animals and study protocol

Ten cynomolgus monkeys (*Macaca fascicularis*, aged 3 to 8 years) were raised at the Covance Laboratories (Muenster, Germany) under standard conditions. All animals were housed and handled in strict accordance with good animal practice under supervision of veterinarians in accordance with the German Animal Welfare Act and were monitored for evidence of disease and changes in attitude, appetite or behaviour suggestive of illness. Full details are shown in [Table 1](#).

Table 1. Details of the animals used in this study.

| Covance Study 8260977 | Covance Study 8274007 |
|---|---|
| Species: Cynomolgus monkeys (<i>Macaca fascicularis</i>) | Species: Cynomolgus monkey (<i>Macaca fascicularis</i>) |
| Origin: Mauritius | Origin: Mauritius |
| Age at predose start: 3 to 8 years | Age at predose start: 3 to 8 years |
| Predose body weight: 4 to 12 kg | Predose body weight: 4 to 12 kg |
| Number and sex: 5 healthy male animals | Number and sex: 5 healthy male animals |
| Animal housing: Pair and single, due to the single control animal | Animal housing: Pair and single, due to the single control animal |

doi:10.1371/journal.pone.0113701.t001

The naive Cynomolgus fascicularis monkeys are from a closed breeding colony (Noveprim Mauritius). Tests for TB, B-Virus, SIV, SRV, STLV, are carried out during export and import quarantine. Additionally tests for TB, B-Virus, SIV, SRV, STLV are carried out regularly for all animals on site regardless if they are in studies or not.

Cynomolgus monkeys are housed in social groups before and during studies. The space requirements are according to the EU directive (DIRECTIVE 2010/63/EU OF THE EUROPEAN PARLIAMENT AND OF THE COUNCIL of 22 September 2010 on the protection of animals used for scientific purposes).

The animals live under a 12 hour dark light cycle, have ad libitum access to water and food provided twice daily, lab diet plus fresh fruit. The foremost enrichment is social housing. Additionally mirrors, wooden trunks, balls are supplied as a standard. Further enrichment devices are available and made available on a rotating scheme.

The animal welfare officer on site regularly checks the housing and handling conditions.

Since animals are housed in groups during the study the individuals are not randomised to the dose group, but rather a stable group of animals created a long time before the study.

Both eyes of four animals were intravitreally injected with ranibizumab and another four animals with aflibercept. The doses of anti-VEGF agents were the same as clinically used in humans and as provided and recommended by the manufacturers: 2 mg of aflibercept and 0,5 mg of ranibizumab, respectively.

All injections were carried out in the morning, following slight sedation with ketamin and diazepam. One and seven days after intravitreal injection, the animals were sacrificed under general anaesthesia and the kidneys were removed (except the left kidney of a monkey that was sacrificed on day seven after injection of aflibercept showing aplasia). The left kidney of each animal was prepared for immunohistochemistry, specimens of the right kidneys served for electron microscopy as described below. One untreated monkey sacrificed on day seven and one monkey injected with aflibercept's vehicle and sacrificed one day after injection served as controls. Blood samples were taken before injection (predose) and on days one and seven after injection. Platelet-poor plasma was prepared by centrifugation. For injection specifications, ophthalmic examinations as well as

fixation methods and histological procedures, please see our previous publications [21, 32].

Ethical Statement

Handling and housing of the animals were only done at Covance Laboratories GmbH. All animals were housed and handled in strict accordance with good animal practice under supervision of veterinarians in accordance with the German Animal Welfare Act and were monitored for evidence of disease and changes in attitude, appetite or behaviour suggestive of illness. The animals were sacrificed, and their kidneys were fixed at Covance Laboratories GmbH. The animals were sacrificed under general anaesthesia, i.e., intramuscular injection of ketamine hydrochloride followed by an intravenous sodium pentobarbitone (Lethabarb, Virbac, Australia) overdose. Only the further investigations: electron microscopy and immunohistochemistry were performed in our lab in Tuebingen. These investigations did not necessitate approval by an institutional review board. Covance Laboratories GmbH test facility is fully accredited by the AAALAC. This study was approved by the local IACUC, headed by Dr. Jörg Luft, and performed in consideration of the following recommendation:

Commission Recommendation 2007/526/EC on guidelines for the accommodation and care of animals used for experimental and other scientific purposes (Appendix A of Convention ETS 123).

2. Kidneys samples and fixation

On days one and seven after intravitreal injection, the animals were sacrificed under general anaesthesia, i.e., intramuscular injection of ketamine hydrochloride followed by an intravenous sodium pentobarbitone (Lethabarb, Virbac, Australia) overdose. The kidneys were extracted five minutes post-mortem. The left kidney of each animal was fixed in paraformaldehyde uncut for immunohistochemistry, a specimen of the right kidneys was dissected into small cube-like pieces with a length of 2–3 mm and then fixed in glutaraldehyde (ice cooled) for electron microscopy (the only available kidney of the monkey described above was prepared for electron microscopy). The kidneys of the monkey without treatment, or with aflibercept's vehicle injection, were handled in the same manner.

3. Immunohistochemistry

Sections (4 μ m) were cut from formalin-fixed, paraffin embedded tissue and mounted on superfrost Plus microscope slides (R. Langenbrinck Labor- u. Medizintechnik).

The slides were deparaffinised and rehydrated, and heat induced epitope retrieval in TRIS EDTA (pH 9) using a pressure cooker was performed. After two washing steps in TBS (0.5% TWEEN) immunohistochemical staining of VEGF was performed according to the instructions provided by the manufacturer in a humid chamber. The slides were incubated for 60 min with the primary mouse

anti-VEGF antibody (1:50, DAKO, Denmark) at 37°C and then processed using the DAKO REAL Detection System Alkaline Phosphatase/RED kit rabbit/mouse, then counterstained with hematoxylin and covered. The same procedure was performed for immune reactivity analysis against ranibizumab and aflibercept using respectively a primary mouse antibody against the human IgG-Fab-fragment (Dianova, 1:100) and a primary mouse antibody against the human IgG-Fc-fragment (Dianova, 1/150). These samples were used for the quantification and normalisation of VEGF or ranibizumab/aflibercept stainings.

Additionally an immune reactivity analysis using fluorescent antibodies was performed. A mouse antibody against the human IgG-Fab-fragment of IgG (dilution 1:400, Jackson ImmunoResearch) and a goat anti-mouse alexa488 labelled secondary antibody (dilution 1:400, Invitrogen) were used for ranibizumab staining. Goat anti-human IgG-Fc antibody (dilution 1:200, Novus Biologicals) and a donkey anti-goat alexa488 labelled secondary antibody (dilution 1:500, molecular probes) were used for aflibercept staining.

4. Quantification and normalisation of VEGF and ranibizumab/aflibercept stainings

From each tissue sample, photos from 10 randomly chosen glomeruli-containing regions were taken using a Zeiss Axioscop microscope with AxioVision image capture software at a magnification of 400x. On these photos the glomeruli were defined as the area of interest (aoi). These aoi were isolated using the image j software. In the next step the nuclei in the aoi were counted using a semi-quantitative computer assisted method (image j). Then the stained area of each aoi was determined (Fig. 1). Briefly, the image j program offers a colour deconvolution plug which splits images into three color-channels and is widely used for immunohistochemistry analysis [33]. The number of nuclei could be calculated after the hematoxylin stained areas were isolated using the “H&E” filter of the color deconvolution plug in. After that “watershed” and “particle counter” algorithms were run for the nuclei count as described by others [34, 35]. This method was compared with manual counting and was found to be as accurate as the manual method. For the determination of the stained area we used the colour deconvolution plug in with the RGB (red, green, blue) filter. The red image was used for the calculation of the stained area.

For the determination of the background for the stained area determination the red dye intensity from a control which was treated only with the secondary antibody and the red dye was set as threshold for the filter settings for the image j analysis. The ratio of stained area/nuclei was calculated and the statistical analysis was performed as further described.

5. VEGF-A plasma levels

Blood samples of all monkeys were collected in tubes containing EDTA before intravitreal injection (predose) and on day one and seven after injection of anti-

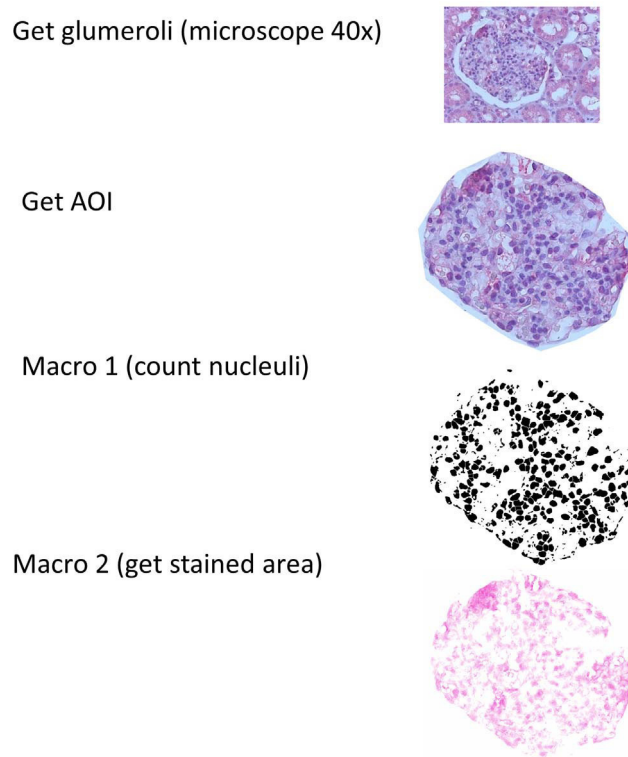


Figure 1. Semi-quantitative computer assisted method used for the quantification and normalisation of the VEGF staining. Glomeruli were defined as the area of interest (AOI), and then the AOI were isolated using the image j software. The nuclei in the AOI were then counted and finally the stained area of each AOI was determined.

doi:10.1371/journal.pone.0113701.g001

VEGF agents, and plasma was prepared by centrifugation, transferred to new tubes and stored at -70°C . Plasma samples were analyzed using commercially available ELISA kits for human VEGF-A (DVE00) (R&D Systems, Minneapolis, Minnesota). Briefly, the microtitration plates were coated with monoclonal antibodies specific for VEGF-A, standards and probes were added, incubated and washed. Then, an enzyme-linked polyclonal antibody specific for VEGF-A was added and its substrate solution followed after a second incubation and wash step. After stopping the colour development, the intensity of colour (Optical Density) was measured by photospectrometry with the lower detection limit of VEGF-A set at 30 pg/ml. Calculation of VEGF concentration was performed according to the manufacturer's recommendations.

6. Light and electron microscopy

Specimens were postfixed with 1% OsO₄ at room temperature in 0.1 M cacodylate buffer (pH 7.4), en bloc stained with uranyl acetate and lead citrate, and embedded in Epon after dehydration in a graded series of acetones. Semithin sections were stained with Toluidine Blue and examined by light microscopy

(Zeiss Axioplan2 imaging, Zeiss, Jena, Germany). For electron microscopy, the sections were cut ultrathin and analyzed with a Zeiss 902 A electron microscope (Zeiss, Jena, Germany).

7. Quantification of the glomerular endothelial fenestrations

Under the light microscope at a low magnification (x10) glomeruli were identified in semi-thin sections and checked on mechanical or fixation artifacts and pathological features at a higher magnification. Three glomeruli per kidney (six per time point for ranibizumab and aflibercept, three for controls) with middle to large diameter and intact bowman's capsules were chosen and cut ultrathin for electron microscopy. After examination of the probes at a magnification of 3000 fold, montages of transmission electron micrographs were performed by using the multiple image arrangements = MIAs in order to provide montages of the entire glomeruli (Fig. 2). The montages consist of overlapping images that were taken using an image analysis software (iTEM, Olympus Soft Imaging Solutions, Muenster, Germany). Similarly to a previously described method [36], high-magnification images were taken from the chosen glomeruli according to a systematic uniform random sampling protocol (SURS). Starting at the top-most portion of the glomerular tuft, $\times 20000$ images were taken moving the position of the thin section grid with the help of the X and Y grid position control keys. For this purpose, the grid was moved ten units horizontally taking a picture at each stop point until the opposite portion of the capsule was reached. Then the position of the grid was moved 10 units vertically and 5 units to the right or left, respectively. This procedure was continued until the entire glomerular profile was scanned through (Fig. S1). After pictures were scanned through for artefacts by a blinded observer, high-magnification images were used for quantification of glomerular fenestration using a counting tool of the iTEM software. Only pictures on which glomerular endothelium was undoubtedly identifiable were analyzed. A line was drawn and measured along the lamina rara interna of the endothelial basement membrane adjacent to the fenestrated endothelium and fenestrations were counted by a single observer under standardised conditions. As capillary walls can be divided into peripheral and mesangial regions [36], only peripheral portions where glomerular basement membranes and capillary walls show parallelism were considered. We found that the quantification in the mesangial portions is not comparable to the peripheral parts as the predominant amount of mesangial endothelium is not fenestrated whereas on the other hand there are parts with increased fenestration (as described as "alveolus fenestratus endothelialis" by Kondo et al., [37]). Thus, this endothelium is morphologically not comparable to the single layered endothelium in the peripheral portions so that applying the same quantification method would not be admissible (Fig. 3A–B). Therefore, the mesangial portions were excluded from the quantification of the fenestrations.

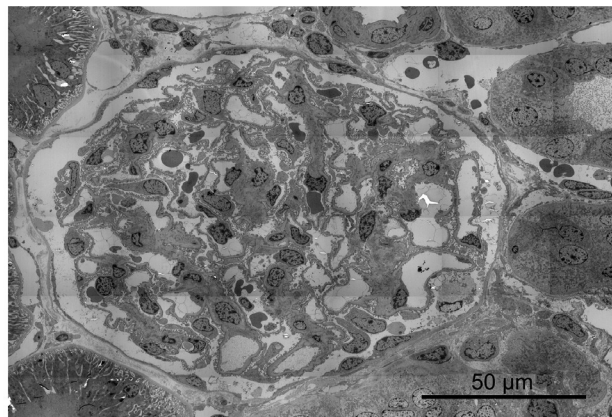


Figure 2. Example of a montage of transmission electron micrographs by using multiple image arrangements (MIAs) in order to provide the entire renal glomerulus. These images were taken using the image analysis software iTEM at the magnification of $\times 3000$. Here one day after aflibercept injection.

doi:10.1371/journal.pone.0113701.g002

8. Statistical analysis

The ratio of fenestrae per μm was calculated using Microsoft-Office-Excel for each image considered. Statistical significances for the evaluation of the fenestrae per μm of the glomerular capillaries and for the quantification of VEGF as well as ranibizumab/aflibercept were determined by using the Student's t test from the JMP10 statistical program (SAS, Heidelberg, Germany). $P < 0.05$ was considered statistically significant.

Results

1. Immunohistochemistry

1.1. Ranibizumab/aflibercept fluorescence staining.

Kidney sections from the control animal did not show any specific staining in the glomeruli after staining either with an antibody against the anti-human IgG-Fc fragment (Fig. 4A) or against the anti-human Fab fragment of IgG (not shown). Only the erythrocytes within the capillaries showed a weak autofluorescence (Fig. 4A). After omitting the first antibodies, the same staining pattern as in Fig. 4A was observed (not shown). One day after aflibercept injection, the endothelium cell layer and material within the capillaries of many glomeruli were highly fluorescent (Fig. 4B–C). Occasionally, glomeruli in which only the endothelium was stained were localised close to others that contained high amounts of IgG-Fc reactive material within the capillaries (Fig. 4B). Erythrocytes within the glomeruli were highly fluorescent (Fig. 4C). Seven days after aflibercept injection, the fluorescent material within the capillaries was fewer and the fluorescence intensity became weaker (Fig. 4D). One day after ranibizumab injection, the endothelium cell layer and erythrocytes of most glomeruli became

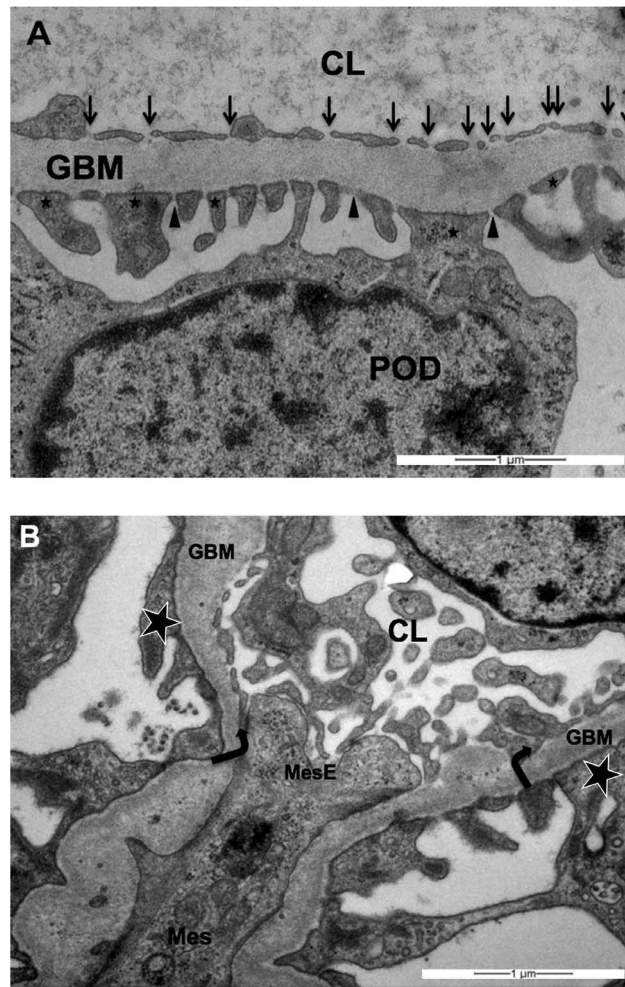


Figure 3. Examples of representative transmission electron micrographs of (A) a fenestrated glomerular endothelium and of (B) peripheral versus mesangial portions of the glomerular endothelium (both one day after aflibercept injection). (A) Blood lumen on the upper part, urinary space on the lower part of the image. The healthy glomerular filtration barrier consists of three layers [6]: the fenestrated glomerular endothelial cells, the intervening glomerular basement membrane and the podocyte processes and slit diaphragm. GBM= glomerular basement membrane, CL= capillary lumen, POD= podocyte. Arrows mark glomerular endothelial cells fenestrae (note the absence of diaphragm), asterisks mark podocyte foot processes, arrowheads mark podocyte slit diaphragm. (B) At this magnification, podocyte foot processes (asterisks) allow the clear identification of the capillary lumen (CL). In accordance with our definition, the peripheral portion begins where the endothelium and the glomerular endothelial basement membrane (GBM) run approximately parallel (marked by arrows). Arrows mark direction into which peripheral endothelium begins. In between the arrows the mesangium (Mes) and the mesangial portion of the capillary endothelium (MesE) is located. Note that in the mesangial portion there is no GBM adjacent to the fenestrated endothelium so that the described counting method is not applicable and the endothelium does not show the typical single-layered configuration. Magnification $\times 20000$.

doi:10.1371/journal.pone.0113701.g003

fluorescent after labelling with an antibody against the human Fab fragment of IgG (Fig. 4E). However, the specific fluorescence was nearly lost seven days after injection of ranibizumab (Fig. 4F).

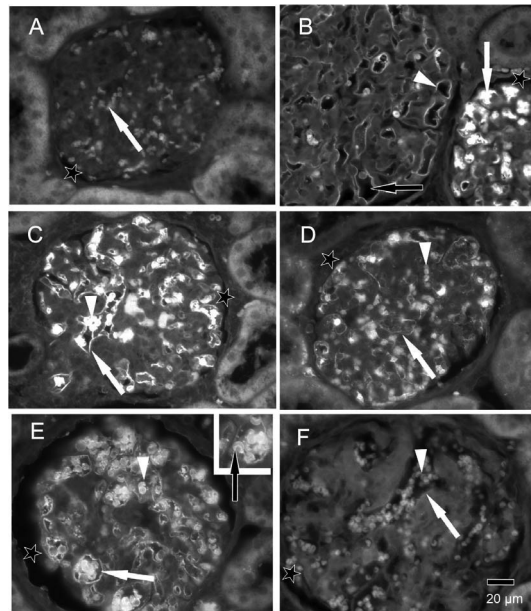


Figure 4. Immune fluorescent photomicrographs of glomeruli from control (A), aflibercept-treated (B–D) and ranibizumab-treated (E–F) monkeys eyes. In all figures, the asterisks label the spaces of the Bowman capsule. **A)** Kidney sections from the control animal did not show any specific staining with anti-human IgG-Fc antibody in the glomeruli. Only the erythrocytes (arrow) within the capillaries showed a weak fluorescence. **B)** One day after aflibercept injection, the endothelium cell layer and material within the capillaries of a glomerulus were highly fluorescent (white arrow) after labelling with an antibody against the Fc region of IgG. In an adjacent glomerulus, only the endothelium was stained (white arrowhead) whereas the lumina of the vessels did not contain IgG-Fc positive material (black arrow). **C)** Erythrocytes within the glomeruli (arrowhead) as well as the endothelium (arrow) were highly fluorescent. **D)** Seven days after aflibercept injection, the fluorescent material within the capillaries (arrowhead) and the fluorescence intensity of the endothelium became weaker. **E)** One day after ranibizumab injection, the endothelium cell layer (white arrow) and erythrocytes (arrowhead and black arrow in the inset) were fluorescent after staining with an antibody against human Fab of IgG. **F)** The specific fluorescence of the endothelium (arrow) and erythrocytes (arrowhead) was nearly lost seven days after injection of ranibizumab.

doi:10.1371/journal.pone.0113701.g004

1.2 Quantification and normalisation of ranibizumab/aflibercept stainings.

Immune reactivity against aflibercept or ranibizumab was only detected in aflibercept- or ranibizumab-treated animals respectively and did not show any significant differences between days one and seven (Fig. 5A–B).

1.3 Quantification and normalisation of VEGF staining.

The anti-VEGF stained area to cells ratio in the aoi of the samples (representing the mean VEGF level/cell ratio) from the tissue of the ranibizumab-treated animals showed no significant changes at any of the analysed time points (486 ± 55 (day 1) and 451 ± 66 (day 7)) compared to the untreated control-animal samples (456 ± 99). However, the stained area to cells ratio of the tissue-samples of the aflibercept-treated animals showed a significant decrease one day (383 ± 85) after treatment ($p < 0.05$) and an even stronger decrease seven days (233 ± 41) after treatment ($p < 0.0001$) compared to the untreated control-animal samples (456 ± 99). The levels of VEGF were found to be significantly lower in the

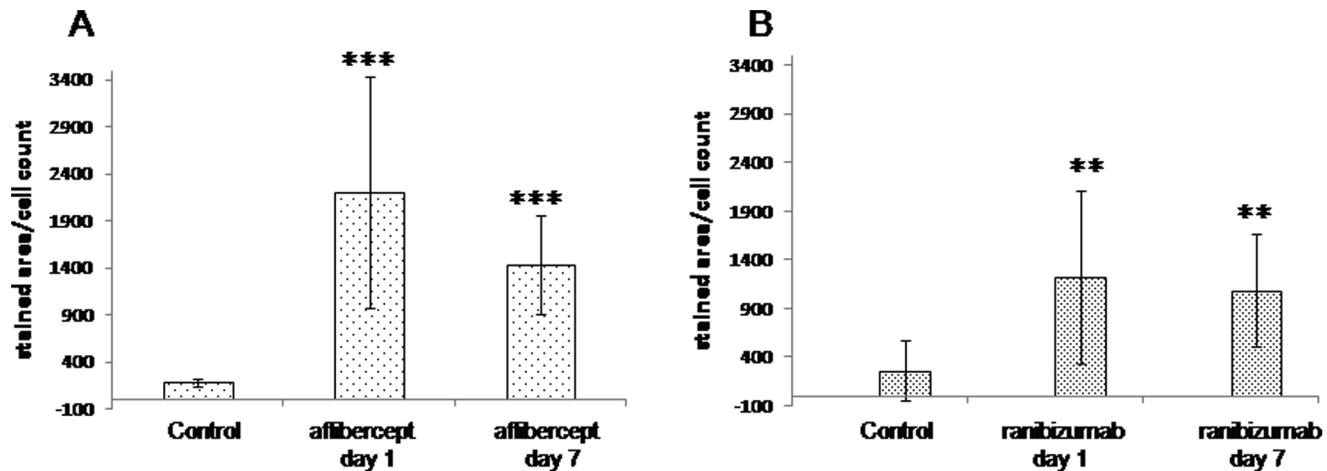


Figure 5. Quantification and normalisation of aflibercept/ranibizumab staining. Results of the analysis of aoi of glomeruli from kidneys of monkeys one and seven days after aflibercept (A) or ranibizumab (B) treatment and the corresponding controls, respectively after staining with the anti-Fc-fragment antibody for aflibercept and the anti-Fab fragment antibody for ranibizumab immune reactivity analysis; t-test against the corresponding control was performed: ** for $p < 0.001$, *** for $p < 0.0001$.

doi:10.1371/journal.pone.0113701.g005

aflibercept-treated animals on days one (383 ± 85 vs. 486 ± 55 ; $p < 0.05$) and seven (233 ± 41 vs. 451 ± 66 ; $p < 0.0001$) after treatment as compared to the corresponding ranibizumab-treated ones. The decrease of the VEGF level from day one to day seven after treatment was also found to be significant (383 ± 85 vs. 233 ± 41 ; $p < 0.0001$) (Fig. 6).

2. Measurement of VEGF-A¹⁶⁵ plasma levels

All doses were below the detectable limit of the assay meaning under 30 pg/ml (not shown).

3. General examinations by light and transmission electron microscopy

The biopsies of all the kidneys were first studied by light microscopy and also by TEM with increasing magnification in order to scan the specimens on artefacts and pathologic features. None of the glomeruli was sclerotic. The podocyte foot processes were well-formed and did not show effacement, and a continuous slit diaphragm could be observed. The glomerular basement membrane (GBM) was of normal thickness and did not show duplication in all specimens without widening of the subendothelial space or cellular interposition. The well-defined glomerular endothelium was flattened though there were slight variations in thickness without endotheliosis. In all samples, it was mostly adjacent to the GBM.

The capillary loops were filled with more or less electron-dense serum. The density difference could be observed in glomeruli of all of the kidneys (Fig. 7).

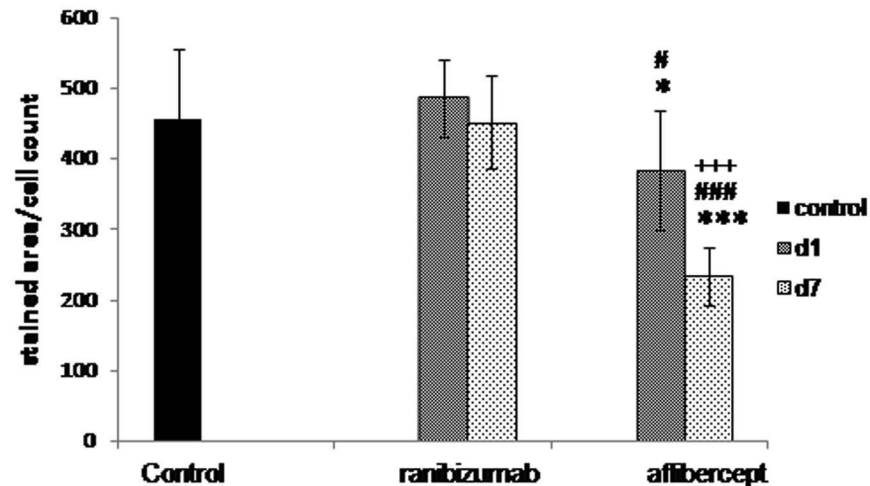


Figure 6. Quantification and normalisation of the VEGF staining. Results of the analysis of aoi of glomeruli from kidneys of monkeys one and seven days after ranibizumab and aflibercept treatment and the corresponding controls after anti-VEGF staining; t-test against control: * for $p < 0.05$, *** for $p < 0.0001$; t-test ranibizumab day 1 versus aflibercept day 1 and ranibizumab day 7 versus aflibercept day 7: # for $p < 0.05$, ### for $p < 0.0001$; t-test aflibercept day 1 versus aflibercept day 7: +++ for $p < 0.0001$.

doi:10.1371/journal.pone.0113701.g006

4. Quantification of the glomerular endothelial cells fenestrations

In total, 30 glomeruli e.g. three glomeruli per monkey fulfilling the criteria described above were investigated. The total amount of pictures taken was 4855 of which 1327 (27.3%) were evaluated. After the ratio of fenestrae per μm was calculated for each image, the values obtained for the two monkeys of aflibercept and ranibizumab for each time point were pooled. Student's test was performed with values of the untreated monkey as control values and it showed a statistically significant increase ($p < 0.05$) in the number of fenestrae per μm one day after aflibercept injection (median: 2.05) compared to all other groups (medians: 1.27 for aflibercept day 7, 1.46 for ranibizumab day 1, 1.29 for ranibizumab day 7 and 1.25 for the untreated group) (Fig. 8). The other conditions did not show any statistical significance compared to the controls (Fig. 8).

Discussion

In the normal kidney, VEGF is expressed on podocytes. Dysregulation of VEGF expression within the glomeruli has been associated with a wide range of renal diseases that may occur within weeks to months after intravitreal administration of VEGF inhibitors [14, 27]. The dose of anti-VEGF agents used in ophthalmology is minute compared with that used intravenously, but there is evidence of systemic absorption and diffuse inhibition of VEGF [14, 17, 38, 39]. Pelle *et al.*, reported a non diabetic patient with normal kidney function who developed kidney toxicity after four injections of ranibizumab for the treatment of age-related macular degeneration [14]. Several studies evaluating the safety and efficacy of intravitreal

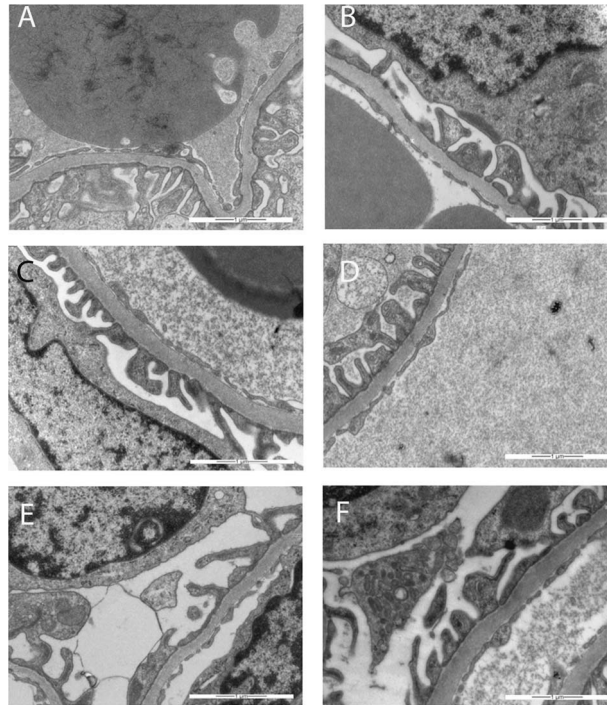


Figure 7. Examples of transmission electron micrographs used for the quantification of the glomerular endothelial cells fenestrations. The red line drawn a long lamina rara interna, the length of line is in μm , the red crosses point out fenestrations. (A) after injection of the vehicle; (B) in the untreated control; (C) one day after injection of ranibizumab; (D) seven days after injection of ranibizumab; (E) one day after injection of aflibercept; (F) seven days after injection of aflibercept. Magnification $\times 20000$.

doi:10.1371/journal.pone.0113701.g007

anti-VEGF in diabetic patients have reported renal adverse effects [17, 39, 40]. Georgalas et al., postulated that plasma levels of anti-VEGF could possibly cause deregulation of VEGF expression in the kidney and cause renal damage. Of course the fact that the patients were diabetic should be taken into consideration since such patients are prone to develop renal failure [17]. Previous studies [41] have shown that intravitreally injected ranibizumab is cleared from the eye into the circulation with a half-life of approximately three days in monkeys [42] and that ranibizumab can be found in the serum but the concentrations detected were considered below the necessary threshold for a sufficient VEGF inhibition [43]. Since ranibizumab is not protected from serum elimination by an Fc-fragment, it has been suggested that it is rapidly cleared from the circulation *via* renal elimination. Our data is in accordance with these studies since indeed ranibizumab was indeed localised in the glomeruli one and seven days after intravitreal injection and it did not affect the VEGF level in the glomeruli nor the number of glomerular endothelial fenestrations. We were unable to measure plasma VEGF levels since the concentrations were always below the detectable limit (30 pg/ml) of the assay. Larsson et al., have determined in 80 plasma samples of healthy humans that the mean value \pm SD of VEGF was 32 ± 21 pg/ml [44]. Moreover, the use of serum instead of plasma would be preferable since serum

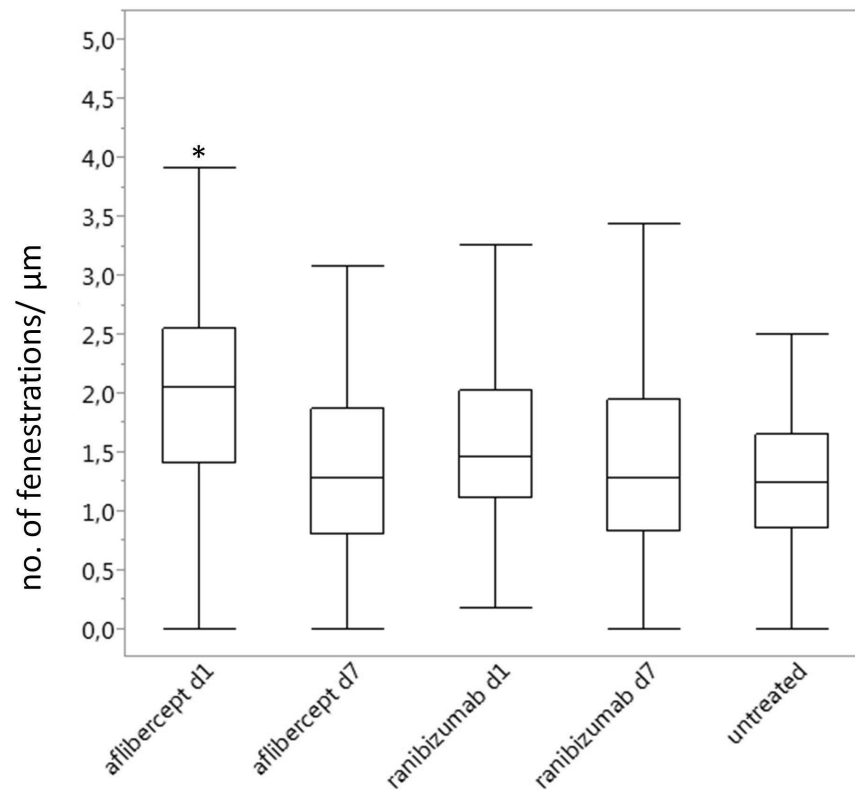


Figure 8. Box plot representation of the quantification of the fenestrations per μm depending on the treatment and its duration. Application of the Student's test showed no significant differences in the number of fenestrations per μm except one day after aflibercept's injection where the number was increased compared to all other groups (*, $p < 0.05$).

doi:10.1371/journal.pone.0113701.g008

VEGF levels are several fold higher than plasma levels, because platelets express VEGF and secrete it during blood clotting [45].

Unfortunately we have no data concerning the urinary sediments. It would be of great interest to analyse them, especially as there are indications that anti VEGF therapies have influence on the kidneys, and can cause proteinuria and hypertension [3–5]. The analysis of the urinary sediments will also be an aim of our further studies.

It has been published that aflibercept, in contrast to bevacizumab, binds VEGF-A in a 1:1 stoichiometry which remains stable in the circulation [46]. The authors speculated that because of this stoichiometry and the inert nature of the complexes, aflibercept is not expected to accumulate in renal glomeruli as has been found for bevacizumab [46]. The present study shows for the first time that in reality aflibercept is found in the glomeruli after intravitreal injection and moreover that it significantly decreases their VEGF level. Whether pathological alterations were caused by ranibizumab or aflibercept in a different manner or not is out of the focus of this pilot study. Surprisingly one day after injection, aflibercept was able to increase the number of glomerular endothelial cells

fenestrations compared to the controls or ranibizumab-treated monkeys. Since the glomerular VEGF level was reduced, we rather expected a reduction or a stabilisation of the number of fenestrations, as apparent in the choriocapillaris after intravitreal injection of an anti-VEGF agent [19]. This result suggests a complex regulation of glomerular endothelial cell fenestrations which is not completely elucidated. Indeed in contrast to the choriocapillaris, it has been shown that the fenestration of glomerular capillaries requires the action of TGF- β 1 [47]. Moreover, in systemic endothelial fenestrations, the intracellular pathways through which VEGF acts to induce fenestrations include a key role for the fenestral diaphragm protein plasmalemmal vesicle-associated protein-1 (PV-1). However, the role of PV-1 in glomerular endothelial cell fenestrations is less clear, not least because of controversy over the existence of glomerular endothelial cell fenestral diaphragms [48]. Satchell and Braet thought that the glomerular endothelial cell fenestrations generally do not express PV-1 and, it is generally asserted, do not possess diaphragms. However, they should note that a number of observations challenge this position. To some extent, appearance of this feature may be dependent on the fixation and labelling techniques used, since a diaphragm is seen in some preparations but not in others. It could be either that some techniques destroy a very delicate diaphragm or that other techniques result in an artefactual appearance of a diaphragm, perhaps through condensation/cross-linking and labelling of glycocalyx, other plasma proteins, or the outer surface of the glomerular basement membrane. Another careful study demonstrated that glomerular endothelial cells in the rat adult kidney, apart from a small fraction, do not furnish diaphragms with their fenestrae; most glomerular endothelial cells in the immature glomeruli of rat embryos have diaphragmed fenestrations and the number of glomerular endothelial cells with diaphragmed fenestrations is increased in the glomeruli of Thy-1.1 nephritis rats, presumably reflecting a process of restorative remodelling of the glomerular capillary tuft after injury [49]. Along with the appreciation that the intraglomerular portion of efferent arterioles and direct tributaries may express fenestrated diaphragm [50], this goes a long way toward clarifying the position. In our study, the fenestrations of the glomerular endothelial cells of adult monkeys were clearly not closed by diaphragms (Fig. 3A) which contrast to those observed in the choriocapillaris and reported in one of our previous monkey studies (Fig. 6 in [19]). Since the same technique was used in these two studies, technical artefacts can be excluded. The glomerular changes observed in our study are not very extensive, but one has to keep in mind, that in the present model anti-VEGF treatment was given only once and the animals used have no overt renal pathology. Usually patients with e.g. diabetic retinopathy get the anti-VEGF treatment on regular basis and as proliferative diabetic retinopathy is a microvascular disease, we have to assume in these patients also microvascular disturbances in the kidney including microalbuminuria. Under this condition VEGFA secreted from podocytes is essential to maintain proper cellular functions [51].

What might happen if VEGFA is affected in a stimulated system is speculative and should be investigated. This might be a consequence of different antibody

design. The immune complexes might be inductor of thrombotic microangiopathy in the kidney [52]. Caution is needed when patients which might also have already renal disease get these substances locally, which have definitive systemic effects.

Conclusions

In conclusion, we showed that intravitreal ranibizumab and aflibercept can escape from the blood-retinal barrier and are also distributed to distant organ like the kidneys. Our study demonstrated that a single dose of intravitreally injected aflibercept already decreases the VEGF level in the glomeruli one and seven days after treatment whereas ranibizumab did not affect the glomerular VEGF level. In clinical practice, it is therefore important to monitor patients receiving intravitreal injection of VEGF inhibitors for possible systemic side-effects, particularly kidney injury, which may not be immediately apparent. Because of the increasing use of intravitreal anti-VEGF agents in the treatment of age-related macular degeneration, as well as for other indications such as diabetic retinopathy, further studies are highly needed to elucidate the effects of repeated anti-VEGF injections on VEGF concentrations in distant organs.

Supporting Information

Figure S1. Demonstration of the systematic uniform random sampling protocol (SURS) on a multiple image arrangement (MIA). Transmission electron microscopy, magnification $\times 3000$. Probe: Aflibercept day 1, Glomerulus 1. Asterisk marks starting position (first picture), double asterisks mark end position (last picture), arrows mark direction into which SURS was performed. doi:10.1371/journal.pone.0113701.s001 (DOCX)

Acknowledgments

The authors warmly thank Sigrid Schultheiss for her excellent technical assistance.

Author Contributions

Conceived and designed the experiments: SJ US. Performed the experiments: AT SC. Analyzed the data: AT SC SJ ML MG US. Contributed reagents/materials/analysis tools: US. Wrote the paper: AT SC SJ.

ReferencesReferences

1. Ferrara N (2009) Vascular endothelial growth factor. *Arterioscler Thromb Vasc Biol* 29: 789–791.
2. Eremina V, Quaggin SE (2004) The role of VEGF-A in glomerular development and function. *Curr Opin Nephrol Hypertens* 13: 9–15.

3. **Zhu X, Wu S, Dahut WL, Parikh CR** (2007) Risks of proteinuria and hypertension with bevacizumab, an antibody against vascular endothelial growth factor: systematic review and meta-analysis. *Am J Kidney Dis* 49: 186–193.
4. **Roncone D, Satoskar A, Nadasdy T, Monk JP, Rovin BH** (2007) Proteinuria in a patient receiving anti-VEGF therapy for metastatic renal cell carcinoma. *Nat Clin Pract Nephrol* 3: 287–293.
5. **Lafayette RA, McCall B, Li N, Chu L, Werner P, et al.** (2014) Incidence and relevance of proteinuria in bevacizumab-treated patients: pooled analysis from randomized controlled trials. *Am J Nephrol* 40: 75–83.
6. **Eremina V, Jefferson JA, Kowalewska J, Hochster H, Haas M, et al.** (2008) VEGF inhibition and renal thrombotic microangiopathy. *N Engl J Med* 358: 1129–1136.
7. **Izzedine H, Brocheriou I, Deray G, Rixe O** (2007) Thrombotic microangiopathy and anti-VEGF agents. *Nephrol Dial Transplant* 22: 1481–1482.
8. **Frangie C, Lefaucheur C, Medioni J, Jacquot C, Hill GS, et al.** (2007) Renal thrombotic microangiopathy caused by anti-VEGF-antibody treatment for metastatic renal-cell carcinoma. *Lancet Oncol* 8: 177–178.
9. **Bollee G, Patey N, Cazajous G, Robert C, Goujon JM, et al.** (2009) Thrombotic microangiopathy secondary to VEGF pathway inhibition by sunitinib. *Nephrol Dial Transplant* 24: 682–685.
10. **Stewart MW** (2012) The expanding role of vascular endothelial growth factor inhibitors in ophthalmology. *Mayo Clin Proc* 87: 77–88.
11. **Stewart MW** (2012) Clinical and differential utility of VEGF inhibitors in wet age-related macular degeneration: focus on aflibercept. *Clin Ophthalmol* 6: 1175–1186.
12. **Lobo ED, Hansen RJ, Balthasar JP** (2004) Antibody pharmacokinetics and pharmacodynamics. *J Pharm Sci* 93: 2645–2668.
13. **Proetzel G, Roopenian DC** (2014) Humanized FcRn mouse models for evaluating pharmacokinetics of human IgG antibodies. *Methods* 65: 148–153.
14. **Pelle G, Shweke N, Duong Van Huyen JP, Tricot L, Hessaine S, et al.** (2011) Systemic and kidney toxicity of intraocular administration of vascular endothelial growth factor inhibitors. *Am J Kidney Dis* 57: 756–759.
15. **Bressler NM** (2009) Antiangiogenic approaches to age-related macular degeneration today. *Ophthalmology* 116: S15–23.
16. **Csaky K, Do DV** (2009) Safety implications of vascular endothelial growth factor blockade for subjects receiving intravitreal anti-vascular endothelial growth factor therapies. *Am J Ophthalmol* 148: 647–656.
17. **Georgalas I, Papaconstantinou D, Papadopoulos K, Pagoulatos D, Karagiannis D, et al.** (2014) Renal Injury Following Intravitreal Anti-VEGF Administration in Diabetic Patients with Proliferative Diabetic Retinopathy and Chronic Kidney Disease- A Possible Side Effect? *Curr Drug Saf*.
18. **Heiduschka P, Fietz H, Hofmeister S, Schultheiss S, Mack AF, et al.** (2007) Penetration of bevacizumab through the retina after intravitreal injection in the monkey. *Invest Ophthalmol Vis Sci* 48: 2814–2823.
19. **Peters S, Heiduschka P, Julien S, Ziemssen F, Fietz H, et al.** (2007) Ultrastructural findings in the primate eye after intravitreal injection of bevacizumab. *Am J Ophthalmol* 143: 995–1002.
20. **Schraermeyer U, Julien S** (2013) Effects of bevacizumab in retina and choroid after intravitreal injection into monkey eyes. *Expert Opin Biol Ther* 13: 157–167.
21. **Schraermeyer U, Julien S** (2012) Formation of immune complexes and thrombotic microangiopathy after intravitreal injection of bevacizumab in the primate eye. *Graefes Arch Clin Exp Ophthalmol* 250: 1303–1313.
22. **Papadopoulos N, Martin J, Ruan Q, Rafique A, Rosconi MP, et al.** (2012) Binding and neutralization of vascular endothelial growth factor (VEGF) and related ligands by VEGF Trap, ranibizumab and bevacizumab. *Angiogenesis* 15: 171–185.
23. **Investigators IS, Chakravarthy U, Harding SP, Rogers CA, Downes SM, et al.** (2012) Ranibizumab versus bevacizumab to treat neovascular age-related macular degeneration: one-year findings from the IVAN randomized trial. *Ophthalmology* 119: 1399–1411.

24. **Dinc E, Yildirim O, Necat Yilmaz S, Canacankatan N, Ayaz L, et al.** (2013) Intravitreal bevacizumab effects on VEGF levels in distant organs: an experimental study. *Cutan Ocul Toxicol*.
25. **Qian J, Lu Q, Tao Y, Jiang YR** (2011) Vitreous and plasma concentrations of apelin and vascular endothelial growth factor after intravitreal bevacizumab in eyes with proliferative diabetic retinopathy. *Retina* 31: 161–168.
26. **Matsuyama K, Ogata N, Matsuoka M, Wada M, Takahashi K, et al.** (2010) Plasma levels of vascular endothelial growth factor and pigment epithelium-derived factor before and after intravitreal injection of bevacizumab. *Br J Ophthalmol* 94: 1215–1218.
27. **Anto HR, Hyman GF, Li JP, Spitalowitz S, Thomas D** (2012) Membranous nephropathy following intravitreal injection of bevacizumab. *Can J Ophthalmol* 47: 84–86.
28. **Sato T, Kawasaki Y, Waragai T, Imaizumi T, Ono A, et al.** (2013) Relapse of minimal change nephrotic syndrome after intravitreal bevacizumab. *Pediatr Int* 55: e46–48.
29. **Perez-Valdivia MA, Lopez-Mendoza M, Toro-Prieto FJ, Cabello-Chaves V, Toro-Ramos M, et al.** (2014) Relapse of minimal change disease nephrotic syndrome after administering intravitreal bevacizumab. *Nefrologia* 34: 421–422.
30. **Heier JS, Brown DM, Chong V, Korobelnik JF, Kaiser PK, et al.** (2012) Intravitreal aflibercept (VEGF trap-eye) in wet age-related macular degeneration. *Ophthalmology* 119: 2537–2548.
31. **Nguyen DC, Scinicariello F, Attanasio R** (2011) Characterization and allelic polymorphisms of rhesus macaque (*Macaca mulatta*) IgG Fc receptor genes. *Immunogenetics* 63: 351–362.
32. **Julien S, Biesemeier A, Taubitz T, Schraermeyer U** (2014) Different effects of intravitreally injected ranibizumab and aflibercept on retinal and choroidal tissues of monkey eyes. *Br J Ophthalmol*.
33. **Ruifrok AC, Johnston DA** (2001) Quantification of histochemical staining by color deconvolution. *Anal Quant Cytol Histol* 23: 291–299.
34. **Kachouie N, Kang L, Khademhosseini A** (2009) Arraycount, an algorithm for automatic cell counting in microwell arrays. *Biotechniques* 47: x–xvi.
35. **Drury JA, Nik H, van Oppenraaij RH, Tang AW, Turner MA, et al.** (2011) Endometrial cell counts in recurrent miscarriage: a comparison of counting methods. *Histopathology* 59: 1156–1162.
36. **Najafian B, Mauer M** (2011) Quantitating glomerular endothelial fenestration: an unbiased stereological approach. *Am J Nephrol* 33 Suppl 1: 34–39.
37. **Kondo H, Ushiki T** (1985) Stratified laminae fenestratae (alveolus fenestratus endothelialis) in the glomerular capillaries of the mouse kidney. *Arch Histol Jpn* 48: 117–122.
38. **Davidovic SP, Nikolic SV, Curic NJ, Latinovic SL, Draskovic DO, et al.** (2012) Changes of serum VEGF concentration after intravitreal injection of Avastin in treatment of diabetic retinopathy. *Eur J Ophthalmol* 22: 792–798.
39. **Diabetic Retinopathy Clinical Research N, Scott IU, Edwards AR, Beck RW, Bressler NM, et al.** (2007) A phase II randomized clinical trial of intravitreal bevacizumab for diabetic macular edema. *Ophthalmology* 114: 1860–1867.
40. **Jamrozy-Witkowska A, Kowalska K, Jankowska-Lech I, Terelak-Borys B, Nowosielska A, et al.** (2011) [Complications of intravitreal injections—own experience]. *Klin Oczna* 113: 127–131.
41. **Klettner A** (2014) VEGF-A and its inhibitors in age-related macular degeneration - pharmacokinetic differences and their retinal and systemic implications. *Journal of Biochemical and Pharmacological Research* 2: 8–20.
42. **Gaudreault J, Fei D, Rusit J, Suboc P, Shiu V** (2005) Preclinical pharmacokinetics of Ranibizumab (rhuFabV2) after a single intravitreal administration. *Invest Ophthalmol Vis Sci* 46: 726–733.
43. **Barbazetto IA, Saroj N, Shapiro H, Wong P, Ho AC, et al.** (2010) Incidence of new choroidal neovascularization in fellow eyes of patients treated in the MARINA and ANCHOR trials. *Am J Ophthalmol* 149: 939–946 e931.
44. **Larsson A, Skoldenberg E, Ericson H** (2002) Serum and plasma levels of FGF-2 and VEGF in healthy blood donors. *Angiogenesis* 5: 107–110.

45. **Webb NJ, Bottomley MJ, Watson CJ, Brenchley PE** (1998) Vascular endothelial growth factor (VEGF) is released from platelets during blood clotting: implications for measurement of circulating VEGF levels in clinical disease. *Clin Sci (Lond)* 94: 395–404.
46. **Rudge JS, Holash J, Hylton D, Russell M, Jiang S, et al.** (2007) VEGF Trap complex formation measures production rates of VEGF, providing a biomarker for predicting efficacious angiogenic blockade. *Proc Natl Acad Sci U S A* 104: 18363–18370.
47. **Liu A, Dardik A, Ballermann BJ** (1999) Neutralizing TGF-beta1 antibody infusion in neonatal rat delays in vivo glomerular capillary formation 1. *Kidney Int* 56: 1334–1348.
48. **Satchell SC, Braet F** (2009) Glomerular endothelial cell fenestrations: an integral component of the glomerular filtration barrier. *Am J Physiol Renal Physiol* 296: F947–956.
49. **Ichimura K, Stan RV, Kurihara H, Sakai T** (2008) Glomerular endothelial cells form diaphragms during development and pathologic conditions. *J Am Soc Nephrol* 19: 1463–1471.
50. **Elger M, Sakai T, Kriz W** (1998) The vascular pole of the renal glomerulus of rat. *Adv Anat Embryol Cell Biol* 139: 1–98.
51. **Tufro A, Veron D** (2012) VEGF and podocytes in diabetic nephropathy. *Semin Nephrol* 32: 385–393.
52. **Stokes MB, Erazo MC, D'Agati VD** (2008) Glomerular disease related to anti-VEGF therapy. *Kidney Int* 74: 1487–1491.

9.5 Curriculum Vitae

Personal Information

Name: Tschulakow, Alexander, Viktor
 Birthday&-place: October 02 1981, Gomel, Belarus
 Citizenship: German

EDUCATION

1987-2000 F.L. Jahn Gymnasium, Greifswald

10.jul.2000

Degree: General qualification for university entrance (Allgemeine Hochschulreife) grade: 1.9

Study of Human biology

2001-2007 Diploma- Study of Human Biology at the Ernst-Moritz-Arndt-Universität Greifswald

Prediploma:

Subjects: Chemistry, morphology, biochemistry, microbiology, mathematics/statistics

Diploma:

Subjects: Immunology, human genetics, molecular micro-biology
 Subsidiary subject: molecular micro-biology, supervisor Prof. Dr. M Hecker

Diplomathesis: Physiological stress signatures in *Staphylococcus aureus* (Physiologische Stresssignaturen in *Staphylococcus aureus*)

Degree: diploma human biologist (Diplomhumanbiologe) grade: 1.9

Scientific Activities during Study

11.2003-02.2004 Student trainee at the Institute of Molecular Microbiology of the Ernst-Moritz-Arndt- Universität Greifswald, Department of Molecular Microbiology (supervisor: Dr. S. Engelmann; fields of study/techniques: protein- and RNA-studies in bacteria)

02.2005-04.2005 Student trainee at the International Institute of Biophysics (IIB) Neuss, Germany (supervisor: Prof. Dr. F.-A. Popp; fields of study/techniques: biophysical-, biophotonic-, water-studies, some of the results are published)

05.2005-09.2005 Student trainee at the Institute of Human Genetics of the Ernst-Moritz-Arndt- Universität Greifswald (supervisor: Dr. W. Schroeder; fields of study/techniques: PCR, cell culture)

Scientific Activities

- 03.2008-09.2009 Research assistant at the Universitätsklinikum-Schleswig-Holstein, Lübeck, institute of neuroendocrinology, department of immunology (supervisor: Dr. T Lange; fields of study/techniques: ELISA, flow-cytometry, cell cultures, flow-chamber, immunological sleep-studies, vaccination studies)
- 06.2010-09.2010 Research assistant at the J.G.-University Mainz, Department of Pharmacological Biology (supervisor: Prof. T. Efferth; fields of study/techniques: cancer biology, immunohistochemistry, assistance in education of students of pharmacy, cell culture work)
- 09.2010-11.2011 Research assistant at the School of Chinese Medicine Baptist University, Hong Kong (supervisor: Prof. W. Hsiao; fields of study/techniques: cancer biology, molecular biology, cell culture, transfection, assistance in education of students)
- 02.2013 - now PhD student at the University Hospital of Tuebingen, Division of Experimental Vitreoretinal Surgery (supervisor: Prof. U. Schraermeyer; fields of study/techniques: animal studies, cancer biology, ophthalmological studies (OCT, SLO, ERG), radiological studies, cell culture, histology, electron microscopy, 3d modelling)

Additional Skills

Computer skills: Good knowledge of standard computer programs (MS office etc., working knowledge of special programs like Statistica, DIVA, AMIRA and others)

10.1999-09.2003 Basic-study of Traditional Chinese Medicine (TCM)

Languages: German and Russian: native speaker,
English: fluently written and spoken,
French, Spanish and Mandarin: basic knowledge.

Others: Intensive study of Asian and Russian martial arts, trainer assistant

9.5 Erklärungen

Vorname, Name: Alexander Viktor Tschulakow

Titel der Arbeit: Prevention of radiotherapy-induced side effects in retinoblastoma animal models

Ich erkläre hiermit, dass ich die zur Promotion eingereichte Arbeit selbständig verfasst, nur die angegebenen Quellen und Hilfsmittel benutzt und wörtlich oder inhaltlich übernommene Stellen als solche gekennzeichnet habe. Ich erkläre, dass die Richtlinien zur Sicherung guter wissenschaftlicher Praxis der Universität Tübingen (Beschluss des Senats vom 25.5.2000) beachtet wurden. Ich versichere an Eides statt, dass diese Angaben wahr sind und dass ich nichts verschwiegen habe. Mir ist bekannt, dass die falsche Abgabe einer Versicherung an Eides statt mit Freiheitsstrafe bis zu drei Jahren oder mit Geldstrafe bestraft wird.

Tuebingen,

Ort, Datum Unterschrift

9.6 Acknowledgements

I would like to thank my supervisor Prof. Dr. Schraermeyer for providing me with the opportunity to work in his department, his support and for being always kindly open for discussions. I also wish to express my sincere thanks to Prof. Dr. Rammensee for his support.

Very special thanks go to to my co-supervisor and the project leader PD Dr. Sylvie Julien-Schraermeyer, who planned and supervised this project.

I am also indebted to our cooperation partners from the Division of Radiobiology & Molecular Environmental Research, Department of Radiation Oncology, University of Tübingen, Prof. Dr. Hans-Peter Rodemann and Prof. Dr. Klaus Dittmann for their assistance and consultations. Many thanks also to Prof. Dr. Stephan Huber, Dominik Klumpp and Benjamin Steegen from the laboratory of Experimental Radiooncology, Dept. of Radiooncology, University of Tuebingen for their assistance during the Irradiations of the cell cultures and mice, and their support.

I would like to thank Dr. Tobias Peters and Norman Rieger for their support of the SLO/OCT experiments.

I am very grateful to Monika Rittgarn and Sigrid Schultheiss, for their excellent technical assistance and also Dr. Antje Biesemeier, Tatjana Taubitz, Shan Liu, Yuan Fang, Dr. Barbara Illing and Judith Birch from the Division of Experimental Vitreoretinal Surgery for the very warm and friendly atmosphere in our team.

I would like to thank the Deutsche Kinderkrebsstiftung (DKKS), whose financial support made this project possible. Thank you also to my friends beyond the lab, and my family.

Finally, I would like to thank my parents - for everything.